ETUDE DE LA CINETIQUE ET DE LA THERMODYNAMIQUE DES SYSTEMES REACTIONNELS (X-I-O-H) PAR SPECTROMETRIE DE MASSE HAUTE TEMPERATURE

Fatima-Zahra Roki

INSTITUT POLYTECHNIQUE DE GRENOBLE

T H E S E

pour obtenir le grade de

DOCTEUR DE Grenoble INP

Spécialité : *« Mécanique des Fluides, Energétique, Procédés »*

préparée au laboratoire Science et Ingénierie des Matériaux et Procédés
dans le cadre de l'Ecole Doctorale **« Ingénierie, Matériaux, Mécanique, Environnement, Energétique, Procédés, Production »**

présentée et soutenue publiquement

par

Fatima-Zahra ROKI

le 29 Janvier 2009

ETUDE DE LA CINETIQUE ET DE LA THERMODYNAMIQUE DES SYSTEMES REACTIONNELS (X-I-O-H) PAR SPECTROMETRIE DE MASSE HAUTE TEMPERATURE

DIRECTEUR DE THESE : Christian Chatillon
CO-DIRECTEUR DE THESE : Alexander Pisch

JURY

M.	Yann BULTEL	Grenoble INP/LEPMI	Président
M.	Jean-Claude TEDENAC	LPMC, Montpellier	Rapporteur
M.	Rudy KONINGS	ITU-Euratom, Allemagne	Rapporteur
M.	Christian CHATILLON	CNRS / SIMaP, Grenoble	Directeur de thèse
M.	Alexander PISCH	CNRS-Lafarge, Lyon	Co-Directeur
M^{me}	Marie-Noëlle OHNET	IRSN / DPAM, Cadarache	Examinateur
M.	Didier JACQUEMAIN	IRSN / DS, Cadarache	Examinateur

REMERCIEMENTS

Ce travail a été réalisé en collaboration avec l'IRSN/DPAM (l'Institut de Radioprotection et Sureté Nucléaire/ Direction de la Prévention des accidents majeurs de Cadarache) que je tiens à remercier de m'avoir choisie en tant que candidate pour la réalisation de ces travaux de recherche.

Je remercie, M^{me} Marie-Noëlle OHNET (mon tuteur IRSN), M^{r} Didier Jacquemin, M^{me} Sylvie Fillet et M^{me} Béatrice Simondi-Teisseire pour la confiance, l'autonomie et l'intérêt que vous m'avez accordé tout au long de ce travail. Marie-Noëlle, je souhaite te remercier plus particulièrement pour ta patience, ta motivation, ton encouragement, ton suivi et tes services qui n'ont fait que rapprocher les distances entre Cadarache et Grenoble.

Je tiens également à remercier le service engineering de l'IRSN: Messieurs C. Marquie, B. Durville, J. Huret (les 3 Z') et F. Bot-Robin… pour leur bonne humeur pendant le montage et les qualifications du réacteur. Et je n'oublie pas le service SEMIC en particulier F. Cousin et L. Cantrel pour leur aide à comprendre la modélisation de l'accident grave avec le code ASTEC.

Je remercie également toute personne de l'IRSN ayant participé de près ou de loin à la réalisation de ce travail.

Cette étude n'aurait pu se faire sans le cofinancement d'EDF et je tiens aussi à lui exprimer ma gratitude.

Je souhaite aussi manifester toute ma gratitude à M^{r} Christian Chatillon, mon directeur de thèse qui a su m'encadrer et qui n'a pas ménagé ses efforts pour m'aider à mener à son terme ce travail. Il a aussi fait preuve de beaucoup de patience à mon égard et il a su supporter mes caprices et coups de têtes tout au long de ces trois années de thèse. Merci Christian, ton enthousiasme, ton dynamisme et ta motivation m'ont vraiment touchée et encouragée à mener à bien ce travail.

Je souhaite aussi remercier A. Pisch (mon co-directeur) et L. Michelutti pour leur aide, leurs bons conseils et leur accueil chaleureux…

Je remercie également l'équipe SMHT: H. Collas, L. Artaud, I. Nuta, M. Gouello, G. Honstein… pour leur aide, leur sympathie et pour les bons moments passés ensemble surtout à l'heure du goûter.

Je suis également reconnaissante envers le personnel du SIMaP ainsi que les doctorants et stagiaires (E. Fischer, M. Botella, L. Di-Giacomo, J. Cuoq, Fabienne, Nadine, Alain L.M, Manu…) et je les remercie vivement pour l'ambiance chaleureuse du premier étage du bâtiment recherche. Je n'oublie pas l'équipe Yavari (Mustafa, Kostas, Yan…) surtout pour le chocolat…

Un grand merci pour une amie « Nourhane » qui a su m'épauler et me supporter durant les moments difficiles et qui a aussi su partager avec moi les moments de joie et de bonheur.

Je souhaite aussi remercier M^{r} H. Kahil pour son soutien et ses précieux conseils lors de la préparation de la soutenance.

Et je n'oublie pas de remercier mon mari qui a fait preuve de beaucoup de patience, qui a toujours été à l'écoute et qui m'a aidé à surmonter les passages les plus difficiles…

Fatima-Zahra

Table de matière/ Contents

INTRODUCTION GENERALE

Le présent travail sur les composés à base d'Iode susceptibles de se dégager dans l'environnement lors d'un accident nucléaire grave (accident de fusion du cœur d'un réacteur à eau sous pression, dont la probabilité d'occurrence est très faible) a été entrepris en collaboration entre le CNRS/INPG/ SIMaP[1] (Grenoble) et l'IRSN/DPAM[2] (Cadarache) et est cofinancé par Electricité de France (EdF). Ce projet se situe dans le cadre plus vaste d'une collaboration internationale visant à évaluer ce que l'on appelle dans le milieu du nucléaire le «terme source», définissant les quantités de produits radioactifs susceptibles d'être rejetées dans l'environnement. La collaboration internationale nécessitant des communications et des rapports en langue anglaise, le présent document a été rédigé pour ce qui est des études détaillées en anglais et sous la forme de publications scientifiques. Parmi celles-ci, la publication concernant l'étude spectrométrique de la vaporisation de CsOH(s,l) - (Thermodynamic study of the CsOH(s,l) vaporization by high temperature mass spectrometry F. Z. Roki, C. Chatillon, M. N. Ohnet, D. Jacquemain, J. Chem. Thermodyn. 40 (2008) 401-416) - constitue telle quelle une partie du chapitre II.

En première partie, et à la demande de l'INP-Grenoble – Formation doctorale -, un exposé des motivations de ce travail et des outils utilisés est présenté en français, complété par des résumés étendus des résultats obtenus ainsi que de la stratégie de recherche qui sous-tend ces travaux. Ce travail permet de proposer des pistes de recherche pour évaluer plus exactement à l'aide des outils thermodynamiques et cinétiques le terme source.

Ce que l'on nomme dans l'industrie nucléaire le « terme source » comporte un nombre important d'éléments chimiques qui doivent être surveillés soit à cause de leur nocivité chimique soit à cause de leur radioactivité. Ces éléments sont produits à partir de la fission du combustible nucléaire. En cas d'accident nucléaire grave résultant de la défaillance cumulée de plusieurs systèmes de sécurité indépendants – comme celui de Three Mile Island (USA) ou plus récemment Tchernobyl (Ukraine) – la fusion du combustible et la rupture des gaines de confinement conduisent à la libération des éléments de fission les plus volatiles qui peuvent alors se répandre en premier lieu dans le circuit de refroidissement, puis vers l'enceinte de confinement du réacteur ou dans l'environnement extérieur quand ces barrières de

[1] Sciences et Ingénierie des Matériaux et Procédés, St Martin d'Hères.
[2] Institut de Radioprotection et Sureté Nucléaire de Cadarache / Direction de la Prévention des Accidents Majeurs

confinement sont défaillantes. Pour un réacteur à eau pressurisée, parmi ces éléments volatils, le Caesium et l'Iode sont les plus importants, suivis par le Tellure, le Molybdène, etc…
Des expériences de fusion du combustible et de sa gaine à différentes échelles ont été réalisées depuis une vingtaine d'années (Vercors, Vulcano,…….Phébus) au CEA[3] puis conjointement CEA-IRSN.. Ces expérimentations ne sont pas toujours suffisamment analytiques pour comprendre les différents mécanismes mis en jeu mais ont permis de cibler les principales questions que pose l'accident nucléaire grave. Notamment, les calculs thermodynamiques indiquaient qu'il ne devait pas y avoir d'iode gazeux à la brèche du circuit primaire alors qu'expérimentalement, dans les essais Phébus, il en a été observé une quantité significative au vue des conséquences possibles sur la population environnante. L'explication pourrait être une limitation cinétique. Afin d'avoir une meilleure compréhension des phénomènes impliquées, il a été décidé de réaliser des essais à une échelle plus réduite et plus « analytique » afin d'observer un nombre réduit de phénomènes et de permettre de valider cette hypothèse.

Sur le plan théorique, le comportement de ces éléments a d'abord été analysé historiquement à l'aide de l'outil thermodynamique, c'est-à-dire par calculs d'équilibres sur les bilans de matière originale contenue dans le cœur du réacteur, cet ensemble étant placé dans différentes conditions de température et de pression correspondant aux différentes zones d'un réacteur nucléaire, ou aux différentes phases d'un accident. Le transport de ces éléments nécessite aussi de prendre en compte le couplage de la thermodynamique et des flux de matière et de chaleur – exactement comme cela se fait pour comprendre l'élaboration des matériaux dans un four ou réacteur chimique -. Dans le cas d'un phénomène accidentel, la rapidité de certaines séquences demande aussi de prendre en compte les cinétiques de réaction dans un couplage avec des flux. Ce sont ces outils de simulation qui sont en phase de mise au point au service modélisation de la DPAM à l'IRSN pour analyser le comportement de l'iode lors de son transfert entre le cœur en fusion du réacteur et l'enceinte de confinement. Ce travail de thèse porte plus particulièrement sur les conditions en début du circuit de refroidissement dans la zone dite « brèche en branche chaude », c'est-à-dire entre 800 et 1300 K, correspondant à l'entrée des générateurs de vapeur.

[3] Le Commissariat à l'Energie Atomique

La simulation plus fine des phases de l'accident prend alors une démarche plus scientifique qui va requérir des données de base comme les propriétés thermodynamiques, les constantes cinétiques ainsi que celles liées au transport de matière et de chaleur, sans oublier les effets de radiolyse due au milieu fortement radioactif. Le présent travail se situe à ce niveau de la recherche scientifique. L'objectif était donc d'établir des données thermodynamiques et cinétiques sur la volatilisation et le transport de l'iode, c'est-à-dire des principaux composés iodés susceptibles d'être rencontrés dans la zone de la branche chaude en sortie de cœur dégradé. La complexité des phases vapeurs de l'iode a nécessité l'utilisation d'un outil d'analyse suffisamment universel et pour cela la méthode de Knudsen associée à un spectromètre de masse à haute température (SMHT) a été choisie. Deux objectifs étaient poursuivis en parallèle: - (i) une étude thermodynamique classique, avec les moyens existants, sur les vapeurs connues ou à mettre en évidence qui peuvent expliquer le transport de l'iode, et - (ii) une étude cinétique visant à comprendre quels mécanismes expliquent la présence d'iode volatile à la brèche en branche chaude. Cette étude thermo-cinétique nécessitait la mise en place d'un réacteur spécifique se couplant au SMHT, son dimensionnement jusqu'à sa conception et sa mise en service sont présentés dans ce travail.

CHAPITRE I

MOTIVATION DE L'ETUDE ET OUTILS SCIENTIFIQUES D'ANALYSES

I.1. CONTEXTE: L'EVALUATION DU TERME SOURCE IODE EN CAS D'ACCIDENT GRAVE DE REACTEUR NUCLEAIRE

I.1.1. Accident grave de réacteur nucléaire

Dans un réacteur nucléaire, le combustible nucléaire et les produits radioactifs qu'il contient sont confinés par trois enveloppes étanches successives:

- la première est constituée par le gainage métallique à base de zirconium qui contient les pastilles de combustible à base de UO_2 (l'ensemble pastilles et gainage formant un crayon combustible),
- la seconde est constituée par le circuit primaire de refroidissement du cœur. Ce circuit est composé (figure I-1):
    - de la cuve du réacteur contenant les crayons combustible montés en assemblage,
    - de générateurs de vapeur qui assurent le refroidissement de l'eau du circuit primaire par échange de chaleur,
    - d'un circuit assurant la circulation de l'eau de refroidissement dans la cuve autour du cœur vers les générateurs de vapeur, et constitué de branches chaudes (eau chauffée par le cœur) entre la sortie de la cuve et l'amont des générateurs de vapeur et de branches froides (eau refroidie au niveau des générateurs de vapeur) entre l'aval des générateurs de vapeur et l'entrée dans la cuve.
- la troisième est constituée par l'enceinte de confinement en béton qui contient l'ensemble des éléments ci-dessus.

L'occurrence d'un accident de réacteur conduisant à la fusion du cœur est de très faible probabilité car elle suppose une combinaison de défaillances des systèmes de sécurité du réacteur et/ou d'erreurs humaines et l'impossibilité de ramener le réacteur dans une situation

sûre. Cependant, un tel accident peut conduire à des rejets radioactifs importants dans l'environnement. Une séquence d'évènements typiques pouvant survenir dans un accident grave de réacteur, qui conduirait à la rupture du confinement, peut-être décrite de la manière suivante:

- une brèche (rupture de canalisation) dans le circuit primaire où circule l'eau de refroidissement du cœur du réacteur peut constituer l'évènement initiateur; la brèche entraîne une perte de l'eau de refroidissement du circuit primaire qui se déverse dans le puisard de l'enceinte de confinement (Figure I-1) et un abaissement soudain de la pression de confinement jusqu'à 2 bars environ.

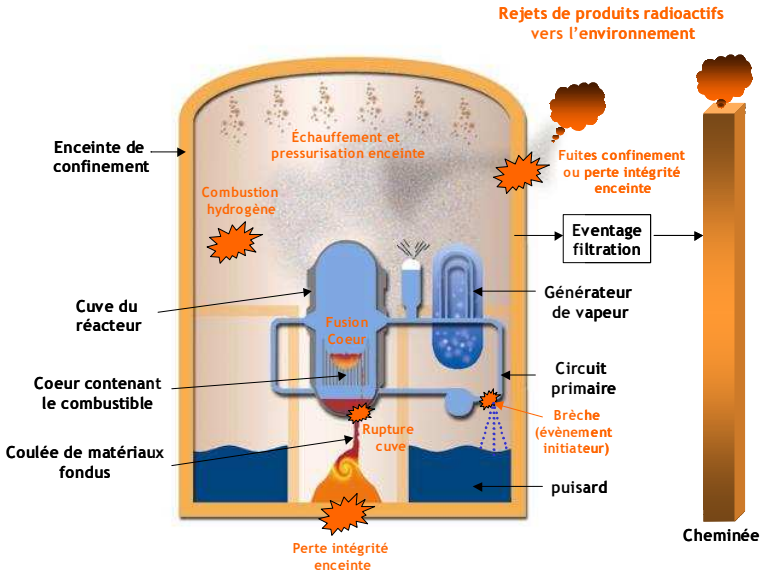

Figure I.1: L'accident grave de réacteur nucléaire: représentation schématique du déroulement et des conséquences possibles

- le cœur contenant le combustible nucléaire s'échauffe (plus de 2300 K) car il n'est plus refroidi, entraînant la dégradation mécanique et thermique des matériaux qui le constituent et le relâchement, par vaporisation, de certains produits de fission radioactifs,
- les produits de fission radioactifs (PF) forment des aérosols par condensation/nucléation/agglomération (phase condensée solide ou liquide) et/ou des vapeurs qui sont transportés par l'écoulement de gaz provenant du cœur dégradé, essentiellement entraînés par la vapeur d'eau et/ou l'hydrogène vers la brèche du circuit primaire et atteignent l'enceinte de confinement,

- dans le circuit primaire comme dans l'enceinte de confinement, les produits de fission radioactifs peuvent se déposer et être remis en suspension au cours de l'accident,
- la dégradation du cœur peut entraîner la formation de mélanges de matières en fusion, lesquelles s'écoulent à travers le cœur, et vont s'accumuler en partie basse de la cuve du réacteur, avec des réactions chimiques de dissolution-reprécipitation (création d'un système complexe U-O-Zr-Fe-Cr-Ni etc) qui causent la rupture de celle-ci (Figure I-1). Les matériaux fondus peuvent ensuite entrer en contact avec le béton du sol de l'enceinte (radier) de confinement produisant la libération de gaz (H_2, CO, CO_2) dans l'enceinte de confinement et éventuellement au percement du béton avec ouverture de l'enceinte vers le sol (perte d'intégrité de l'enceinte),
- l'atmosphère de l'enceinte de confinement se réchauffe sous l'effet de la présence de gaz chaud (vapeur, hydrogène,…) et des produits radioactifs et la pression dans l'enceinte augmente. Une combustion de l'hydrogène accumulé dans l'enceinte peut survenir et induire une augmentation de pression supplémentaire,
- une fraction des produits radioactifs en suspension dans l'enceinte peut être émise vers l'environnement par différentes voies:
    - soit par les chemins de fuite existant dans les parois de l'enceinte (rejets faibles mais continus) ou par le sol après le percement du radier de l'enceinte,
    - soit par l'intermédiaire d'une ligne d'éventage de l'enceinte (Figure I-1). Cette ligne d'éventage n'est utilisée, au bout de quelques heures, que si la montée en pression, menace l'intégrité de l'enceinte. L'éventage se fait par ouverture de l'enceinte sur l'environnement au travers d'un système de filtration dont l'objectif est de limiter le rejet de produits radioactifs.

Divers moyens de mitigation peuvent être mis en œuvre pour tenter de sauvegarder l'intégrité de l'enceinte de confinement du bâtiment réacteur comme par exemple des recombineurs de l'hydrogène.

Même si la prévention des accidents est assurée en premier lieu par la conception du réacteur et de ses systèmes de sûreté et par la mise en œuvre du concept de défense en profondeur, il est indispensable de caractériser les processus physiques décrits plus haut susceptibles d'intervenir dans le déroulement de l'accident dans le but d'être en mesure :

- de mettre en place des mesures de gestion des accidents afin de contribuer à la prévention aussi bien qu'à la limitation des conséquences d'un accident pour l'homme et l'environnement, et d'évaluer leur efficacité,
- de fournir une bonne évaluation de la cinétique, de la composition et du niveau du rejet de produits radioactifs vers l'environnement – ce que l'on appelle *l'évaluation du terme source* - de manière à consolider les plans particuliers d'intervention (PPI) à mettre en œuvre pour la sécurité des populations et évaluer l'efficacité des moyens de mitigation mis en place.

C'est l'objectif de la recherche menée dans le domaine des accidents graves à l'IRSN/DPAM[1] et des programmes expérimentaux réalisés au SERCI/L2EC[2].

I.1.2. Objectif du programme CHIP (CHimie de l'Iode dans le circuit Primaire)

En cas d'accident nucléaire dans un Réacteur à Eau Pressurisée (REP), l'iode[3] du fait de son caractère volatil peut être relâché du cœur du réacteur et être transporté dans le circuit primaire de refroidissement (eau) vers l'enceinte de confinement, sous forme gazeuse (vapeur ou par les gaz produits lors de la propagation de l'accident) ou aérosol. L'iode faisant partie des radio contaminants les plus critiques car ayant des conséquences sanitaires sur la population (fixation sur la thyroïde) et sur l'environnement, il est essentiel de disposer d'outils de calcul validés permettant, pour les séquences accidentelles les plus probables, d'évaluer les conséquences radiologiques possible pour l'homme d'un relâchement de l'iode dans l'environnement. Une des difficultés majeures dans la mise en œuvre de ces outils de calcul est qu'il n'existe pas suffisamment de données expérimentales validées concernant le comportement physico-chimique de l'iode dans le circuit primaire jusqu'à la brèche où va s'effectuer le premier relâchement (fissuration dans le circuit qui peut être produit par rupture ou dégradation du matériau).

[1] Institut de Radioprotection et Sureté Nucléaire de Cadarache / Direction de la Prévention des Accidents Majeurs
[2] Service d'Etude et de Recherche expérimentale sur la Chimie et l'Incendie / Laboratoire d'Expérimentations Environnement et Chimie
[3] Elément issu de la réaction de fission de l'uranium

Depuis l'accident du réacteur n°2 de la centrale nucléaire américaine de Three Mile Island (TMI-2), le 28 mars 1979, qui s'est traduit par la fusion de la moitié du cœur du réacteur et des rejets de produits de fission limités, un ensemble de programmes expérimentaux de recherche en sûreté a été réalisé par de nombreux organismes internationaux à travers le monde. De nombreux modèles de simulation ont également été développés pour calculer le déroulement de tels accidents, en évaluer les conséquences et apprécier l'efficacité des différentes mesures qui pourraient être mises en œuvre pour en limiter les effets.
Le programme expérimental Phébus PF, lancé par l'Institut de Protection et de Sûreté Nucléaire en 1988, est l'un des principaux programmes de recherche internationaux consacrés aux accidents graves de réacteurs à eau (avec fusion de cœur). Un bon nombre de résultats obtenus lors de ce programme, dont certains importants pour les évaluations de sûreté, étaient inattendus. L'analyse de l'ensemble de ces résultats et leur utilisation dans les études d'évaluation des rejets radioactifs potentiels vers l'environnement en cas d'accident a permis de dégager un certain nombre d'enseignements [1-4]. Des essais spécifiques à petite échelle ont été réalisés pour comprendre les phénomènes inattendus observés et valider les nouveaux modèles. A l'issue du programme Phébus PF, une liste des principales incertitudes restantes a été établie. Le projet européen EURSAFE intégré au 5ème Programme Cadre de Recherche Européen, dont l'objectif était de conduire à une évaluation réaliste des rejets possibles dans l'environnement pour une meilleure gestion des risques associés, a conduit à une hiérarchisation des recherches à mener en vue de réduire ces incertitudes. Une partie de ces recherches fait l'objet du nouveau programme international lancé conjointement par l'Institut de Radioprotection et de Sûreté Nucléaire (IRSN), le Commissariat à l'Energie Atomique (CEA) et Electricité de France (EDF) en 2005: le programme «Terme Source» [5] comprenant une série d'essais analytiques relatifs notamment à la chimie de l'iode (comportement dans le circuit primaire du réacteur et à l'intérieur de son enceinte de confinement), la dégradation du combustible en présence de carbure de bore, l'oxydation des gaines sous air et les cinétiques de relâchement des produits de fission à partir du combustible.

Un des résultats les plus inattendus et ayant un impact important pour la sûreté est la mise en évidence expérimentale d'une petite fraction d'iode volatil à basse température dans l'enceinte de confinement très tôt durant les essais Phébus FPT-0-1-2 [6]. En se basant sur des mesures expérimentales d'iode dans les capsules gazeuses du circuit primaire, l'iode gazeux mesuré dans l'enceinte de confinement à cet instant a été interprété comme provenant du circuit, contrairement aux prédictions des modèles de thermochimie qui prévoyaient que tout

l'iode se trouvait sous une forme condensée (CsI) à la sortie du circuit. Des limitations d'ordre cinétique dans les réactions chimiques en phase gazeuse sont l'explication la plus plausible puisqu'aucun des calculs présupposant un équilibre chimique dans le gaz ne permet de reproduire les résultats expérimentaux [7, 8].

De manière générale, les essais Phébus ont montré que la concentration en iode volatil dans l'enceinte de confinement à long terme (au delà de 24 heures) dépend principalement des processus physico-chimiques intervenant dans la phase gazeuse et donc de la concentration en iode volatil provenant du circuit primaire ou formé dans l'enceinte lors de la fusion du coeur. Les enseignements issus de l'analyse des résultats relatifs au comportement de l'iode lors des essais Phébus PF ont été utilisés pour l'amélioration et le développement de modèles traitant de la chimie de l'iode dans l'enceinte, par la suite intégrés dans la plupart des logiciels de simulation utilisés pour les analyses de sûreté. Une meilleure compréhension de la chimie de l'iode dans le circuit primaire est nécessaire à la levée d'incertitudes concernant la quantification des rejets accidentels dans l'environnement et fait l'objet du programme de recherche CHIP (CHimie de l'Iode dans le circuit Primaire). Celui ci fait partie du programme international Terme Source et est cofinancé par l'IRSN, le CEA, EDF, la Communauté Européenne (C.E.), l'United State Nuclear Regulatory Commission (USNRC), l'Atomic Energy Canada Limited (AECL), Suez-Tractebel et l'Institut Paul Scherrer (PSI - Suisse) sur la période 2005-2010. Il vise à acquérir les données nécessaires au développement et à la validation des modèles décrivant les mécanismes de formation de l'iode gazeux en branche chaude et en branche froide du circuit primaire en situation accidentelle. Les données obtenues permettront de développer et de valider des modèles développés par l'IRSN pour représenter le comportement chimique de l'iode dans le circuit primaire d'un réacteur en situation accidentelle. Les objectifs du programme CHIP sont hiérarchisés de la façon suivante:

- trouver un moyen d'observation des formes gazeuses de l'iode dans les conditions de la brèche pour repérer les espèces responsables de son transport,
- déterminer (expérimentalement) les données thermodynamiques et cinétiques conduisant à la formation de ces espèces,
- développer des modèles simulant le transport de l'iode pour alimenter les outils de calculs de l'accident.

Lors de la dégradation du cœur, les PF issus du combustible ainsi que les matériaux des barres de commande -en carbure de bore (B_4C) ou à base d'alliage absorbant d'Argent, d'Indium et

de Cadmium (Ag-In-Cd)- et les matériaux de structure génèrent de nombreux composés dont les formes chimiques peuvent variées. Compte-tenu de la complexité des systèmes chimiques mis en jeu, les objectifs précédents seront traités au niveau expérimental selon deux axes d'expérimentation différents :

- le premier axe correspondant aux essais dit ***«analytiques»*** (ligne analytique) vise à étudier un nombre réduit d'éléments chimiques pour faciliter l'analyse de la phase gazeuse. Compte tenu de la présence du gaz porteur et de l'iode, il s'agit au moins de systèmes quaternaires de type {X-I-O-H}.
- le deuxième axe correspondant aux essais dit ***«phénoménologiques»*** (ligne phénoménologique) prendra en compte l'ensemble des principaux éléments chimiques produits par la dégradation du cœur du réacteur (produits de fission: Cs, Mo, Te…), éléments du crayon absorbant les neutrons (Ag, In, Cd) et ou des matériaux de structure (Sn)).

Le travail de thèse se situe dans le cadre de la ligne analytique. Parmi les méthodes d'analyses des phases gazeuses à haute température – (i) méthodes optiques: Raman, Infra rouge ou absorption atomique, – (ii) méthode par ionisation du gaz: spectrométrie de masse- seule la spectrométrie couplée à une cellule d'effusion possède une capacité d'analyse importante et universelle car elle ne dépend pas étroitement de l'espèce mesurée. Ainsi pour cette ligne analytique l'IRSN a choisi de collaborer dans le cadre de cette thèse avec le SIMAP/CNRS[4] qui dispose d'un spectromètre de masse à haute température avec le double objectif: -(i) d'effectuer un diagnostic des espèces existant à la brèche en branche chaude en concevant un réacteur spécifique, -(ii) d'établir des données thermodynamiques et cinétiques pour les espèces gazeuses repérées. Ces données seront intégrées dans les bases de données utilisées pour modéliser l'accident à l'aide du logiciel SOPHAEROS (module cinétique du logiciel en cours de développement) [9].

[4] Science et Ingénierie des Matériaux et Procédés, UMR 5614 CNRS, Saint Martin d'Hères

I.1.3. Spécifications des conditions aux limites pour la réalisation des essais analytiques

Pour mener les essais dits «analytiques» à objectif de modélisation, le procédé et le dispositif associé devront être conçus de manière à pouvoir obtenir – (i) des données d'équilibre et des données cinétiques relatives à différents systèmes réactionnels impliquant chacun un nombre restreint d'éléments chimiques, - (ii) diagnostiquer le comportement des espèces pour des conditions aux limites intéressant le domaine d'étude des accidents graves. Pour les études thermodynamiques et cinétiques, les conditions de mesures doivent optimiser les phénomènes dans la gamme où ils sont mesurables. Par contre pour le diagnostic « accident grave » , la maîtrise des paramètres d'études suivants est requise:

- ***Systèmes réactionnels**:* les systèmes à étudier sont du type {X-I-O-H}, l'élément X pouvant être du Cs, In, Ag, Cd… Il a été décidé de débuter le programme d'essai avec le système (Cs, I, O, H) qui a été le plus étudié jusqu'à présent, il s'agit donc de valider ou préciser les données cinétiques et thermodynamiques existantes de la littérature, de générer les données manquantes pour les modèles et de valider le bon fonctionnement du dispositif expérimental qui sera mis en place.
- ***Niveaux de températures**:* la température de la cellule à haute température simulant les conditions de la sortie du cœur du réacteur, appelé craqueur, doit être comprise entre 1500 et 1900 K (il est estimé qu'une température de l'ordre de 1900 K est suffisante pour mener des études cinétiques). La température de la cellule simulant les conditions de la brèche en branche chaude, appelé condenseur, doit être comprise entre 1000 et 1300 K.
- ***Niveaux de concentrations***: ce paramètre intervient directement dans la modélisation des phénomènes cinétiques et il est donc important de bien le maîtriser. Le dispositif d'essai doit permettre de couvrir les gammes de concentration les plus larges possibles. Les évaluations faites par l'IRSN/DPAM montrent que les gammes de rapports molaires suivantes doivent pouvoir être étudiées pour le système {Cs, I, O, H}:
  - Cs/H_2O compris entre 10^{-4} et 10^{-1} et I/H_2O entre 10^{-5} et 10^{-2};
  - Cs/H_2 compris entre 10^{-3} et 10^{-1} et I/H_2 entre 10^{-4} et 10^{-2} ;

  L'étude de dimensionnement du dispositif a permis de déterminer avec plus de précision les gammes de concentration à atteindre [10].
- ***Temps de séjour moyen**:* c'est le temps qu'il faut pour qu'une espèce gazeuse passe de la zone de craquage à la cellule de recombinaison (condenseur). Par analogie à un réacteur

à eau pressurisée en condition accidentelle, il représente le temps de parcours de la sortie du cœur du réacteur vers le circuit primaire au niveau de la brèche en branche chaude. La gamme est de 1 à 10 s. Les contraintes sur ce paramètre d'étude sont du même type que celles sur les concentrations: l'objectif est de bien maîtriser ce paramètre qui intervient directement dans la modélisation et de couvrir les plus larges gammes possibles.

L'étude présentée ici vise à concevoir et à tester un réacteur qui à la fois respecte les exigences des mesures spectrométriques (pression totale condenseur < 10^{-4} bar) et assure les spécifications demandées par l'IRSN. Ce réacteur a pour objectif final de diagnostiquer les espèces présentes à la brèche en branche chaude. Les études thermochimiques et cinétiques seront ensuite limitées à ces espèces. Ce réacteur de diagnostic n'est pas habituel en spectrométrie de masse à haute température et c'est pourquoi nous avons fait une étude de dimensionnement pour appréhender les gammes de fonctionnement pouvant être atteintes [10] et pour concevoir ce réacteur et les lignes d'introduction. Nous avons ensuite effectué des tests spectromètriques visant à valider la calibration des mesures de pressions partielles par rapport à celle du gaz porteur qui est l'Argon. Cette étude fait l'objet du chapitre V. L'objectif de ce réacteur de diagnostic n'est pas d'être représentatif de toutes les conditions rencontrées dans le circuit primaire, en particulier au niveau des pressions totales, mais de déceler les paramètres qui vont avoir un impact sur les équilibres chimiques ou les cinétiques de réaction - rapport de pressions partielles, niveaux de température et temps de séjour -. Il est utile de rappeler qu'en terme de réaction chimique, la constante d'équilibre et les constantes cinétiques ne dépendent que de la température et très peu de la pression.

Avant la mise au point du réacteur de diagnostic, des calculs thermodynamiques couplés à des calculs de flux effectués à l'IRSN (SEMIC[5]) n'ont pas permis d'expliquer les quantités d'iode volatile (totale et sous toutes les formes chimiques et physiques) mesurées à la brèche du circuit de refroidissement lors des essais intégraux PHEBUS. Dès lors, du point de vue des mécanismes chimiques au moins trois voies peuvent expliquer ce fait:

- Il existerait des molécules gazeuses nouvelles et inconnues, non prises en compte dans les banques de données thermodynamiques à la base des calculs de transfert. Ce fait acquiert une certaine probabilité si l'on se référe au travail spectrométrique de

[5] Service d'Etudes et de Modélisation de l'Incendie, du corium et du Confinement

Blackburn et Johnson [11], ces auteurs ayant montré l'existence d'un complexe CsICsOH(g) stable.

- Il existerait une cinétique de recombinaison en phase gazeuse homogène relativement lente comparée au temps de transfert (1 à 10 s) dans la branche chaude et, en conséquence, de l'iode volatile (I_2(g), I(g) ou HI(g) par exemple) résiduelle serait transférée vers les zones plus froides.
- Il se produit au cours de la détente et du refroidissement un passage du fluide de l'état supercritique - mélange homogène de tous les constituants avec solubilité totale de tous ces éléments - à un état d'équilibre ou de pseudo-équilibre qui va entraîner un partage entre phases gazeuses et phases condensées ce qui explique la présence de très nombreux aérosols. Dans le partage des éléments entre ces phases l'excès de vapeur d'eau peut entraîner l'expulsion de ces éléments les moins solubles, dont précisement l'iode.

Le présent travail entrepris avec l'IRSN a été conduit prioritairement sur les deux premiers axes :

- études thermodynamiques classiques réalisées avec l'équipement existant du SIMaP et le savoir faire en thermodynamique, et
- étude cinétique pour laquelle un réacteur spécifique a du être consçu (chap. V).

I.1.4. Principe de conception du dispositif d'essai

Pour obtenir des données thermodynamiques et cinétiques pour les systèmes quaternaires, le dispositif d'essai pourrait être constitué d'un réacteur ouvert permettant de maîtriser les écoulements de gaz et le temps de séjour entre la zone où la température est maximale (T_{max}) et le point de mesure ($T_{branche\ chaude}$). Les paramètres température, rapport des pressions partielles et temps de séjour devront permettre de couvrir les gammes des conditions accidentelles dans le circuit primaire d'un REP et, en particulier, celles de la branche chaude.

Il pourrait être constitué de trois parties. Une première partie appellée cellule de craquage des réactifs dite «craqueur» (figure I-2) dans laquelle les réactifs injectés (H_2, H_2O, I_2 et X = Cs ou In) seront amenés à une température suffisamment élevée pour obtenir une composition

aussi proche que possible des mélanges obtenus à la sortie du cœur du réacteur, dans la partie chaude du circuit primaire en situation d'accident. Une deuxième partie appellée cellule de recombinaison ou condenseur (figure I-2) dans laquelle les réactifs se recombinent à une température uniforme qui sera la température d'étude (température de la branche chaude située entre 1000 et 1300 K). Une troisième partie qui doit permettre d'échantillonner les réactifs présents dans le réacteur pour réaliser une analyse quantitative (mesure des pressions partielles des gaz) par spectrométrie de masse à haute température (Figure I-2).

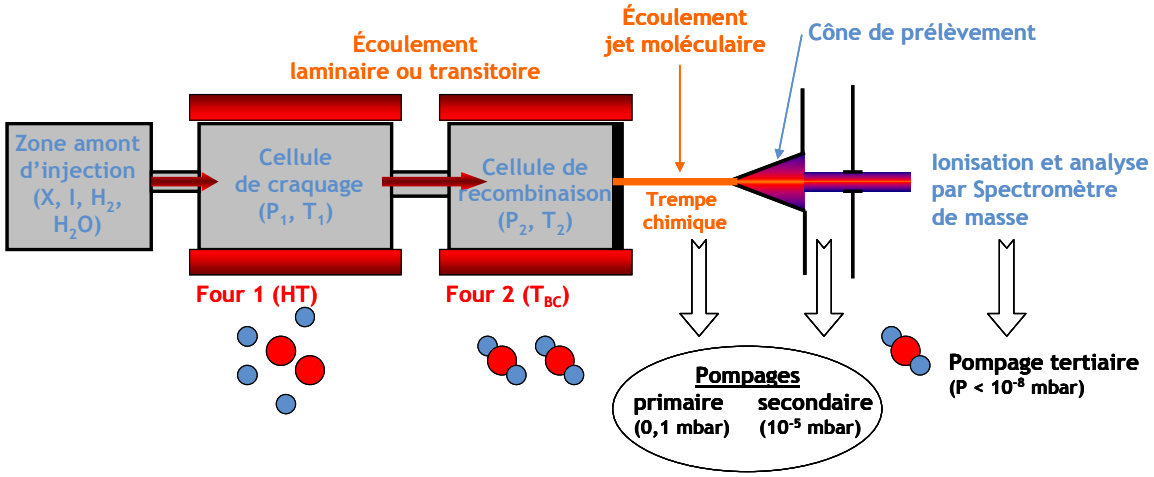

Figure I-2: Principes du dispositif expérimental pour la ligne analytique

Pour pouvoir étudier les réactions entre différents élements, il a été décidé d'utiliser des lignes d'injection séparées autant que possible pour chaque gaz ou élément:

- une ligne d'injection composé d'un mélange de H_2 et de vapeur d'eau,
- une ligne d'injection d'iode moléculaire,
- une ligne d'injection ou un évaporateur pour l'élement X étudié.

Le but de ces lignes indépendantes est d'essayer d'obtenir des variations de concentration relatives importantes et si possible rapides. Ce schéma de réacteur idéal constitue le point de départ de ce travail dont l'objectif est d'évaluer la «faisabilité» tant en terme de structure d'ensemble qu'en terme de réalisation, notamment sur le plan du choix des matériaux et de leur mise en forme. Ces contraintes vont guider les choix successifs.

I.2. SPECTROMETRIE DE MASSE A HAUTE TEMPERATURE

Cette technique a été choisie car elle est particulièrement bien adaptée à l'étude des phases vapeurs à haute température: elle est la seule à pouvoir s'adapter à l'étude de la vaporisation de tout type de composés ainsi qu'à celle des réactions en phase gazeuse homogène.

I.2.1. Principe

La spectrométrie de masse à haute température (SMHT) est une technique d'analyse des phases gazeuses à partir d'un jet moléculaire plus généralement appelée spectrométrie de masse sur cellule d'effusion ou sur faisceau moléculaire. De nombreux travaux sur la thermodynamique des phases gazeuses utilisant la spectrométrie de masse ont été effectués depuis 1954, année de sa mise au point [12, 13] (environ 2500 publications à l'heure actuelle).

Le principe de la spectrométrie de masse à haute température consiste à associer un réacteur chimique fonctionnant sous vide dont l'étage terminal est effusif et qui contient le système à étudier avec un spectromètre de masse à ionisation de gaz par bombardement électronique (figure I-3).

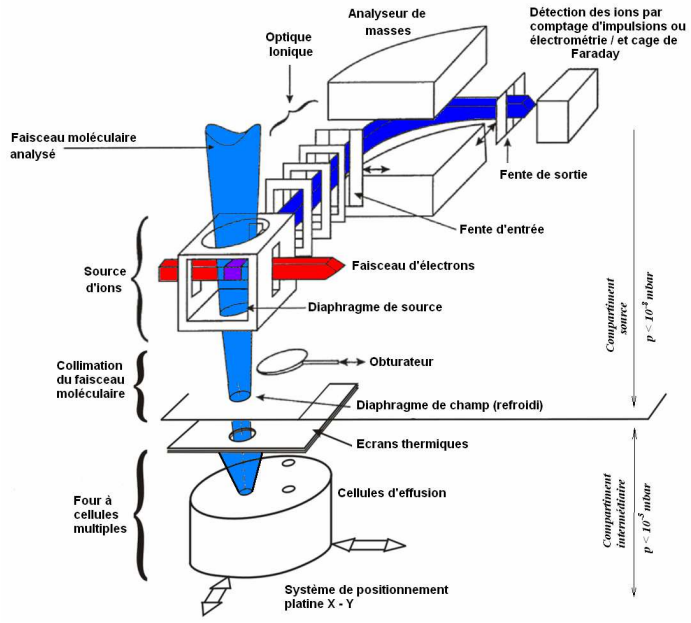

Figure I-3: Principe général de la mesure spectrométrique au SIMaP

Un système de collimation sélectionne un faisceau de molécules qui est ionisé par un faisceau d'électrons au niveau de la source d'ions suivant le processus simple le plus général, l'ionisation adiabatique:

$$M + e^- \longrightarrow M^+ + 2\,e^- \quad (1)$$

Les ions produits sont accélérés et séparés en fonction de leur rapport masse/charge par un prisme magnétique qui fait fonction d'analyseur de masse. Ils sont ensuite collectés sur une cage de Faraday ou un multiplicateur d'électrons secondaires. L'abondance isotopique de chaque ion permet de remonter à sa composition atomique. Le jet moléculaire (processus effusif) produit via un petit orifice est un faisceau de molécules ou atomes gazeux produits à des pressions suffisamment basses pour que le «vol» des espèces gazeuses s'effectue sans collision. Le détecteur spectrométrique verra alors des gaz représentatifs du lieu de leur production. En pratique cela signifie que l'orifice par lequel «effuse» ce jet a des dimensions comparables au libre parcours moyen dans le gaz considéré avant effusion. Par exemple, pour un orifice de diamètre 1 mm, la pression est de 10^{-4} bar environ.

La loi de Beer-Lambert appliquée à l'absorption des électrons dans un milieu raréfié [14] conduit à l'expression de la pression partielle p_i d'une espèce dans le réacteur en fonction de l'intensité mesurée au spectromètre I_i, de la température T dans le réacteur et de la sensibilité du spectromètre S_i selon la relation de base spectrométrique suivante:

$$p_i S_i = I_i T \quad (2)$$

La sensibilité S_i est définie par la relation suivante:

$$S_i = G\eta\sigma_i(E)\gamma_i f_i \quad (3)$$

où G est un facteur géométrique qui fait intervenir l'angle solide entre la chambre d'ionisation et la source du faisceau moléculaire (orifice d'effusion), η est le facteur de transmission des ions dans l'analyseur spectrométrique (pour notre secteur magnétique $\eta=1$), $\sigma_i(E)$ est la section efficace d'ionisation au potentiel E des électrons ionisants, γ_i est le rendement de la détection (=1 pour notre comptage d'impulsions), f_i est l'abondance isotopique de l'ion détecté, connue ou calculable à partir des atomes constituants l'ion.

La sensibilité du spectromètre S_i ne peut être obtenue que par calibration de l'appareillage à chaque expérience et par estimation des sections efficaces d'ionisation σ_i. La section efficace d'ionisation d'une molécule se calcule sur la base d'une règle dite «d'additivité» à partir de

celles des atomes la constituant [13]. Cette règle s'applique pour l'ensemble du processus d'ionisation en prenant en considération l'ion parent plus les ions fragments (ceux-ci sont nombreux dans le cas des hydroxydes et des iodures). Les sections efficaces d'ionisation des

atomes ont été paramétrées en fonction de l'énergie d'ionisation (eV) dans la référence [13]. Dans le cas d'un dimère, la règle d'additivité conduit à un rapport dimère/monomère égal à 2.

L'étude des processus d'ionisation permet de remonter aux molécules à l'origine des ions et donc de connaître la composition des vapeurs formées dans le réacteur. Cette analyse se fait par différents moyens:

- Tracé et étude des courbes d'efficacité d'ionisation (Intensités mesurées en fonction de l'énergie des électrons ionisants),
- Variation de la chimie du système en vue de faire varier la composition des vapeurs.

I.2.2. Les cellules d'effusions couplées au SMHT

Différentes types de cellules peuvent être couplées au SMHT comme illustré sur la figure I-4.

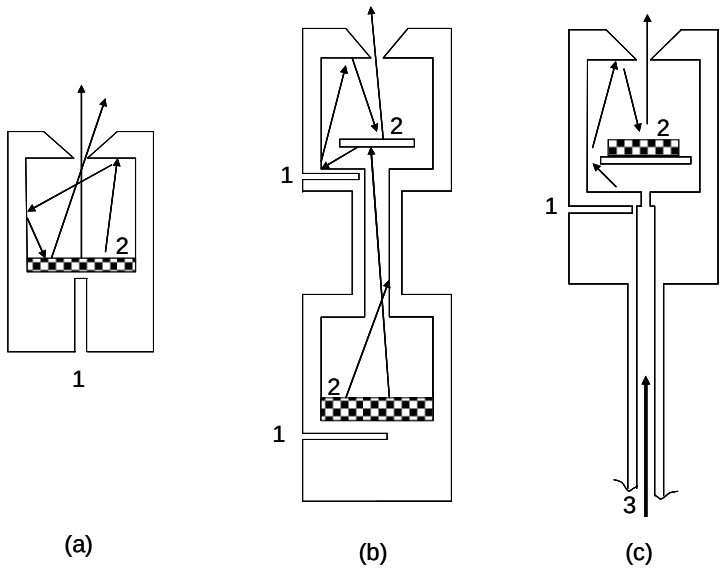

Figure I-4: Différentes cellules d'effusion utilisées au SMHT: (a) Cellule de Knudsen – (b) cellule Tandem pour le craquage des vapeurs saturées – (c) cellule avec introduction de gaz à faible pression. 1. Accès pour mesures de température par thermocouple ou par pyrométrie, 2. échantillon solide ou liquide, 3. ligne d'introduction de gaz réactif.

La cellule d'effusion dite de Knudsen est la plus répandue. C'est un récipient fermé composé d'un creuset et de son couvercle dans lequel est pratiqué l'orifice d'effusion dont la section *s* est petite vis-à-vis de la surface de l'échantillon *S* disposé dans ce récipient (fig. I-4-a). Un rapport $s/S \leq 10^{-2}$ est généralement utilisé. Cette cellule est entourée d'une enveloppe facilitant l'équilibre thermique, et l'ensemble est disposé à l'intérieur d'un four spécialement conçu. L'échantillon étudié doit générer une pression inférieure à 10^{-4} bar afin d'assurer un régime moléculaire au niveau de l'orifice de sortie ou l'orifice d'effusion. L'analyse des vapeurs va porter sur le jet moléculaire produit par les vapeurs à l'orifice: les molécules prélevées sur l'axe normal à l'orifice ne touchent aucune paroi avant la détection spectrométrique (conservation de leur température).

Le flux de molécules ou d'atomes dN_i/dt par unité de temps effusé par l'orifice de section *s* est calculé par la relation de Hertz-Knudsen [13]:

$$\frac{dN_i}{dt} = \frac{p_i \, sC}{\sqrt{2\pi M_i RT}} \qquad (4)$$

avec p_i la pression dans la cellule, M_i la masse molaire de l'espèce gazeuse effusante, *R* la constante des gaz parfaits, *T* la température de la cellule et *C* un coefficient dit de Clausing utilisé dans le cas d'un orifice à paroi non idéalement mince.

Le calcul du coefficient de Clausing a été revu par Santeler et al. [15] pour un canal cylindrique et est donné par la relation suivante:

$$C = \frac{1}{1 + \frac{3 * l'}{8 * r}} \qquad (5)$$

où l' est la longueur équivalente de la canalisation et r le rayon de la canalisation. La longueur équivalente – calculée pour tenir compte de la conductance dite «d'extrémité» ou sortie des molécules de l'orifice - est exprimée en fonction de la longueur l et du rayon r de l'orifice d'effusion par la relation suivante [15]:

$$l' = l * \left[1 + \frac{1}{3 + \frac{3 * l}{7 * r}} \right] \qquad (6)$$

Dans le cas de l'étude de réactions entre un gaz et un solide, ou entre différents gaz, la cellule est alors munie d'une ou plusieurs lignes d'introduction de gaz ou vapeurs sous pression

réduite de façon à respecter le régime d'effusion à l'orifice de sortie (fig. I-4-c). Ceci correspond alors à des flux très faibles.

I.2.3. Etalonnage/Calibration du spectromètre

L'étalonnage du spectromètre de masse ou calibration (connaissance de S_i ou passage de I_i à p_i) se fait habituellement en combinant la relation spectrométrique (2) avec la perte de masse de l'échantillon Δm (7) pour obtenir la sensibilité (8):

$$\Delta m = \sum \frac{dN_i}{dt} \times M_i \tag{7}$$

$$S = \left(sC\sqrt{M}\right) / \left(\Delta m \sqrt{2\pi R}\right) \sum_{i=1}^{n} \left(I\sqrt{T}\right)_i \delta t_i \tag{8}$$

où s est la section de l'orifice, C son coefficient de Clausing, t le temps et i=1 à n correspondant aux différents paliers de température. Les produits $I\sqrt{T}\delta t$ sont obtenus par intégration de l'observation spectrométrique tout au long de l'expérience.

Pour plusieurs espèces gazeuses j en présence, l'expression devient:

$$S_1 = \left(sC\sqrt{M_1} / \Delta m \sqrt{2\pi R}\right) \sum_{j=1}^{p} \left(\sum_{i=1}^{n} S_1 / S_j \sqrt{M_j / M_1} \left(I_j \sqrt{T}\right)_i \delta t_i \right) \tag{9}$$

i = 1 à n correspondant aux différents paliers de température de l'expérience, j au nombre d'espèces. Cette dernière expression nécessite soit de connaître soit d'estimer les rapports de sensibilité S_1/S_j rapportés à une sensibilité de référence S_1.

I.2.4. Description du spectromètre

La cellule d'effusion est couplée avec un spectromètre de masse. Le spectromètre se compose de trois parties principales: la source d'ions, l'analyseur de masse et la détection (Figure I-5).

- ***La source d'ions***

La chambre d'ionisation est en µ-métal (protection contre les champs magnétiques parasites) et assure l'extraction des ions à l'aide d'une lentille à «immersion» et d'un repousseur d'ions. Les ions extraits sont ensuite accélérés et focalisés par une lentille électrostatique fonctionnant entre 5000 V et la masse avant de pénétrer dans l'analyseur de masse. La chambre d'ionisation est munie d'un diaphragme d'entrée ajustable afin de collimater le faisceau venant de la cellule d'effusion. Ce système permet de s'assurer que les molécules ionisées sont bien issues de la cellule mais limite aussi le volume d'ionisation.

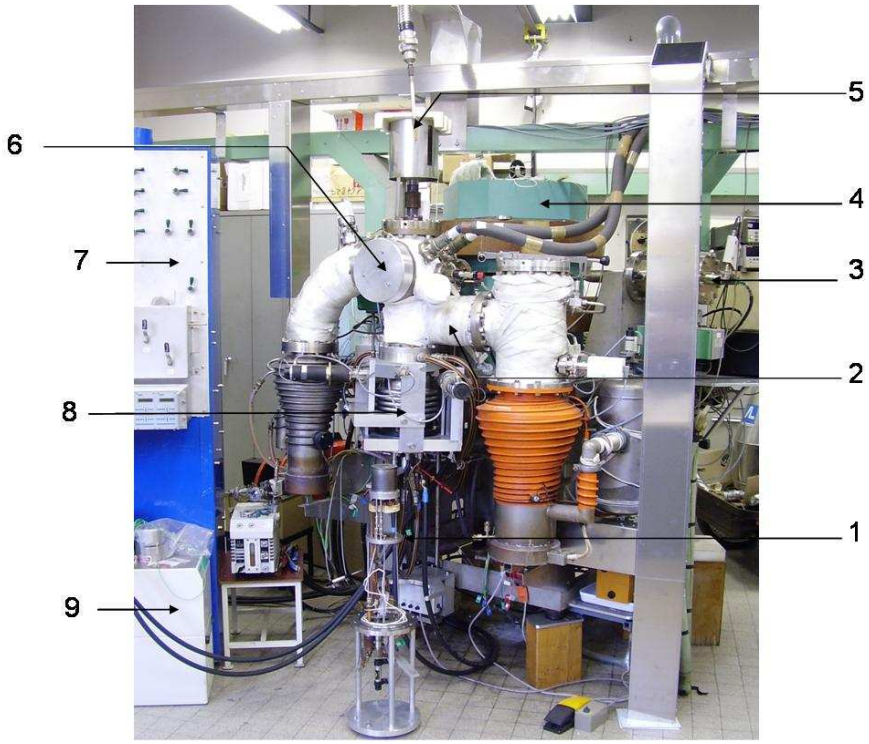

Figure I-5: Photographie du spectromètre de masse du SIMAP. 1: Réacteur à cellule d'effusion simple, 2: Enceinte four, 3: Détection des ions, 4: Champ magnétique, 5: N_2 liq., 6: Enceinte source des ions, 7: Armoire régulation gaz (Ar-H_2-H_2O), 8: Système électromécanique asservi de positionnement du réacteur, 9: Générateur d'iode.

La source d'ionisation est soudée à un piège froid en verre rempli d'azote liquide situé au-dessus de la chambre. Ceci permet d'éviter la ré-évaporation des composés issus du jet moléculaire utile qui se seraient condensés sur la partie haute de la source en cours

d'expérience. Le piège permet aussi un meilleur vide local (diminution très nette du spectre résiduel du vide source).

Deux filaments en tungstène chauffés par circulation d'un courant assurent une émission régulière d'électrons tout en les maintenant à un potentiel fixe – potentiel d'ionisation– compris entre -4 et -80 V par rapport à la chambre d'ionisation. Le système à 2 filaments est préféré au cas d'un filament simple car il permet une meilleure homogénéisation de la densité des électrons dans la chambre et un doublement du courant d'ions. Ces filaments sont responsables de l'échauffement des parois de la chambre d'ionisation qui sont à une température proche de 600 K dans une source d'ions non refroidie à l'azote liquide ce qui provoque des réactions secondaires des produits déposés en cours d'expérience. Dans notre cas il n'y a plus d'évaporation secondaire puisque nos produits sont piégés. De plus, les dépôts de molécules sur les parois de la chambre d'ionisation sont faibles (de 10 à 50 fois par rapport à un montage classique) car le jet moléculaire est issu d'un système de collimation dite «restreinte» [16]. Les avantages de ce dispositif sont plus particulièrement exposés dans le chapitre portant sur l'évaporation de CsOH(s,l), soit le chapitre II. L'absence de collisions entre le jet moléculaire (utilisé pour l'analyse) et une quelconque paroi garantie des propriétés de température et de pression des molécules étudiées représentatives de la cellule d'effusion.

La tension d'accélération des ions est obtenue par une alimentation FUG-0-6500V de stabilité inférieure à 10^{-4} commandée par une interface IEEE.

La source d'ions est aussi munie d'une fente fixe de focalisation des ions et d'une fente d'ouverture (réglage manuel) qui permet d'affiner les pics en vue d'une meilleure résolution en éliminant une partie des aberrations. L'intensité ionique est alors un peu plus faible.

- ***L'analyseur de masse***

L'analyse de masse est faite par un prisme magnétique de rayon 30,5 cm et d'angle $\theta = 90°$ (d'origine «Nuclide Corporation» - 1967). Le champ magnétique peut varier entre 0 et 1 T. Le bobinage a été modifié par la société Drusch pour fonctionner à basse tension et le champ magnétique est régulé par une alimentation Drusch/Bouhnik (0-60 V, 0-10 A) de stabilité 2.10^{-5}, munie d'une interface IEEE.

L'ensemble source et prisme magnétique assurent une transmission η constante des ions quelle que soit la masse mesurée. C'est une caractéristique avantageuse (par rapport aux quadrupoles) des prismes magnétiques lorsque les sources d'ions sont de types purement électrostatiques et correctement protégées des champs magnétiques.

La résolution du spectromètre, qui dépend des caractéristiques du prisme magnétique, est de manière générale définie par la plus grande masse pour laquelle un critère établi au préalable est respecté [17]. Pour notre spectromètre, nous avons retenu comme critère «la hauteur de vallée » qui exprime la résolution comme la plus grande masse à laquelle deux pics adjacents d'intensité équivalente, séparés par une unité de masse atomique, présente une hauteur de vallée entre les deux pics inférieure à un certain pourcentage de l'intensité du pic. Le pourcentage choisi est de 10% et ainsi ΔH/H doit être inférieure ou égale à 0.1 (Figure I-6). Ce critère permet de nous assurer que lors de la mesure de l'intensité d'un pic (qui est faite au sommet du pic), cette mesure n'est pas interférée par la présence du pied du pic adjacent. Dans notre cas, le spectromètre possède une résolution ≥ 600.

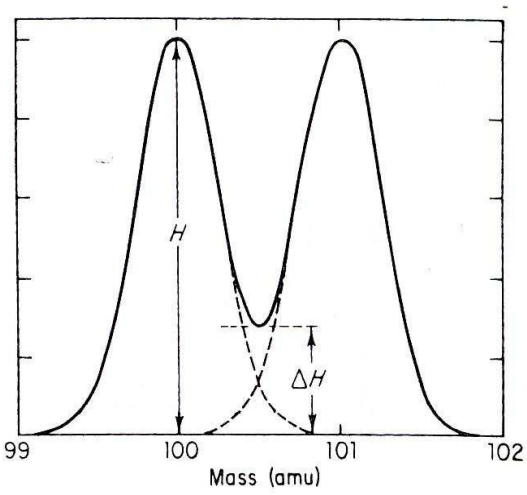

Figure I-6: Résolution entre deux pics adjacents d'intensité H et de hauteur de vallée ΔH.

- ***La détection***

La détection peut se faire selon deux modes:

- une cage Faraday équipée d'un électromètre KEITHLEY modèle 6517A permettant de détecter des courants d'ions > 10^{-15} A.

- un multiplicateur d'électrons ETP 1000 (dynodes Ag/Mg) de dimension réduite conçue pour le comptage d'impulsions (réduction des temps de transit et pulses de 2-3 ns).
  Le bruit de fond est inférieur à 1 coup.s^{-1} pour un gain de 10^7 à 10^8 électrons par ion incident. Un préamplificateur rapide ORTEC 9327 met en forme le signal. Nous disposons ensuite de deux chaînes de comptage d'impulsions:
    - LEAS[6]
    - Compteur Hewlett Packard modèle 53132 A

  Ces deux chaînes possèdent des réglages de seuil de tension d'entrée et de pente pour discriminer les pulses provenant du bruit de fond électronique de celles provenant des ions. Les pulses provenant du bruit de fond ont une amplitude en tension très faible (< 0,15 mV en sortie du préamplificateur) mais sont très nombreuses (10^8 s^{-1}) tandis que celles provenant des ions correspondent à des amplitudes de 0,8 à 1V. Entre ces deux séries, lorsque le multiplicateur est en bon état, il existe une bande sans aucune pulse. La séparation entre le bruit de fond et les ions par un seuil est donc parfaite.
  Malgré les trois blindages existant autour du multiplicateur d'électrons secondaires, depuis l'extérieur vers l'intérieur, fer ARMCO (pour absorber les champs magnétiques résiduels), cuivre OFHC (blindage contre les courants HF) et µ-métal (pour repousser les champs magnétiques de la zone interne où est situé le multiplicateur), des pulses parasites (0-1 coup.s^{-1}) provenant soit des rayons cosmiques soit d'interférences électriques par les alimentations, malgré un transformateur d'isolement, peuvent survenir. Les mesures à très bas niveau sont donc à analyser plus finement avant d'être retenues.

La télécommande des interfaces et l'acquisition des données se fait avec une station de travail HP Kayak XM 600 (Ets BOURBAKY, Tournon) sur laquelle est implanté un programme réalisé au SIMaP en langage HT Basic. L'esprit du programme n'est pas de réaliser des expériences entièrement automatisées mais de pouvoir s'adapter à chaque expérience. Par exemple, il n'est pas réalisé de balayage sur toute la gamme de masse pour obtenir en une seule fois tous les pics car la résolution serait faible et cela prendrait beaucoup de temps. Le programme est constitué de plusieurs commandes élémentaires telles que le réglage de la haute tension, du repousseur d'ions, du champ magnétique et de taches scientifiques comme un balayage sur un pic donné avec ou sans obturateur, l'obtention de courbes d'efficacité d'ionisation ou simplement de mesures d'intensité et de température. Ces commandes

[6] ZA La Bâtie, BP 38, 38332 St Ismier

élémentaires sont pilotées à la demande par l'expérimentateur au cours des expériences. Des modules supplémentaires sont régulièrement programmés en fonction du type d'expérience: cela a été le cas par exemple pour la conduite des tests et des mesures avec le réacteur CHIP.

I.2.5. Gamme de mesure spectrométrique

La gamme de mesure du spectromètre de masse à haute température est comprise entre 10^{-5} et 10^{-10} bar, ce qui représente respectivement les limites du régime moléculaire à l'orifice et le seuil de détection du spectromètre. Si l'on prend par exemple les spécifications de l'IRSN en terme de concentrations des gaz attendues dans le circuit primaire du réacteur en cas d'accident nucléaire:

Espèces gazeuses	Rapport de pressions partielles/1bar dans le réacteur (en cas d'accident) en bar	Pressions partielles attendues au spectromètre en bar
Cs/H_2O ou Cs/H_2	10^{-4} à 10^{-1}	10^{-8} à 10^{-5}
I/H_2O ou I/H_2	10^{-5} à 10^{-2}	10^{-9} à 10^{-6}
H_2/H_2O	10^{-1}	10^{-5}

Table I-1: comparaison entre la gamme de mesure spectrométrique et les rapports de pression attendus dans le circuit primaire du réacteur nucléaire en conditions accidentelles.

Les pressions totales représentatives de l'étude étant au delà de la limite des mesures du spectromètre, une détente de 10^4 est nécessaire. Les concentrations alors attendues au niveau du spectromètre de masse à haute température sont bien dans la gamme de mesure de l'appareil (entre 10^{-5} et 10^{-10} bar).

I.3. METHODE D'INTERPRETATION: 2IEME ET 3IEME LOI DE LA THERMODYNAMIQUE

Dans une configuration avec cellule d'effusion, la mesure spectrométrique conduit à l'obtention de pressions partielles, et donc à la détermination de la constante d'équilibre d'une

réaction (vaporisation, dissociation, équilibre gazeux) K_p directement liée à l'enthalpie standard de réaction $\Delta_r G°_T$ par la relation:

$$\Delta_r G°_T = -RT \ln K_p \qquad (10)$$

L'enthalpie libre standard $\Delta_r G^\circ$ est elle-même reliée à l'enthalpie $\Delta_r H^\circ$ et l'entropie $\Delta_r S^\circ$ de réaction,

$$\Delta_r G°_T = -RT \ln K_p = \Delta_r H°_T - T\Delta_r S°_T \qquad (11)$$

De manière générale, sur le plan de l'exploitation des résultats expérimentaux, deux voies sont possibles pour déterminer l'enthalpie d'une réaction:

1- L'application de la 2ième loi de la thermodynamique conduit à la relation de Van t'Hoff ou Clausius Clapeyron:

$$\frac{d(\ln K_p)}{d(1/T)} = \frac{-\Delta_r H°_T}{R} \qquad (12)$$

Cette relation est la dérivée de la relation générale :

$$\ln K_p = \frac{-\Delta_r G°_T}{RT} = \frac{-\Delta_r H°_T}{RT} - \frac{-\Delta_r S°_T}{R} \qquad (13)$$

Comme Kp peut être décomposée à partir de la relation spectrométrique P = IT / S en $K_p = K_{IT} \cdot K_S$, la relation (12) devient:

$$\frac{d(\ln K_p)}{d(1/T)} = \frac{d \ln K(IT)}{d(1/T)} = \frac{-\Delta_r H°_T}{R} \qquad (14)$$

à condition que la mesure spectrométrique soit menée de façon à ce que K_S reste bien constant (sensibilité constante à l'intérieur d'une même expérience). Le $\Delta_r H°_T$ à T moyen de l'expérience est ainsi directement déterminé. On obtient une seule valeur pour l'ensemble des données expérimentales.

2- La méthode dite de la 3ième loi (ou de l'entropie nulle à 0 K, un des postulats de la thermodynamique): si l'expérimentateur est à même de déterminer les sensibilités par une calibration adéquate, il est capable de connaître les pressions partielles et le $\Delta_r G°_T$ à chaque température car le Kp(T) est connu. En utilisant la relation (11) et connaissant par ailleurs l'entropie, et donc la fonction d'énergie libre Fel (Fef en anglais), il détermine $\Delta_r H°_T$ pour chaque mesure de température via la relation:

$$\Delta_r H°_T = -RT \ln K_p - T\Delta Fel°_T \qquad (15)$$

La fonction d'énergie libre Fel et définie par:

$$fel = \frac{G°(T) - H°(298.15\ K)}{T} \text{ (dans les tables la fonction tabulée souvent est –fel)} \qquad (16)$$

A partir de la relation G°(T) = H°(T) - TS°(T) on aboutit à:

$$S°(T) = -\frac{[G°(T) - H°(T)]}{T} = \frac{[H°(T) - H°(298.15K)]}{T} - \frac{[G°(T) - H°(298.15K)]}{T} \qquad (17)$$

Et donc : $fel(T) = -S°(T) + \frac{[H°(T) - H°(298.15\ K)]}{T}$ (18)

En utilisant la relation (11) on obtient pour une réaction:

$$\frac{\Delta_r G^0(T)}{T} = \Delta_r\ fel(T) + \frac{\Delta_r H^0(298.15K)}{T} = -R \ln K_p(T) \qquad (19)$$

D'où l'expression de la 3ième loi:

$$\Delta_r H°_{(298,15K)} = -RT \ln K_p(T) - T\Delta_r\ fel°_T \qquad (20)$$

Avec: Δ_rFel = Fel (produits) – Fel (réactifs). (21)

La fonction d'énergie libre Fel est tabulée pour les espèces gazeuses comme CsOH(g), $Cs_2O_2H_2$(g) etc… dans différentes compilations, Gurvich et al. [18], JANAF [19] ou bien doit être évaluée indépendamment. L'exploitation des résultats par la troisième loi demande alors un travail plus important qui fait appel à des modèles d'estimation des fonctions thermodynamiques. Cela requiert pour le spectrométriste une culture scientifique plus vaste. En contre partie, l'exploitation par la troisième loi est en général plus fiable [13].

I.4. PROPRIETES THERMODYNAMIQUES DU SYSTEME CS-I-O-H

Le diagramme de phase du système Cs-I-O-H est présenté sur la figure I-7 qui rassemble l'ensemble des composés solides, liquides ou gazeux binaires soit connus, soit répertoriés dans les tables thermodynamiques. La section pseudobinaire CsI-CsOH est la section de basses pressions car ce sont ces composés qui possèdent les pressions de vapeur les plus faibles.

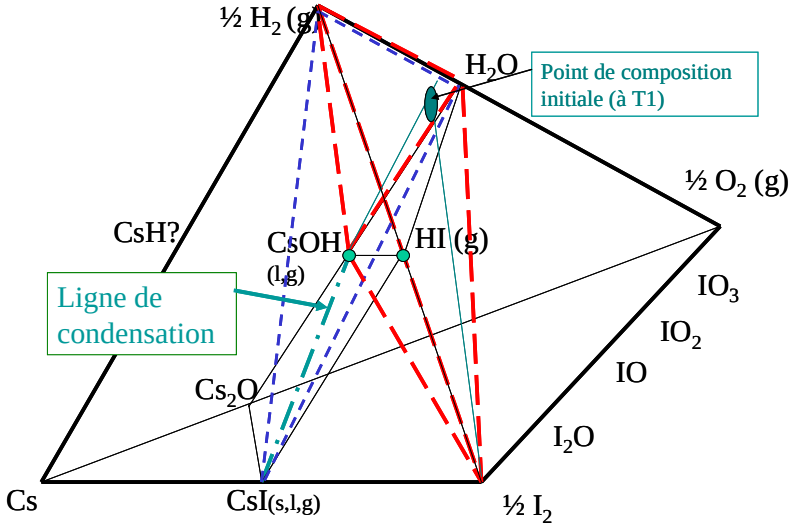

Figure I-7: Esquisse du diagramme de phase du système quaternaire Cs-I-O-H

Les molécules les plus stables sont alors: CsOH, $(CsOH)_2$, CsI, Cs_2I_2, Cs_3I_3 et Cs_4I_4. Ces molécules gazeuses ont été étudiées par spectrométrie de masse. De plus, Blackburn et Johnson [11] ont mis en évidence la présence d'une nouvelle molécule mixte $Cs_2IOH(g)$ qui selon eux pourrait être très stable. Le transport de l'iode pourrait alors être influencé par cette nouvelle molécule. En effet, Blackburn et Johnson ont d'une part:

- identifié la molécule complexe CsOHCsI (Cs_2IOH).
- estimé le coefficient d'interaction de la solution liquide CsOH-CsI.

Ce sont ces «réalités» chimiques qui nous ont permis de penser que l'introduction d'iode pourrait précipiter des composés à base de Cs au niveau de la cellule de recombinaison (analogue de la brèche en branche chaude). C'est pourquoi les données de base de ces produits ont été ré-analysées et au besoin des déterminations plus fiables réalisées et dans un contexte renouvelé.

I.4.1. Données thermodynamiques sur le système Cs-O-H

La réaction entre le Cs et H_2O en conditions accidentelles donne CsOH(s, l ou g) qui est alors un des principaux composés du circuit primaire. Pour cette raison et compte-tenu des concentrations de gaz injectés dans le réacteur «thermocinétique CHIP», les rapports Cs/H_2O à examiner permettent d'envisager d'injecter le Cs sous forme de CsOH (transporté par l'Ar).

Cependant, dans la littérature, les propriétés thermodynamiques associées à $CsOH/H_2O$ ne sont pas toujours en accord en termes de composition de la phase gazeuse, de pressions de vapeur, de fraction exacte du dimère et d'enthalpie de dissociation de la réaction $Cs_2O_2H_2(g) \leftrightarrow 2\ CsOH(g)$. La vaporisation du CsOH(s,l) par SMHT (chap. II) a été entreprise afin de caractériser la phase vapeur et d'obtenir des données thermodynamiques plus justes que celles proposées jusqu'à présent dans la banque SGTE [20] (basée sur les données de Gurvich et al. [18]) utilisée dans les outils de simulation numérique des accidents graves. Les efforts entrepris ont porté sur:

- La préparation de CsOH(s,l) pur à partir du produit commercial monohydraté en se basant sur les travaux de Rollet et al. [21]. L'élimination de l'eau peut se faire à partir d'un dégazage préliminaire sous vide primaire. L'échantillon commercial de $CsOH\text{-}H_2O$ mis dans sa cellule (creuset+couvercle) est dégazé sous vide pendant 16 à 20 heures à 443 K (fig. I-8), ensuite l'ensemble a été chauffé lentement jusqu'à 623 K pendant environ 2 heures ce qui conduit à la fusion du produit. L'ouverture de la cellule se fait en présence d'azote. Il est possible de casser le vide avec de l'argon ou avec de l'air sec, l'eau étant l'élément qui réagit le plus avec le CsOH. Cette procédure est analogue à celle appliquée par Konings et Cordfunke [22]. Le stockage du creuset ainsi préparé se fait dans un dessiccateur lorsqu'il n'est pas utilisé instantanément. Différentes pesées ont montré que dans ces conditions le produit présentait une reprise d'eau négligeable.

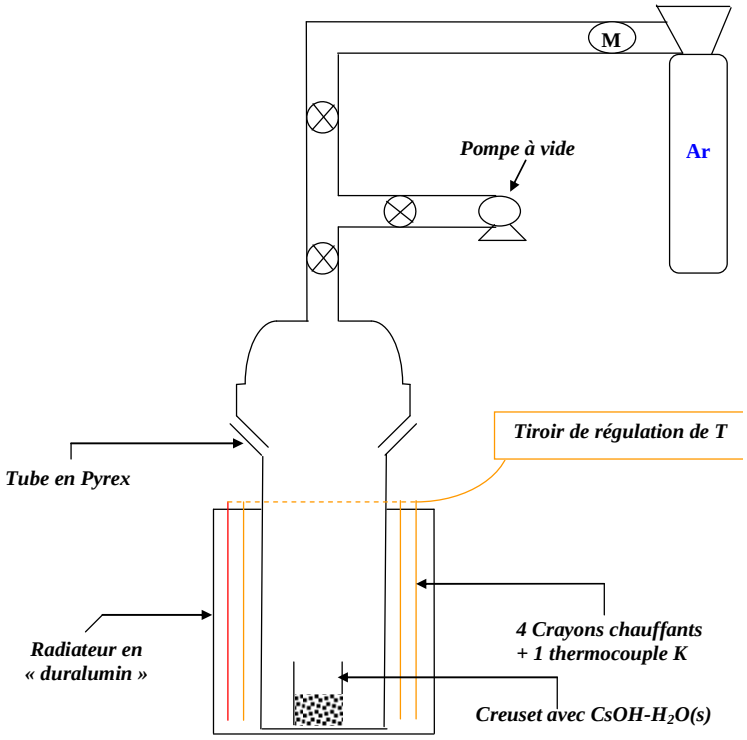

Figure I-8: Schéma du principe de distillation par vaporisation du CsOH-H_2O

- Le choix du matériau à utiliser pour le conteneur recevant CsOH dans le réacteur thermocinétique qui doit répondre à certaines conditions : résistance à la corrosion, absence de réaction avec CsOH et mouillabilité limitée. Des effets parasites ont été observés, comme le débordement du CsOH et la diffusion de surface: la préparation sous vide des échantillons de CsOH a permis de tester le comportement de creusets en MgO dense, Ni, Pt-Rh et Au. Lors de ces préparations, des débordements par le couvercle du creuset ont fréquemment été observés. Dans ces cas, le couvercle est plus au moins scellé par le produit qui n'a pas été attribué précisément au produit hydraté ou au produit final (CsOH anhydre). Contrairement à la MgO dense, le creuset en Pt-Rh semble le mieux adapté pour ce type d'étude. Les expériences spectrométriques faites avec ces creusets ont montré un débordement continu du produit par l'orifice d'effusion -observation d'auréoles plus au moins denses sur la surface extérieure - et dans certains cas, le collage de l'enveloppe extérieure sur la cellule et même du produit qui se répand jusqu'au thermocouple situé sous la cellule.
- La détermination d'un palier de fusion à $T_f = 649 \pm 2$ K plus élevé que celui proposé dans la littérature $T_f = 623$ K. Nous avons observée l'évaporation d'eau résiduelle par spectrométrie de masse en début d'expérience, celle-ci disparaissant ensuite par

distillation due à l'effusion. En effet, la température de fusion proposée par Rollet et al. [21] pourrait ne pas correspondre à un composé pur du à la présence d'eau résiduelle dans leur échantillon lors des analyses par ATD (Analyse Thermique Différentielle): ceci explique la différence par rapport à nos mesures (fig. I-9)

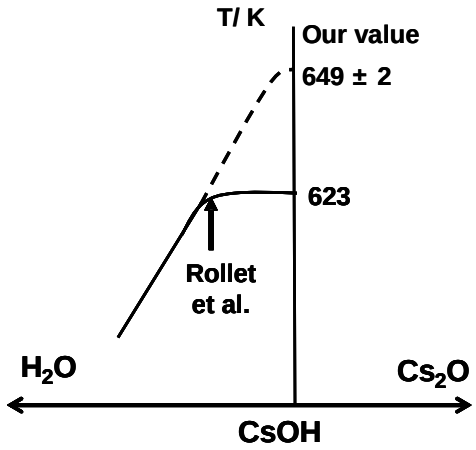

Figure I-9: Diagramme de phase solide-liquide CsOH-Cs_2O (côté CsOH(s,l) proposé par Rollet et al) [21] avec une forme aplatie anormale qui serait due à la présence d'eau résiduelle non analysée.

- La détermination de la composition de la phase gazeuse: CsOH(g), $Cs_2O_2H_2$(g), $Cs_3O_3H_3$(g) (< 6 10^{-4} CsOH(g)) et quelques traces d'eau H_2O (< 100ppm) au début de chaque expérience. La molécule trimère a été mise en évidence pour la première fois lors de ce travail. Les enthalpies de formation du monomère et du dimère ont été déterminées via la 2^{ième} et la 3^{ième} lois de la thermodynamique.
- L'analyse critique des données de la littérature en vue de proposer des valeurs améliorées. Les données issues de ce travail conduisent à des pressions 30% en dessous de celles proposées par Gurvich et al. [18] . Le transport de Cs s'en trouvera réduit.

I.4.2. Données thermodynamiques sur le système Cs-I

Jusqu'à présent, dans les conditions d'un accident grave, il est admis au vu des calculs thermodynamiques que l'iode est transportée majoritairement sous forme de CsI et de son dimère. Le CsI a été étudié en phase solide, liquide et gazeuse. Cependant, pour la phase gaz, entre 900 à 1500 K (température de la brèche en branche chaude), les données de la littérature

sont très dispersées. L'analyse thermodynamique et critique de ce système a été faîte (chap. III) et a montré que:

- Les données thermodynamiques de la phase solide sont cohérentes.
- A température élevée, la fraction du dimère est largement supérieure à celle proposée par Glushko et al. [23] (données actuellement répertoriées dans la base SGTE utilisée pour la simulation de l'accident grave).
- Les pressions totales données lors des études plus récentes montrent systématiquement des pressions plus élevées par rapport à Glushko et al. en phase liquide.

L'analyse critique des données de la littérature relative à CsI en incluant les diverses études publiées depuis la compilation de Glushko et al a permis la sélection d'une nouvelle enthalpie de dimérisation pour le $Cs_2I_2(g)$, donc des enthalpies de formation du monomère et du dimère, ainsi qu'une correction de l'enthalpie de fusion de CsI(s) et de la chaleur spécifique de CsI(l). Les pressions de vapeurs recalculées sur le CsI pur sont de 15 à 20% plus élevées par rapport à celles fournies par Glushko et al. [23]. Le transport de l'iode par les différentes formes du CsI sera donc plus conséquent.

I.4.3. Thermodynamique du système CsI-CsOH

Le mélange CsI-CsOH a été étudié par Blackburn et Johnson [11] à l'aide d'un spectromètre de masse quadrupolaire. Les auteurs ont mesuré des quantités d'ions dimères Cs_2I^+ et Cs_2OH^+ supérieures à celles obtenues lors de la vaporisation des composées purs CsI(g) et CsOH(g). Ils ont attribué cette augmentation à la présence d'une nouvelle molécule mixte $Cs_2IOH(g)$ qui donnerait essentiellement Cs_2OH^+ selon le processus d'ionisation suivant:

$$Cs_2IOH(g) + e^- \rightarrow Cs_2OH^+(g) + I(g) + 2\,e^- \qquad (22)$$

Tout comme pour les dimères des composés purs, il n'y a pas de phénomènes d'ionisation adiabatique conduisant à l'ion parent Cs_2IOH^+, phénomène typique des molécules à caractère ionique [24]: ceci est due aux valeurs relatives des potentiels d'ionisation de Cs, de l'affinité électronique de l'halogène et des énergies des différentes liaisons dans la molécule. L'existence de la molécule mixte va probablement jouer un rôle qui s'ajoute à celui du CsI et de son dimère, dans le transport de l'iode en conditions accidentelles.

Compte-tenu des superpositions entre les mêmes ions venant de différentes origines, nous avons préparé des échantillons de compositions différentes pour produire en phase gazeuse des proportions de molécules différentes puisque les pressions de vapeur dépendent de l'activité en phase condensée. Ce choix était d'ailleurs suggéré par Blackburn et Johnson [11]. Deux mélanges CsI-CsOH ont été préparés, un riche en CsOH (fraction molaire CsOH: 0.77-0.79) et un riche en CsI (fraction molaire en CsI: 0.83-0.86). Ces mélanges ont été vaporisés au SMHT dans la gamme de température 650-860 K (chap. IV), gamme légèrement plus faible que celle utilisée par Blackburn et Johnson due à une meilleure sensibilité de notre spectromètre de masse. Ce fait présente aussi l'avantage d'une meilleure analyse des vapeurs car l'évolution de la composition du liquide (et partant du gaz) avec le processus d'effusion est plus restreint.

Les résultats obtenus ont montré une augmentation anormale des quantités des ions dimères Cs_2I^+ et Cs_2OH^+ par rapport aux corps purs. Ceci confirme la présence de $Cs_2IOH(g)$ comme suggéré par Blackburn et Johnson. Cependant, l'analyse des rapports d'intensité pour différentes compositions du mélange CsOH-CsI par rapports aux corps purs a montré que l'ionisation de la molécule mixte est dissociative non pas selon le seul processus évoqué par Blackburn et Johnson mais selon cinq processus donnant lieu aux ions fragments: Cs_2OH^+, Cs_2I^+, Cs^+, $CsOH^+$ et CsI^+. Pour une seule composition de mélange, les deux premiers ions ne peuvent pas être détectés ensemble à cause de la superposition des ions avec ceux issus de l'ionisation des dimères $Cs_2O_2H_2(g)$ et $Cs_2I_2(g)$. L'ion Cs^+ est toujours présent alors que les ions $CsOH^+$ et CsI^+ s'ajoutent aux ions issus des monomères parents. La présence d'ions fragments CsI+ et CsOH+ – non mise en évidence par Blackburn et Johnson – a été rendue possible grâce à la compilation critique des données de vaporisation de ces corps purs – notamment les constantes de dimèrisation – mais aussi par les expériences que nous avons réalisées sur CsOH(s,l). Pour CsI(s), des expériences préliminaires de vaporisation ont permis de fixer les rapports d'ions sur le corps pur.

Après analyse par étape des différentes contributions d'ions, les pressions de vapeur relatives à la molécule $Cs_2IOH(g)$ ont été établies et la constante d'équilibre Kp de la réaction:

$$CsI(g) + CsOH(g) = Cs_2IOH(g) \quad (23)$$

$$K_p(T) = \frac{p(Cs_2IOH)}{p(CsI) \cdot p(CsOH)} \quad (24)$$

a été calculée et comparée à celle proposée par Blackburn et Johnson [11] (fig. I-10).

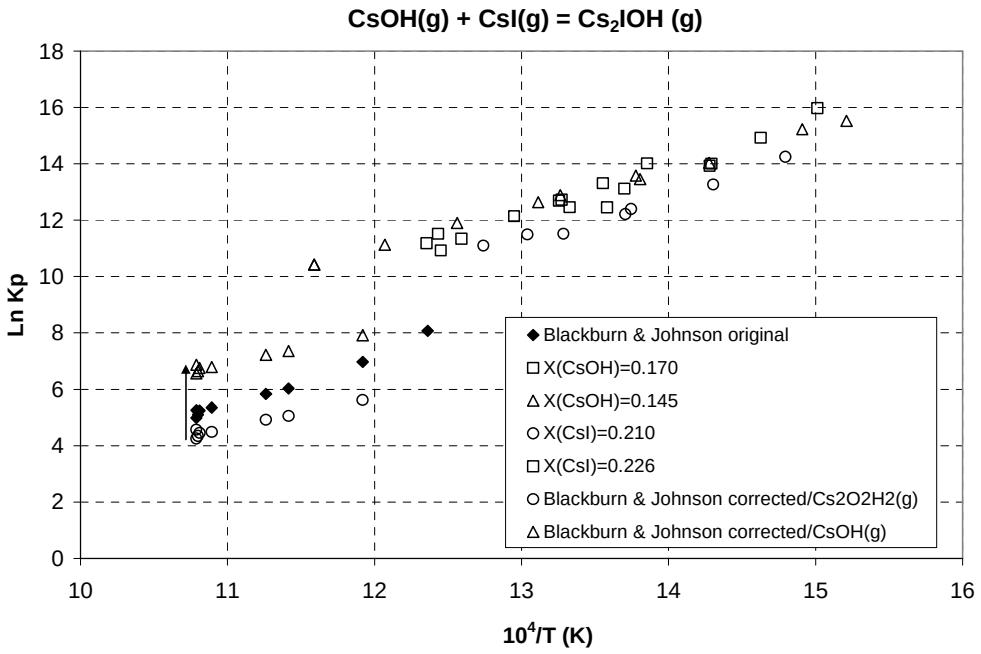

Figure I-10: Comparaison entre les données de Blackburn et Johnson (originales et corrigées) et nos mesures expérimentales pour la réaction CsOH(g) + CsI(g) = $Cs_2IOH(g)$ avec prise en compte de la totalité des ions provenant de la molécule mixte: $Cs_2OH^+ + Cs_2I^+ + Cs^+ + CsI^+ + CsOH^+$ (cf. chapitre IV).

Les corrections appliquées aux données de Blackburn et Johnson sont dues au fait que les auteurs ont sous-estimé les pressions du dimère $Cs_2O_2H_2(g)$ ($1^{ière}$ correction) et par conséquent surévalué les pressions de CsOH ($2^{ième}$ correction) comme cela a été montré lors de l'étude de la vaporisation de CsOH et dans la compilation critique des données (Chap. II). Les pressions mesurées dans ce travail sont plus élevées d'un facteur 13 par rapport à celles de Blackburn et Johnson. Ceci s'explique par la prise en compte du processus d'ionisation complet de la molécule mixte contrairement à l'étude précédente.

Les propriétés thermodynamiques de Cs_2IOH (g) (S°_T, Fel_T, C°_p) ont été évaluées de la façon suivante:

- Tout d'abord par estimation de la géométrie de la molécule mixte par analogie aux deux dimères purs $Cs_2I_2(g)$ et $Cs_2O_2H_2(g)$ et sur la base du modèle ionique de Pauling [25, 26] appliqué aux molécules appartenant à la famille des halogénures alcalins comme NaCl et

leurs dimères. Ce modèle permet l'optimisation de la géométrie (distances inter atomiques) par calcul de l'énergie de liaison minimale et donc de l'état le plus stable de la molécule.

- Calculs des fonctions d'énergies libres de la molécule mixte à l'aide des méthodes statistiques exposées dans les tables JANAF (1998) [19] et Gurvich et al. [27] en utilisant la formulation correspondante au «vibrateur oscillateur harmonique rigide, pour les molécules polyatomiques non linéaires». Ces méthodes prennent en compte dans le calcul de l'entropie les quatre contributions suivantes: translation et rotation, vibration, électronique et les corrections anharmoniques.
  - Translation et rotation: cette contribution sur l'entropie peut être calculée à l'aide de l'équation proposée par Margrave (1967) [28] suivante:

$$S^{\circ}_T = 6.8634\log M + 18.3025\log T - 4.5756\log\sigma + 2.2878\log(I_A I_B I_C)\cdot 10^{117} - 2.3493$$

(en cal.mole^{-1}.K^{-1}) (25)

où M est la masse molaire, $I_A I_B I_C$ le produit des trois moments d'inertie principaux de la molécule, T la température et σ le nombre de symétrie. Le nombre de symétrie est obtenu après détermination du nombre de configurations non distinctes dans laquelle la molécule peut tourner par simple rotation rigide ou à partir du groupe de symétrie de la molécule [28]. Les moments d'inertie sont définis par les longueurs de liaison et les angles. Ils peuvent être soit évalués par spectroscopie, soit calculés selon la méthode de Hirschfelder [29] dans le cas des molécules compliquées -comme pour la molécule mixte- pour lesquelles la détermination de directions des axes principaux n'est pas simple.

  - Vibration: la contribution vibrationnelle à l'entropie est évaluée par la relation suivante: $S^{\circ}_T = 1.9873\mu\, e^{-\mu}/(1-e^{-\mu}) - 4.5756\log(1-e^{-\mu})$ $cal.mole^{-1}.K^{-1}$ (26)
    avec $\mu = (1.4388/T)\omega$ où ω est la fréquence fondamentale d'un oscillateur harmonique en nombre d'onde.
  - Electronique: la contribution électronique à l'entropie s'évalue à partir des niveaux électroniques ε_i et de leur poids statistique g_i à l'aide de la relation suivante,

$$S^{\circ}_T = \frac{2.8591}{T}\frac{\sum \varepsilon_i g_i e^{-1.4388\varepsilon_i/T}}{\sum g_i e^{-1.4388\varepsilon_i/T}} + 4.5756\log\sum g_i e^{-1.4388\varepsilon_i/T} \quad cal.mole^{-1}K^{-1} \qquad (27)$$

En règle générale, et en l'absence d'informations adéquates, seul l'état fondamental est considéré, soit $\varepsilon_i = 0$ (pas de contribution significative des niveaux excités des molécules polyatomiques) [28]. Le poids statistique $g_0 = 1$ dans le cas où le composé est à valence saturée et donc il n'y a pas de contribution électronique. Si la molécule possède un seul électron célibataire, g = 2S+1 avec S = n/2 (n le nombre d'électrons manquants).

- Corrections anharmoniques: celles-ci sont négligées dans le cas des molécules polyatomiques non linéaires car elles sont difficilement évaluables.

L'entropie finale est obtenue après prise en compte des différentes contributions et les fonctions d'énergie libre sont déduites par la suite à partir de l'équation (18).

- Après évaluation des fonctions d'énergie libre de la molécule mixte, la 2^{ième} et la 3^{ième} lois de la thermodynamique ont été utilisées pour calculer l'enthalpie de la réaction pour chaque expérience: CsI(g) + CsOH(g) = $Cs_2IOH(g)$
  L'enthalpie moyenne de réaction est égale à: $\Delta_r H^\circ_{298.15} = -172 \pm 12$ kJ.mole^{-1}
  En utilisant notre sélection d'enthalpies de formation des corps purs CsI(g) et CsOH(g), l'enthalpie de formation de $Cs_2IOH(g)$ a été calculée : $\Delta_f H^\circ_{298.15} = -577.97 \pm 13$ kJ.mole^{-1}.

En conclusion, le présent travail sur cette molécule permet d'enrichir les bases de données thermodynamiques qui permettent le calcul du transport de l'iode dans le cas d'accidents graves. La stabilité de cette molécule relativement aux vapeurs des corps purs permet d'affirmer qu'elle participe effectivement de façon notable au transport de l'iode sauf à envisager une barrière cinétique conséquente.

I.5. ETUDE CINETIQUE: REACTEUR THERMOCINETIQUE CHIP

Dans le cas d'un accident grave et pour une certaine catégorie de scenarii, le temps de séjour des gaz et vapeurs entre le cœur du réacteur et la brèche en branche chaude du circuit primaire est de l'ordre de 1 à 10 s. Les composés présents dans la phase gazeuse au départ ont probablement une forme dissociée, c'est-à-dire majoritairement atomique, ou diatomique simple ou même radicale. Pour une phase vapeur homogène les principales réactions de

recombinaison qui peuvent avoir lieu lors de la détente et du refroidissement sont par exemple du type:

$$Cs(g) + I(g) \rightarrow CsI(g) \quad (28)$$

$$Cs(g) + OH(g) \rightarrow CsOH(g) \quad (29)$$

$$Cs(g) + H_2O(g) \rightarrow CsOH(g)+H(g) \quad \text{etc....} \quad (30)$$

Ce type de schéma réactionnel a été examiné par Cantrel et Krausmann [7] afin de comprendre l'excès de production d'iode au niveau de la brèche par rapport à un simple calcul thermodynamique. Il en ressort qu'il est important d'analyser les réactions qui peuvent présenter une limitation cinétique. Ainsi, le réacteur thermocinétique CHIP a été conçu non seulement afin de donner un diagnostic des espèces présentes à la branche chaude, mais aussi afin d'évaluer les constantes cinétiques à l'aide d'un couplage avec le SMHT (chap. V).

I.5.1. Conception du réacteur

Compte tenu des très faibles valeurs de flux de gaz ou de vapeur à introduire dans le «réacteur thermocinétique» (flux effusif au spectromètre de masse) un calcul selon la formule de l'écoulement laminaire (loi de Hagen-Poiseuille ou formule de Newton) [30] montre que des buses de quelques microns doivent être utilisées ou bien des capillaires très longs. Cependant, en présence de vapeurs condensables (CsOH par exemple) seules des buses maintenues à haute température sont utilisables à cause des pressions d'introduction et du régime d'écoulement (figure I-11). Les difficultés principales sont alors – (i) le passage de pressions relativement élevées (quelques mbar à 1 bar) au niveau des lignes d'introduction à des pressions faibles correspondant à l'écoulement effusif ($< 10^{-4}$ bar) qui impose une bonne tenue mécanique à chaud, - (ii) la corrosion ou la tenue chimique des matériaux des buses par rapports aux produits introduits.

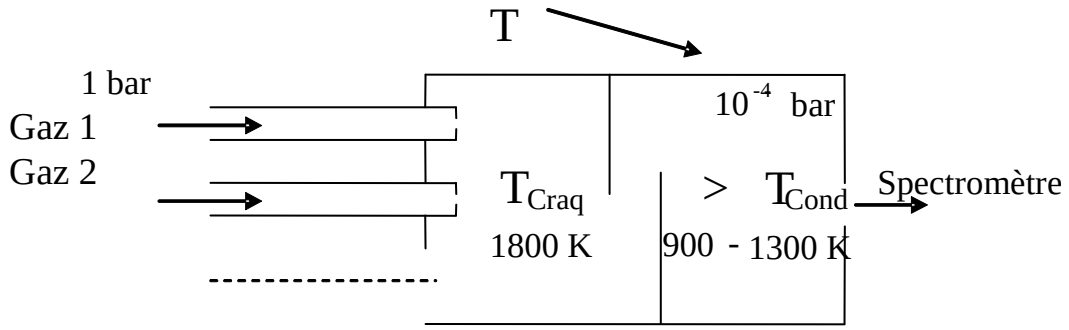

Figure I-11: réacteur idéal pour le diagnostic cinétique

Une étude bibliographique n'a pas permis d'identifier le matériau adéquat qui assurerait toutes ces exigences au niveau même de la cellule de craquage qui doit être portée pour l'étude aux environs de 1900 à 2000 K. Une solution moins contraignante a été envisagée: elle consiste à abaisser le niveau de température des buses d'injection afin de résoudre à la fois les problèmes de tenue mécanique et d'étanchéité sous vide et de diminuer les niveaux de corrosion (figure I-12), tout en espérant que des condensats ne viendront pas se produire dans les lignes entre buse et craqueur (une certaine dilution sera nécessaire).

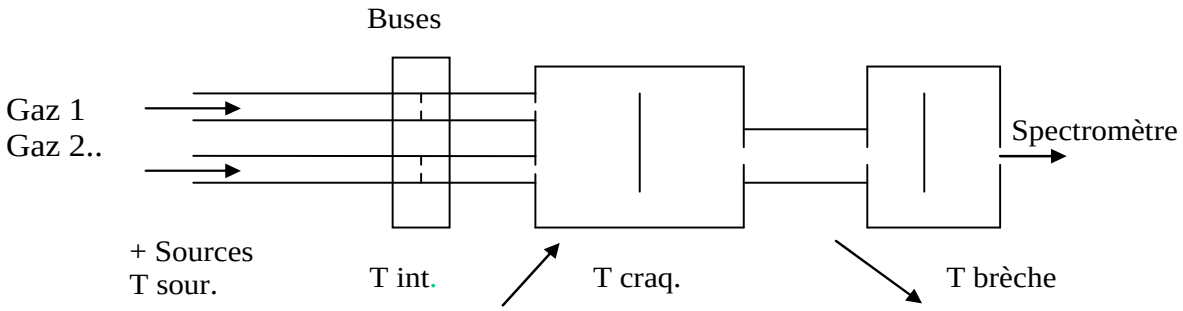

Figure I-12: réacteur possible à réaliser

C'est sur ce principe que le réacteur thermocinétique CHIP a été conçu en collaboration avec le LR2E[7] pour étudier le système Cs-I-O-H. Le dispositif expérimental complet peut être divisé en 4 éléments principaux:

- un générateur d'iode moléculaire gazeux et un générateur d'hydrogène/vapeur d'eau (disposant d'une armoire gaz sécurisée), tous deux situés à l'extérieur du réacteur ;

[7] Laboratoire de Réalisation des Equipements Expérimentaux, de la DPAM/IRSN

- trois lignes d'injections avec gaz porteur Ar dont une ligne avec iode, l'autre avec la vapeur d'eau et/ou l'hydrogène ;
- un réacteur thermocinétique situé entièrement sous vide accueillant en partie basse les trois lignes d'injections ;
- une colonne de fours instrumentés assurant le chauffage indépendant de chacun des 4 étages du réacteur;
- et un spectromètre de masse de type magnétique pour l'analyse de la phase gazeuse du effusant du dernier étage du réacteur (spectromètre du SIMaP).

I.5.2. Descriptif du réacteur thermocinétique

Le réacteur thermocinétique consiste en trois amenées indépendantes de gaz, à savoir: mélange Ar/I_2, mélange Ar/CsOH (CsOH source de Cs) et mélange $Ar/H_2/H_2O$ (fig. I-13). Ces trois arrivées passent par des buses (étage 2) et débouchent ensuite dans une zone de mélange et de décomposition des espèces qui est nommé « craqueur » (étage 3) qui est maintenue à haute température (1900 K) pour représenter les vapeurs issues du cœur du réacteur nucléaire en conditions accidentelles. Ce craqueur communique via un tube avec une zone de recombinaison dite « condenseur » (étage 4) simulant certaines conditions de la brèche en branche chaude (1000-1500 K). Les réactions de recombinaison au niveau de cette cellule seront déduites d'une analyse par spectrométrie de masse des composés formés qui transitent via un orifice d'effusion.

Le CsOH est préalablement introduit dans l'étage 1 «évaporateur CsOH» du réacteur thermocinétique où la température sera inférieure à 1000 K. Il sera entraîné par l'argon. Compte tenu des températures de vaporisation de l'iode (< 120°C), le générateur d'iode est disposé dans un bain thermostatique (dispositif HETO^{TM} du SIMaP) extérieur à l'enceinte à vide du spectromètre. L'iode est entraîné par un courant d'argon, le mélange I_2+Ar est régulé en pression au sein du générateur iode (à l'aide d'un manomètre à capacitance chauffé Baratron type 631A MKS$^{®}$) et transporté par un tuyau thermostaté jusqu'à l'entrée du réacteur. Pour le générateur vapeur d'eau/hydrogène, le montage retenu est celui Contrôleur d'Evaporation et de Mélange CEM «Bronkhorst^{TM}» sous vide. Nous n'utiliserons que des lignes d'introduction régulées en pressions amonts (pressiostats et non débitmètres) (voir

annexe I-A). Pour le mélange $H_2/H_20/Ar$, la concentration de chaque gaz est contrôlée à partir de la température et des débits d'introduction des gaz et le résultat du mélange est ensuite pressurisé à l'entrée de la ligne.

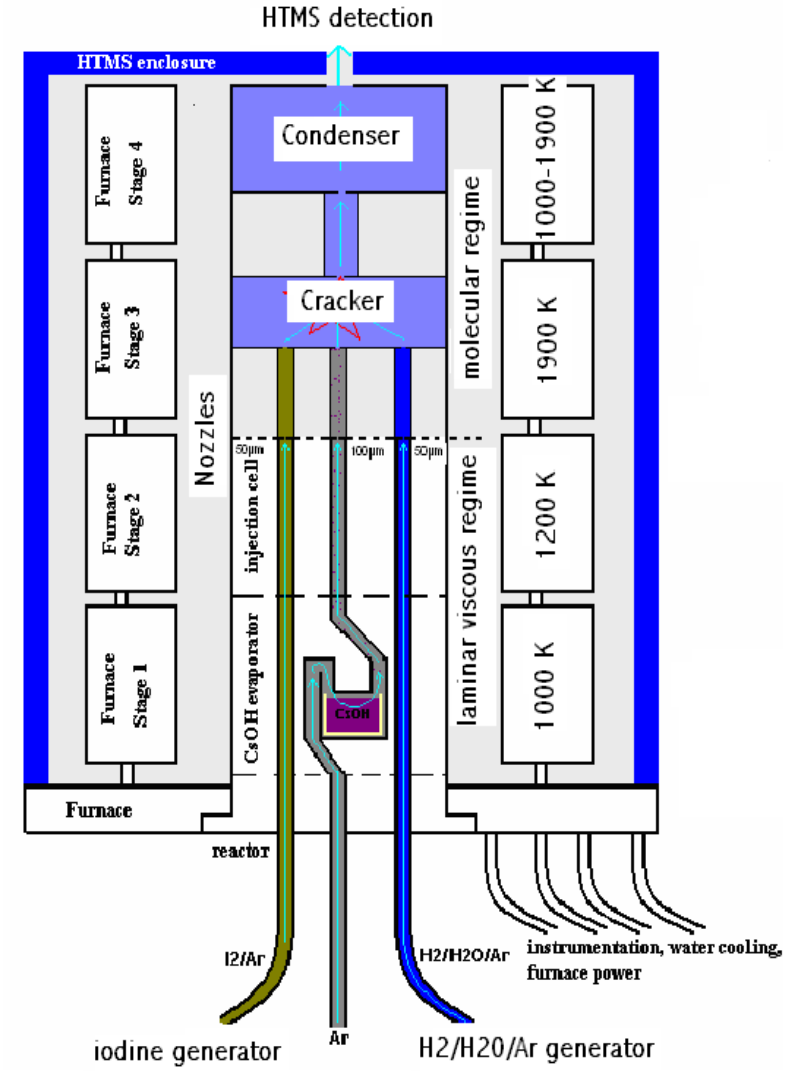

Figure I-13: Schéma des gaz et vapeurs dans le réacteur thermocinétique CHIP

I.5.3. Régime d'écoulement

Un flux de gaz en écoulement dans une canalisation peut être caractérisé en relation avec trois régimes d'écoulement:

- le régime moléculaire
- le régime de transition

- le régime visqueux

Le nombre de Knudsen Kn permet de déterminer dans quel régime d'écoulement se trouve une canalisation. Il se calcule par:

$$Kn = \frac{d}{\lambda} \tag{31}$$

où d est le diamètre de la canalisation et λ est le libre parcours moyen des molécules dans le gaz à cet endroit. λ est défini par la relation:

$$\lambda = \frac{kT}{p \cdot \sqrt{2} \cdot \sigma} \tag{32}$$

Où k est la constante de Boltzmann (k = 1,38066.10^{-23} J/K), T est la température (en Kelvin), p est la pression (en Pascal) et σ est la section efficace de l'espèce gazeuse considérée (en m^2).

Les différents régimes d'écoulements sont définis à partir du nombre de Knudsen comme suit:

- si K ≤ 3, l'écoulement est moléculaire, c'est à dire qu'il n'y a que des collisions avec les parois,
- si 3 ≤ K ≤ 80, le régime est dit transitoire (entre moléculaire et visqueux),
- si K ≥ 80, l'écoulement est visqueux. L'écoulement visqueux peut être de deux types: laminaire ou turbulent. La distinction entre ces deux types se fait grâce au nombre de Reynolds qui se calcule pour la canalisation par:

$$\mathrm{Re} = 0{,}153 \cdot \frac{M}{\eta \cdot T} \cdot \frac{Q}{d} \tag{33}$$

où M est la masse molaire du gaz considéré, η sa viscosité à la pression et température considérée, T la température, Q le flux volumique dans la canalisation et d le diamètre de la canalisation, tous ces paramètres étant exprimés en unités S.I. On distingue deux cas:

- si Re > 2200, l'écoulement est sûrement turbulent,
- si Re < 1200, l'écoulement est sûrement laminaire.

L'ensemble de ces concepts a été utilisé dans une étude préliminaire par L. Michelutti [10] pour concevoir et dimensionner l'écoulement dans le réacteur. Ainsi, les lignes d'introduction doivent être en régime laminaire afin d'éviter tout retour de gaz. Les buses doivent fonctionner en régime laminaire choqué [31] afin de passer directement en régime moléculaire. Le reste du réacteur doit être en régime d'écoulement moléculaire [15] condition essentielle pour la détection spectrométrique. La validation de ces régimes a été faite en

calculant les libres parcours moyens λ et le nombre de Knudsen pour le régime moléculaire. Les dimensions des cellules et orifices pour une configuration du réacteur (fonctionnement en mode thermodynamique) sont présentées sur le tableau I-2

		Diamètre/mm	Longueur/mm
Buses	Ar/I_2	0.05	0.5 dont chanfrein de 0.2 mm
	$Ar/H_2/H_2O$	0.05	0.5 dont chanfrein de 0.2 mm
	Ar/CsOH	0.1	0.5 dont chanfrein de 0.05 mm
Tube de connexion buse-craqueur		8.9	72
Craqueur	cellule	38	≈ 20 (espace utile)
	Orifice d'entrée gaz	0.3	4
	Orifice de sortie gaz	4	4
Tube de transfert craqueur-condenseur		12	72.5
condenseur	cellule	38	≈ 20 (espace utile)
	orifice d'entrée gaz	4	4
	Orifice d'effusion	2	2

Tableau I-2: Dimensions des cellules et des orifices de la configuration actuelle du réacteur CHIP. Les dimensions des orifices d'entrée et sortie craqueur ainsi que l'orifice d'entrée condenseur peuvent être modifiées selon le mode de fonctionnement du réacteur: mode thermodynamique ou mode cinétique.

Afin de respecter le fonctionnement du réacteur en terme de régime d'écoulement au niveau des buses, celles-ci doivent avoir un diamètre très petit (50 µm de diamètre et 500 µm de long pour les buses d'introduction Ar/I_2 et $Ar/H_2/H_2O$ et 100 µm par 500 µm pour la ligne Ar/CsOH). La pression à ce niveau étant forte vis-à-vis de l'enceinte à vide du spectromètre de masse, il faut des lignes soudées étanches. Le matériau choisi est le Nickel pour la partie basse du réacteur dont la température n'excède pas 1200 K (jusqu'aux buses incluses). Le reste du réacteur travaillant à haute température (1900-1000 K) fonctionne en régime moléculaire ce qui évite des problèmes majeurs d'étanchéité d'une part et facilite le choix du matériau qui peut être une céramique (alumine pure) sous forme d'empilement de disques et de tubes correctement ajustés (fig. I-14 et I-15). Le dernier étage – condenseur – doit de toute façon travailler en régime moléculaire pour les besoins de la détection spectrométrique.

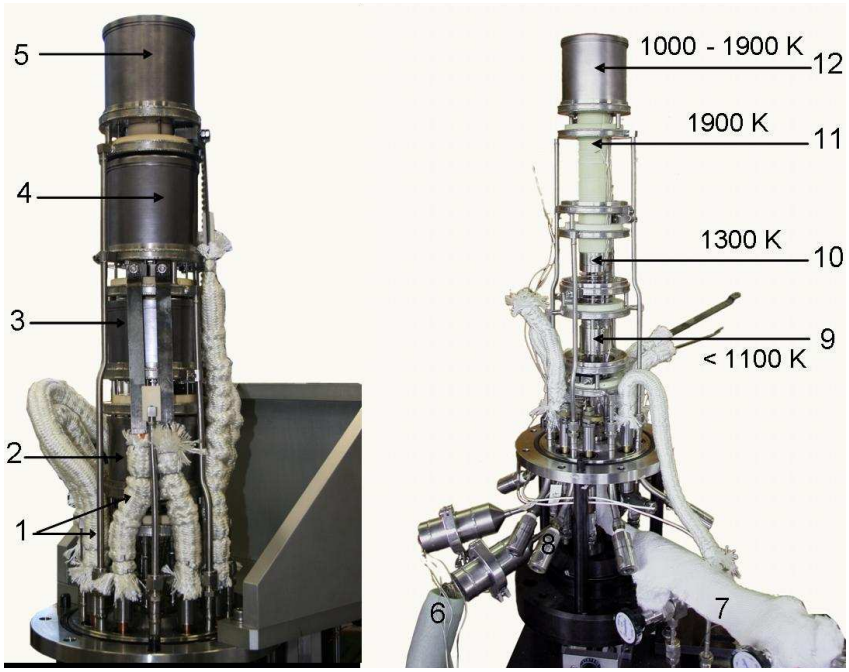

Figure I-14: Photos du réacteur CHIP et de la colonne des fours instrumentés. 1: amenées de courant en Cu avec tresse d'isolement. 2: four de l'étage évaporateur CsOH. 3: four de l'étage buses. 4: four de l'étage craqueur. 5: four de l'étage condenseur. 6: thermocouples. 7: arrivée des 3 lignes de gaz. 8: circuits de refroidissement. 9: évaporateur CsOH. 10: trois buses. 11: craqueur. 12: condenseur.

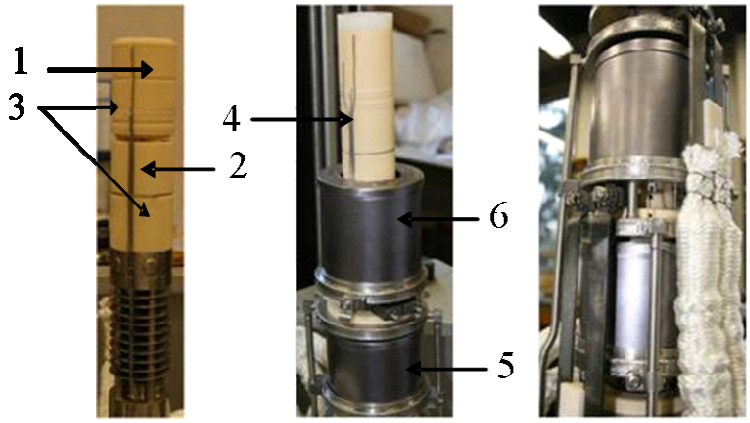

Figure I-15: assemblage et montage du réacteur (partie Nickel et partie alumine) dans les fours. 1: cellule condenseur, 2: cellule craqueur, 3: connexions tubulaires, 4: thermocouples, 5: four buses, 6: four craqueur

L'assemblage du réacteur se fait étape par étape en assemblant tout d'abord la partie basse du réacteur en Nickel avec la partie en céramique (empilement) et les fours instrumentés un par un tout en vérifiant l'alignement de chaque composant dans le réacteur (fig. I-15).

Ce réacteur thermocinétique à 4 étages composé d'environ 600 pièces (1er réalisé de ce type pour des études en phase gazeuse à haute température) est de grande complexité et a nécessité deux années de mise au point. Sa conception a du prendre en compte les principales contraintes suivantes:

- volume disponible réduit de l'enceinte du spectromètre de masse,
- étanchéité élevée pour être compatible avec le vide poussé (10^{-9} bars) du spectromètre de masse,
- forts gradients de température entre les différents étages du réacteur,
- faibles dilatations thermiques tolérées,
- compatibilité chimique avec les réactifs utilisés (non complètement satisfaisante à ce jour),
- réalisation de buses de très faibles diamètres (< 100 µm) pour atteindre les conductances requises.

Cette complexité de réalisation associée notamment à une réaction avérée entre l'Iode et le Nickel qui forme NiI_2(s) au niveau de la buse Ar/I_2 vers 900 K (buse bouchée après quelques heures d'utilisation) contrairement aux prédictions thermodynamiques (pas de formation de NiI_2(s) à T≥ 800 K) ne nous a pas permis de mener à bien les études cinétiques initialement prévues dans ce travail de thèse. Néanmoins, des tests de qualification préliminaires ont été réalisés afin de vérifier le fonctionnement du réacteur thermocinétique:

- ✓ Les gradients thermiques entre chaque étage du réacteur ont montré qu'il existe un gradient thermique régulier et correct entre craqueur et condenseur dans une gamme de température de 900 à 1300 K correspondant à la brèche en branche chaude. Au-delà, il existe un point plus froid.
- ✓ Le centrage du réacteur avec le spectromètre de masse et pour différentes températures du condenseur certifie le bon alignement du réacteur pour des mesures spectrométriques fiables.
- ✓ Le dimensionnement pour chaque section du réacteur à l'aide d'un calcul préliminaire a été validé expérimentalement avec l'Ar pour des pressions d'introduction de gaz allant de

100 à 600 mbar (buse de 50 microns de diamètre) et 100 à 400 mbar (buse de 100 microns de diamètre). Le flux effusif détecté par le spectromètre de masse est strictement proportionnel aux pressions introduites. Il reste cependant un problème de coefficient de proportionnalité qui est moindre que celui attendu par les calculs préliminaires d'écoulement des gaz dans le réacteur.

- ✓ La calibration envisagée du SMHT sur le flux d'argon (et donc sur sa pression mesurée par le spectromètre de masse au niveau du condenseur) a été testée par rapport à Ag et Ni en se référant aux mesures de pressions de ces corps purs au palier de fusion (cf. chap. V).

En conclusion, le réacteur actuel – sous réserve de modifications mineures concernant le matériau des buses (travail en cours à l'IRSN) – sera apte à fournir un diagnostic concernant les espèces gazeuses qui présentent une limitation d'ordre cinétique. Obtenir des données quantifiables de cette limitation cinétique va nécessiter, dans un premier temps, de valider définitivement le modèle d'écoulement entre le craqueur et le condenseur et, dans un second temps, d'effectuer des tests complémentaires portant sur la fusion de corps purs placés dans le craqueur afin de vérifier une bonne étanchéité de la partie haute du réacteur. Pour mieux maîtriser le régime d'écoulement moléculaire, il sera alors peut-être nécessaire d'envisager des améliorations de la partie haute température du réacteur CHIP.

.

BIBLIOGRAPHIE

[1] M.Schwarz, B.Clément, and AV.Jones, "Applicability of Phebus FP results to severe accident safety evaluations and management measures," Nuclear Engineering and Design, Vol. 209, 2001, pp. 173-181.

[2] B.Clément, "Summary of the Phebus FP Interpretation status", in *Proc. 5th Technical seminar on the Phebus FP programme*, 2003, Aix-en-Provence, France.

[3] J.Birchley, T.Haste, H.Bruchertseifer, R.Cripps, S.Güntay, and B.Jäckel, "Phebus-FP: Results and significance for plant safety in Switzerland," Nuclear Engineering and Design, Vol. 235, 2005, pp. 1607-1633.

[4] J.M.Evrard, C.Marchand, E.Raimond, and M.Durin, "Use of Phebus FP Experimental Results for Source Term Assessment and Level 2 PSA", in *Proc. 5th Technical seminar on the Phebus FP programme*, 2003, Aix-en-Provence, France.

[5] B.Clément, "Towards reducing the uncertainties on Source Term Evaluations: an IRSN/CEA/EDF R&D programme", in *Proc. Eurosafe Forum*, 2004, Berlin, Germany.

[6] D.Jacquemain, N.Hanniet, C.Poletiko, S.Dickinson, C.Wren, D.Powers, E.Kraussmann, F.Funke, R.Cripps, and B.Herrero, "An Overview of the Iodine Behaviour in the Two First Phebus Tests FPT-0 and FPT-1", in *OECD Workshop on Iodine Aspects of Severe Accident Management*,, 1999, Vantaa, Finland.

[7] L. Cantrel and E. Krausmann, "Reaction Kinetics of a Fission-Product Mixture in Steam-Hydrogen Carrier Gas in the Phebus Primary Circuit," J. Nucl. Technol., Vol. 144, 2003, pp. 1-15.

[8] N.Girault, S.Dickinson, F. Funke, A.Auvinen, L.Herranz, and E.Krausmann, "Iodine behaviour under LWR accidental conditions: lessons learnt from analyses of the first two Phebus FP tests," Nuclear Engineering and Design, Vol. 236, 2006, pp. 1293-1308.

[9] F.Cousin, K.Dieschbourg, and F.Jacq, "New capabilities of simulating fission product transport in circuits with ASTEC/SOPHAEROS v.1.3," Nuclear Engineering and Design, Vol. 238, 2008, pp. 2430-2438.

[10] C.Chatillon, L.Michelutti, and F.Z.Roki, "Etude de dimensionnement et de conception d'un dispositif d'essai pour la ligne analytique du programme CHIP", Note Techn. DPAM/SEREA-2005-0148 2005, 45 p.

[11] P.E.Blackburn and C.E.Johnson, "Mass Spectrometry Studies of Fission Product Behavior. II- Gas phase species in the CsI-CsOH system," J. Nucl. Mater., Vol. 154, 1988, pp. 74-82.

[12] M.G.Inghram and J.Drowart, "In High Temperature Technology", McGraw-Hill, New York, 1959, pp. 219-281.

[13] J.Drowart, C.Chatillon, J. Hastie, and D. Bonnell, "High-Temperature Mass Spectrometry: Instrumental Techniques, Ionisation Cross-Sections, Pressure Measurements, and Thermodynamic Data," J. Pure Appl. Chem., Vol. 77, 2005, pp. 683-737.

[14] C.Chatillon, M.Allibert, and A.Pattoret, "In Characterization of High Temperature Vapors and Gases", J.W.Hastie, NIST, Gaithersburg, MD, 1979, pp. 181-210.

[15] D.J.Santeler, "New Concepts in Molecular Gas Flow," J. Vac. Sci. Technol, Vol. A4, 1986, pp. 338-343.

[16] P.Morland, C.Chatillon, and P.Rocabois, "High Temperature Mass Spectrometry Using the Knudsen Effusion Cell. I-Optimization of Sampling Constaints on the Molecular Beam," J. High Temp. & Mat. Sci., Vol. 37, 1997, pp. 167-187.

[17] J.Roboz, "Introduction to Mass Spectrometry - Instrumentation and Techniques", Ed. John Wiley and sons, 1968.

[18] L.V.Gurvich, L.N.Gorokhov, G.A.Bergman, V.S.Iorish, V.Ya.Leonidov, and V.S.Yungman, "Thermodynamic Properties of Alkali Metal Hydroxides. Part II. Potassium, Rubidium, and Cesium Hydroxides," J. Phys. Chem. Ref. Data, Vol. 26 (4), 1997, pp. 1031-1109.

[19] M.W.Chase, J., "NIST-JANAF Thermochemical Tables," J. Phys. Chem. Ref. Data, Fourth Edition, Part I, 1998.

[20] SGTE, *Scientific Group Thermodata Europe*; www.sgte.com

[21] A.Rollet, R.Cohen-Adad, and C.Ferlin, "Le Système Eau-Hydroxide de Césium," Compt. Rend. Acad. Sci. Paris, Vol. 256, 1963, pp. 5580-5582.

[22] R.J.M.Konings and E.H.P.Cordfunke, "The Vapour Pressures of Hydroxides. I-The alkali hydroxides KOH and CsOH," J. Chem. Thermodynamics, Vol. 20, 1988, pp. 103-108.

[23] V.P.Glushko, L.V.Gurvich, G.A.Bergman, I.V.Veits, V.A.Medvedev, G.A.Khachakuruzov, and V.S.Yungman, "Thermodynamics of Individual Substances", Part 1, Vol. IV, Nauka, Moscow, 1982, pp. 492-495.

[24] R.I.Reed, "Ion Production by Electron Impact", Academic Press, New York, 1962, 242 p.

[25] L.Pauling, "A Simple Theoretical Treatment of Alkali Halide Gas Molecules", in *Proc. National Academy of Sciences India*, 1956, California Institute of Technology, pp. 1-19.

[26] L.Pauling, "The Nature of The Chemical Bond and The Structure of Molecules and Crystals, Chapt. 13", 3, Cornel University Press, New York, 1960, pp. 504-562.

[27] L.V. Gurvich, I.V. Veyts, and C.B. Alcock, "Thermodynamic properties of individual substances", Hemisphere Publishing Corporation, 4th edition, New York, 1989.

[28] J.L.Margrave, "The characterization of high temperature vapors", Chapter 13, John Wiley & sons, New York, 1967, pp. 359-424.

[29] J.O.Hirschfelder, "Simple Method for Calculating Moment of Inertia," J. Chem. Phys., Vol. 8, 1940, pp. 431.

[30] R.P.Henry, "Cours de Science et Technique du vide", Vol. Livre I, Tome II, Soc. Franç. Vide, Paris, 1968.

[31] D.J.Santeler, "Exit loss in viscous tube flow," J. Vac. Sci. Technol, Vol. A 4 (3), 1986, pp. 348-352.

ANNEXES

ANNEXE I-A: Description du circuit «BRONKHORST^{TM}» générateur de vapeur d'eau / hygrogène avec l'argon comme gaz porteur.

Le montage retenu s'inspire du schéma du fonctionnement du Contrôleur d'Evaporation et de Mélange CEM « Bronkhorst^{TM} » sous vide. Nous n'utiliserons que des lignes d'introduction régulées en pression (pressiostats et non débitmètres). La purge du système se fait par un by-pass (figure I-A1) sur les lignes d'introduction (ligne aval). Pour éviter d'introduire du CO_2 ou O_2, il est utile de faire une purge et un dégazage du réservoir d'eau. En cas de changement de bouteille sans ouverture de la ligne aval, il est utile de faire une purge des manomètres. Cette purge n'est toutefois pas nécessaire si l'on peut pomper le manomètre par la ligne aval car les capacités des lignes permettent une manœuvre rapide.

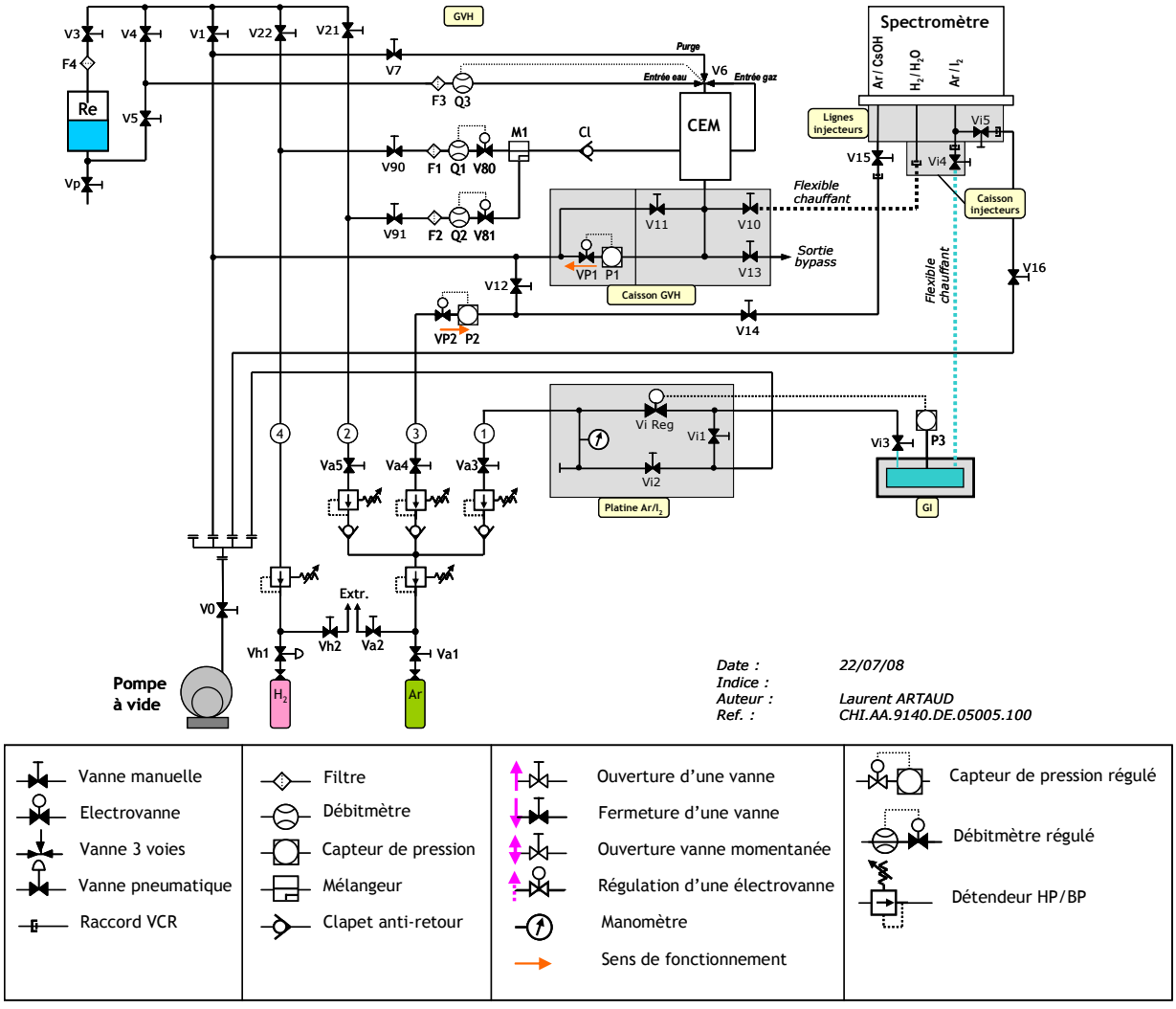

Figure I-A1: schéma de principe du circuit Bronkhorst pour l'injection des gaz $H_2/H_2O/Ar$.

CHAPTER II

PART I: THERMODYNAMIC STUDY OF THE CSOH(S,L) VAPORIZATION BY HIGH TEMERATURE MASS SPECTROMETRY

Available online at www.sciencedirect.com
ScienceDirect
J. Chem. Thermodynamics 40 (2008) 401–416
JCT
www.elsevier.com/locate/jct

Thermodynamic study of the CsOH(s,l) vaporization by high temperature mass spectrometry

F.Z. Roki [a,*], C. Chatillon [b], M.N. Ohnet [a], D. Jacquemain [a]

[a] IRSN, DPAM, SEREA, Laboratoire d'Essais Analytiques, Centre de Cadarache, BP 3, 13115 St. Paul-Lez-Durance Cedex, France
[b] Science et Ingénierie des MAtériaux et Procédés (SIMAP), Associé au CNRS-UMR 5266 (UJF/INPG) 1130, rue de la piscine, Domaine Universitaire, BP75, 38402 Saint Martin d'Hères, France

Received 27 June 2007; received in revised form 17 September 2007; accepted 23 September 2007
Available online 6 October 2007

Abstract

The present study deals with thermodynamic data for the gaseous phase of the Cs–O–H system as studied by high temperature mass spectrometry using the Knudsen cell effusion method. The vapour phase is analyzed and is composed of the monomer CsOH(g), the dimer $Cs_2O_2H_2(g)$, and a small amount of trimer. The vaporization behavior of CsOH(s or l) is analyzed in relation with different physico-chemical phenomena that interfere with the Knudsen method, like creeping and surface diffusion along the walls of the effusion orifice. Besides, the ionization processes are complex and render the interpretation of the mass spectrometric results difficult. Thus, calibration procedures have been carefully analyzed in order to evaluate reliably the uncertainties. The two main independent reactions that lead to thermodynamic data are the following:

$Cs_2O_2H_2(g) = 2CsOH(g)$ with $\Delta_{diss}H^\circ(298\ K) = 146.6 \pm 7.3\ kJ \cdot mol^{-1}$ (3rd law method).
$CsOH(s,l) = CsOH(g)$ with $\Delta_{subl}H^\circ(298\ K) = 163.3 \pm 6.5\ kJ \cdot mol^{-1}$ (3rd law method).

Keywords: Cesium hydroxide; Mass spectrometry; Enthalpy of vaporization; Partial vapour pressures

1. Introduction

In the low probable event of a nuclear reactor accident leading to fuel melting, iodine and its radioactive isotopes are major volatile components which can be released to the environment. Iodine is a radiotoxic element that may cause serious damage to man health and environment and it is thus essential to dispose of means to evaluate the pertinence of measures that authorities will take to reduce the consequences of iodine release. For that purpose, the French ''Institut de Radioprotection et de Sûreté Nucléaire'' launched an international program to study the behavior of iodine in components of the reactor during an accident. Owing to the complexity of the resulting mixture, iodine may be transported by a variety of compounds (fission products, control rod materials, *etc.*) either as vapours, particles or aerosols. The present publication deals with the first step in the thermodynamic study of the system Cs–I–O–H which has been chosen as the first candidate in the study of complex mixtures expected in a reactor accident – cesium being one of the main fission products reacting with iodine. The reaction between gaseous cesium and H_2O during severe nuclear accident may produce cesium hydroxide which is one of the main components in the primary cooling lines.

The present work was undertaken in order to study the gaseous phase chemical behavior of the Cs–O–H system. Different methods such as transpiration [1] and high

* Corresponding author. Tel.: +33 4 76 82 65 11; fax: +33 4 76 82 67 67.
E-mail addresses: fatima.roki@ltpcm.inpg.fr (F.Z. Roki), christian.chatillon@ltpcm.inpg.fr (C. Chatillon), marie-noelle.ohnet@irsn.fr (M.N. Ohnet), didier.jacquemain@irsn.fr (D. Jacquemain).

0021-9614/$ - see front matter © 2007 Elsevier Ltd. All rights reserved.
doi:10.1016/j.jct.2007.09.013

TABLE 1
Summary of preceding mass spectrometric studies of CsOH(s,l) vaporizations according to the literature

Authors and references	Samples and preparation	Cell and material	T range/K	Studied reactions or processes	Observations
Schoonmaker and Porter [7]	CsOH–KOH ($x = 0.5$)	Pt lined with MgO	650 to 900	$2CsOH(g) + K_2O_2H_2(g) = 2KOH(g) + Cs_2O_2H_2(g)$	– $S_{eff}/S_{vap} < 0.003$ (see section 2.4) – Dimer/monomer ratio may not correspond to saturation ($x = 0.5$)
	CsOH–RbOH ($x = 0.5$)	or pure silver		$2CsOH(g) + Rb_2O_2H_2(g) = 2RbOH(g) + Cs_2O_2H_2(g)$	– MgO is spongy and allows the penetration of liquid hydroxide and retains it to avoid creeping – Cs^+ observed as fragment ion of CsOH(g) – Hydroxides trimers not detected – Use isomolecular reactions in order to avoid calibration (internal compensation of sensitivity factors)
Gorokhov et al. [2]	Pure CsOH	MgO		$CsOH(g) + e^- = Cs^+ + OH(g) + 2e^-$	– Born–Haber cycles from dissociative ionization of Cs^+/CsOH(g) – by reference to known ionization potential of Cs^+/Cs(g)
	$KOH + K_2CO_3 + CsOH$		795 to 1044	$CsOH(g) + K(g) = KOH(g) + Cs(g)$	– Isomolecular reaction (internal compensation of sensitivity factors)
Blackburn and Johnson [3]	Pure CsOH(l)	Silver	622 to 772	$CsOH(l) = CsOH(g)$	– Calibration of HTMS by weight loss – $S_{monomer}/S_{dimer} = 0.5$ (estimated)
			681 to 772	$2CsOH(l) = Cs_2O_2H_2(g)$	– Sensitivity of CsOH = 10 times sensitivity of CsI
	Pure CsI(l)		917 to 1035	$CsI(l) = CsI(g)$	– Factor 2 in uncertainties for dimer (proposed)
			924 to 1041	$2CsI(l) = Cs_2I_2(g)$	– CsOH(g) properties measured agree reasonably well with the literature data – The partial pressures of dimer are 100-fold lower than that calculated from retained in JANAF tables
	CsOH–CsI mixtures Preparation of CsOH by vaporization of CsOH–H_2O progressively up to 720 K, 2 h heating Cooling under He Weighing to determine water loss then immediately placed in the vacuum chamber of HTMS		809 to 927	$CsI(g) + CsOH(g) = Cs_2IOH(g)$	– The presence of the complex molecule CsI–CsOH(g) should increase the iodine concentration in the vapour (CsI and CsOH could be deposited and form aerosols) – CsI–CsOH(g) not identified directly by a parent ion due to fragmentation under ionization. This molecule seems to be the more stable molecule at high pressure since its fragment ions hide the same ions coming from the pure dimers

temperature mass spectrometry (HTMS) [2–8] have been used to study hydroxides vaporization and particularly CsOH(s,l) vaporization. The preceding HTMS studies are presented with their experimental conditions and observations in table 1. These studies showed that the gaseous phase contains at least the CsOH(g) "monomer" and $(CsOH)_2$ "dimer" with quite equivalent proportions. The knowledge of the equilibrium constant between these two species is necessary for the interpretation of total pressure data obtained by transpiration. Owing to large discrepancies in the mass spectrometric literature results, the present experimental effort is aimed first at the investigation of the CsOH(s,l) vaporization using high temperature mass spectrometry [9,10] in order to clarify earlier difficulties encountered in these studies and to determine at a first step the gas composition and the dissociation enthalpy of the dimer which is controversy. Gurvich *et al.* [11] performed an assessment of different published studies of the CsOH(s,l,g) system. In this compilation, the monomer and dimer structures are known with a quite good accuracy, C_p°, S_T° and free energy functions are reliable in view of third law calculations. However, in Gurvich compilation the enthalpies of formation have been obtained from a set of largely scattered original data (within 40 kJ) that renders their assigned uncertainty for the monomer and the dimer, respectively, ±5 and 8 kJ, quite optimistic. Gurvich *et al.* [11] recommended for future investigations to study the vaporization of CsOH directly by mass spectrometry in order to obtain reliable quantitative data for vapour composition, including relative concentration of trimeric and possibly tetrameric molecules. Besides, they stated that the selected dimer structure needs to be confirmed.

2. Experimental

2.1. Principle of the HTMS method

The high temperature mass spectrometric method has been presented and its capabilities analyzed in a recent and complete IUPAC report [10] on the mass spectrometric Knudsen cell method. Atoms or molecules traveling as a molecular beam issued from an effusion cell are ionized by an electron beam – the energy of which can be monitored – and the resulting ions extracted from the ion source of a mass spectrometer, then separated in a magnetic prism and focused on a secondary electron multiplier. The measured ionic intensity I_i of any ion is related to the partial pressure of its original molecule p_i in the cell and to the cell temperature T according to the basic mass spectrometric relation:

$$p_i S_i = I_i T \tag{1}$$

in which S_i is the sensitivity given by the general relation [10]:

$$S_i = G\eta\sigma_i(E)\gamma_i f_i, \tag{2}$$

where G is a geometrical factor related to the solid angle for molecular beam sampling defined by the ionization chamber aperture and the effusion orifice, η is the extraction and transmission efficiency of the formed ion in the mass spectrometer (for our ion source and magnetic sector $\eta =$ constant whatever is the measured ion), $\sigma_i(E)$ is the ionization cross-section depending on the electron energy E, γ_i is the efficiency of the ion detector (for our discriminated pulse-counting detection $\gamma_i = 1$ whatever is the measured species i), f_i is the isotopic abundance of the detected ion that is calculated exactly for any atomic composition of each ion. In our case, the sensitivity is reduced to:

$$S_i = G\sigma_i(E)f_i. \tag{3}$$

The sensitivity is obtained by different type of calibration and is to be performed for each experiment. In our study, the calibration is performed combining the spectrometric relation (1) with the total mass loss of the sample Δm according to the Hertz–Knudsen relation [10],

$$\frac{\mathrm{d}N_i}{\mathrm{d}t} = \frac{p_i s C}{(2\pi M_i RT)^{1/2}} \tag{4}$$

in which the number of moles effused $\mathrm{d}N_i/\mathrm{d}t$ per second is related to p_i and M_i the partial pressure and the molar mass of the effused species i, s and C the orifice cross-section and Clausing coefficient and $R$the gas constant [10]. Then the sensitivity can be calculated *a posteriori* after integration all along the experiment of the $I_i T^{1/2}\mathrm{d}t$ products according to:

$$S = \left(sCM^{1/2}\right) \Big/ \left(\Delta m(2\pi R)^{1/2}\right) \sum_{i=1}^{n} \left(IT^{1/2}\right)_i \delta t_i. \tag{5}$$

For several species in the same vapour phase, another version of equation (5) is used:

$$S_1 = \left(sC(M_1)^{1/2}/\Delta m(2\pi R)^{1/2}\right) \times \sum_{j=1}^{p} \left(\sum_{i=1}^{n} S_1/S_j (M_j/M_1)^{1/2} \left(I_j T^{1/2}\right)_i \delta t_i \right), \tag{6}$$

where the summation over $i = 1$ to n corresponds to the various temperature plateaus of the experiment, and j enumerates the species. This last relationship requires knowledge or estimates of the ratios S_1/S_j. In our case, this ratio is directly the ionization cross-section ratio according to (3). No other estimated parameters are required.

The ionization cross-section of a molecular gaseous species is calculated using the so-called "additivity" rule based on each atom constituting it [10]. This rule is to be applied to the whole ionization process of a molecule and takes into account the total ionic current – parent and fragment ions. The ionization cross-sections of the atoms were parameterized according to the potential of ionization (V) in the IUPAC report [10]. In the case of a dimer, the additivity rule leads to a dimer/monomer ionization cross-section ratio equal to 2.

2.2. Improvements in our mass spectrometric method

Three main transformations of our original device have been performed in order to improve the reliability of the measurements, especially when high volatile species have to be detected. These concern: (i) the collimation of the useful molecular beam, (ii) the shutter device, and (iii) the ionization chamber.

- The collimation of the useful molecular beam concerns the so-called "restricted collimation" [12]. Indeed, coupling the effusion cell vapour source to the ion source of the mass spectrometer is achieved by interposing a cooled separation, *i.e.* a water jacket in order to protect the ion source from heat flow of the furnace and from molecular deposits from outer parts of the whole effused beam. In a conventional device (figure 1i), the different apertures (thermal shields, cooled jacket, ion source entrance, *etc.*) allow molecules to enter the ionization chamber from a quite large solid angle, even when careful collimation of the effused beam is done. Thus, the ion source observes at the level of the effusion orifice a large area defined by the umbra and penumbra zones (figure 1): a molecular beam coming from parasitic surface vaporizations is thus detected in addition to the useful (equilibrium) molecular beam [13,14] issued directly from the effusion orifice. Our restricted collimation (figure 1ii) involves the introduction of a small aperture (field aperture) located in the cooled jacket separating the furnace and ion source housings. Together with the source aperture, the field aperture fully defines the sampled molecular beam. The size of the field and source apertures defines the size of the only useful molecular beam in such manner that at the effusion entrance orifice level the penumbra zone (diameter D_p) is less than the effusion diameter D_e. With respect to the conventional collimation, the restricted collimation device presents the advantage to discard definitively any surface contributions occurring with the useful molecular beam effusion. The second advantage is that the solid angle of detection as defined by both apertures remains fixed and independent of the effusion cell (in contrast with a conventional collimation) and is only dependent on the mass spectrometer. This advantage will be used in the evaluation of surface diffusion flow contributions as shall we seen later. The use of restricted collimation device imposes that the distance between the effusion orifice (from the inner face of the lid, *i.e.* the entrance of the effusing molecules in the effusion orifice) and the first (field) aperture must be short and systematically checked for any new cell geometry and associated furnace device to be certain to detect molecules coming only from the inner gas phase of the effusion cell. Moreover the mechanical positioning of the effusion cells must be performed with the best accuracy (± 0.025 mm in our case [14]). Besides, the overall molecular transmission of the restricted collimation has been previously optimized by the correct choice of the two source and field aperture sizes in relation with different distances according to the earlier work performed by Morland *et al.* [12].

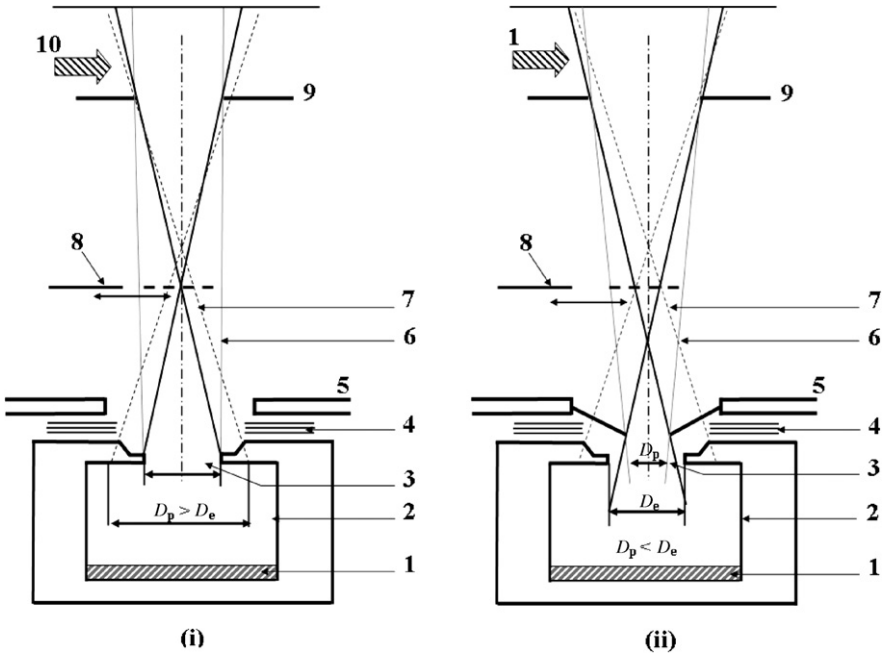

FIGURE 1. Conventional collimation (i) and restricted collimation (ii) of the effused molecular beam showing the various molecular emitting surfaces seen in each sampling method by the ionization chamber: 1: sample; 2: Knudsen cell; 3: effusion orifice; 4: thermal shields; 5: cooled field aperture; 6: solid angle corresponding to effusion orifice alone; 7: supplementary surface viewed by the detector; 8: shutter; and 9: source aperture. 10: ionizing electron beam. D_p is the diameter of the penumbra zone for detection of molecules and D_e the effusion diameter.

- A shutter is a small disk or a blade which can be moved mechanically to cut off perpendicularly the direct molecular beam and by this way we are able to distinguish the background molecular flow (from source background pressure) from the useful molecular beam. This is particularly important when the gaseous species existing in the background are the same as those detected from the cell (H_2O for instance in this study) or appear at the same non-resolved masses. This shutter is located mid-way between the two apertures. Its movement is ''free'' from any mechanical part linked to the water jacket in order to avoid any partial closing of the field aperture during the shutter movement. The vacuum pumped permanent flow between the furnace and source housings, which are rarely at the same background pressure due to the furnace heating [12], is therefore not disturbed.
- The ionization chamber contains an entrance aperture which defines the restricted collimation transmission but at the same time reduces the overall ionization volume. We use a version of ionization chamber (set at 5000 V) which is cooled by direct contact with liquid-nitrogen to prevent any re-vaporization of molecular gaseous species that have entered into the ionization chamber for analysis. This ionization chamber was built intentionally for the measurement of high volatile species from As, P [15].

These three above improvements are prerequisites for reliable measurements with high volatile species since usually these species undergo re-vaporization from thermal shields and from usual ionization chamber devices that are maintained at about 573 K by the electron emitting filament.

2.3. Sample preparation

Pure CsOH(s,l) does not exist as delivered but the monohydrate CsOH–H_2O does. The interaction between cesium hydroxide and H_2O is provided in the H_2O–CsOH solid–liquid phase diagram which is a part of H_2O–Cs_2O phase diagram. Following the Rollet *et al.* [16] work, elimination of water was done by degassing the product in a crucible or an effusion cell under primary vacuum at 440 K during (16 to 20) h. Then temperature was slowly increased (a 50 K/h ramp) to about (620 to 640) K. Temperature was then maintained constant for about (1 to 2) h leading to the melting of the sample. The effusion cell was then cooled, filled with nitrogen, opened at air and weighted to determine water loss. The results showed that the initial amount of water is not a constant, probably because the initial monohydrate crystals catch some water in excess. Curiously, authors in the literature do not mention this phenomenon. This procedure is similar to that applied by Konings and Cordfunke [1] who checked the formation of pure CsOH(s) by X-ray diffraction but not from the weight loss. The CsOH(s) and its cell were immediately stored in a drier (vacuum pumping was not necessary) when not directly introduced in the mass spectrometer. Regularly performed sequential weightings showed that in these storage conditions there is no mass gain of the product (the gain of water seems very slow for a bulk solid).

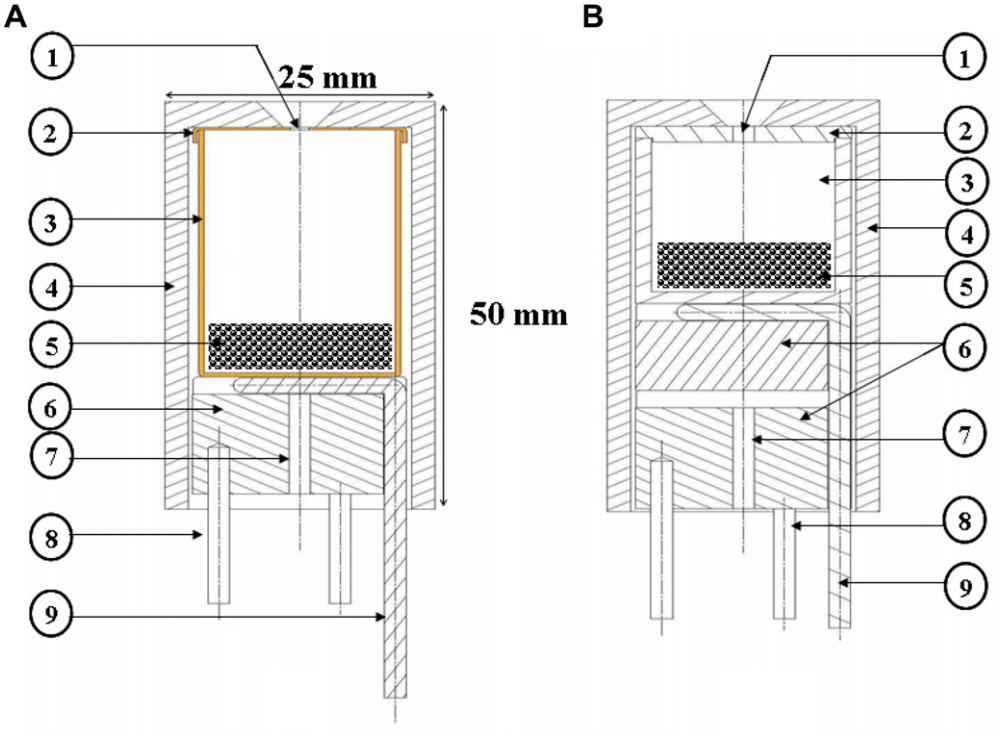

FIGURE 2. Schematics of effusion cells used for vaporization of CsOH. (A) Pt–20% Rh effusion cell. (B) Nickel effusion cell. 1: effusion orifice; 2: lid; 3: crucible; 4: external envelope; 5: sample; 6: holder 7: hole for pyrometric sighting; 8: three thin tungsten poles; and 9: thermocouple K type.

2.4. Effusion cells

In order to choose the suitable cell material for CsOH(s,l) vaporization studies, and from already published investigations, crucibles and lids in dense MgO, Ni, Pt–20% Rh and Au have been tested during the sample preparation stage. Moreover, the cell material has to show in principle bad wetting properties in order to avoid any creeping of the liquid. The preparation stages showed frequent "flow out" of the CsOH either along the cell walls or by the orifice lid of the cell – the lid being more or less sealed by the CsOH product – and exceptionally we observed creeping of the liquid. At that time, we did not know precisely if this behavior was related to the still (partly) hydrated product or to the final anhydrous CsOH(l). Mass spectrometric experiments were performed with cells as shown in figure 2. The whole set of our observations is mentioned in table 2. The spectrometric studies made with different materials showed a "flow out" of the product by the effusion orifice – observation of material rings around the effusion orifice. Figure 3 illustrates the flow out phenomenon. According to our observations, the Pt–Rh(20%) crucible seems to be the more convenient but gold crucibles remain good candidates in terms of wetting properties. The capability of an effusion cell to establish equilibrium conditions for vaporization is directly related to the ratio of the effusion flow to the total vaporization flow at the surface of the sample. The ratio $(s \cdot C)/S$ – as mentioned in table 2 – represents the ratio of effective effusion cross-section ($s \cdot C$) *versus* vaporization section (S cell cross-section) that characterizes equilibrium conditions in the cell [17,18]. Some authors in earlier mass spectrometric investigations published ratio values less than 0.003 [7] or equal to 0.001 [2]. The usual solution to obtain so small ratios is to decrease the orifice effusion diameter at constant cell diameter. This solution, as discussed by Ward and Fraser [19], presents the disadvantage to increase the relative proportion of surface diffusion contributions along the orifice walls and at the external surface (see our further observations) to the genuine effusion flow which is the useful one to characterize vaporization. Ward and Fraser [19] recommended the use of large and cylindrical orifices, this solution being adopted systematically for our mass spectrometric analysis.

2.5. Effusion process analysis and parasitic contributions

The effusion orifice alignment along the ionization chamber axis (restricted collimation axis) is performed by moving the effusion cell furnace in two X and Y directions orthogonal to this axis [14] as showed in figure 4A. In this figure, the various configurations of the restricted collimation positioning relative to the cell orifice are displayed. At the top of the peak (a), the sighting is perfectly inside the orifice and we observe a plateau which corresponds to the measure of the saturated pressure in the cell (genuine effusion). At the basis of the peak (b), the signal corresponds to outside surface vaporizations just around the

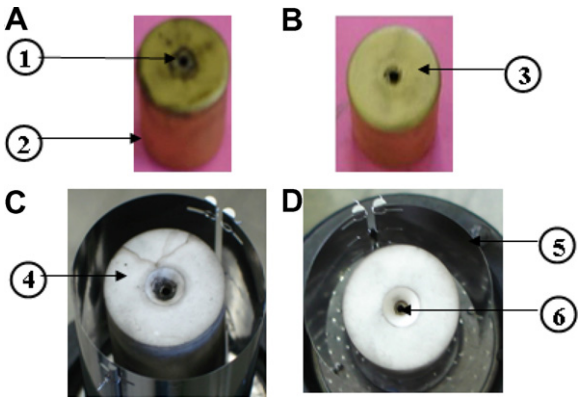

FIGURE 3. (A) and (B) Pictures of gold cell after HTMS experiments: (A) lid showing flow out of the sample, (B) lid after cleaning, (C) and (D) pictures of effusion cells and their external envelopes after HTMS experiments. (C) Gold cell with visible flow out of the sample (D) Pt–Rh cell with no flow out. (1) Material rings around effusion orifice due to flow out. (2) Crucible made of gold. (3) Cell's lid after cleaning (error on weight loss $\delta(\Delta)m \approx 3\%$). (4) External alumina envelope. (5) W-Resistor. (6) Effusion orifice.

TABLE 2
Observations of the behavior of cells made of different materials loaded with CsOH during HTMS experiments

Material cell	Experience label	Temperature range/K	$(s \cdot C)/S$	Observations after HTMS experiments
Ni[a]	CsOH-02 s	515 to 761	$7.1 \cdot 10^{-3}$	Flow out around the effusion orifice Thick residual rings
MgO[b]	CsOH-03 s	572 to 769	$7.1 \cdot 10^{-3}$	Large flow out and sticking of the crucible to the external envelope: no weight loss determination could be performed
Pt–Rh[c]	CsOH-04 s	496 to 765	$6.6 \cdot 10^{-3}$	No flow out detected except some slight grey rings around the effusion orifice
	CsOH-05 s	522 to 758	$6.6 \cdot 10^{-3}$	Same observation as for CsOH-04 s
Au[a]	CsOH-06 s	531 to 753	$11.3 \cdot 10^{-3}$	Sometimes flow out around the effusion orifice by grey rings observations
	CsOH-07 s	530 to 753	$11.3 \cdot 10^{-3}$	Same observation as for CsOH-06 s

The ratio $(s \cdot C)/S$ (s orifice cross-section, C Clausing coefficient, S cell cross-section) characterizes the vaporization equilibrium conditions in the cell (according to Motzfeldt relation [17]).

[a] Pure material.
[b] Dense.
[c] 20% Rh.

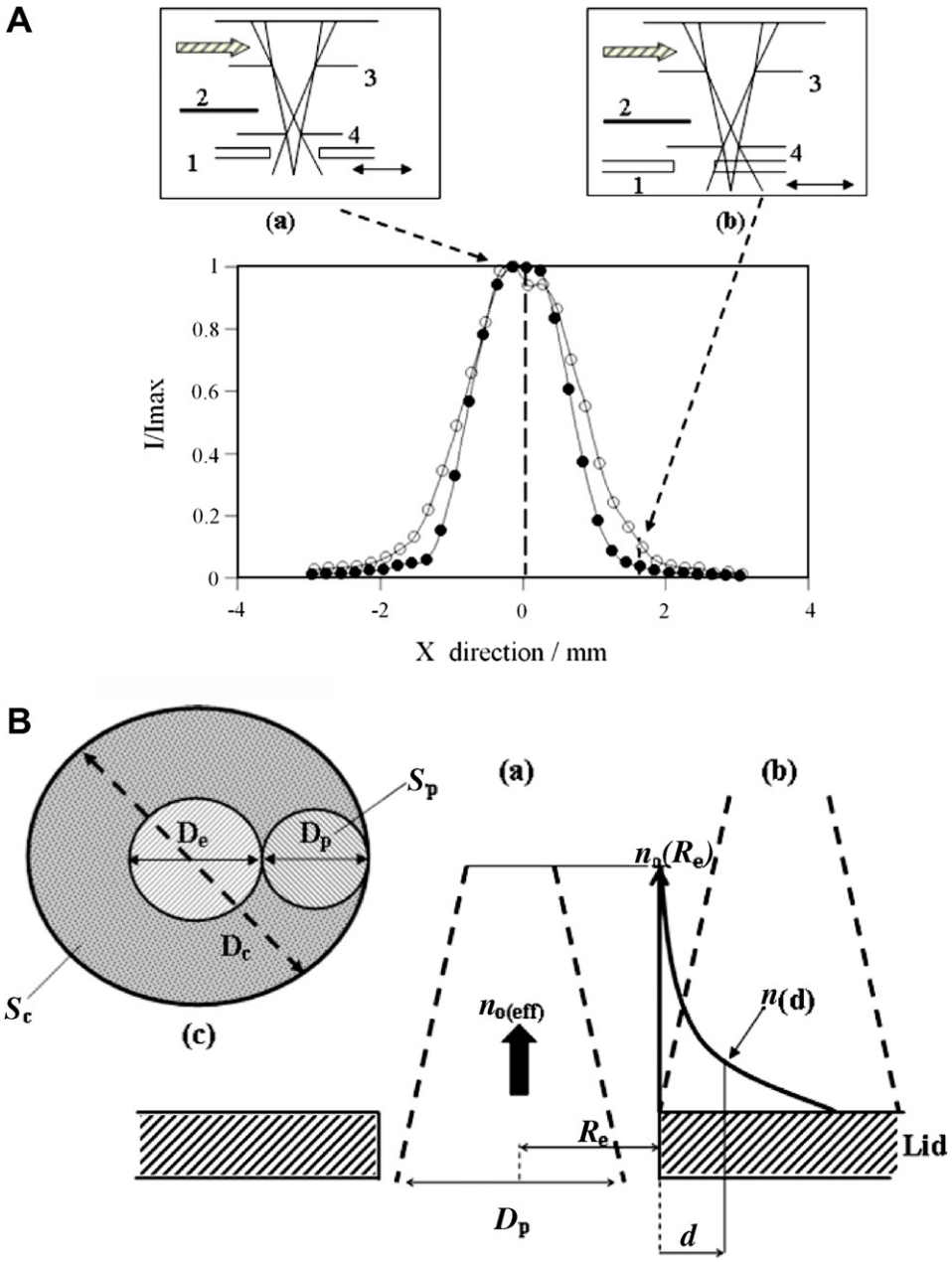

FIGURE 4. (A) Normalized registration of Cs^+ ion intensity during scanning of the position of the effusion orifice of a Pt–Rh cell containing CsOH sample. (a) The sighting is through the orifice; (b) the sighting is the signal coming from outside (surface). ○: $T = 563$ K; ●: $T = 676$ K. 1: 1.7 mm diameter effusion orifice; 2: shutter; 3: source aperture; 4: field aperture. (B) Attended molecular emission of the different surfaces seen by our detector through the restricted collimation. Position in (a) for the restricted collimation: emission of molecules from a cylindrical Knudsen effusion-cell orifice of a radius Re, a length l(eff) with a flow concentration n_o(eff) that corresponds to the saturated pressure in the cell. Collimation in (b) position: n(d): emission of molecules by desorption in competition with surface diffusion. D_p penumbra diameter. d: positioning from the effusion orifice edge. $n(R_e)$ can be calculated as a function of orifice length (l_{eff}) and n_o(eff): $n(\mathrm{Re}) = f(l_{eff}) \cdot n_o(\mathrm{eff})$ according to Winterbottom and Hirth [20]. (c) D_e: orifice diameter. D_p: penumbra diameter. D_c: total diameter (D_e plus D_p).

effusion orifice edge. The accuracy (±0.025 mm) [14] of the cell and furnace positioning device allows us to locate exactly the penumbra zone tangentially to the border of the effusion orifice.

In order to be able to manage the cell temperature in this low temperature range (570 K to 770 K) as well as to avoid any re-vaporization of the peripheral molecular beam zones on thermal shields we did not use any thermal shields. Schoonmaker and Porter operated similarly [7]. Doing so, the residual ionic intensity observed in figure 4A at the basis of the peak (position (b)) is related to the only ''flow out'' process of molecular gaseous species adsorbed along the effusion orifice wall and on the outside surface of the lid in competition with vaporization under vacuum. This phenomenon does not disturb the MS detection with the restricted collimation (performed at the

summit of the peak at (a) position) but gives an additional contribution to the mass loss of the cell which is different from the only genuine effusion taken into account in the Hertz–Knudsen relation. Consequently, it is necessary to evaluate this contribution in order to correct the total mass loss of the sample which in this case takes into account both the effusion and the flow out processes. In effusion and mass spectrometric studies, creeping of liquids leads usually to large overflow of liquid samples (in our case melting is at $T > 630$ K) that contributes so largely to mass loss evaluation that any calibration of the mass spectrometer becomes ineffective: with non-restricted collimation devices – conventional ones – the ionic intensities may increase abnormally – *i.e.* additional detected parasitic flows increase drastically – and generally the liquid creeping is observed to have sealed all parts of the cell assembly after experiment. We observed this feature when using MgO cells. When the liquid had totally disappeared from the crucible or if some clogging of the effusion orifice occurs (more frequent case due to freezing at the orifice), the ionic intensity finally decreases due to cooling effects on outside surfaces. Schoonmaker and Porter [7] observed such a behavior and finally they used a porous MgO crucible inserted in a stainless steel or nickel effusion cell to trap the liquid hydroxide in the pores. We used also (open) porous MgO, but the liquid wetted MgO and leaked through this material. With dense MgO (sintered with ZrO_2 additives) we observed large creeping. Finally, Schoonmaker and Porter did not vaporize quantitatively (using mass loss calibration) the pure CsOH(s,l) but mixtures with KOH or RbOH, probably because CsOH is more difficult to retain in its container.

For other materials the analysis of the mass spectrometric response to the cell position scanning (e.g. Figure 4A) showed systematically that the profile becomes sharper when temperature increases, meaning that the contribution of the flow out decreases relatively to genuine effusion at high temperature. This is typically related to a surface diffusion phenomenon occurring along the effusion orifice walls: the total contribution according to such a phenomenon was analytically resolved by Winterbottom and Hirth [20] and numerically (Monte-Carlo method) analyzed by Ward *et al.* [21]. In figure 4B, position (a) depicts the observation by our restricted collimation of the orifice of a Knudsen effusion cell with a saturated concentration n_o(eff) for evaporated molecules *i.e.* coming from the interior of the cell at equilibrium pressure p_e. In figure 4B, position (b) represents the observed surface through which the diffusion flow competes with free vaporization. Winterbottom and Hirth [20] showed that the surface diffusion contribution becomes relatively more important for decreasing radii of the orifice. As we use large orifices – *i.e.* ~2 mm diameter, the diffusion contribution to the total flow will remain limited. Besides, as the activation enthalpy for diffusion is lower than for vaporization, the relative contribution of diffusion to effusion decreases with temperature as predicted by Winterbottom and Hirth. With our restricted collimation we observed this feature systematically (see figure 4A as an example) whatever is the cell material (except MgO) when monitoring the direct contribution ratio by measurement at the top and at the basis of the peak observed when scanning the orifice position. Using different positioning of the effusion orifice in a plane perpendicular to the ionization chamber axis (restricted collimation axis), it is possible to evaluate the percentage of the diffusion contribution. We know, according to Winterbottom and Hirth [20] and Ward *et al.* [21] that the emission of molecules decreases sharply when starting from the orifice edge (as depicted in figure 4B, position b) and we can postulate that with our large observed zone (our penumbra zone) we detect all the surface contribution: more simply the whole surface diffusion flow is evaporated before reaching the external limit of the observed penumbra zone. This is readily checked by comparing the penumbra diameter from the orifice edge with the extinction of the signal at about $x = 3$ mm (see figure 4A). The corresponding intensity as measured for a penumbra zone positioned tangentially to the orifice relative to the maximum is thus equal to 0.13 at 563 K and 0.04 at 676 K. The total diffusion intensity on the whole surface of diameter D_c can be obtained with the proportion between the penumbra zone section S_p and the total ring surface S_c (figure 4B). So the total calculated diffusion contribution becomes equal to 53% at 563 K and 25% at 676 K of the genuine effusion process. This result agrees with the fact that the surface diffusion contribution decreases with temperature. The total mass loss corrected $\Delta m_{(corr)}$ – that is the only resulting genuine effusion mass loss – is then calculated as following:

$$\Delta m_{(corr)} = \Delta m_{(exp)} \cdot (1/(1 + (\%\ \mathrm{diff}/100)), \qquad (7)$$

where $\Delta m_{(exp)}$ is the experimental total mass loss (effusion + diffusion process), $\Delta m_{(corr)}$ is the corrected mass loss which only takes into account of the effusion process, % diff is the total diffusion contribution and 1 is the normalized I_{eff}/I_{max} at $X = 0$ mm on the axis of the restricted collimation. We recalculated for each temperature the intensity

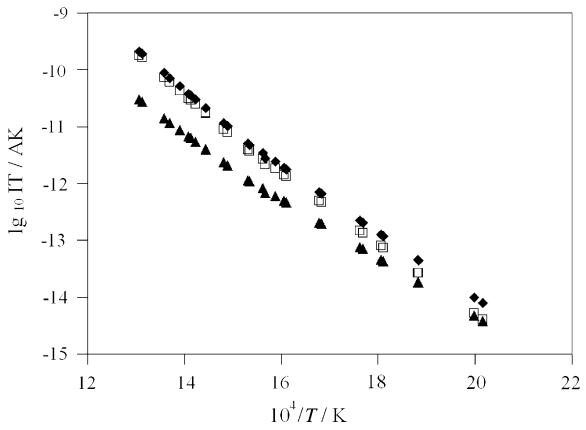

FIGURE 5. Effusion, diffusion and total contribution of Cs^+ measured ion when vaporizing CsOH(s,l) in a Pt–Rh effusion cell. ▲: Cs^+ diffusion. □: Cs^+ effusion. ◆: Cs^+ effusion + diffusion (hypothetical).

related to the total diffusion contribution for the Cs^+ ion using a Pt–Rh cell as it is shown in figure 5, compared to the genuine effusion (center line or I_{max}). The sum of the two contributions is the one which would be usually observed with a conventional collimation device. As the IT product is proportional to the partial pressure p (relation (1)), the obtained curves agree with the predictions of Winterbottom [22]: (i) with surface diffusion contribution the apparent partial pressure curve escaping from a Knudsen cell – that is the total intensity that would be measured in a conventional device – lies above the true partial pressure from genuine effusion, (ii) the absolute value of the slope of the total apparent pressure is always lower than the true one *i.e.* genuine effusion.

3. Results

3.1. Detected ionic species

The following ions were detected: Cs^+, $CsOH^+$, CsO^+, CsH^+ (small quantity), Cs_2OH^+, Cs_2O^+, Cs_2H^+, $Cs_3O_2H^+$, $Cs_3O_2H_2^+$, H_2O^+ (figure 6). Compared to the preceding spectrometric studies [3,7], CsH^+, Cs_2H^+ and the trimers ions are new ones. The Cs_3XY^+ ions in the spectrum mean that the trimer molecule exists. Contrary to what is proposed by Schoonmaker and Porter [7] we did not detect the ion Cs_2^+ but Cs_2H^+. Considering the square structure of the dimer (Gurvich *et al.*) [11] and the ionic character of the parent molecule, the Cs_2^+ formation seems less probable than the Cs_2H^+ during any dissociation ionization process. It is important to note that we systematically observed a relative decrease of measured intensity within the higher temperature range (713 to 753) K of our measurements (figure 6). This slight inflexion of the intensities is due to vapour deposits on the first (field) aperture of the restricted collimation device located close to the cell orifice. To take into account these vapours deposit effects, we ended systematically each run by 2 measurements at low temperature (650 K to 660 K) in order to calculate the correction to be applied to the few measurements performed in the high temperature range due to partial clogging of the field aperture.

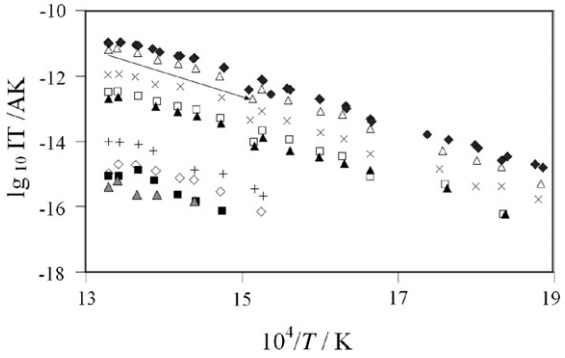

FIGURE 6. Evolution of ionic intensities detected by HTMS for the vaporization of CsOH(s,l) (Exp.CsOH-07,Gold cell). ◆: Cs^+, △: Cs_2OH^+, ×: CsOH, □: Cs_2O^+, ▲: Cs_2H^+, +: $Cs_3O_2H_2^+$, ◇: CsO^+, ■: $Cs_3O_2H^+$, ⧋: CsH^+.

3.2. Melting temperature of pure CsOH(s)

The solid–liquid phase change appears clearly as a plateau in both the IT products and the temperature as a function of time (figure 7). The corresponding mean temperature of this plateau is 647 K. In comparison with the melting point of CsOH(s) (considered pure) given by Rollet *et al.* [16] *i.e.* $T_m = 623$ K, our melting point is higher. Consequently, the melting point given by Rollet *et al.* may not correspond to a pure CsOH(s) and presence of traces of water in their samples for DTA analysis may explain the difference with our results. By comparison, Rollet *et al.* [23] also studied the solid–liquid phase diagram of $RbOH–H_2O$. Looking at the phase diagram shape close to the melting point for the RbOH compound, contrary to $CsOH–H_2O$ the water distillation of $RbOH–H_2O$ seems to proceed easier since no inflexion of the liquidus curve at the final stage of purification for small concentrations of water in RbOH was observed (a straight line is observed). We believe that Rollet *et al.* [16] had problems in the final purification stage of $CsOH–H_2O$. We measured the corresponding melting temperature of CsOH(s) for each run which was determined to range within 647 to 651 (±2 K).

3.3. Gaseous phase composition

The essential point in mass spectrometry is to relate each ion observed to its molecule of origin. In fact, ions can be parent ions obtained by simple adiabatic ionization process:

$$CsOH(g) + e^- \rightarrow CsOH^+ + 2e^- \quad (8)$$

or fragment ions obtained by dissociation ionization process:

$$CsOH(g) + e^- \rightarrow Cs^+ + OH(g) + 2e^- \quad (9)$$

To distinguish these various processes, we can use different methods:

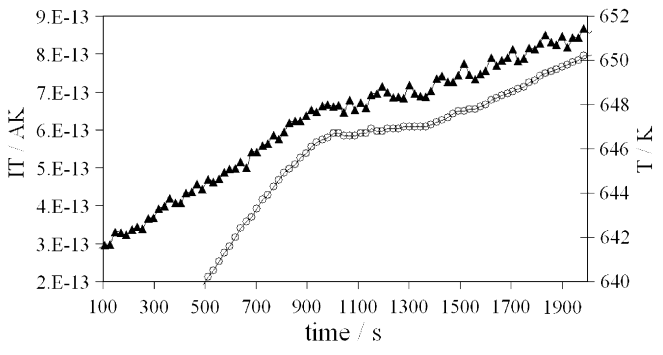

FIGURE 7. Observed melting temperature of CsOH(s) to CsOH(l) when increasing the temperature of the cell. ▲: IT product, ○: Temperature.

- Determination of the appearance potentials of each ion (for the parent ion it is the ionization potential).
- Breaks in the shape of the ionization efficiency curves.
- Study of the ions ratios as a function of chemical variations in the system under study (temperature, concentration, saturation, or non-saturation, *etc.*).

Using the ionization efficiency curves (figure 8), the appearance potential for ionization of the different ions were estimated (table 3) and their relative proportions summarized in table 4. For the Cs^+ ion, we observed an early slow increase as early as 4.6 V (the ionization potential of Cs(g)) with a very low intensity, about 10^{-4} to 10^{-3} times the maximum of the curves). This may be related to a very small proportion of Cs(g) in the vapour. Then at a potential of 7.6 V, Cs^+ ion intensity increased promptly. Gorokhov *et al.* [2] proposed an apparition potential of 7.6 ± 0.15 V for Cs^+ ion coming from CsOH(g) with much better ionization efficiency curve shapes close to the appearance potential. Logarithms of the product IT (proportional to the partial pressure) as a function of the inverse of the temperature were plotted and ions for which these curves behave in a strictly parallel way come from the same molecule. It is the case of the ions Cs^+ and $CsOH^+$ which thus come from CsOH(g). The same feature was observed for the ions Cs_2O^+ and Cs_2OH^+, which come from the dimer $Cs_2O_2H_2$(g). This analysis was already made by other authors [3,7]. The presence of a significant number of fragment ions implies, in the quantitative determination runs, carrying out a systematic recording of all the ions in order to calculate the total intensity resulting from each molecule. This is a prerequisite for applying the "additivity" rule in the estimates of the relative ionization cross-section [10]. After analyzing the ionization efficiency curves as well as studying the ions origins, we conclude that the vapour phase is composed by: CsOH(g), $Cs_2O_2H_2$(g), $Cs_3O_3H_3$(g) and traces of H_2O (<100 ppm) at the beginning of any run. However, there is no significant Cs(g) in the vapour contrarily to the observation of Schoonmaker and Porter in case of stainless steel containers, a feature that have been attributed by the authors to the reducing action of the container material. This Cs(g) could also come from contributions of outer surface re-

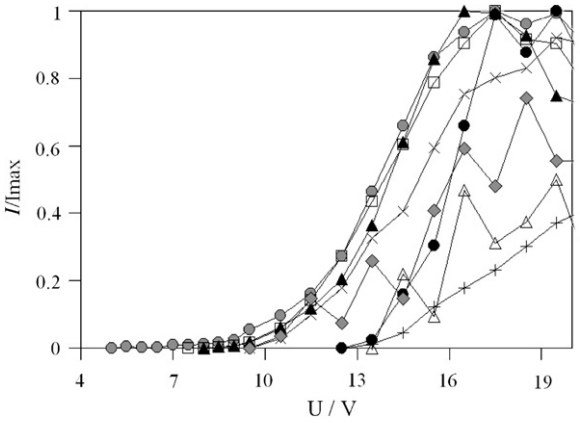

FIGURE 8. An example of the ionization efficiency curves obtained during the MS vaporization of CsOH in a cell of Gold. ◯: Cs^+, □: Cs_2OH^+, ▲: $CsOH^+$, ×: Cs_2O^+, △: CsO^+, ●: Cs_2H^+, ◇: $Cs_3O_2H_2^+$, +: H_2O^+.

TABLE 4
Ions detected by HTMS, their origins and relative proportions

Detected ions	Molecular origins	Ratio at 720 K and 24 V
Cs^+	CsOH(g), $Cs_2O_2H_2$(g)	8.7
$CsOH^+$	CsOH(g), $Cs_2O_2H_2$(g)	1
CsO^+	CsOH(g), $Cs_2O_2H_2$(g)	$1.25 \cdot 10^{-3}$
CsH^+	CsOH(g)	
Cs_2OH^+	$Cs_2O_2H_2$(g)	5.73
Cs_2O^+	$Cs_2O_2H_2$(g)	0.3
Cs_2^+	Not detected	
Cs_2H^+	$Cs_2O_2H_2$(g)	0.18
$Cs_3O_2H^+$	$Cs_3O_3H_3$(g)	$6 \cdot 10^{-4}$
$Cs_3O_2H_2^+$	$Cs_3O_3H_3$(g)	$7.5 \cdot 10^{-3}$
H_2O^+	H_2O^a	$<10^{-3}$

For water the value corresponds to the beginning of the experiment, since it disappeared during the run.

[a] From sample only by use of the shutter.

TABLE 3
Appearance potentials (V) of measured ions, working potentials used in our different experiments and comparison with the appearance potentials of Cs^+ and $CsOH^+$ ions given by Gorokhov *et al.* [2]

Gaseous ions species	Cell in Ni		Cell in Pt–Rh		Cell in Gold		Gorokhov *et al.*
	Apparition potential (V)	Work voltage (V)	Apparition potential (V)	Work voltage (V)	Apparition potential (V)	Work voltage (V)	Apparition potential (V)
CsH^+			10.1	32	12	24	
Cs^+	4.6 to 7.6	38	5.6 to 7.6	32	5.5 to 7.5	24	7.6 ± 0.15
$CsOH^+$	7.6	38	7.6	32	8.5	24	7.4 ± 0.15
CsO^+					14.5	24	
Cs_2OH^+	6.6 to 7.6	36			8.5	24	
Cs_2O^+	9.1	36			10	24	
Cs_2H^+	13.1	36			13	24	
$Cs_3O_2H^+$	8.1	36	8.6	32	12.5	24	
$Cs_3O_2H_2^+$			8.6	32	10	24	

Potential scale was calibrated with H_2O at the beginning of the experiments, then water disappeared. Usual accuracy is ±0.5 V at best.

vaporizations which occur mainly under non-saturated conditions and with reducing conditions in metallic furnaces.

3.4. Thermodynamic calculations

Partial pressures mass spectrometric measurements lead to the determination of the equilibrium constant K_p for any reaction, which is directly related to the standard enthalpy of the reaction $\Delta_r G^\circ_T$ by relation:

$$\Delta_r G^\circ_T = -RT \ln K_p = \Delta_r H^\circ_T - T\Delta_r S^\circ_T. \quad (10)$$

Second and third law of thermodynamics were used to calculate the reactions enthalpies at 298 K. Enthalpy increments and free energy functions (Fef) come from tabulated values in the Gurvich *et al.* compilation [11] for the CsOH(s, and l), and CsOH(g), $Cs_2O_2H_2$(g) molecular gaseous species. In third law results, the number of obtained enthalpy values is equal to the number of original data and these enthalpy values should be distributed around a constant mean value. If some trend is observed as a function of temperature either the sensitivity or Fef could be incriminated [10].

3.5. Thermodynamic results

3.5.1. The dissociation of the dimer

Taking into account the composition of the vapour phase, the main studied reaction is the reaction of dissociation of the dimer $Cs_2O_2H_2$(g):

$$(CsOH)_2(g) = 2CsOH(g) \quad (11)$$

The accurate knowledge of the equilibrium constant of this reaction will make it possible to perform calculations from any other result of total pressure measurements. An example of 2nd law is presented in figure 9. The enthalpies of reaction resulting from the 3rd law calculation are presented in figure 10 as a function of the measurement temperature. A summary of our $\Delta_r H^\circ$ (298 K) determinations according to the 2nd and 3rd law calculations is presented in table 5. Figure 9 presents the measured dissociation constant K_d as a function of temperature, pressure values were

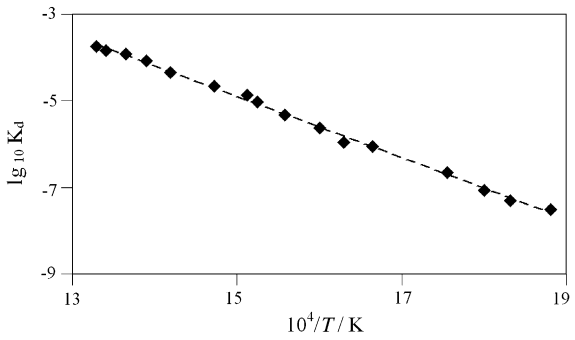

FIGURE 9. Results using 2nd law of thermodynamics for the dissociation reaction of the dimer: $Cs_2O_2H_2(g) \leftrightarrow 2CsOH(g)$ (Exp. CsOH-07 s, gold cell). ◆: Corrected pressure data which takes into account the correction for deposit of the vapours on the field aperture and mass loss from surface diffusion phenomenon.

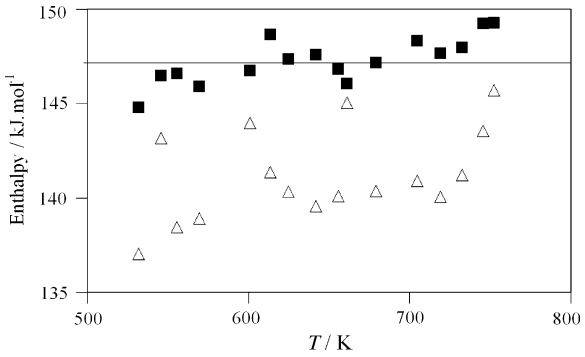

FIGURE 10. 3rd law results for the dissociation of dimer: $Cs_2O_2H_2(g) \leftrightarrow 2CsOH(g)$ (Exp. CsOH-07 s, gold cell). △: Experimental data. ■: Corrected pressure data which takes into account the correction for deposit of the vapours on the field aperture and the surface diffusion phenomenon in the mass loss.

TABLE 5
Summary of 2nd and 3rd law results at 298 K for the reaction $Cs_2O_2H_2$ (g) = 2CsOH(g) using different cells materials and their standard deviations

Material cell	Experience label	Temperature range/K	$\Delta_r H^{298\,K}/(kJ \cdot mol^{-1})$	
			2nd law	3rd law
Ni[a]	CsOH-02 s	515 to 761	133.6 ± 3.1	145.9 ± 1.9
Pt–Rh[b]	CsOH-04 s	496 to 765	134 ± 1.6	144.4 ± 1.5
	CsOH-05 s	522 to 758	134.6 ± 9.1	149.3 ± 4.4
Au[a]	CsOH-06 s	531 to 753	135.9 ± 3.3	149 ± 1.9
	CsOH-07 s	530 to 753	138 ± 1.8	147.3 ± 1.2
Average value ± total evaluated uncertainty[c]			135.4 ± 5.9	146.6 ± 7.3

Exp. CsOH-05 s has been discarded in the mean value calculation because of sensitivity evolution directly related to the change of working potential during the experiment: in a temperature range (693 to 723) K (45 V) rather than 32 V. Consequently, the measured intensity for each gaseous species was higher. Using the ionization efficiency curves, we recalculated the corresponding intensity at 32 V introducing larger uncertainties.

[a] Pure material.

[b] 20% Rh.

[c] See appendix A and B for calculation of total evaluated uncertainty.

corrected for partial clogging of the field aperture, otherwise the impact on the slope would be high since the 2nd law is very sensitive to trends in experimental errors. Figure 10 displays the third law enthalpies of the dissociation reaction at 298 K as a function of temperature. As shown in table 5, the standard deviation in the third law results is smaller (as usual in mass spectrometry). The difference between the 2nd and 3rd law results is due to the fact that the second law is very sensitive to systematic experimental errors – not taken into account in a conventional derivation – either during each run or due to the chemistry of the system under investigation. The total uncertainty per experiment is calculated when taking into account every operation or parameter used in the enthalpy calculation (see appendix A and B). The final retained total uncertainty is calculated with the assumption of compensation of the errors including also the standard deviation (S_d) of all the enthalpies values as explained in appendix A and B.

The mean enthalpy value from 2nd and 3rd law of thermodynamics calculations in our different experiments, discarding the 05 experiment (see table 5), is:

- 2nd law: $\Delta_r H(298\ \mathrm{K}) = 135.4 \pm 5.9\ \mathrm{kJ \cdot mol^{-1}}$.
- 3nd law: $\Delta_r H(298\ \mathrm{K}) = 146.6 \pm 7.3\ \mathrm{kJ \cdot mol^{-1}}$.

The quoted uncertainties being the total evaluated ones. Regarding these uncertainties, the second law seems more accurate but we cannot explain the large difference between the two laws. Systematic difference observed between second and third law results could come from too main features, – (i) temperature effects, *i.e.* self-cooling of the sample surface due to insufficient heat flow provided in this low temperature range to compensate the vaporization flow, (ii) chemical effect, *i.e.* non-reversible vaporization due to low evaporation coefficient [24] or composition evolution in the H_2O–Cs_2O pseudo-binary system. The temperature effect occurrence seems less probable for the following reasons:

- This effect has been observed with better resolution in activity measurements of Ag–Ge system using the multiple cell method [25] and was explained at that time by competition between provided radiation heat flow at the surface of the sample (liquid) and vaporization heat flow associated to effusion flow, neglecting conduction heat flow. The departure of the measured pressure from the expected one from thermodynamic law does not show a regular trend but a threshold effect since the effused flow evolution is exponential with temperature, while the heat conduction and radiation are proportional to temperature gradient between the surface and the walls. Figures 6 and 9 provided as examples do not show such thresholds.
- This effect should depend on the shape of the cell. As shown in figure 2, the Pt/Rh cells were longer than the Ni or Au cells – the wall surface was increased by a factor 2. Although the cell section and the mass of the samples were quite the same, we did not observe any smaller differences between the two 2nd and 3rd law results than for other cells.
- The main characteristic of effusion cells is not the orifice size but the ratio $(s \cdot C)/S$ as defined in table 2. This ratio not only fixes the quality of the molecular flow equilibrium [24] in the cells, but is analogous to the black-body conditions: large orifices correspond to large cells to compensate for radiation of orifices.
- Some systematic residual trends are observed in third law results (see figure 10 for example) which could be associated to temperature gradients. This evolution should be according to the derivation of third law relation:

$$\partial H^{\circ}_{298} = \partial T(-R \ln K + \Delta \mathrm{Fef}^{\circ}). \tag{12}$$

As the term in parenthesis is positive, any decrease of the surface temperature – $\delta T = T_{\mathrm{surf}} - T_{\mathrm{meas}} < 0$ – would decrease the third law result, contrarily to what is observed.

The chemical effect may have two origins:

- Non-reversible evaporation due to low value for the evaporation coefficient. According to equations as presented in reference [24] our $(s \cdot C)/S$ ratio implies a very low value for evaporation coefficient *i.e.* $\leqslant 0.05$, which seems unlikely since the rare tentative to determine evaporation coefficients for pure liquids [26] concluded that these values are close to 1. This feature is explained by the rapid adsorption and desorption of vapours on disordered or defects surfaces. Moreover, usually the associated activation enthalpy favours the decrease of the pressure gap when temperature increases, contrarily to our observations for CsOH vaporization.
- CsOH is not a pure compound but a mixture in the pseudo-binary H_2O–Cs_2O system. Consequently, the congruent vaporization of CsOH(s, or l) cannot correspond rigorously to a "line" compound since the vapour phase may contain small amounts of H_2O(g) or Cs(g), *etc*. that show small departures from the CsOH composition. Following this congruent line as a function of temperature, the activity of CsOH may vary according to the thermodynamics of "indifferent" states [27]. The evolution of the congruent line for a liquid has been discussed for the U–O liquid phase in reference [28]. In the case of the H_2O–Cs_2O liquid system, there is some high probability that the congruent line composition goes towards Cs_2O rich compositions due to higher volatility of H_2O in this system. Consequently, small amounts of Cs(g) should vaporize.

The correct evaluation of this last feature is related to the knowledge of the thermodynamics of the Cs–O–H ternary system and its H_2O–Cs_2O pseudo-binary system which would be interesting to study also in the framework of nuclear accident since the water vapour content is in excess and condensates as solutions for decreasing temperatures.

As proposed by Drowart *et al.* [10] in recent analysis of the mass spectrometric method, we retain the third law enthalpy results that are less sensitive to systematic errors not detectable by definition. This procedure could be applied only because the free energy functions for the gaseous molecules are assumed to be reliable enough to apply the third law calculations. Indeed, trends in third law measurements were observed to be very small. Gurvich *et al.* [11] chose in their compilation a value of enthalpy obtained by the 3rd law of thermodynamics using the $CsOH(l) + CsOH(g) = (CsOH)_2(g)$ isomolecular reaction with a fixed dimer/monomer pressure ratio equal to 0.2 (mean geometrical value) at a mean temperature. The enthalpy of dissociation of the dimer is deduced to be $\Delta_r H(298\ K) = 141 \pm 11\ kJ \cdot mol^{-1}$. The difference with our results remains significant although the two values lies within their respective uncertainty ranges.

3.5.2. Monomer vaporization

Among the three reactions observed by mass spectrometry – dissociation of the dimer, vaporization of the monomer and vaporization of the dimer – only two are independent reactions. As we have chosen to study the dissociation of the dimer, the other independent reaction must be selected as a function of the *a priori* minimum associated uncertainties. For this reason, we choose the monomer vaporization:

$$CsOH(s,l) = CsOH(g) \quad (13)$$

Since this molecule seems more important in the gas phase, and consequently its weight on the mass loss is more important in the calibration procedure. 2nd and 3rd law calculations with their standard deviations for the reaction of vaporization of monomer are summarized in table 6. The mean enthalpy value from 2nd and 3rd law of thermodynamics calculations in our different experiments, discarding the 05 experiment, is:

- 2nd law: $\Delta_{subl}H\ (298\ K) = 146.8 \pm 11.7\ kJ \cdot mol^{-1}$.
- 3rd law: $\Delta_{subl}H\ (298\ K) = 163.3 \pm 6.5\ kJ \cdot mol^{-1}$.

The uncertainty estimated for each experiment is summarized in appendix B (table B2). Using the formation enthalpy selected by Gurvich *et al.* for CsOH(s, 298 K) equal to $-416.2 \pm 0.5\ kJ \cdot mol^{-1}$ and retaining the third law enthalpy we propose:

$$\Delta_f H(CsOH, g, 298\ K) = -252.7 \pm 6.5 \text{ (total evaluated uncertainty) } kJ \cdot mol^{-1}.$$

Using the enthalpy of formation of CsOH(g) as well as the enthalpy of dissociation of the dimer $Cs_2O_2H_2(g)$, we calculated the enthalpy of formation of the dimer:

$$\Delta_f H(Cs_2O_2H_2, g, 298\ K) = -652 \pm 11.7 \text{ (total evaluated uncertainty) } kJ \cdot mol^{-1}.$$

Although our dissociation enthalpy is significantly different from the one proposed by Gurvich *et al.*, the present proposed values for the enthalpies of formation of the monomer and dimer agree due to compensation of errors.

4. Conclusion

The vaporization of CsOH(s,l) in view of determining the composition of the gaseous phase as well as the thermodynamic properties of the existing molecules has been performed using new and improved experimental tools in order to circumvent the numerous difficulties that preceding researchers encountered in the high temperature study of this hydroxide by mass spectrometry. These efforts concerned:

- The preparation of the compounds and the monitoring of the final stage of water distillation in relation with the determination of a new melting temperature.
- The use of different cells materials in view of chemical analysis of crucible physico-chemical interactions with CsOH and determinations of surface diffusion contributions to the genuine effusion flow.
- The use of restricted collimation device in order to monitor the only genuine effusion phenomenon.
- The use of *in situ* liquid nitrogen cooled ionization chamber in order to discard any disturbing re-vaporization processes in the ionization chamber during measurements.

TABLE 6
Summary of 2nd and 3rd law results at 298 K obtained for the reaction CsOH (s,l) = CsOH(g) using different cells materials and their standard deviations

Material cell	Experience label	Temperature range/K	$\Delta_r H^{298\ K}/(kJ \cdot mol^{-1})$	
			2nd law	3rd law
Ni[a]	CsOH-02 s	515 to 761	136.3. ± 1.9	163.9 ± 3.4
Pt–Rh[b]	CsOH-04 s	496 to 765	140.3 ± 1.5	160.1 ± 2.2
	CsOH-05 s	522 to 758	150.7 ± 0.8	163.3 ± 1.1
Au[a]	CsOH-06 s	531 to 753	153.3 ± 0.9	164.7 ± 1
	CsOH-07 s	530 to 753	157.4 ± 0.8	164.4 ± 0.6
Average value ± total evaluated uncertainty [c]			146.8 ± 11.7	163.3 ± 6.5

[a] Pure material.
[b] 20% Rh.
[c] See appendix A, B and C for calculation of total evaluated uncertainty. Exp. CsOH-05 s has been discarded in the mean value calculation for the same reasons as explained before in table 5.

- A careful analysis of all the fragments ions contribution to the ionization process of the molecules.
- A configuration of the mass spectrometer that reduces the number of parameters in the calibration procedure to the only ionization cross-section ratios.
- The selection of the two main independent reactions – *i.e.* dissociation of the dimer and vaporization of the monomer – that led to minimal uncertainties.
- The systematic use of the third law calculations which are known to be more reliable compared to second law results more sensitive to undetected systematic errors.
- A careful estimate of the total uncertainties associated with our two studied reactions.

As concluded earlier by Gurvich *et al.*, the CsOH compound was the less reliable one (altogether with RbOH) in the alkaline hydroxide series, and the present study brings more information on the vaporization behavior and we propose improved and more reliable thermodynamic data for the monomer CsOH(g) and the dimer $Cs_2O_2H_2$(g). This work provides sound basis for the thermodynamic study of the more complex Cs, I, O, H system.

Acknowledgements

This program is conducted within the framework of the International Source Term Program, funded by IRSN, EDF[a], CEA[b], European Commission, USNRC[c], Suez-Tractebel, AECL[d] and PSI[e]. [a] Electricité de France, [b] Commissariat à l'Energie Atomique, [c]US Nuclear Regulatory Commission, [d]Atomic Energy Canada Limited, [e]Paul Scherrer Institut.

Appendix A. Total uncertainty estimates for the dissociation of the dimer

Studied reaction: $Cs_2O_2H_2\ (g) = 2CsOH(g)$

A.1. Uncertainty on 3rd law determinations

From the following relation:

$$\Delta_r H^\circ_T = -RT\ln K_p - T\Delta \mathrm{Fef}^\circ_T. \tag{A1}$$

The uncertainty on 3rd law determination can be obtained by derivation

$$\partial(\Delta H^\circ_{298}) = \partial T(-R\ln K_p + \Delta \mathrm{Fef}^\circ(T)) + RT(\mathrm{d}K_p/K_p) + T\partial(\Delta \mathrm{Fef}^\circ(T)), \tag{A2}$$

where

$$(-R\ln K_p + \Delta \mathrm{Fef}^\circ) = \Delta_r H^\circ_{298}/T_{\mathrm{mean}}, \tag{A3}$$

The uncertainty on the equilibrium constant K_p is related to the total uncertainty on the products IT and on the sensitivity for each gaseous species (υ_i being the stoechiometric coefficient of each gas):

$$\partial K_p/K_p = \upsilon_i \sum \partial IT/IT + \upsilon_i \sum \partial S/S. \tag{A4}$$

The uncertainty on the sensitivity S can be obtained from the calibration by mass loss:

$$\partial S/S = \sum \partial\sigma/\sigma + \sum \partial\Delta m/\Delta m + \sum \partial C/C + \sum \partial s/s + \sum \partial \int IT^{1/2}\,\mathrm{d}t/\int IT^{1/2}\,\mathrm{d}t, \tag{A5}$$

which is a function of the total uncertainties on the ionization cross-sections, the mass loss, the Clausing coefficient, the section of the orifice cell and the products $IT^{1/2}\,\mathrm{d}t$.

A.2. Uncertainty on 2nd law determination

The uncertainty on the 2nd law determinations is given by the following relations:

$$\mathrm{d}(\ln K_p)/\mathrm{d}(1/T) = -\Delta_r H^\circ_T/R, \tag{A6}$$

$$\partial K_p/K_p = (\Delta H^\circ/R)\cdot(\partial T/T^2) \quad \text{or} \quad \Delta H^\circ = (RT^2/\partial T)\cdot(\partial K_{IT}/K_{IT}), \tag{A7}$$

$$\partial \Delta H^\circ_{Tm} = 2RT_m\cdot(\partial K_{IT}/K_{IT}) = 2RT_m \sum \upsilon_i(\partial I_i T/I_i T). \tag{A8}$$

This uncertainty does not take into account any other kind of uncertainty like systematic errors due to trends in temperature or in ionic intensity measurements.

Appendix B. An example of uncertainties calculation: Gold crucible (Exp.CsOH-07 s)

B.1. Uncertainty on 3rd law determinations

According to the relation (A2):

$$(-R\ln K_p + \Delta \mathrm{Fef}^\circ) = 230.8\ \mathrm{J\cdot mol^{-1}\cdot K^{-1}}$$

where $\Delta_r H^\circ_{298} = 147.3\ \mathrm{kJ\cdot mol^{-1}}$ and $T_{\mathrm{mean}} = 638\ \mathrm{K}$.

B.1.1. Uncertainty on temperature δT

The uncertainty on the temperature is directly related to:

- Thermocouple positioning/cell (considered correct, as seen in figure 1).
- Manufacturer accuracy (≈1 to 2) K.
- Uncertainty due to total T change during a temperature plateau ⩽6 K.
- Electric monitoring line according to HP data acquisition booklet (including the cold reference temperature) ≈ 1.8 K.

So the total δT can be estimated to ≈7 K

B.1.2. Uncertainty on the equilibrium constant K_p

B.1.2.1. Uncertainty on the product IT. It can be obtained from the relation:

$$\upsilon_i \sum \delta IT/IT = \upsilon_i \sum \delta I/I + \delta T/T. \quad \text{(A9)}$$

The uncertainty on the intensities is obtained from the following relation:

$$\upsilon_i \sum \delta I/I = 2(\delta I/I)_{\text{mono}} + (\delta I/I)_{\text{dim}}. \quad \text{(A10)}$$

The uncertainty for intensities is calculated from the ion monomer ($CsOH^+$) and the ion dimer (Cs_2OH^+) intensity measurements (from maximum deviations in pulse counting mode) at high and low temperature (high T (746 K): $(\delta I/I)_{\text{total}} = 10\%$ and low T (355 K): $(\delta I/I)_{\text{total}} = 46\%$). We have to quote that the uncertainty on the dimer contribution at low T are 10 times higher than for the monomer.

B.1.3. Uncertainty on the sensitivity

According to the relation (A4), the uncertainty on the sensitivity is the sum of the following uncertainties:

1. The uncertainty on the ionization cross-section ratio is estimated to 34% as the ratio $\sigma_{\text{dimer}}/\sigma_{\text{monomer}}$ could vary from 2 to 1.5 as observed in mass spectrometry [10].
2. The uncertainty on the Clausing coefficient $\delta C/C$ is lower than 1% as estimated in [29]. We choose a value of 0.7%.
3. According to our visual observation, the uncertainty on the section of the effusion orifice is estimated to 0.05%.
4. The uncertainty on the sum of the products $\sum IT^{1/2}\delta T$ takes into account the uncertainty due to temperature plateaus for measurements and to intervals due to intermediate regimes – increasing or decreasing temperatures – when using the trapeze method. In this method, during intermediate regimes, the sample temperature is necessarily different from the thermocouple temperature located in the envelope and the two measured quantities – I and T – do not correspond. Moreover, the trapeze method underestimates or overestimates the products $IT^{1/2}\delta T$ when, respectively, increasing and decreasing the temperature.

Usually at high temperature the intermediate regimes contribute to a small part (sometimes neglected) of the total mass loss because the time for thermal equilibration is short compared to plateau's time for measurements of all species. At low temperature, the proportion is reversed (equilibration time here is about 1 h 30 min) and the error in the trapeze method becomes relatively important. In order to evaluate this error, we randomly monitored the main intensity during intermediate regimes – up and down. For other intermediate regimes we did not monitor the evaporated species by moving the cell position out of the source axis in order to prevent the field aperture from clogging. Finally, we evaluated the relative difference of area according to the relation:

$$A = \left(\int IT^{1/2}\,\mathrm{d}t(\text{real}) - IT^{1/2}\,\mathrm{d}t(\text{trapeze}) \right) \Big/ IT^{1/2}\,\mathrm{d}t(\text{trapeze}). \quad \text{(A11)}$$

The mean total value of A is about 11%. Weighting the intermediate regimes error by the sum $\sum IT^{1/2}\delta T$ for this experiment, we obtain a final uncertainty equal to ±4.7%. For the different experiments, the proportion varied from 0.8 to 15%.

B.1.4. Uncertainty on mass loss $\delta(\Delta m)$

The uncertainty on mass loss is related to:

- Balance accuracy which is negligible.
- Transfer time influence (mass spectrometer → to balance): we tested the mass gain of the product when it is stored in a drier and we observed that the mass gain of the sample between the MS opening and the weighting was not measurable. So the uncertainties due to transfer time influence is considered to be negligible (the sample is a bulk solid).
- Uncertainty on the flow out at the orifice cell (tested by cleaning and weighting) has been evaluated to 3% maximum.
- Surface diffusion process contribution was already taken into account in the thermodynamics calculations of each experiment.

So in this experience the total mass loss uncertainties can be estimated to 3% for the genuine effusion process.

B.1.5. Uncertainty on the free energy functions $\delta\Delta Fef(T)$

Using Gurvich *et al.* thermodynamics tables [11], the free energy function uncertainty at the mean temperature of our experiments is for the monomer $\delta Fef_m(CsOH(g)) = \pm 0.56\ \text{J}\cdot\text{mol}^{-1}\cdot\text{K}^{-1}$ and for the dimer $\delta Fef_m(Cs_2O_2H_2(g)) = \pm 1.77\ \text{J}\cdot\text{mol}^{-1}\cdot\text{K}^{-1}$. So when multiplying by the mean temperature, the uncertainty on the ΔFef of the reaction of dissociation of the dimer is:

$T\delta\Delta Fef(T) = \pm 1.24\ \text{kJ}\cdot\text{mol}^{-1}\cdot\text{K}^{-1}$ when applying a compensation of the uncertainties.

Table B1 summarizes the uncertainty on each parameter for this experiment. Finally, we obtained for this experi-

TABLE B1
Uncertainties on each parameter leading to the 2nd and 3rd law uncertainties determination for the experiment CsOH-07 s in Gold cell

Independent uncertainties	Value
δT	7.18
$\sum \delta I/I$ monomer	0.04
$\sum \delta I/I$ dimer	0.27
$\sum \delta\sigma/\sigma$	0.34
$\sum \delta\Delta m/\Delta m$	0.03
$\sum \delta C/C$	0.007
$\sum \delta s/s$	0.0005
$\sum \delta\left[IT^{1/2}\,\mathrm{d}t\right/\int IT^{1/2}\,\mathrm{d}t$	0.047
$\delta S/S$	0.35
$\delta K_p/K_p$	0.45
$\delta\Delta$Fef	1.94

TABLE B2
Summary of 2nd and 3rd law results with their total estimated uncertainties obtained for the reactions: $Cs_2O_2H_2(g) = 2CsOH(g)$ and CsOH (s,l) = CsOH(g) using different cells materials

Material cell	Experience label	Temperature range/K	$\Delta_rH^{298\,K}/(kJ\cdot mol^{-1})$			
			$Cs_2O_2H_2(g) = 2CsOH(g)$		CsOH (s,l)=CsOH(g)	
			2nd law	3rd law	2nd law	3rd law
Ni[a]	CsOH-02 s	515 to 761	133.6 ± 3.6	145.9 ± 4.9	136.3. ± 2.3	163.9 ± 4.1
Pt–Rh[b]	CsOH-04 s	496 to 765	134 ± 1.7	144.4 ± 4.9	140.3 ± 1	160.1 ± 4.5
	CsOH-05 s	522 to 758	134.6 ± 1.9	149.3 ± 4.5	150.7 ± 1	163.3 ± 3.9
Au[a]	CsOH-06 s	531 to 753	135.9 ± 6	149 ± 6.3	153.3 ± 1.8	164.7 ± 4.5
	CsOH-07 s	530 to 753	138 ± 3	147.3 ± 5.3	157.4 ± 0.5	164.4 ± 4.4
Average value ± total evaluated uncertainty[c]			135.4 ± 5.9	146.6 ± 7.3	146.8 ± 11.7	163.3 ± 6.5

[a] Pure material.
[b] 20% Rh.
[c] Exp. CsOH-05 s has been discarded in the mean value calculation as already explained in table 5.

ment (CsOH-07 s) the uncertainty on the third and second laws determination:

$$\delta\Delta_dH_{298}\ (2nd\ law) = \pm 3\ kJ\cdot mol^{-1}.$$
$$\delta\Delta_dH_{298}\ (3rd\ law) = \pm 5.3\ kJ\cdot mol^{-1}.$$

The uncertainty related to each experiment is summarized in table B2.

The total uncertainty for the mean value retained from our set of experiments is calculated with the assumption of compensation of the errors including also the standard deviation of the set of enthalpies values according to the relation:

$$\delta\Delta_rH_m(298) = \left\{\left(\delta\Delta_rH^2_{(Ni\text{-}02)} + \delta\Delta_rH^2_{(Pt\text{-}04)} + \delta\Delta_rH^2_{(Au\text{-}06)} + \delta\Delta_rH^2_{(Au\text{-}07)}\right)\Big/4\right\}^{1/2} + S_d, \quad (A12)$$

where S_d is the standard deviation of the whole set of enthalpy values.

$$\delta\Delta_rH_{298}\ (2nd\ law) = \pm 5.9\ kJ\cdot mol^{-1}.$$
$$\delta\Delta_rH_{298}\ (3rd\ law) = \pm 7.3\ kJ\cdot mol^{-1}.$$

Appendix C. Total uncertainty estimates for the vaporization of monomer

Studied reaction: CsOH(s,l) = CsOH(g)

Same uncertainties calculations, as explained before for the reaction of dissociation of dimer, were performed for the reaction of vaporization of the monomer. The obtained results are summarized in table B2. According to the relation (A12), the total uncertainty obtained with the 2nd and 3rd law of thermodynamics is thus:

$$\delta\Delta_rH_{298}\ (2nd\ law) = \pm 11.7\ kJ\cdot mol^{-1}.$$
$$\delta\Delta_rH_{298}\ (3rd\ law) = \pm 6.5\ kJ\cdot mol^{-1}.$$

References

[1] R.J.M. Konings, E.H.P. Cordfunke, J. Chem. Thermodyn. 20 (1988) 103–108.
[2] L.N. Gorokhov, A.V. Gusarov, I.G. Panchenkov, Russ. J. Phys. Chem. 44 (1) (1970) 150–151.
[3] P.E. Blackburn, C.E. Johnson, J. Nucl. Mater. 154 (1988) 74–82.
[4] R.C. Schoonmaker, R.F. Porter, J. Phys. Chem. 64 (1960) 457–461.
[5] R.C. Schoonmaker, R.F. Porter, J. Phys. Chem. 62 (1958) 234–237.
[6] R.C. Schoonmaker, R.F. Porter, J. Phys. Chem. 62 (1958) 486–489.
[7] R.C. Schoonmaker, R.F. Porter, J. Chem. Phys. 31 (1959) 830–833.
[8] R.C. Schoonmaker, R.F. Porter, J. Chem. Phys. 28 (1958) 454–457.
[9] C. Chatillon, Rev. Métall.-CIT/Sci. Génie Matér. (1998) 1077–1099.
[10] J. Drowart, C. Chatillon, J. Hastie, D. Bonnell, J. Pure Appl. Chem. 77 (2005) 683–737.
[11] L.V. Gurvich, L.N. Gorokhov, G.A. Bergman, V.S. Iorish, V.Ya. Leonidov, V.S. Yungman, J. Phys. Chem. Ref. Data 26 (4) (1997) 1031–1109.
[12] P. Morland, C. Chatillon, P. Rocabois, J. High Temp. Mater. Sci. 37 (1997) 167–187.
[13] C. Chatillon, M. Allibert, A. Pattoret, J. High Temp. Sci. 8 (1976) 233–255.
[14] M. Heyrman, C. Chatillon, H. Collas, J.-L. Chemin, Rapid Commun. Mass Spectrom. 18 (2004) 163–174.
[15] M. Tmar, C. Chatillon, J. Chem. Thermodyn. 19 (1987) 1053–1063.
[16] A. Rollet, R. Cohen-Adad, C. Ferlin, Compt. Rend. Acad. Sci. Paris 256 (1963) 5580–5582.
[17] K. Motzfeldt, J. Phys. Chem. 59 (1955) 139–147.
[18] M. Heyrman, C. Chatillon, J. Phys. Chem. Solids 66 (2005) 494–497.
[19] J.W. Ward, M.V. Fraser, J. Chem. Phys. 50 (1969) 1877–1882.
[20] W.L. Winterbottom, J.P. Hirth, J. Chem. Phys. 37 (1962) 784–793.
[21] J.W. Ward, R.L. Bivins, M.V. Fraser, J. Vac. Sci. Technol. 7 (1970) 206–210.
[22] W.L. Winterbottom, J. Chem. Phys. 47 (1967) 3546–3556.
[23] A.P. Rollet, R. Cohen-Adad, M. Michaud, A. Tranquard, Compt. Rend. Acad. Sci. Paris 246 (1958) 3249–3251.
[24] G.M. Rosenblatt, in: N.B. Hannay (Ed.), Evaporation from Solids, in Treatise on Solid-State Chemistry VI. Surfaces, Plenum Press, New York, 1976, pp. 165–239.
[25] L. Martin-Garin, C. Chatillon, M. Allibert, J. Less-Common Met. 63 (1979) 9–23.
[26] G.M. Pound, J. Phys. Chem. Ref. Data 1 (1) (1972) 135–146.
[27] I. Prigogine, R. Defay, D.H. Everett, Chemical Thermodynamics, Longman, London, 1965, pp. 450–510.
[28] M. Baïchi, C. Chatillon, G. Ducros, K. Froment, J. Nucl. Mater. 349 (2006) 57–82.
[29] D.J. Santeler, J. Vac. Sci. Technol. A 4 (1986) 338–343.

CHAPTER II

PART II: CRITICAL ASSESSMENT OF THERMODYNAMIC DATA FOR CSOH GAS PHASE MOLECULES

II.1. INTRODUCTION

This work is part of the CHIP analytical program (in the framework of the International Source Term Program), the aim of which is to analyze with a high temperature mass spectrometer (HTMS) the behavior of gaseous vapors in condition as close as possible to those at the high temperature break of a primary cooling circuit of a nuclear reactor in case of severe pressurized water reactor accident. This analytical program has been undertaken in two ways: - (i) identification of existing gaseous molecules and analysis of their stability *i.e.* determination of their thermodynamic data, - (ii) analysis of non-equilibrium conditions in a high temperature reactor in order to determine kinetic data for molecules identified as undergoing some kinetic barrier.

The present study deals with the first step that is the thermodynamic study of the complex Cs-I-O-H system which has been chosen as the first candidate in the study of severe accident. The present work was undertaken in order to establish reliable thermodynamic properties for the gaseous phase of the Cs-O-H system which is one of the main component that transports Cesium under excess of water. Indeed, the reaction between gaseous Cesium and H_2O during severe nuclear accident produces Cesium Hydroxide which is one of the main component in the primary cooling lines either in the gas phase or in aerosols.

Owing to large discrepancies in the mass spectrometric results for CsOH gaseous phase, a preceding experimental effort was aimed first at the investigation of the pure CsOH(s,l) vaporization using High Temperature Mass Spectrometry “HTMS” [1] in order to clarify earlier difficulties encountered in these studies and to determine at a first step the gas composition and the dissociation enthalpy of the dimmer which were controversy. The present critical analysis aimed at the selection of reliable thermodynamic properties for the CsOH gaseous phase, starting from a preceding assessment performed by Gurvich et al. [2] which is enriched by more recent experimental works.

II.2. PRECEDING GURVICH ET AL. ASSESSMENT

In 1997, Gurvich et al. [2] collected and critically reviewed data on thermodynamic and molecular properties of alkaline hydroxides, particularly KOH, RbOH and CsOH (cr, liq, g). Tables of thermodynamic properties in condensed and gaseous states have been calculated using the results of their selection including also some estimated values. Their recommendations are compared with earlier evaluations given in the JANAF Tables [3] and in Thermodynamic Properties of Individual Substances by Gurvich et al. [4]. The considered properties are: the temperature and enthalpy of phase transitions and fusion, heat capacities, spectroscopic data and structures of gaseous molecules, bond energies and enthalpies of formation at 298.15 K.

For gaseous CsOH system, the molecular constants of monomer CsOH(g) and dimmer $Cs_2O_2H_2$(g) are well-established, and consequently C°_p (heat capacity), S°_T (standard entropy) and Fef°_T (free energy functions) are considered as reliable within their assigned uncertainties.

In order to obtain the enthalpy of formation of CsOH(g) and $Cs_2O_2H_2$(g), different reactions including these molecules have to be studied. Among them, the following ones can be quoted:

- dimmerization: $2CsOH(g) = Cs_2O_2H_2(g)$ (1)
- flame dissociation: $Cs(g) + H_2O(g) = CsOH(g) + H(g)$ (2)
- ionization process: $CsOH(g) + e^- = Cs^+ + OH(g) + 2e^-$ (3)

For studies in flames with simplified reactions set [5-7], the excited states are not necessarily identified when existing, and equilibrium conditions are difficult to ascertain. High Temperature Mass Spectrometry (HTMS) allows the direct determination of monomer and dimmer equilibrium constant K_d. The p(dimmer)/p(monomer) pressures ratio (p_2 / p_1) has been determined by different authors to vary from 0.7 [8], 0.07 [9-12] to ≈ 10^{-3} [9]. The last value has been discarded by Gurvich et al. due to “probable mass discrimination effects” *(sic)* in the quadrupole mass analyzer. As a compromise, Gurvich et al. chose the value $p_2 / p_1 = 0.2$ which is the geometrical mean of the minimum and maximum values 0.07 and 0.7 calculated according to the relation,

$$\bar{x} = \sqrt[n]{\prod_{i=1}^{n} x_i} \qquad (4)$$

This mean value has been taken constant in the range of mass spectrometric measurements (570-770 K) in order to obtain a mean third law enthalpy value for the isomolecular reaction,

$$CsOH(l) + CsOH(g) = Cs_2O_2H_2(g) \quad (5)$$

and using the assumption of internal compensations for the sensitivities – *i.e.* ionization cross sections times multiplier yields canceled-. Total ionic intensities as measured coming from the ionization of the CsOH(g) molecule have been taken into account (sum of the ions Cs^+ and $CsOH^+$) contrarily to the dimmer intensity which has been attributed to the only Cs_2OH^+ ion.

Our recent determinations [1] (4 experiments) of the dimmer to monomer pressure ratio show it varies from 0.14 to 0.6 within the above temperature range, and this feature leads to a value slightly different for the dimmerization enthalpy in comparison to Gurvich et al.. Thus, the mass spectrometric method remains the most appropriate one to determine the formation enthalpies of the two species (CsOH(g) and $Cs_2O_2H_2(g)$) or similarly the enthalpy of dimmerization.

In the Blackburn and Johnson work (1988) [9], Gurvich et al. retains the vaporization enthalpy of the monomer – corrected from the dimmer contribution which has been recalculated from their above retained mean value ($p_2 / p_1 = 0.2$) – as a reliable enthalpy value.

Konings and Cordfunke [10] by transpiration method determined the total cesium atoms transported by the gaseous phase ($p_{(apparent)} = p_1 + 2\,p_2$,) in the 676 to 976 K temperature range. They considered only the monomer contribution in their study because they could not separate the contributions of monomer and dimmer contrarily to Gurvich et al. who did it using their above selected values for dimmerization equilibrium constant. The deduced value for the CsOH(cr,l) = CsOH(g) reaction is in agreement with Blackburn and Johnson value corrected with the dimmer contribution in the same manner.

Finally, the Gurvich et al. proposed values for the enthalpies of formation of the gaseous monomer and dimmer are based on the choice of the p_2 / p_1 ratio mean value and the two works of Blackburn and Johnson [9] and Konings and Cordfunke [10]. As a partial

conclusion, considering that the compiled values are largely scattered, the Gurvich et al. estimated mean values seem proposed with quite optimistic uncertainties. The dimmerization equilibrium constant K_d and the p_2 / p_1 ratio values remains important key values. So, we considered that a new way for critical assessment is needed in conjunction with our new mass spectrometric study.

Original data leading to the dissociation energy of the Cs-OH bond have been revised by Gurvich et al. (flames [5-7], HTMS/Ionization processes [9-12], ab-initio calculation [13]) using third-law calculations on the basis of their selected data (Cp°, S°_T and Fef°_T, given with uncertainties). The obtained results for $\Delta_f H^\circ_{298.15}$ (CsOH, g) are presented in table II-1.

Authors	$D°_0$(Cs-OH)	$\Delta_f H^\circ$(CsOH,g) kJ.mol^{-1}
Smith and Sugden (Flames) [5]	381[a] ± 4	-269 ± 4
Jensen and Padley (Flames, linear molecule) [6]	380 [a] ± 12	-268 ± 12
Cotton and Jenkins (Flames, linear molecule) [7]	377 [a] ± 8	-265 ± 8
Gorokov et al. (HTMS, Born-Haber) [11]	357.6 [b] ± 12.6	-245.6 ± 12.7
Gorokov et al. (HTMS, isomolecular reaction) [11]	388.8 [c] ± 5.6	-276.8 ± 5.8
Emellyanov et al. (HTMS, Born-Haber)[12]	341 [b] ± 13.6	-229 ± 13.7
Bauschlicher et al. (ab-initio, ionic bond)[13]	365 [a] ± 10	-253 ± 10

[a] from Gurvich et al. compilation, $\delta D°_0$ original uncertainty; [b] calculated from the observed dissociative ionization at ≈ 900 K, Cs(g) and OH(g) data from NIST-JANAF Tables (1998)[3] and $\delta D°_0$ obtained from error compensation relation $\sqrt{\sum \delta x^2}$; [c] referred to KOH from Gurvich et al. compilation [2] , Cs(g) and K(g) data from NIST-JANAF Tables (1998)[3] and $\delta D°_0$ uncertainty estimated from original data, $\delta D°_0$(K-OH) from Gurvich et al. [2] and δfef from table 58 Gurvich et al. [2](1000 K) within $\sqrt{\sum \delta x^2}$ relation.

Table II-1 : Thermodynamic properties from authors cited in Gurvich et al. compilation [2]

II.3. CRITICAL ASSESSMENT OF THERMODYNAMIC DATA FOR THE GAS PHASE

II.3.1. CsOH(g) flames studies

In order to obtain the enthalpy of formation of CsOH(g), H_2 + O_2 + N_2 + CsOH (dopant) flames dissociation studies were performed assuming the main dissociation reaction (2):

$Cs(g) + H_2O(g) = CsOH(g) + H(g)$

Assumptions - based on this unique reaction or on a simplified set of elementary reactions - have been chosen for interpretation of measurements. Usually, CsOH is introduced in the

flames as a spray of diluted solution in water and the ionization of Cs into Cs^+ liberates electrons at high temperature. The proportion of Cs^+ is small as well as the CsOH(g) formed at equilibrium, and the introduced concentration of Cs is often chosen as a first approximation to be the existing one in the flame - sometimes including different species -. Different detection systems were used - electron concentration by attenuation method using radiofrequency waves [5], resonant cavity for electron concentration measurement, absorption spectroscopy for atoms [6] and double-beam atomic absorption using Cs hollow-cathode lamps [7] - .

Smith and Sugden (1953) [5] observed that the Saha relation for equilibrium ionization of alkaline components,

$$[CsOH] = Cs^+ + e^- + [OH] \quad (6)$$

was not observed for Rb and Cs hydroxides, even with a modified burner protecting the flame by a nitrogen flow against atmospheric interferences, or using different mixtures. As temperature uncertainties could not explain the difference between measurements and attended results, a competitive reaction was proposed, *i.e.* the electron capture by the hydroxyl radical,

$$OH + e^- \rightarrow OH^- \quad (7)$$

that decreases the electron concentration as detected by radio frequency. The enthalpies of the two reactions assumed to occur altogether – ionization of Cs and electron capture by OH^- were deduced from determination of the attenuation coefficient. But yet the electron affinity of OH was estimated to be 288.7 $kJ.mol^{-1}$ instead of 175.7 $kJ.mol^{-1}$ as presently retained from more recent and accurate measurements using laser methods as compiled by Lias et al. (1988) [14]. This difference implies that the OH^- concentration is underestimated, then the Cs^+ concentration overestimated. Finally the obtained value for the Cs-OH dissociation is overestimated as shown in table II-2 when compared to cotton and Jenkins [7] (at least 3 kJ) using a different method.

In fact, in this study the Cs-OH bond dissociation was not determined directly but referred to the Li-OH bond dissociation, these two metals having similar dissociation values. As a result, the authors assumed quite identical chemical behavior by comparison with NaOH which was

chosen to be entirely decomposed for calibration of the electron concentration in the flame. Thus, the CsOH dissociation was referred in a trend to LiOH dissociation which is well known (value so far unchanged).

Besides, the molecular parameters for the two molecules LiOH and CsOH – used in the pre-exponential factor of the equilibrium constant (partition function) – have been estimated by the authors. For this reason and using the presently known parameters – from JANAF98 [3] for LiOH and Gurvich et al. [2] for CsOH – free energy function has been recalculated by using JANAF formula for a linear polyatomic molecule [3] and compared to those calculated with the same manner by using Smith and Sugden molecular parameters for LiOH and CsOH [5]. The free energy function contribution difference into the dissociation energies has been calculated for the reaction LiOH(g) + Cs(g) → CsOH(g) + Li(g) with the following relations:

$$\Delta H^\circ_{0(Smith)} = -RTLnKp + T\Delta fef_{(Smith)} = D^\circ_0(Li-OH) - D^\circ_0(Cs-OH) \quad (8)$$

$$\Delta fef = fef_{(CsOH)} + fef_{(Li)} - fef_{(LiOH)} - fef_{(Cs)} \quad (9)$$

$$\Delta H^\circ_{0(corr)} = \Delta H^\circ_{0(Smith)} - T\Delta fef_{(smith)} + T\Delta fef_{(our\ cal.)} \quad (10)$$

$$T(-\Delta fef_{(Smith)} + \Delta fef_{(our\ cal.)}) = T\left[\left(-fef_{(CsOH)} + fef_{(LiOH)}\right)_{Smith} - fef^{\,Janaf}{}_{(Li)} + fef^{\,Janaf}{}_{(Cs)} + \left(fef_{(CsOH)} - fef_{(LiOH)}\right)_{our\ cal.} + fef^{\,Janaf}{}_{(Li)} - fef^{\,Janaf}{}_{(Cs)}\right] \quad (11)$$

$$T(-\Delta fef_{(Smith)} + \Delta fef_{(our\ cal.)}) = T\left[\left(-fef_{(CsOH)} + fef_{(LiOH)}\right)_{Smith} + \left(fef_{(CsOH)} - fef_{(LiOH)}\right)_{our\ cal.}\right] \quad (12)$$

$\Delta H^\circ_{0(corr)}$ is the corrected enthalpy, $\Delta H^\circ_{0(smith)}$ is Smith and Sugden enthalpy, $\Delta fef_{(smith)}$ the free energy function calculated with Smith and Sugden molecular parameters for CsOH(g) and LiOH(g), $\Delta fef_{\ our\ cal.}$ our recalculated free energy function using Janaf parameters for LiOH(g) and Gurvich et al. parameters for CsOH(g) (see appendix II-B), free energy functions of Li(g) and Cs(g) considered taken from Janaf tables [3].

The product $T(\Delta Fef_{(our\ cal.)} + \Delta Fef_{(Smith)})$ at the flame temperature (T = 2245 K) amounts to -16.7 kJ.mol^{-1} that has to be added to the proposed value by Smith and Sugden: D°_0 (Li-OH) - D°_0 (Cs-OH) = 46 - 16.7 = 29.3 kJ.mol^{-1} . The resulting dissociation energy D°_0 (Cs-OH) = 398.8 kJ.mol^{-1}. D°_0 (Li-OH) has been calculated from Janaf tables [3] for the dissociation reaction LiOH(g) → Li(g) + OH(g) at 0 K using the following relation:

$$D^\circ_0(Li-OH) = \Delta_f H_0(Li,g) + \Delta_f H_0(OH,g) - \Delta_f H_0(LiOH,g) \quad (13)$$

$\Delta Fef_0(i)$ is the formation enthalpy of the gas i (i = Li(g), OH(g) and LiOH(g)) at 0 K. The dissociation energy $D°_0$ (Li-OH) has been obtained to be 428.1 kJ.mol^{-1}. $D°_0$ (Cs-OH) has been transformed into $D°_{298.15\ K}$(Cs-OH) according to relation (14):

$CsOH(g) \rightarrow Cs(g) + OH(g)$ $\quad D°_0$ (Cs-OH) at 0 K

$CsOH(g) \rightarrow Cs(g) + OH(g)$ $\quad D°_{298.15}$ (Cs-OH) at 298.15 K

$$D°_{298.15}(Cs-OH) = D°_0(Cs-OH) + (H_{298.15} - H_0)Cs(g) + (H_{298.15} - H_0)OH(g) - (H_{298.15} - H_0)CsOH(g) \quad (14)$$

$D°_0$(Cs-OH) dissociation enthalpy at 0 K, $D°_{298.15}$(Cs-OH) dissociation enthalpy at 298.15K, $(H_{298.15}-H_0)$ enthalpy increment taken from Janaf tables for Cs(g)and OH(g) and from Gurvich et al. table for CsOH(g).

The formation enthalpy of CsOH(g) at 298.15 K has been calculated within the following relations:

$$D°_{298.15}(Cs-OH) = \Delta_f H_{298.15}(Cs,g) + \Delta_f H_{298.15}(OH,g) - \Delta_f H_{298.15}(CsOH,g) \quad (15)$$

$$\Delta_f H_{298.15}(CsOH,g) = \Delta_f H_{298.15}(Cs,g) + \Delta_f H_{298.15}(OH,g) - D°_{298.15}(Cs-OH) \quad (16)$$

The enthalpies of formation of Cs(g) and OH(g) have been taken from Janaf tables [3]. Results before and after correction of Smith and Sugden free energy functions are presented in table II-2.

Jensen and Padley (1966) [6] values further corrected by Jensen (1970) [15] for the linear Cs-O-H structure used high temperature flames (2475 K) and determined electron concentration by resonant cavity, with special calibration procedure and keeping values in the linear range response of the cavity versus the inverse of temperature in the range 2000 – 2500 K.
The alkaline component concentration was determined by optical absorption measurements using the first resonant doublets of the alkaline component. For the Cs study, the authors added small quantities of Cs in Rb in order to suppress the Cs ionization – feature which was not reached – and in addition the residual concentration of CsOH(g) could not be neglected. Finally the Cs concentration has been increased – according to the ionization theoretical equilibrium – in order to decrease the CsOH concentration below the detection threshold. The

balance between the Cs introduced concentration in the flame and the one deduced from electron concentration measurements amounts to a factor ≈ 6. This factor will induce a decrease of the dissociation energy of about RTln6 = 33 kJ.mol^{-1} (at T = 2250 K, R: gas constant) (see table II-2). Besides, we can question about the formation of the OH^- ion as postulated by Smith and Sugden (1953) [5] that may decrease the electron concentration.

Cotton and Jenkins (1969) [7] used low flame temperature (1570 K) in order to avoid (or limit) the ionization of Cs, and obtained the Cs concentration by atomic absorption (Cs lamps) using a double-beam for calibration. Some usual techniques were used to measure the H flame concentration. The equilibrium constant is deduced from the trend of the ratio H_2O/H as a function of the introduced volume (and thus concentration) of the solution in the flame. Entropies are those from Jensen and Padley (1966) [6], consequently the correction to be applied is ≈ - 1kJ as re-calculated by Jensen (1970) [15] (see table II-2).

Authors	D°_0 original (kJ.mol^{-1})	D°_0 corrected (kJ.mol^{-1})	$\Delta_f H^\circ$(298.15 K) (kJ.mol^{-1})	Method
Smith & Sugden [5]	380.7[a] ± 12.6 (2nd law)	**398.8 ± 12.6**	-268.7 ± 12.7 **-286.8 ± 12.7**	electron concentration by resonant cavity
Jensen & Padley [6] Jensen [15]	380[a] ± 12 (3rd law)	**347 ± 12**	-268 ± 12 **-235 ± 12**	electron concentration by resonant cavity
Cotton & Jenkins [7]	376.6[a] ± 8.4 (3rd law)	**375.6 ± 8.4**	-264.6 ± 8.5 **-263.6 ± 8.5**	Flame photometry

[a] *original authors data and estimated uncertainty*

Table II-2. Summary of flame studies of the Cs-OH bond dissociation and our corrected values as discussed in the text. Corrected values are presented in bold. $\delta\Delta_f H^\circ$(298.15 K) has been calculated with assumption of error compensation using the $\sqrt{\sum \delta x^2}$ relation

Concerning the flame studies, excited states are not necessarily identified when existing, and equilibrium conditions are difficult to ascertain since the only observed evolution in the flame does not warranty sufficient long time to achieve equilibrium till fundamental electronic level of the reactants and products even when analysis are performed along the flame propagation. Moreover, Gurvich et al. [2] invoked a significant uncertainty on third law analysis due to the high temperatures used in flames (2475 K for Jensen & Padley [6], Jensen [15]) but this is not so significant for Cotton & Jenkins [7] who worked at rather low temperatures ≈ 1570 K. In

fact the pre-exponential factor – taking into account the rotational and vibrational states - in the equilibrium constant for the main postulated reaction has been estimated on the basis of no electronic contribution (sigma ground state), and this assumption may introduce large errors in the third law analysis if some low laying states exist. Farther, the choice of a single reaction or of a simplified set of reactions (usually only two main reactions) does not correspond to the real complex equilibria occurring in the flames within the temperature and concentration ranges of the experimental determinations. Clearly flame studies necessitate a panel of technical analysis in view to consider the complexity of the gaseous phase.
For all these reasons, we believe that the above flame studies are likely to be approximate values. Indeed their results differ significantly from those obtained using more conventional methods as Knudsen effusion, transpiration and mass spectrometry.

II.3.2. Mass spectrometric studies

- ***Equilibrium constants of isomolecular reactions***

Schoonmaker and Porter [8] studied by HTMS mixed alkali hydroxides condensed phases including CsOH. Monomeric and dimmeric species have been detected and the ratios of fragment to parent ions published at 100 V ionizing voltage. Their ion spectrum is very similar to our observations for pure CsOH vaporization [1]. Thermochemical data were reported for the dimmerization reactions $2MOH(g) = M_2O_2H_2(g)$ and $M_2(OH)_2(g) + N_2(OH)_2(g) = 2MN(OH)_2(g)$ with M and N = Na, K, Rb and CsOH respectively. For the isomolecular studied reactions of the type,

$$(CsOH)_2\ (g) + 2\ MOH\ (g) = (MOH)_2\ (g) + 2\ CsOH(g) \qquad (17)$$

with M = Rb or K as reference, Schoonmaker and Porter made the assumption that the mass spectrometer sensitivity factors cancelled which make it possible to write the equilibrium constant as following:

$$K_p = [I(M_2OH^+).I(CsOH^+)^2/I(Cs_2OH^+).I(MOH^+)^2] \qquad (18)$$

From ionization cross-section values and secondary electron multiplier yields relations as proposed by Drowart et al. [16], and using the sum of the ionic intensities issued from each molecule (parent plus fragment ions *i.e.* $Cs^+ + CsOH^+$ for the total ionic current issued from the CsOH molecule), the authors assumption has been checked and remains valid within 9% for RbOH reference and 3% for KOH reference.

If the original thermochemical data obtained for the RbOH-CsOH systems at 673 K and KOH-CsOH at 692 K [8] are taken into consideration, using Gurvich et al. free energy functions (Fef) for the reference molecules RbOH(g) or KOH(g) [2], the dimmerization enthalpy is obtained to be: $\Delta_{dim}H^\circ$ (CsOH) = 146 ± 11 kJ.mol^{-1} with RbOH as reference and 156 ± 10 kJ.mol^{-1} with KOH as reference. Note that the dimmer $Rb_2O_2H_2$ reference is not well known since Gurvich et al. estimated the bond using trends in the hydroxides that were then compared to flame experiments due to lack of direct vaporization studies.

Gorokov et al. (1970) [11] determined by HTMS the difference of dissociation energies of KOH and CsOH: D_0(Cs-OH)- D_0(K-OH)=31.8 ± 4.6 kJ.mol^{-1}. At the beginning of their experiment or in the first one, some invoked carbonates impurities (earlier studies on carbonates – including preparation of the samples - were performed by the authors) produced Cs(g) and K(g) in the gas phase. Note that this feature would be related to reducing conditions in the cell that can not be obtained by the only Pt container (used in their experiment), but necessarily by sample impurities clearly different from water pollution. As the ionization process of the hydroxides produce more Cs^+ (or K^+) ions than $CsOH^+$ (or KOH^+) ions, the convolution of the different contributions remains a necessary step that increases the total uncertainty of the measurements. From their equilibrium constant of the gas-phase exchange reaction (isomolecular),

$$Cs(g) + KOH(g) = CsOH(g) + K(g) \qquad (19)$$

i.e. CsOH referred to KOH from Gurvich et al. compilation [2] (D_0(K-OH)=357± 3 kJ.mol^{-1}) , and using Fef (free energy functions) of Janaf tables for Cs and K [3], the dissociation energy of CsOH(g) has been obtained to be D_0(Cs-OH) = 388.8 ± 5.6 kJ.mol^{-1} (uncertainty takes into account the assumption of error compensation using $\sqrt{\sum \delta x^2}$ relation and including the free energy function uncertainty= ±1 kJ.mol^{-1}) and $\Delta_f H_{298.15}$CsOH(g) = -276.8 ± 5.8 kJ.mol^{-1}.

- ***Born-Haber cycles from ionization processes***

From Gorokov et al. (1970) [11] measurement of the Cs^+ dissociative ionization potential using the following Born-Haber cycle (at 900 K),

$CsOH(g) + e^- \leftrightarrow Cs^+ + OH(g) + 2\ e^-$ (dissociative ionization potential at 900 K) (3)

$Cs(g) + e^- \rightarrow Cs^+ + 2\ e^-$ (known adiabatic ionization potential) (20)

$CsOH(g) = Cs(g) + OH(g)$ (deduced bond energy at 900 K) (21)

and considering the measurement performed at 900 K: $D°_{900K}(Cs\text{-}OH) = 359.8 \pm 12.5$ kJ.mol^{-1} , dissociation energy has been calculated at 0 K using enthalpy increments,

$$D°_0\,(Cs - OH) = D°_{900K}\,(Cs - OH) + (H_{900} - H_0)_{CsOH(g)} - (H_{900} - H_0)_{OH(g)} - (H_{900} - H_0)_{Cs(g)} \quad (22)$$

The enthalpy increments have been obtained from Janaf tables for OH(g) and Cs(g) and from Gurvich et al. tables for CsOH(g). The resulting dissociation enthalpy $D°_0(Cs\text{-}OH) = 357.6 \pm 12.6$ kJ.mol^{-1}(uncertainty takes into account the errors compensation). As Gorokhov et al., we assume no contribution of ion (and/or neutral) kinetic energy in process (3) by analogy with K^+/KOH analyzed using electrostatic deflection at the ion source output. Our recalculated value is slightly different from the one presented in Gurvich et al. compilation (358 ± 12 kJ. mol^{-1}).

From Emellyanov et al. (1967) [12] and the same Born-Haber cycle, we obtained $D°_0(Cs\text{-}OH) = 341 \pm 13.6$ kJ.mol^{-1} different from the original value given by the authors at about 900 K: $D°_{900K}(Cs\text{-}OH) = 344 \pm 13.5$ kJ.mol^{-1} . The resulting value for the enthalpy of formation is $\Delta_f H^\circ_{298.15}CsOH\ (g) = -229 \pm 13.7$ kJ.mol^{-1} including the proposed uncertainty for the enthalpy increment of CsOH(g) by Gurvich et al. [2].

It is to notice that the differences in these two preceding studies have to be related to difficulties in obtaining accurate values for ionization potentials: namely 0.1 eV is rarely reached as total uncertainty (0.1 eV = 11.2 kJ).

- ***Vaporization studies***

Konings and Cordfunke [10] total apparent pressure p_{app} from the transpiration experiment – calculated on the basis of the transported and analyzed Cs atoms at the condenser - gives the partial pressure of the monomer and dimmer using our dissociation constant K_d (inverse of dimmerization constant) for the reaction $(CsOH)_2(g) \leftrightarrow 2CsOH(g)$ according to the following relations,

$$p_{app} = p_1 + 2p_2 \quad (23)$$

$$K_d = \frac{p_1^{\,2}}{p_2} \quad (24)$$

$$p_2 = \frac{p_1^{\,2}}{K_d} \quad (25)$$

$$p_{app} = p_1 + 2\frac{p_1^{\,2}}{K_d} \quad (26)$$

$$2p_1^{\,2} + K_d \cdot p_1 - K_d \cdot p_{app} = 0 \quad (27)$$

$$\Delta = K_d^{\,2} + 8K_d \cdot p_{app} = K_d\left(K_d + 8p_{app}\right) \quad (28)$$

$$p_1 = \frac{-K_d + \sqrt{K_d(K_d + 8p_{app})}}{4} = \frac{K_d}{4} \cdot \left[-1 + \sqrt{1 + \frac{8p_{app}}{K_d}}\right] \quad (29)$$

p_1 and p_2 correspond respectively to monomer and dimmer pressures.

As the monomer remains the main species, third law calculation of the CsOH(cr,l) = CsOH(g) equilibrium is chosen as the main result : $\Delta_{subl}H^{\circ}_{298.15}$ = 162.8 ± 0.9 (standard deviation) kJ.mol^{-1}. The third law results are presented in figure II-1 as a function of the measured temperature and compared to authors results with their assumption that monomer is the only present component in the gaseous phase. Our corrected values discarding the dimmer contribution lead to a less scattered mean value and to a smaller trend (thermodynamics should show no trend). The original pressures and corrected ones are presented in table II-3.

The total uncertainty is calculated from the third law relation:

$$\delta\Delta_{subl}H = \delta T.(\Delta_{subl}H/T_{mean}) + \delta(\Delta_{subl}Fef).T_{mean} + R.T_{mean}.\delta P/P = \pm 6.5 \text{ kJ.mol}^{-1} \quad (30)$$

We estimated - (i) the total monomer pressure uncertainty on the basis of maximum deviation of the original apparent pressure ($\delta P/P = \pm 0.46$ in fig. II-2 of Konings and Cordfunke [17]) for p_{app}, adding the uncertainty on the dimmer existence or not ($0 < p_2 / p_1 < 0.6$ leading to $\delta P/P = \pm 0.3$), the total $\delta P/P = \pm 0.76$, - (ii) T_{mean} = 800 K and $\delta T = \pm 5$ K, - (iii) $\delta(\Delta_{subl}Fef) = 2 + 2$ according to Gurvich et al. tables. The assumption of errors compensation has been used for the calculation of total uncertainty. The deduced enthalpy of formation $\Delta_f H^\circ_{298.15}CsOH(g)$ is equal to -253.4 ± 6.5 kJ.mol^{-1} (uncertainty takes into account the errors compensation and $\Delta_f H^\circ_{298.15}CsOH(s,l)$= 416 ± 0.5 kJ.mol^{-1} from Gurvich et al. [2].

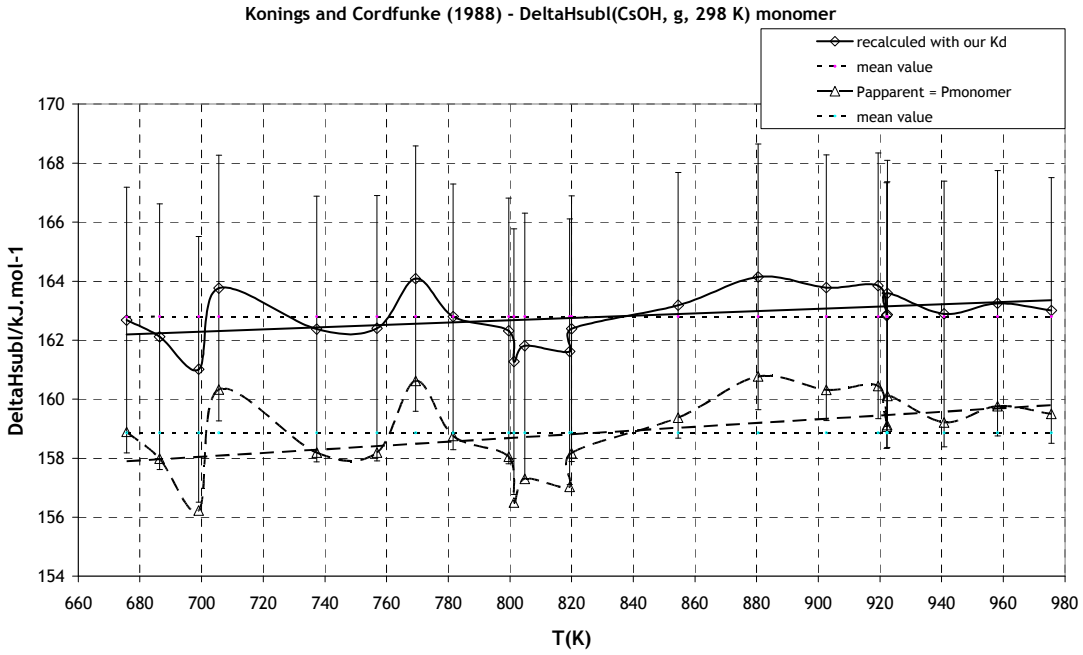

Figure II-1: Third law enthalpy of the vaporization reaction CsOH(l) = CsOH(g) versus temperature for Konings & Cordfunke data [10] and Konings & Cordfunke corrected values discarding the dimmer contribution to the total apparent pressure data .

T(K)	Measured pressure = P_{app} (Pa*) Konings	Konings assumption: $P_1 = P_{app}$ $\Delta_{sub}H_{298.15}$(Konings) kJ.mol^{-1}	Our calculation: $P_1 = P_{app}-2P_2$ (bar)	Without dimmer $\Delta_{sub}H^\circ_{298.15}$ (recalculated) kJ.mol^{-1}
675.7	1.4	158.9	7.13E-06	162.7
686.4	2.42	158.0	1.17E-05	162.1
699.1	5.08	156.2	2.23E-05	161.0
705.6	3.13	160.3	1.74E-05	163.8
737.3	12.22	158.2	6.17E-05	162.4
756.9	21.5	158.2	1.10E-04	162.4
769.4	20.73	160.6	1.21E-04	164.1
781.6	38.34	158.8	2.06E-04	162.8
799.6	67.16	158.0	3.53E-04	162.3
801.3	88.29	156.5	4.31E-04	161.3

804.8	85.09	157.3	4.34E-04	161.8
819.4	124.57	157.0	6.36E-04	161.6
820	106.76	158.2	5.76E-04	162.4
854.6	191.77	159.4	1.12E-03	163.2
880.5	267.36	160.8	1.69E-03	164.1
902.6	432.6	160.3	2.73E-03	163.8
919.4	575.43	160.5	3.69E-03	163.8
922.2	723.88	159.1	4.43E-03	162.8
922.3	720.23	159.1	4.42E-03	162.9
922.4	633.74	160.1	4.03E-03	163.6
940.8	972.77	159.2	6.08E-03	162.9
958.1	1199.93	159.8	7.75E-03	163.3
975.6	1627.13	159.5	1.06E-02	163.0
Mean value at 298 K		**158.9**		**162.8**
Standard deviation		1.3		0.9

** the published unit in table 1 of Konings and Cordfunke paper [17] is Pascal and not kPa as mentioned.*

Table II-3 : In the third column, the third law enthalpy is calculated with the Fef of Gurvich et al.[2] and with Konings assumption of only monomer in the gas phase. In the fourth column, the monomer pressure is calculated using our dissociation enthalpy for the dimmer. The last column corresponds to the calculated third law enthalpy for the sublimation of the only monomer (CsOH(cr,l) = CsOH(g)).

Blackburn and Johnson (1988) [9] vaporized CsOH(l) by HTMS (quadrupole mass spectrometer) and calibrated the mass spectrometer using the mass loss of the sample during the experiment. When compared with earlier mass spectrometric studies and our determinations [1] performed with a conventional magnetic mass spectrometer, their dimmer ionic intensities are much lower - at least by a factor 100. As we confirmed the values for the ionic intensities dimmer to monomer ratio of Schoonmaker and Porter [8] performed with a magnetic mass analyzer, we agree with the existence of an uncontrolled mass discrimination in the quadrupole MS as invoked by Gurvich et al. [2]. Indeed, Blackburn and Johnson attempted to check this mass discrimination "using perfluorotripentylamine for the mass range 50 to 602" but they were not convinced by their tests and did not use the mass discrimination results. So, the Blackburn and Johnson determinations cannot be used for the determination of the dimmerization equilibrium constant. Moreover, due to their attributed small contribution of dimmer in their gas phase, Blackburn and Johnson calculated the monomer vaporization from the full mass loss and so doing they over-evaluated the monomer's pressure. Gurvich et al. took off the dimmer contribution to the monomer pressure, but no details are published about the correction done probably to the total mass loss. Similar process has been done using our selected dimmerization (or dissociation) constant in the following way:

- the total relative mass loss (from tables II-1 and II-2 in Blackburn and Johnson paper [9]) have been recalculated due to the monomer and dimmer effusion according to the Hertz-Knudsen equation,
- The total pressure in the effusion cell - defined as apparent pressure from the only mass loss - is then used to recalculate the monomer partial pressure using our equilibrium constant K_d (dissociation of the dimmer into two monomers) according to the following relations,

$$p_{app} = p_1 + \sqrt{2}\, p_2 \tag{31}$$

$$\frac{\sqrt{2}}{K_d} p_1^{\,2} + p_1 - p_{app} = 0 \tag{32}$$

$$\Delta = 1 - 4 \cdot \frac{\sqrt{2}}{K_d} p_{app} \tag{33}$$

$$p_1 = \frac{-1 + \sqrt{\Delta}}{2\sqrt{2}/K_d} \tag{34}$$

and finally, using relation (32) dimmer pressure p_2 is deduced according to the following relation:

$$p_2 = \frac{p_{app} - p_1}{\sqrt{2}} \tag{35}$$

The so calculated ratio p_1/p_{app} amounts to about 0.96. For low temperature range, no dimmer pressures have been published by Blackburn and Johnson and as a first approximation, their monomer pressure can be considered as equal to the apparent pressure. Meanwhile in the high temperature range, the apparent pressure has been recalculated from the two contributions (presence of monomer and dimmer in the gaseous phase). Then, from this recalculated apparent pressure (as measured by mass loss) and using our dissociation constant K_d, the real monomer pressure has been recalculated.

The original pressures and corrected ones are presented in table II-4 and figure II-2. From the corrected partial pressure of the monomer, the third law sublimation enthalpy for the reaction CsOH(cr,l) = CsOH(g) has been calculated to be: $\Delta_{subl}H^{\circ}_{298.15}$ = 164.4 ± 1.3 (standard deviation) kJ.mol^{-1}. The estimated total uncertainty has been taken as for Roki et al. mass spectrometric same experiments (± 6.5) and finally the total uncertainty is $\delta(\Delta_{subl}H)$ = ± 7.8 kJ.mol^{-1} (including the standard deviation). Using Gurvich et al. [2] enthalpy of formation

$\Delta_f H^\circ_{298.15}$CsOH(s,l)= 416 ± 0.5 kJ.mol^{-1}, the deduced formation enthalpy is $\Delta_f H^\circ_{298.15}$CsOH (g) = -251.8 ± 7.8 kJ.mol^{-1} (uncertainty takes into account the errors compensation).

N.B. *The authors did not mention any experimental observations concerning the creeping or overflow of the material - as analyzed by Roki et al.[1] - but we observe a relatively large scatter of the original published data (see fig. II-2). Consequently, the third law enthalpy results of the main reaction CsOH(s,l) = CsOH(g) are largely scattered as presented as a function of temperature measurements in figure II-3.*

In order to test the influence of a possible overflow of about 50% in the total mass loss, we calculated also the sublimation enthalpy when the apparent pressure is divided by two (fig II-3). Results show that the enthalpy is increased by about 3kJ but the results show a small trend (comparison between the mean value and the least square fit). Our first calculation with apparent pressure seems better. As the authors used silver Knudsen cell – a material Roki et al. did not test in their experiments – we can conclude that either there is compensation between the overflow and their measured ionic intensities (genuine effusion plus parasitic contribution) or there is no significant overflow with silver cells.

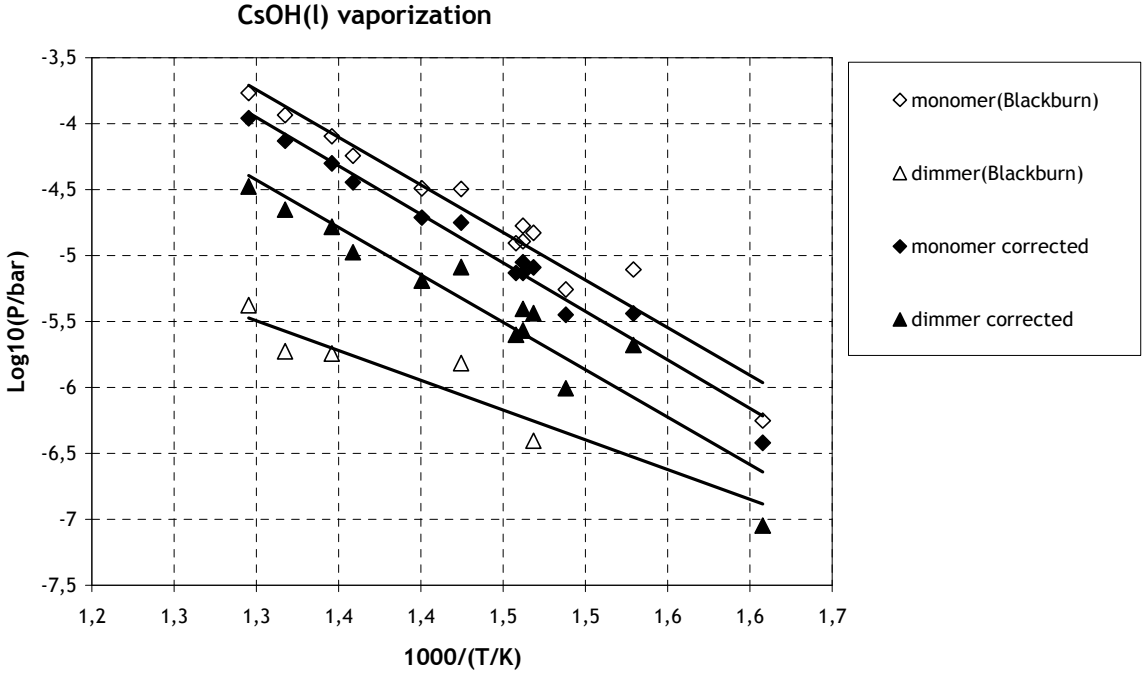

Figure II-2 : Decimal logarithm of partial pressures in equilibrium with CsOH(l) versus 10^3/T for Blackburn and Johnson data [9] and corrected pressures as explained in the text.

T(K)	Monomer pressure (Bar) Blackburn	Dimmer pressure (bar)Blackburn	Apparent Pressure (bar)	Monomer pressure corrected with our K_d	$\Delta_{subl}H(298\ K)$ ($kJ.mol^{-1}$)
622	5.60E-07		5.60E-07	3,81E-07	166.2
654	7.82E-06		7.82E-06	3,64E-06	161.7
672	5.53E-06		5.53E-06	3,56E-06	165.8
681	1.49E-05	3.94E-07	1.55E-05	8,13E-06	163.1
684	1.68E-05		1.68E-05	8,92E-06	163.2
684	1.28E-05		1.28E-05	7,39E-06	164.2
686	1.24E-05		1.24E-05	7,38E-06	164.7
702	3.19E-05	1.53E-06	3.41E-05	1,78E-05	162.9
714	3.23E-05		3.23E-05	1,94E-05	164.8
736	5.70E-05		5.70E-05	3,58E-05	165.5
743	8.04E-05	1.81E-06	8.30E-05	4,99E-05	164.8
759	1.16E-04	1.88E-06	1.19E-04	7,41E-05	165.3
772	1.71E-04	4.21E-06	1.77E-04	1,10E-04	165.1
				Mean value at 298 K	**164.4**
				Standard deviation	**1.3**

Table II-4: Re-calculations of apparent pressure from monomer and dimmer pressure values of Blackburn and Johnson [1] and deduced monomer pressure using our dissociation enthalpy for the dimmer. The last column corresponds to the calculated third law enthalpy for the sublimation of the monomer CsOH(cr,l) = CsOH(g).

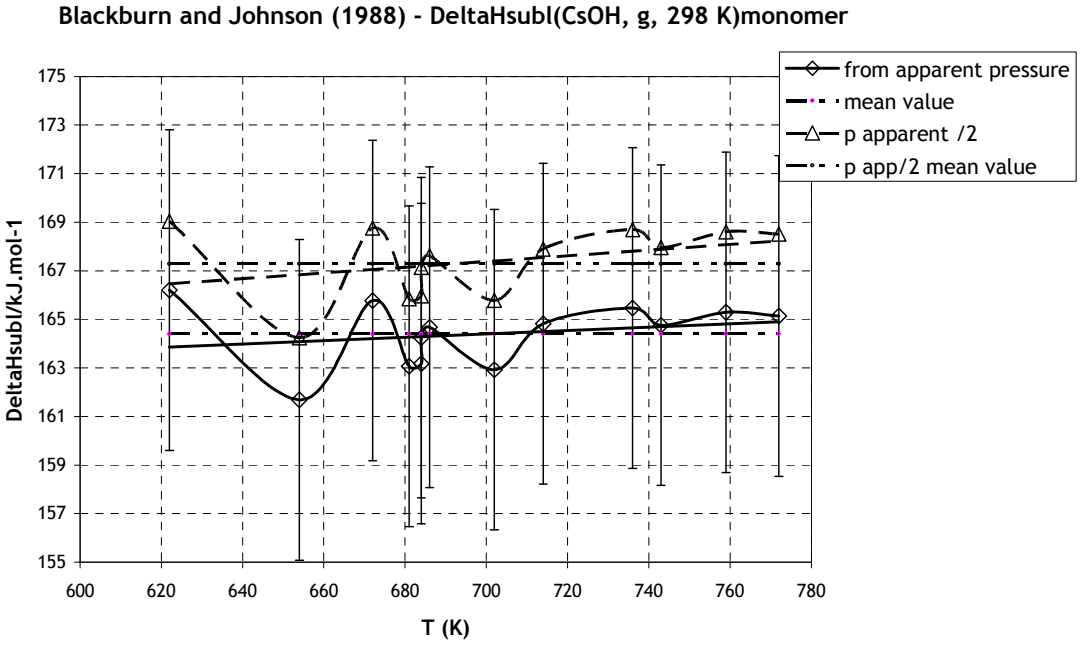

Figure II-3: Third law enthalpy of the reaction CsOH(cr,l) = CsOH(g) from Blackburn and Johnson data recalculated using our dissociation constant for the dimmer (full line). Dashed lines correspond to an arbitrary decrease of mass loss (50%) associated to the assumption of an overflow contribution in the total effusion process.

Roki et al. (2007) [1] performed mass spectrometric vaporization of pure CsOH(l) (see appendix II-A for experimental pressures of CsOH(g) and $Cs_2O_2H_2$(g)) and propose for the sublimation reaction CsOH(cr,l) = CsOH(g) a value $\Delta_{subl}H^\circ_{298.15}$ = 163.3 ± 6.5 kJ.mol^{-1} . Using Gurvich et al. enthalpy of formation for the solid: $\Delta_fH^\circ_{298.15}$CsOH(s) = -416.2 ± 0.5 kJ.mol^{-1}, the CsOH(g) enthalpy of formation has been obtained to be: $\Delta_fH^\circ_{298.15}$CsOH(g) = -252.9 ± 6.5 kJ.mol^{-1}, uncertainty takes into account the error compensation $\sqrt{(6.5^2+0.5^2)}$ (published value in [1] -252.7 ± 6.5, the 0.2 difference is simply due to an error of calculation). The direct determinations of the sublimation enthalpy are compared in table II-5. Results show that all third law enthalpies become more consistent when taking into account our dissociation constant.

Reaction : CsOH(cr,l) = CsOH(g)		Temperature range (K)	Δ_{subl}H(298 K, 2nd law) /kJ.mol^{-1}	Δ_{subl}H(298 K, 3rd law) /kJ.mol^{-1}
Blackburn, Johnson [9]	Authors	622-772 (T_{mean} = 700)	160.9 ± 9.7	151.9 ± 1.9
	Corrected		163.6 ± 7.0	**164.4 ± 1.3**[a]
Konings, Cordfunke [10]	Authors	676-976 (T_{mean} = 830)	152.2 ± 2.6	158.9 ± 1.3
	Corrected		157.9 ± 1.8	**162.8 ± 0.9**[a]
Roki et al. [1]	This work	496-765	146.8 ± 10.1[b]	**163.3 ± 2.1**[b]

[a]*: 1 experiment,* [b]*: 4 experiments standard deviation*

Table II-5: Comparison between literature data and recalculation of sublimation enthalpy with 2nd and 3rd law (with standard deviation).

II.4. SUMMARY AND CONCLUSION

The whole set of formation enthalpies for CsOH(g) is summarized in table II-6. Good agreement is observed for values obtained by direct sublimation, the last value from Roki et al. confirms the original choice of retained methods of measurements by Gurvich et al. [2] who did not retain other kind of determinations.

Following Gurvich et al. [2], we believe that "the high temperatures employed in studies of equilibria in flames [5-7] resulted in significant uncertainties for the 3rd law enthalpies of reaction", due for one part to the uncertainty of the real temperature of the flame and for

another part to uncertainty on the calibration of ions concentration as well as the knowledge of the exact electronic states of the CsOH molecule.

Born-Haber cycles based on dissociative ionization as observed in mass spectrometry are only rough estimates due to the possible excess kinetic energy associated to the fragment ions that are not always detected with sufficient accuracy. Moreover, the calibration of the voltage scale in a Mass Spectrometer ion source is not necessarily reliable due to voltage gradient in the ionization volume.

The isomolecular reaction taking into account Cs(g) and K(g) in addition to the hydroxides (CsOH and KOH) in the gas phase is based on feature that needs from a chemical point of view reducing conditions or pollution by an oxide at very low oxygen potential or a carbonate as invoked by Gorokhov et al. [11]. In fact, the Cs^+ and K^+ parent ions are mixed with the fragment ones coming from hydroxides in a rather important amount. Therefore, the measured isomolecular reaction – notwithstanding easy calibration procedure – can include some uncontrolled uncertainties. But yet, comparing the proposed formation enthalpy value (-278.4 $kJ.mol^{-1}$) with those obtained in flames studies, we observed that the isomolecular value is rather close to those obtained from direct sublimation.

As proposed by Gurvich et al. [2], a mean value has been retained from sublimation experiments that are presently the most reliable ones because:

- the gaseous phase composition has been re-determined and thus the dimmer to monomer dissociation constant;
- the sublimation enthalpies of the monomer have been re-evaluated from different experiments discarding the dimmer contribution.

Our proposed mean value for the formation of CsOH(g) ($\Delta_f H^\circ_{298.15}$CsOH(g) = -252.7 ± 4.1 $kJ.mol^{-1}$) is slightly different from the Gurvich et al. proposed one (-256.0 ± 5 $kJ.mol^{-1}$). The difference in pressures of the monomer can be calculated using the third law relation,

$\frac{\partial p}{p} = \frac{\partial \Delta_f H}{RT} + \frac{\partial \Delta Fef}{R}$ = 3000/RT, with the same Fef (free energy function).

At 1000K, our monomer pressure is 36% lower than the proposed ones by Gurvich et al. [2].

Authors	Experimental Methods	$D°_0$(Cs-OH)	$\Delta_f H°_{298K}$ (CsOH,g) /kJ.mol^{-1}	Comments
Smith, Sugden (1953) [5]	Flames	398.8 [d] ± 12.6	-286.8 ± 12.7 [a]	Possible excited states and unknown temperature
Jensen, Padley (1966) [6]	Flames	347 [d] ± 12	-235 ± 12 [a]	
Coton, Jenkins (1969) [7]	Flames	375.6 [d] ± 8.4	-263.6 ± 8.5 [a]	
Gorokhov, Gusarov (1970) (Born-Haber) ([11]	HTMS Dissociative ionization	357.6 ± 12.6	-245.6 ± 12.7 [a]	Possible kinetic energy and calibration of potential scale
Emellyanov et al. (1967) [12]	HTMS Dissociative ionization	341 ± 13.6	-229 ± 13.7 [a]	
Gorokhov, Gusarov (1970) (isomolecular reaction) [11]	HTMS Isomolecular reaction	388.8 ± 5.6	-276.8 ± 5.8 [a]	Origines of Cs(g) and K(g) ?
Blackburn, Johnson (1988) [9]	HTMS Vaporization		-251.8 ± 7.8 [b]	Corrected with our K_d
Konings, Cordfunke(1988) [10]	Transpiration Vaporization		-253.4 ± 6.5 [b]	
Roki et al. (2007) [1]	HTMS Vaporization		-252.9 ± 6.5 [b]	New K_d determination
Gurvich et al. (1997) [2]	Assessment	368.6 ± 5	-256.0 ± 5 [a]	Compilation assessment
This work	**Our assessment**		**-252.7 ± 4 [c]**	

[a]: original uncertainties proposed by the authors, [b]: uncertainties re-evaluated in this work, [c]: evaluated as $[\sqrt{(7.8^2+6.5^2+6.5^2)}]/n$ (with n=3), [d] corrected value from table II.2

Table II-6: display of all determined and analyzed values for the dissociation enthalpy of Cs-OH and the formation enthalpy of CsOH(g), quoted with total uncertainties.

The formation enthalpy of the dimmer is deduced from our retained dissociation enthalpy and the preceding formation enthalpy of the monomer:

$$\Delta_{diss}H^\circ = 2\,\Delta_f H_{mono} - \Delta_f H_{dim} \qquad (36)$$

The enthalpy of dissociation $\Delta_{diss}H^\circ$ is related to the dissociation constant K_d within:

$$\Delta_{diss}H^\circ = -RTLn\,K_d + T\Delta Fef \qquad (37)$$

The $Cs_2O_2H_2$(g) enthalpy of formation is deduced to be: $\Delta_f H^\circ_{dim}$ = - 652.4 ± 11.7 kJ.mol^{-1} (Roki et al. published value -652 ± 11.7 kJ.mol^{-1} due to an error of calculation of $\Delta_f H^\circ$(CsOH,g)). The calculated uncertainty takes into account the errors compensation.

Gurvich et al. [2] adopted the value -653.0 ± 8 kJ.mol^{-1}, which is in good agreement with our value due to internal compensations in the thermodynamic cycles since their references are not the same. Indeed, Gurvich et al. compared the dimmer series – $K_2O_2H_2$, $Rb_2O_2H_2$ - as done by Schoonmaker and Porter [8] in which the rubidium is already an estimated value.

Looking at the "recommendations for future measurements" proposed in the Gurvich et al. compilation [2], the present work gives response to the item (5) "Mass spectrometric study of potassium, rubidium and cesium hydroxides to obtain reliable quantitative data on vapor composition, including relative concentration of trimeric and possibly tetrameric molecules" at present applied only for the CsOH compound. Our principal thermodynamic results concern:

- the melting temperature of anhydrous CsOH(s to l),
- the dissociation constant dimmer – monomer,
- the enthalpies of formation of these two species,
- the existence of the trimmer.

In the item (7), Gurvich et al. pointed out that the selected structure for the dimmer would present some active modes in Raman spectra that should be detected as a confirmation. Some new results could modify the free energy function and consequently the dissociation energy of the dimmer. As we did not observe any systematic trends in our four retained third law results, the modification of the Free energy function would probably not be very important.
For mass spectrometric future investigations, the proportion of fragment ions has been determined as a basic reference with the pure compound. This step was necessary in view of multi-component systems (CsI-CsOH for example) investigations in order to detect reliably the apparition of new atoms or molecules giving ions at the same mass.

Finally, the proposed thermodynamic properties for the CsOH(s,l), CsOH(g) and $Cs_2O_2H_2$(g) are summarized in table II-7. Selected CsOH(g) and $Cs_2O_2H_2$(g) vapour pressures have been calculated as well as the dimmerization constant K_{dim} for the reaction CsOH(g) = 2 $Cs_2O_2H_2$(g) and presented in figures II-4 and II-5.

Compound or molecule	Thermodynamic function	JANAF 1998 from Janaf 1971 [3]	Gurvich et al. (1997) [2]	Present work retained
CsOH(s)	$\Delta_f H$ (298 K)/kJ.mol^{-1}	-416.73 ± 0.8	-416.2 ± 0.5	Gurvich
	S°(298 K))/J.K^{-1}mol^{-1}	98.7 ±4.2 estimated	104.22 ± 0.10	Gurvich
	$C°_p$ (298.15 K)/J.K^{-1}mol^{-1}	67.87	69.93 ± 0.1	Gurvich
	H(298.15) – H(0) /J. mol^{-1}	unknown	14103 ± 10	Gurvich
	$\Delta_{melting}H°$ (K)	4.56 ±0.4	7.78 ± 0.4	Gurvich
	$T_{melting}$ (K)	588 ± 1	615.5 ± 1.0	**649 ± 2**
CsOH(l)	$C°_p$ ($T_{melting}$)/J.K^{-1}mol^{-1}	83.68	85.0	Gurvich
CsOH(g)	$\Delta_f H°$ (298 K)/kJ.mol^{-1}	-259.4 ± 12.6	-256 ± 5	**-252.7 ± 4**
	S°(298 K))/J.K^{-1}mol^{-1}	254.78 ± 0.42	254.84 ±0.7	Gurvich
	$C°_p$ (298.15 K)/J.K^{-1}mol^{-1}	49.723	49.724 ± 0.3	Gurvich
$Cs_2O_2H_2$(g)	$\Delta_f H°$ (298 K)/kJ.mol^{-1}	-687.8 ± 41.8	-653 ± 8	**-652.4 ± 11.7**
	S°(298 K) /J.K^{-1}mol^{-1}	360.7 ± 12.6	381.267 ± 2	Gurvich
	$C°_p$ (298.15 K)/J.K^{-1}mol^{-1}	82.807	108.293 ± 1	Gurvich

Table II-7: Selected thermodynamic properties for Cs-O-H system.

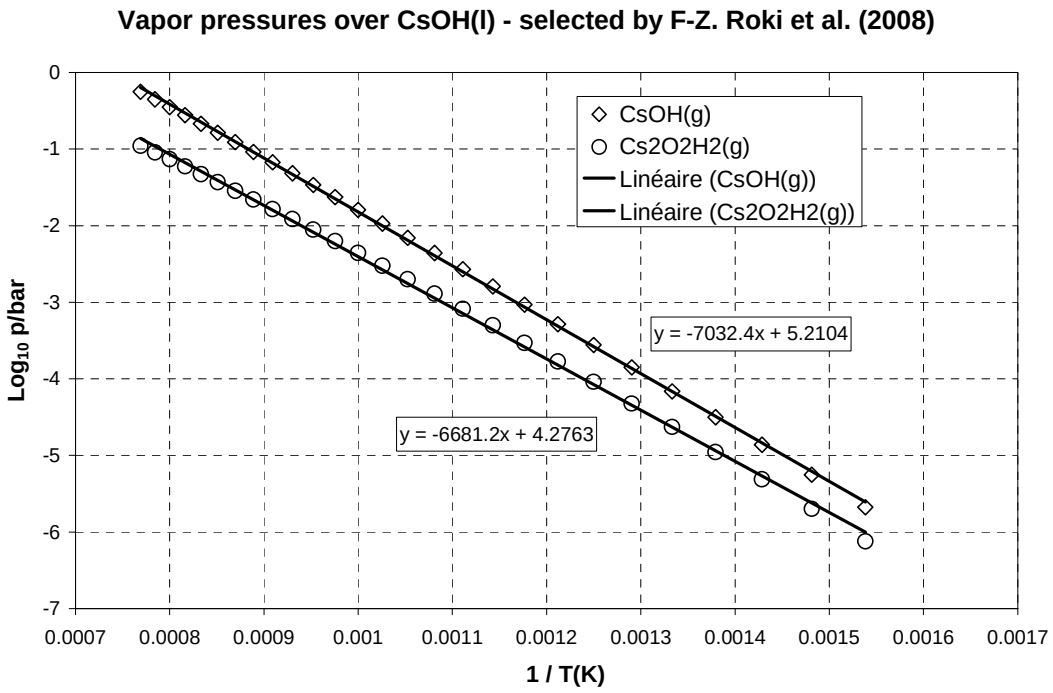

Figure II-4: Selected CsOH(g) and $Cs_2O_2H_2$(g)) vapor pressures over liquid phase

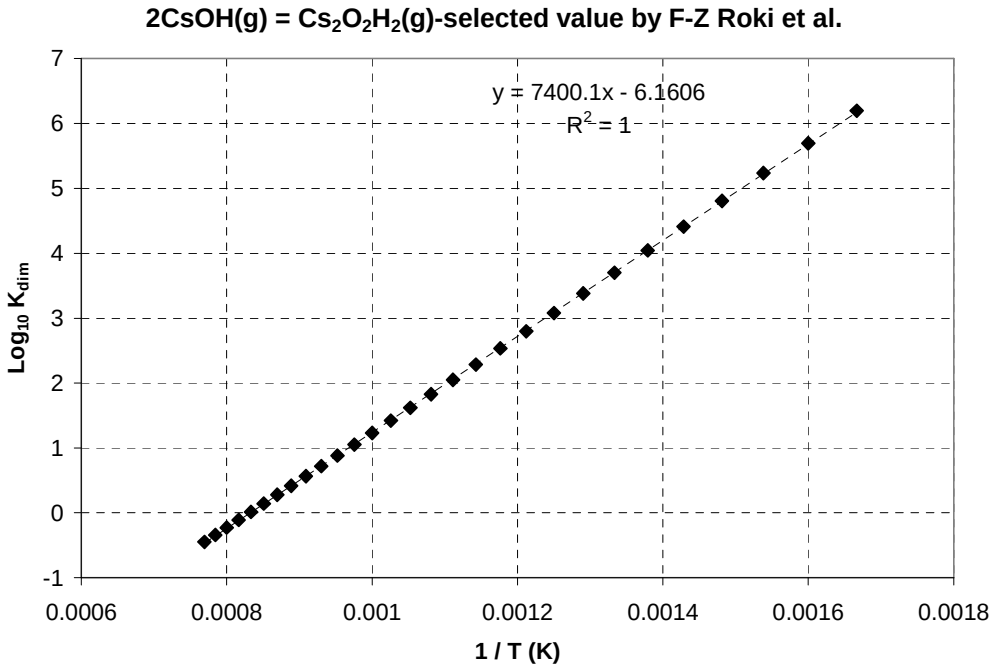

Figure II-5: Selected constant of dimmerization for the reaction CsOH(g) = $Cs_2O_2H_2$(g)

REFERENCES

[1] F.Z.Roki, M.N.Ohnet, C.Chatillon, and D.Jacquemain, "Thermodynamic study of the CsOH(s,l) vaporization by high temperature mass spectrometry," J. Chem. Thermodyn., Vol. 40, 2008, pp. 401-416.

[2] L.V.Gurvich, L.N.Gorokhov, G.A.Bergman, V.S.Iorish, V.Ya.Leonidov, and V.S.Yungman, "Thermodynamic Properties of Alkali Metal Hydroxides. Part II. Potassium, Rubidium, and Cesium Hydroxides," J. Phys. Chem. Ref. Data, Vol. 26 (4), 1997, pp. 1031-1109.

[3] M.W.Chase, J., "NIST-JANAF Thermochemical Tables", Fourth Edition, J. Phys. Chem. Ref. Data, Part II, 1998.

[4] L.V.Gurvich, I.V.Veyts, and V.A.Medvedev, "Thermodynamic Properties of Individual Substances," Hemisphere Publ. Corp., New York, Vol. 1 (Part 1), 1989, pp.

[5] H.Smith and T.M. Sugden, "The stability of gaseous lithium hydroxide at high temperature and its relation with the hydroxyl concentration of flame gases," Proc. R. Soc. London Ser., Vol. 219, 1953, pp. 204-215.

[6] D.E.Jensen and P.J. Padley, "Dissociation Energies of the Alkali Metal Hydroxides," Trans. Faraday Soc., Vol. 62, 1966, pp. 2132-2139.

[7] J.H.Cotton and D.R. Jenkins, "Bond Dissociation Energies of Gaseous Alkali Metal Hydroxides," Trans. Faraday Soc., Vol. 65, 1969, pp. 1537-1543.

[8] R.C.Schoonmaker and R.F. Porter, "Mass Spectrometric Study of Alkali Hydroxide Vapors," J. Chem. Phys., Vol. 31, 1959, pp. 830-833.

[9] P.E.Blackburn and C.E.Johnson, "Mass Spectromety Studies of Fission Product Behavior. II- Gas phase species in the CsI-CsOH system," J. Nucl. Mater., Vol. 154, 1988, pp. 74-82.

[10] R.J.M.Konings, E.H.P.Cordfunke, and W.Ouweltjes, "The standard enthalpies of formation of hydroxides. II-The alkali hydroxides CsOH and KOH," J. Chem. Thermodynamics, Vol. 20, 1988, pp. 777-780.

[11] L.N.Gorokhov, A.V.Gusarov, and I.G.Panchenkov, "Detemination of Dissociation Energies of Potassium and Cesium Hydroxides by Electron Bombardment," Russian Journal of Physical Chemistry, Vol. 44(1), 1970, pp. 150-151.

[12] A.M.Emellyanov, A.V.Gusarov, L.N.Gorokhov, and A.N. Sadovnikova, Teoret. Eksperim. Khymiya, Vol. 3, 1967, pp. 226.

[13] C.W.Jr.Bauschlicher, S.R. Langhoff, and H.J. Partridge, "Ab initio study of the alkali and alkaline-earth monohydroxides," J. Chem. Phys., Vol. 84 (2), 1986, pp. 901-909.

[14] S.G.Lias, J.E.Bartmess, J.F.Liebman, J.L.Holmes, R.D.Levin, and W.G.Mallard, "Gas-Phase Ion and Neutral Thermochemistry," J. Phys. Chem. Ref. Data, Vol. 17 (1), 1988.

[15] D.E.Jensen, "Molecular Structures and Enthalpies of Formation of Gaseous Alkali Metal Hydroxides," J. Phys. Chem., Vol. 74 (N°1), 1970, pp. 207-208.

[16] J.Drowart, C.Chatillon, J. Hastie, and D. Bonnell, "High-Temperature Mass Spectrometry: Instrumental Techniques, Ionisation Cross-Sections, Pressure Measurements, and Thermodynamic Data," J. Pure Appl. Chem., Vol. 77, 2005, pp. 683-737.

[17] E.H.P.Cordfunke and R.J.M.Konings, "Thermochemical Data for Reactor Materials and Fission Products", Elsevier Science Publishers B.V., Amsterdam, 1990, pp. 111-119.

APPENDIX II-A

CsOH(g) and $Cs_2O_2H_2$(g) experimental pressures obtained during CsOH(s,l) vaporization by high temperature mass spectrometry measurements

[a] Pure material, [b] 20% Rh

Material cell	Experience label	T / K	PCsOH(g) / Pa	$PCs_2O_2H_2$(g) / Pa
Ni[a]	CsOH-02s	515.70	4.052E-04	9.406E-05
		531.40	1.086E-03	2.712E-04
		559.60	4.054E-03	1.236E-03
		587.00	1.253E-02	3.778E-03
		621.10	4.493E-02	6.452E-03
		633.10	7.137E-02	1.440E-02
		759.60	5.092E+00	7.883E-01
		693.55	6.393E-01	1.329E-01
		724.20	1.741E+00	3.163E-01
Pt-Rh[b]	CsOH-04s	564.80	1.085E-02	5.072E-03
		530.80	1.959E-03	6.425E-04
		498.90	3.056E-04	1.653E-04
		552.10	5.810E-03	2.134E-03
		594.68	3.992E-02	1.461E-02
		621.30	1.090E-01	3.098E-02
		639.90	2.126E-01	4.820E-02
		628.58	1.502E-01	3.975E-02
		651.60	3.283E-01	9.115E-02
		763.73	1.601E+01	7.046E+00
		673.30	7.660E-01	1.952E-01
		703.83	2.348E+00	7.671E-01
		733.10	6.124E+00	2.387E+00
		717.93	3.698E+00	1.367E+00
		693.80	1.596E+00	5.313E-01
	CsOH-05s	628.00	8.967E-02	2.556E-02
		604.00	3.357E-02	1.244E-02
		582.75	1.207E-02	4.075E-03
		563.60	4.242E-03	1.628E-03
		546.50	1.484E-03	5.850E-04
		523.70	3.976E-04	1.480E-04
		635.05	1.208E-01	4.235E-02
		665.00	3.987E-01	3.195E-01
		758.15	7.757E+00	3.019E+00
		655.60	2.803E-01	2.487E-01
		692.60	1.042E+00	6.451E-01
		747.00	5.654E+00	2.360E+00
		723.55	2.814E+00	1.373E+00
		710.00	1.841E+00	9.876E-01
Au[a]	CsOH-06s	615.38	3.491E-02	1.181E-02
		601.80	1.950E-02	6.389E-03
		591.13	1.188E-02	3.841E-03
		553.10	1.786E-03	4.284E-04
		539.95	8.610E-04	1.613E-04
		531.50	5.242E-04	1.135E-04

		625.95	**5.753E-02**	**3.330E-02**
		666.73	**2.764E-01**	**1.061E-01**
		693.43	**8.021E-01**	**2.515E-01**
		752.33	**6.449E+00**	**2.212E+00**
		710.18	**1.374E+00**	**5.617E-01**
		719.18	**2.132E+00**	**6.898E-01**
		729.28	**2.851E+00**	**1.041E+00**
		741.08	**4.334E+00**	**1.519E+00**
		656.55	**1.834E-01**	**6.382E-02**
		641.15	**1.098E-01**	**4.923E-02**
	CsOH-07s	**600.95**	**1.800E-02**	**3.691E-03**
		570.45	**4.171E-03**	**8.041E-04**
		555.80	**1.844E-03**	**3.998E-04**
		545.90	**1.110E-03**	**2.486E-04**
		532.20	**4.977E-04**	**8.038E-05**
		613.35	**3.293E-02**	**9.864E-03**
		625.00	**5.482E-02**	**1.268E-02**
		642.15	**1.135E-01**	**2.744E-02**
		655.85	**2.399E-01**	**6.009E-02**
		678.45	**5.780E-01**	**1.513E-01**
		703.90	**1.422E+00**	**4.495E-01**
		752.70	**7.023E+00**	**2.724E+00**
		720.10	**2.487E+00**	**7.493E-01**
		733.75	**3.879E+00**	**1.235E+00**
		745.00	**5.525E+00**	**2.073E+00**
		662.05	**3.066E-01**	**6.842E-02**

.

APPENDIX II-B

Molecular parameters	Smith & Sugden [4]		Gurvich et al. [2]	Janaf [3]
	LiOH(g)	CsOH(g)	CsOH(g)	LiOH(g)
r AOH/ Å	1.52	2.78	2.863	2.067
ν_1 /cm^{-1}	800	300	335.6 ± 10	630
ν_2 /cm^{-1}	410	300	306 ± 10	662
ν_3 /cm^{-1}	------	------	3705 ± 100	3666
I (g.cm^2)	22 10^{-40}	20.4 10^{-39}	(15.255 ± 0.03) 10^{-39}	
Ground state quantum weight	1	1	1	1
σ	1	1	1	1
Rotational constant B_0/ cm^{-1}	------	------	------	1.192055

Table II-B1: molecular parameter of gaseous LiOH and CsOH used in calculation of free energy functions. Vibrational frequency ν_3 of LiOH(g) and CsOH(g) not given by Smith and Sugden. In place we used in the calculations those proposed by Gurvich et al. and Janaf

T(K)	Cp	H(T) - H(0)	H(T) - H(298)	S(T)	Gef(0)	Gef(298)
	J K^{-1} mol^{-1}	J mol^{-1}		J K^{-1} mol^{-1}		
298.15	49.7233686	11833.7793	0	254.834095	215.143487	254.834177
300	49.77074	11925.8114	92.0321658	255.141819	215.389196	254.835127
400	51.5241626	17001.6111	5167.83185	269.731993	227.228026	256.812475
500	52.414674	22202.7997	10369.0204	281.334447	236.928897	260.596455
600	52.9735744	27473.7857	15640.0064	290.943058	245.153456	264.876421
700	53.4220619	32793.9634	20960.1842	299.143269	252.294785	269.200183
800	53.8549359	38157.7438	26323.9646	306.304962	258.607812	273.400036
900	54.3044707	43565.5377	31731.7585	312.673909	264.267783	277.416427
1000	54.7728026	49019.2766	37185.4973	318.419566	269.400314	281.234093
1100	55.2501803	54520.4018	42686.6225	323.662339	274.09836	284.856341
1200	55.7244166	60069.2057	48235.4265	328.490133	278.432481	288.293964
1300	56.1850059	65664.8268	53831.0475	332.968775	282.457388	291.560295
1400	56.6243817	71305.4965	59471.7173	337.148761	286.216281	294.66898
1500	57.0378559	76988.8371	65155.0579	341.069698	289.743823	297.633009
1600	57.4230771	82712.124	70878.3448	344.76329	293.068228	300.46434
1700	57.7794034	88472.4881	76638.7088	348.255381	296.212755	303.173802
1800	58.1073525	94267.058	82433.2788	351.567376	299.196802	305.771124
1900	58.4081722	100093.054	88259.2746	354.717258	302.036716	308.265021
2000	58.6835277	105947.843	94114.0642	357.720313	304.746403	310.663293
2100	58.9352853	111828.973	99995.1935	360.589676	307.337796	312.972929
2200	59.1653687	117734.178	105900.399	363.336737	309.821213	315.200204
2300	59.3756671	123661.387	111827.608	365.971452	312.205642	317.350764
2400	59.5679815	129608.712	117774.933	368.502582	314.498962	319.429704
2500	59.7439939	135574.44	123740.661	370.937887	316.708121	321.441633

Table II-B2: CsOH(g) thermodynamic properties calculated with Gurvich et al. [2] molecular parameters

T(K)	Cp	H(T) - H(0)	H(T) - H(298)	S(T)	Gef(0)	Gef(298)
	J K^{-1} mol^{-1}	J mol^{-1}		J K^{-1} mol^{-1}		
298.15	50.1083911	11985.0416	0	258.261267	218.063302	258.261329
300	50.1520623	12077.7826	92.7410276	258.571361	218.312147	258.262286
400	51.7603404	17183.6683	5198.62676	273.24908	230.289955	260.252559
500	52.5728147	22404.2	10419.1585	284.895017	240.086654	264.056737
600	53.0861423	27688.5335	15703.4919	294.528087	248.380562	268.355631
700	53.5060113	33018.4343	21033.3927	302.743341	255.574175	272.695663
800	53.9198382	38389.5969	26404.5553	309.914918	261.927945	276.909247
900	54.3560954	43803.1796	31818.138	316.290699	267.62052	280.937232
1000	54.8148193	49261.576	37276.5345	322.041271	272.779713	284.764755
1100	55.2850281	54766.5278	42781.4862	327.287696	277.49996	288.395453
1200	55.7537775	60318.5305	48333.4889	332.118276	281.852849	291.840384
1300	56.2100761	65916.8647	53931.8231	336.599091	285.893825	295.113088
1400	56.6460343	71559.8643	59574.8228	340.780805	289.66663	298.227374
1500	57.0567432	77245.2272	65260.1857	344.703139	293.206333	301.19636
1600	57.4396955	82970.2858	70985.2442	348.397875	296.541457	304.032108
1700	57.7941376	88732.2147	76747.1731	351.890914	299.695505	306.745529
1800	58.1205051	94528.1767	82543.1351	355.203706	302.688062	309.346419
1900	58.4199844	100355.419	88370.3774	358.354261	305.53563	311.843546
2000	58.6941942	106211.331	94226.2895	361.357892	308.252236	314.244756
2100	58.9449647	112093.476	100108.435	364.227751	310.849914	316.557077
2200	59.1741917	117999.606	106014.564	366.975243	313.339066	318.786813
2300	59.3837426	123927.659	111942.617	369.610332	315.72875	320.939637
2400	59.5754004	129875.758	117890.717	372.141792	318.0269	323.020668
2500	59.750833	135842.198	123857.157	374.577388	320.240516	325.034532

Table II-B3: CsOH(g) thermodynamic properties calculated with Smith & Sugden molecular parameters [4]

T(K)	Cp	H(T) - H(0)	H(T)-H(298)	S(T)	Gef(0)	Gef(298)
	J K^{-1} mol^{-1}	J mol^{-1}		J K^{-1} mol^{-1}		
298.15	55.0628683	13480.7883	0	268.260966	223.046206	268.260991
300	55.1244679	13582.7117	101.923388	268.601763	223.326082	268.262043
400	57.6460288	19233.1068	5752.31849	284.839584	236.756836	270.458807
500	59.1065006	25077.0152	11596.2269	297.873847	247.719832	274.681408
600	60.0004713	31035.7843	17554.996	308.735499	257.009205	279.477185
700	60.5788418	37066.7157	23585.9273	318.03108	265.078639	284.336908
800	60.9714353	43145.4219	29664.6335	326.14748	272.215712	289.066697
900	61.2488549	49257.1953	35776.4069	333.345792	278.615584	293.594238
1000	61.451567	55392.7197	41911.9314	339.810026	284.417314	297.898102
1100	61.6039068	61545.8393	48065.0509	345.674461	289.723705	301.978967
1200	61.7211414	67712.3366	54231.5483	351.039942	294.613001	305.846991
1300	61.8132072	73889.2321	60408.4437	355.984048	299.146183	309.51602
1400	61.8867812	80074.3639	66593.5755	360.56769	303.371721	313.000856
1500	61.9464771	86266.1272	72785.3388	364.839542	307.328796	316.315988
1600	61.9955614	92463.3066	78982.5182	368.839093	311.049531	319.475024
1700	62.0363975	98664.9652	85184.1769	372.598813	314.560603	322.490478
1800	62.0707282	104870.37	91389.5814	376.145715	317.884403	325.373729
1900	62.0998606	111078.938	97598.1496	379.502508	321.039913	328.135065
2000	62.1247905	117290.202	103809.414	382.688465	324.043368	330.783762

2100	62.1462866	123503.782	110022.993	385.720077	326.908756	333.328179
2200	62.1649504	129719.365	116238.577	388.611564	329.64822	335.775851
2300	62.1812571	135936.693	122455.905	391.375273	332.272366	338.133579
2400	62.1955868	142155.551	128674.762	394.021993	334.790517	340.407512
2500	62.2082459	148375.755	134894.967	396.561203	337.210904	342.603219

Table II-B4: LiOH(g) thermodynamic properties calculated with Janaf molecular parameters [3]

	Cp	H(T) - H(0)	H(T)-H(298)	S(T)	Gef(0)	Gef(298)
T(K)	J K^{-1} mol^{-1}	J mol^{-1}		J K^{-1} mol^{-1}		
298.15	43.9442167	10451.0472	0	207.740622	172.688202	207.741186
300	44.024209	10532.4182	81.3709143	208.012702	172.905202	207.742026
400	47.3694607	15116.6352	4665.58799	221.177771	183.386604	209.514222
500	49.3950863	19962.7543	9511.70711	231.983272	192.0581	212.960195
600	50.7229573	24972.6956	14521.6484	241.113862	199.492983	216.911396
700	51.7009643	30095.8648	19644.8176	249.009369	206.015518	220.945585
800	52.5094165	35307.3395	24856.2923	255.967154	211.833191	224.897
900	53.2329992	40594.9726	30143.9254	262.194277	217.088939	228.701214
1000	53.9061046	45952.2814	35501.2342	267.838161	221.886048	232.337096
1100	54.5394909	51374.879	40923.8318	273.005984	226.301702	235.802654
1200	55.1345143	56858.9032	46407.856	277.777347	230.395068	239.104274
1300	55.689922	62400.4609	51949.4137	282.212674	234.212449	242.251716
1400	56.2046471	67995.5303	57544.483	286.35884	237.790725	245.255758
1500	56.6786682	73640.0323	63188.9851	290.252964	241.159722	248.127086
1600	57.1130432	79329.9414	68878.8942	293.925003	244.343896	250.8758
1700	57.5096579	85061.3817	74610.3345	297.399552	247.363545	253.511219
1800	57.8709264	90830.6945	80379.6473	300.697107	250.235704	256.041841
1900	58.1995352	96634.4782	86183.431	303.834976	252.974814	258.475365
2000	58.4982521	102469.605	92018.558	306.827944	255.593226	260.81875
2100	58.7697959	108333.223	97882.1758	309.688763	258.101595	263.078284
2200	59.0167553	114222.745	103771.698	312.428529	260.509176	265.259652
2300	59.241543	120135.835	109684.788	315.056968	262.82407	267.368003
2400	59.4463749	126070.389	115619.342	317.582663	265.053405	269.408008
2500	59.6332646	132024.512	121573.465	320.013232	267.203495	271.383914

Table II-B5: LiOH(g) thermodynamic properties calculated with Smith & Sugden molecular parameters [4]

CHAPTER III

CRITICAL ASSESSMENT OF THERMODYNAMIC DATA FOR THE CS-I SYSTEM: VAPOUR PRESSURE DATA*

*This chapter is ongoing submission to Journal of Nuclear Materials

Critical assessment of thermodynamic data for the Cs-I system: vapour pressure data

F-Z. Roki, M-N. Ohnet, Institut de Radioprotection et de Sureté Nucléaire, DPAM/SERCI, 13115, Saint Paul lez Durance, France.

C. Chatillon, Science et Ingénierie des Matériaux et Procédés (associé au CNRS UMR-5622 UJF/Grenoble- INP), BP 75, 1130 rue de la piscine, 38402 Saint Martin d'Hères, France.

ABSTRACT

Thermodynamic data for the Cs-I system, including solid, liquid and gases are important for the calculation of iodine release in a severe nuclear accident from two points of view: - (i) for the final evaluation of the nature of iodine formed compounds, and – (ii) for scaling kinetic data that are important in the calculations of intermediate states occuring in the primary cooling line. The present study is a critical analysis of available thermochemical data for the whole Cs-I system based on literature. Vapor pressure data are mainly assessed in order to deduce enthalpies of formation of the monomer CsI(g) and the dimmer Cs_2I_2(g). The proposed enthalpies of formation are:

$\Delta_f H°(CsI,g,298.15\ K) = -153.27 \pm 4.2\ kJ.mol^{-1}$ and

$\Delta_f H°(Cs_2I_2,g,298.15\ K) = -470.56 \pm 10\ kJ.mol^{-1}$.

Trimmer Cs_3I_3(g) also exists as well as tetramer species in smaller amounts. In the course of this thermodynamic assessment, condensed phase thermodynamic data were revised in order to obtain consistent set of data for vaporization. New heat capacity is proposed for the liquid phase, as well as for the melting enthalpy within the range of available experimental thermodynamic determinations:

$C°_p(liq) = 74.3\ J.K^{-1}.mol^{-1}$ and $\Delta_{melting} H°(CsI,s,at\ 905\ K) = 27.61 \pm 0.83\ kJ.mol^{-1}$.

III.1. INTRODUCTION

The behaviour of Cesium and Iodine in a nuclear reactor severe accident conditions has been the subject of many thermodynamic studies [1-4]. From those studies it appeared that one of the chemical form in which iodine escapes from the fuel is Cesium Iodide, this compound being stable and less volatile than elemental iodine. Consequently, it is important to select

reliable thermodynamic data for the solid, the liquid and for the gaseous phase of CsI in order to – (i) be used in thermodynamic calculations of any nuclear accident, or - (ii) to serve as references in the acquisition of new thermodynamic and kinetic data of the system Cs-I-O-H which is the first basic quaternary system related to accident chemistry.

Thermodynamic data for the Cesium-Iodine system have been analysed first by Brewer and Bracketts (1967) [5], then Feber (1977) [6] and Glushko et al. (1982) [7]. Brewer and Bracketts work was based on relatively scarce data and part of thermodynamic data were estimated. Feber and Glusko et al. both gave thermodynamic tables of the CsI(s,l), CsI(g) and Cs_2I_2(g). Thermodynamic functions of CsI solid have been further revised by Cordfunke and Prins (1985) [8] after new data acquisitions.

The present work has been undertaken in order to perform a critical assessment including new CsI experimental data – with emphasis on gas phase data - that have been recently published since the Glushko et al. data assessment performed in 1982 which is presently stored in the SGTE data bank [9] (original way of storage explained in [10]) and used as data sources in many nuclear accident thermodynamic simulation tools. More recent propositions for new data have been proposed by Cordfunke and Konings [11] that differ slightly. But yet the new investigations concerning the heat capacities and the vapour pressures of CsI(s,l) show that:

- The experimental total and apparent vapour pressures are higher than the pressures calculated with Glushko et al. tables, mainly in the 900 – 1300 K range,
- The composition of the dimmer in the gaseous phase is more important than calculated with Glushko et al. tables: 10% as total dimmer fraction from Glushko et al. to be compared to experimental measurements in the range 20 to 30% at ≈1300 K.

The origin of this disagreement might be due to the heat capacity Cp° of CsI(l), to the melting enthalpy or to the dimmerization constant of the dimmer K_{dim} (for 2 CsI(g) = Cs_2I_2(g) reaction). These thermodynamic data have to be revised in order to propose new reliable data to be used in a consistent way for the iodine transport calculation in the framework of the CHIP[1] program. Besides, the development of a new effusion reactor associated to our mass spectrometer called ”CHIP reactor” for thermodynamic and kinetic studies of the Cs-I-O-H

[1] CHIP (French acronym for "iodine chemistry in the primary circuit") program is conducted within the framework of the International Source Term Program, funded by IRSN, EDF (Electricité de France), CEA (Commissariat à l’Energie Atomique), European Community, USNRC (U. S. Nuclear Regulatory Commission), AECL (Atomic Energy Canada Limited), Suez-Tractebel and PSI (Paul Scherrer Institut).

system, needs to know more accurately the dimmer partial pressure via its dimmerization constant. Furthermore, as a mixed molecule CsI-CsOH has been proposed by Blackburn and Johnson in 1988 [12] that have a very high stability, the two dimmers related to this molecule would be the basic references to determine the thermodynamic properties of this new gaseous species.

III.2. CONDENSED PHASES DATA PREREQUISITES

Any critical analysis of gaseous molecules requires a reliable knowledge of related condensed phases that are often the source of these molecules since they are involved in different vaporization reactions. Different types of calorimetry, combined with thermochemical cycles calculation method based on literature data, were performed by Cordfunke and Prins [8] and results are summarized in table III-1. These authors performed also a critical assessment of earlier calorimetric data.

The dissolution enthalpy of CsI in water solution was determined by solution calorimetry at 298.15 K for different diluted concentrations. The enthalpy of solution measured by Cordfunke and Prins [8] at various concentration is in agreement with the preceding evaluation of Parker [13] who selected $\Delta_{\infty}H°$ (solution) = 33.346 ± 0.418 kJ.mol^{-1} as the best value from the measurements of Beketov and Beketov (1904) [14], and Forcrand (1911) [15, 16]. Since then, other measurements have been performed by Tsvetkov and Rabinovitch (1969) [17], Montgomery et al. (1978) [18] and Thourey and Perachon (1980) [19]. Due to the apparent small dependence on concentration, Cordfunke and Prins retained $\Delta_{\infty}H°$(CsI in water) = 33.35 ± 0.1 kJ.mol^{-1} as the best value for the enthalpy of solution of CsI(s) in water, but the authors did not detail their method. But yet, results of the two compilations (Parker and Cordfunke) are so close that this value can be retained as a reliable one. Using the above selected CsI(s) enthalpy of solution, the enthalpy of formation of Cs^+(aq) taken from CODATA (1989) [20] $\Delta_fH°(Cs^+,aq)$ = -258.04 ± 0.13 kJ.mol^{-1} and the enthalpy of formation of Iodine ion $\Delta_fH°(I^-,aq)$ = -56.750 ± 0.070 kJ.mol^{-1} given by VanderZee and Sprengel [21] from a recent evaluation of all available data, Cordfunke deduced the enthalpy of formation of CsI(s) to be $\Delta_fH°$ (CsI,s, 298.15 K) = -348.14 ± 0.18 kJ.mol^{-1}. This value is different from the value recommended by NBS [22], -346.6 kJ.mol^{-1}, a difference of about 2 kJ.mol^{-1} due to

different choices for $\Delta_f H°(I^-,aq)$. The selected value by Cordfunke is in perfect agreement with the value recommended earlier by Glushko et al. [7]. Indeed, the 2 $kJ.mol^{-1}$ difference will induce a difference in partial pressure of CsI(g) equal to ≈ 20% at 1000K.

At room temperature, CsI has a CsCl-structure (bcc) till melting. Below 160 K, CsI has a tetragonal lattice [23]. High temperature enthalpy increments have been measured by Cordfunke and Prins [8] using diphenyl ether drop calorimetry. CsI(s) samples were dried under Ar at different temperatures (473-523 K) during 2 to 4 hours before experiment. Data are compared to literature in Fig. III-1. Cordfunke and Prins measurements display two different sets of data: up to about 560 K data have a smooth connection with the low-temperature heat capacity measurements by Taylor et al. [24]. High temperature enthalpy increments have also been measured by Kaylor et al. (1960) [25], and Smith et al. (1961) [26], but their measurements do not agree with Cordfunke and Prins data, or do not connect to low-temperature heat capacity measurements (see Fig. III-1). For this reason Cordfunke discarded their measurements. According to Cordfunke, Takahashi et al.(1985) [27] measurements are rather scattered but the mean value differs by only 0.7% from Cordfunke's measurements. Takahashi et al. Cp° measurements let appear an increase of Cp° above 400 K as proposed by Cordfunke and Prins.

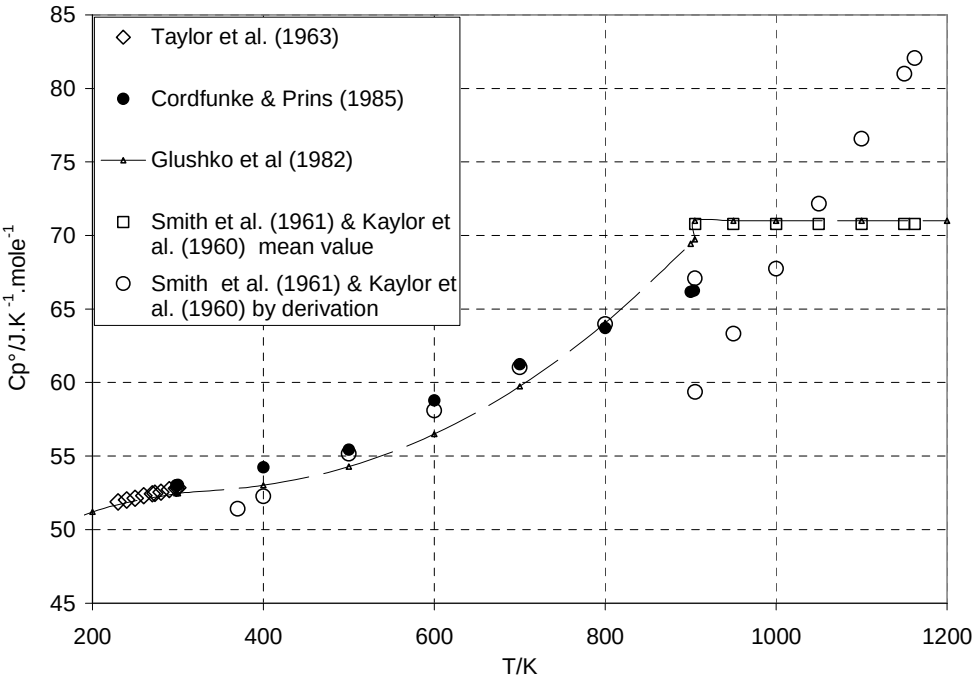

Figure III-1: Comparison of the heat capacities obtained by derivation of enthalpy increments relations as given by different authors at low and high temperatures

For the solid phase, recent values proposed by Cordfunke and Prins are in agreement with Glushko et al. selection on the basis of Taylor et al. low temperature data and taking into account of the uncertainties associated to the enthalpy increments derivation. Glushko et al. proposed data are retained for the solid phase.

For the liquid phase, the constant value adopted by Glushko et al. agrees with the mean value of liquid heat content coming from Smith et al. [26] and Kaylor et al. [25] values. Indeed, the derivation from Smith et al. and Kaylor et al. enthalpy increment values gives a drastic and anomalous Cp° evolution probably because these measurements are not enough accurate and were performed within a too small temperature range. Clearly, new calorimetric measurements are needed in a larger temperature range or with reduced uncertainties. Presently, we propose first to start the analysis with the selected value from Glushko et al. existing in the SGTE data bank.

Low temperature heat capacity measurements have been performed by Taylor et al. (1963) [24], and by Sorai et al. (1968) [28] .The latter authors claim a precision of 0.3% even though there is a systematic deviation between their two sets of measurements (0.5% at 298 K and 2% at 20 K). Marshall and Kunkler (1969) [29] determinations only agree with Sorai et al. [28] data below 5 K. The entropy of solid CsI has been derived from the low temperature heat capacity measurements: by Sorai et al. [28] $S°_{298} = 121.867 \pm 0.4$ $J.K^{-1}.mol^{-1}$ and by Taylor et al. [24] $S°_{298} = 123.05$ $J.K^{-1}.mol^{-1}$ without any details about accuracy. Cordfunke and Prins (1985) [8] propose a value close to Taylor's, $S°_{298} = 123 \pm 0.5$ $J.K^{-1}.mol^{-1}$ on the basis that their measurements in the high temperature range overlap Taylor's low temperature data smoothly. This value is retained, a bit different from Gluskho et al. retained one: 122.2 $J.K^{-1}.mol^{-1}$.

Authors & references	Samples	Experimental technique or Method	T (K) range	Thermodynamic Determinations	Observations
Cordfunke and Prins(1985) [8]	CsI-1 dried at 473 K for 2h (air?) CsI-2 and CsI-4: dried under Ar at 523 K for 4h Sample checked by X-ray diffraction	Dissolution calorimeter (in water) + Thermochemical cycle Diphenyl ether drop calorimeter Fit Fit Scanning calorimetry : Mettler DSC apparatus	298.15 583-851 396-540 396-540 T_m = 903.5 ± 0.2	<u>Enthalpy of solution of CsI in water</u> -Cordfunke best value at infinite dilution $\Delta H°_{\infty}$(dissolution) = 33.35 ± 0.1 kJ.mol^{-1} <u>Calculation of Enthalpy of formation of CsI</u> With CsI(s) = $Cs^+ + I^-$ From: $\Delta_f H°$(I-,aq) = -56.750± 0.070 kJ.mol^{-1} [21] $\Delta_f H°(Cs^+,aq)$ = -258.04 ± 0.13 kJ.mol^{-1} [30] Proposed value: $\Delta_f H°_{298.15}$ (CsI,s) = -348.14 ± 0.18 kJ.mol^{-1}. NBS value: $\Delta_f H°_{298.15}$ (CsI,s) = -346.6 kJ.mol^{-1} <u>Enthalpy increments</u> of CsI(s) $H^0(T)-H^0(298.15)$ (J.mol^{-1}) = 44.0049T+12.3085.10^{-3} T^2-14214.2 $H^0(T)-H^0(298.15)$ (J.mol^{-1}) = 49.4299T+6.00565.10^{-3} T^2-15271.4 <u>Measurement of Melting point and enthalpy of fusion</u> Cordfunke and Prins $\Delta_m H°$ = 24 ± 0.2 kJ.mol^{-1} To be compared with Glushko et al. $\Delta_m H°$ = 25.65 kJ.mol^{-1} Glushko et al.: T_m = 905 K	-In agreement with preceding Parker [13] selection: $\Delta H°_{\infty}$(solution) = 33.346 ± 0.418 kJ.mol^{-1} -Cordfunke [8] and Glushko et al.[7] in agreement -difference NBS [22] and Cordfunke of about 2kJ.mol^{-1} from choice of $\Delta_f H°(I^-,aq)$) Room T heat capacity in agreement with Taylor et al.[24] and Sorai et al. [28] Correction for vaporization effects

Table III-1: New calorimetric determinations since the Glushko et al. compilation. These determinations concern the enthalpy of formation of CsI(s), high temperature heat capacity and melting enthalpy [8]

Cordfunke and Prins determined the melting point with a Mettler DSC apparatus to be 903.5 ± 0.2 K. In fact, in literature, there are significant differences between the given values for the melting point as well as the enthalpy of fusion of CsI. Measurements by Kaylor et al. (1960) [25] have been discarded by Cordfunke due to the disagreement with their high temperature enthalpy increments. This analysis is not pertinent for a data which is an enthalpy difference deduced from measurements in a small temperature range. The melting enthalpy value given by Bousquet et al. (1967) [31] is rather high whereas their melting point is too low. For this reason, as those data were included in the Glushko et al. (1982) [7] analysis, Cordfunke rejected this selection and recommended new values (table III-2).

CsI (s)	**Glushko et al. (1982)**	**Cordfunke (1985)**
$T_{melting}$ (K)	905.1 ± 2.0	903.5 ± 0.2
$\Delta_{melting}H$ (kJ.mol^{-1})	25.65 ± 0.4	24 ± 0.2

Table III-2: Selected values for melting temperature and enthalpy of CsI(s) according to different authors

Cordfunke and Prins observed a very good reproducibility, but have to apply small corrections for vaporization. They discarded Kaylor and Smith melting enthalpy measurements on the basis of their disagreement of enthalpy increments with other authors. But yet this disagreement concerns absolute values and not necessarilly their melting enthalpy which is deduced from a difference between two measurements around melting temperature. Moreover, Kaylor and Smith used sealed Pt vessels and consequently the vaporization enthalpy should have no impact on the measurements at melting temperature, leading to a higher enthalpy effect. Reversely same thermal reasons might lead to decrease in the measured melting temperature for the Cordfunke and Prins DSC experiments with non sealed vessels.

We can thus conclude that there are still some uncertainties on the real value of the melting temperature as well as the melting enthalpy. From Thermodynamic point of view, these later data will affect through the melting of CsI(s) the heat capacity Cp° and the entropy S_T° of the CsI liquid. Moreover these two data are commonly used in the calculation of the enthalpy of formation of the gaseous molecules from pressure data over liquid phase. Conversely, changing these data for the liquid will generate new partial pressures in the vapour phase for the high temperature range. However, the present 2 K uncertainty on the melting temperature

does not generate significant uncertainties on thermodynamic properties of the liquid phase and will not be considered to be evaluated more accurately. We propose to retain the Glushko et al. value, $T_{melting}$ = 905.1 K.

III.3. DISSOCIATION ENERGY DETERMINATIONS

Different spectroscopic measurements - summarized in table III-3 - were performed on CsI(g) that led, using some assumptions, to the enthalpy of the dissociation reaction at 0 K,

$CsI(g) = Cs(g) + I(g)$ $D_0°$(at 0 K)

Authors	Experimental method	$D_0°$ kJ.mol^{-1}	$\Delta_f H°_{298\ K}$ kJ.mol^{-1}	Observations
Sommermeyer (1929) [32]	Absorption Spectroscopy	309.6 ± 17	-128.2 ± 17	Birge-Spooner extrapolation
Bulewitz et al. (1961) [33]	Flame	352 ± 17	-168.8 ± 17	Cs metal adsorption
Gaydon (1968)[34]	Compilation	328 ± 3.9	-146.6 ± 4.0	Mean value with thermochemical works (Sheer and Fine)
Berkowitz (1969) [35]	Photoionization	344.3 ± 4.2	-162.9 ± 4.2	Onset of Cs^+ ionization
Huber and Herzberg (1979) [36]	Compilation	345.3	-162.1	Mean value with thermochemical works
Su and Riley (1979) [37]	Photofragment spectroscopy	332.6 ± 2.1	-151.2 ± 2.1	

Table III-3. Spectroscopic studies from literature aimed to determination of dissociation energy of the molecule CsI(g) and derived formation enthalpies.

The published values are largely scattered due to the different assumptions that are necessary in the interpretation of the results: choice of a simplified set of reactions as well as equilibrium state assumption in flame studies, assumptions on the electronic states of products or on the absence of kinetic energy of neutral fragments. In flame studies the relatively high temperature range (≈ 2250 K) of measurements do not warranty the reliability of the used free energy functions as tabulated from low temperature observations. Moreover the presence of ions and exited states is not often taken into account either in the method of measurement or in the set of considered reactions. Following Glushko et al., these spectroscopic measurements are considered generally as first and rough approach to the enthalpy of formation and thermochemical determinations are needed to obtain more reliable thermodynamic functions. Indeed, Gaydon (1968) [34] and Huber and Herzberg (1979) [36] propose values that take into account of the thermochemical values available at that time. Thus, no reliable CsI(g) enthalpy of formation selection can be done via the CsI (g) enthalpy of dissociation and other techniques have to be analysed.

III.4. TOTAL PRESSURE DETERMINATIONS

Since Glushko et al. compilation (1982) [7], different techniques such as mass spectrometry, Knudsen effusion method, transpiration method, Rodebush-Dixon (also called quasi-static) method have been used to determine the CsI(s,l) total pressure with or without taking into account of the dimmer pressure in their thermodynamic calculations (*i.e.* assumption of gaseous phase composed only with CsI (g)) (see appendix III-A). After the first works of Akishin et al. [38] and Gorokhov [39], Viswanathan and Hilpert (1984) Knudsen cell mass spectrometric investigations [40] of the vapour over CsI(s) between 604 and 833 K showed the existence of a more complex gaseous phase. The analysis of the ionization efficiency curves as well as the ratio of the ions intensities as a function of temperature allowed the identification of the molecular origins of each measured ion:

$$CsI(g) \rightarrow [Cs^+, CsI^+, I^+]$$

$$(CsI)_2(g) \rightarrow [Cs_2I^+, Cs_2^+, Cs_2I_2^+]$$

$$(CsI)_3(g) \rightarrow [Cs_3I_2^+]$$

$$(CsI)_4(g) \rightarrow [Cs_4I_3^+]$$

According to Viswanathan and Hilpert, the vapour phase is composed of the monomer CsI(g), the dimmer $Cs_2I_2(g)$, the trimmer $Cs_3I_3(g)$ (first observation) and the tetramer $Cs_4I_4(g)$ in a

very low proportion because only one ion intensity measurement of $Cs_4I_3^+$ was recorded close to the detection limit. After calibration procedure, the proposed pressures ratio $p_{dimmer}/p_{monomer}$ is about 8.52 10^{-2} and $p_{trimmer}/p_{monomer}$ is about 1.59 10^{-4} at 905 K -the melting temperature selected by Glushko et al. -.

III.4.1. Knudsen effusion method

The Knudsen effusion method has been used by Venugopal et al. (1985) [41] in order to obtain vapour pressure values over solid CsI in the temperature range 753 to 897 K with the assumption of no dimmer contribution (estimated by the authors to be less than 1% at T<863 K). The principle of the Knudsen effusion method consists on determining the CsI (or Cs) mass loss at constant temperature for each experiment to obtain the corresponding pressure using the Knudsen relation [42]:

$$\frac{dN_i}{dt} = \frac{p_i \, sC}{\sqrt{2\pi M_i RT}} \qquad (1)$$

relation in which the number of moles effused dN_i/dt per second is related to the partial pressure p_i, M_i the molar mass of the effused species *i*, *s* and *C* the orifice cross-section and Clausing coefficient and R the gas constant. In case of an unknown complex gaseous phase, the measured pressure can not be considered as a total pressure measurement but more conveniently as an apparent pressure. The apparent pressure concept is used once the experimenter does not know exactly if the analyzed vapours are coming from CsI(g) monomer, Cs_2I_2(g) dimmer or Cs_3I_3(g) trimmer etc… In the effusion method, if the vapours are analyzed as coming from the only CsI monomer the Knudsen relation becomes:

$$dm = \frac{p_{app} \cdot \sqrt{M_1}}{\sqrt{2\pi RT}} \qquad (2)$$

relation in which *dm* is the measured mass loss during an experiment, p_{app} the vapours apparent pressure, *R* the gas constant and *T* the temperature. Once vapours are considered coming from monomer and dimmer, relation (2) becomes:

$$dm = \frac{p_1 \cdot \sqrt{M_1}}{\sqrt{2\pi RT}} + \frac{p_2 \cdot \sqrt{M_2}}{\sqrt{2\pi RT}} \quad (3)$$

p_1 is related to analyzed vapours coming from CsI(g), p_2 is vapours coming from Cs_2I_2(g), M_1 and M_2 are respectively the CsI and Cs_2I_2 molar masses.

With $M_2(Cs_2I_2) = 2M_1(CsI)$ (4)

Relating equations 2 and 3:

$$\frac{p_{app} \cdot \sqrt{M_1}}{\sqrt{2\pi RT}} = \frac{p_1 \cdot \sqrt{M_1}}{\sqrt{2\pi RT}} + \frac{p_2 \cdot \sqrt{2M_1}}{\sqrt{2\pi RT}} \quad (5)$$

and thus the measured apparent pressure is related to the partial pressures by the relation,

$$p_{app} = p_1 + \sqrt{2}\, p_2 \quad (6)$$

If trimmer and tetramer gas are taken into account, equation 6 becomes:

$$p_{app} = p_1 + \sqrt{2}\, p_2 + \sqrt{3} p_3 + \sqrt{4} p_4 + ... \quad (7)$$

Glushko et al.(1982) considered that the vapour phase is composed only of monomer and dimmer gaseous species, with 7% of dimmer fraction at melting point 905K, quantity based on Akishin et al. [38] and Deitz [43] measurements. Using Glushko et al. tables, monomer and dimmer pressures have been calculated via the 3rd law of thermodynamics and using equation (6) apparent pressures have been deduced. Comparison with Venugopal et al. (1982) [41] and others who used the same experimental method (effusion Knudsen) is presented in figure III-2.

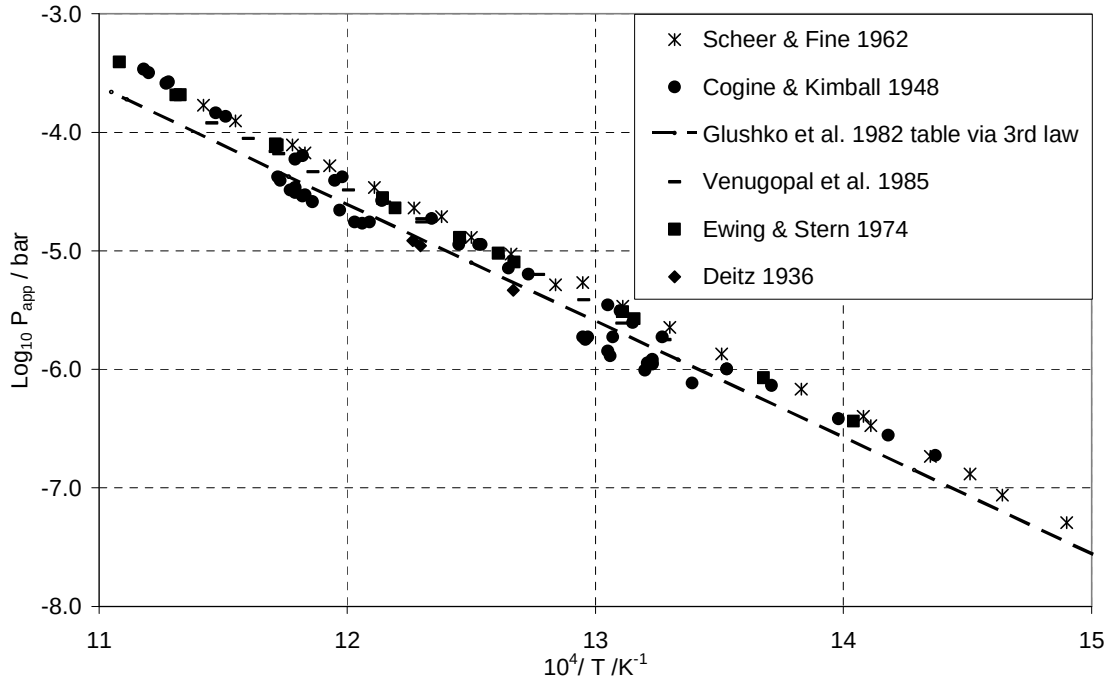

Figure III-2: CsI apparent total pressure determinations over solid given by different authors using the Knudsen effusion method and comparison with calculations from Glushko et al selected data.

Glushko et al.(1982) selected data are generally lower than the measured one's (Scheer and Fine [44] and Ewing and Stern [45]) although some series of data agree with Glushko et al. *i.e* Deitz [43] and Cogin and Kimball [46]. Recent measurements of Venugopal et al. (1985) [41] confirm the higher pressure experimental data sets.

Viswanathan and Hilpert [40] obtained from their data 8% of dimmer molar fraction at 905 K in the gaseous phase. This value was calculated using their spectrometric ionic intensity measurements based on an estimate of the ionization cross sections ratio $\sigma_{dimmer}/\sigma_{monomer}$ = 1.75. Using the spectrometric relation:

$$p_i S_i = I_i T \qquad (8)$$

relation in which I_i is the measured ionic intensity, p_i the partial pressure of the original molecule in the cell, T is the cell's temperature and S_i is the sensitivity which is given by the general relation:

$$S_i = G\eta_i\sigma_i(E)\gamma_i f_i \quad . \qquad (9)$$

G is a geometrical factor related to the solid angle for molecular beam sampling defined by the ionization chamber aperture and the effusion orifice, η_i is the extraction and transmission efficiency of the formed ion in the mass spectrometer, σ_i(E) is the ionization cross section depending on the electron energy *E*, γ_i is the efficiency of the ion detector, f_i is the isotopic abundance of the detected ion that is calculated exactly for any atomic composition of each ion.

For the ion source and magnetic analyser of Viswanathan and Hilpert spectrometer η_i is constant whatever the measured ion is, and for their discriminated pulse-counting detection γ_i = 1 whatever is the measured ion i, and consequently, the sensitivity is reduced to the very simple relation:

$$S_i = G\sigma_i(E)\, f_i \qquad (10)$$

Once considering the reaction of dimmerization:

$2CsI(g) = Cs_2I_2(g)$

the pressures ratio can be defined as:

$$\frac{p_2}{p_1} = \frac{I_2}{I_1} \times \frac{S_1}{S_2} = \frac{I_2}{I_1} \times \frac{\sigma_1}{\sigma_2} \qquad \text{1 for monomer and 2 for dimmer} \qquad (11)$$

Thus, according to relations (10) and (11), the uncertainty on the pressures ratio is directly related to the uncertainty due to the intensities measurements and to the ionization cross sections ratio as follows:

$$\frac{\delta\left(\frac{p_2}{p_1}\right)}{\frac{p_2}{p_1}} = \frac{\delta\left(\frac{I_2}{I_1}\right)}{\frac{I_2}{I_1}} \times \frac{\delta\left(\frac{\sigma_1}{\sigma_2}\right)}{\frac{\sigma_1}{\sigma_2}} \qquad (12)$$

The uncertainty due to the experimental measurements can be estimated to 10-20% and depends on the pulse counting rate that moves with temperature and pressure range in the cell. The uncertainty due to the ionization cross sections ratio is evaluated to be ± 17% by

comparison of the $\sigma_2 / \sigma_1 = 1.75$ chosen value by the authors with usual estimates that range from the additivity rule and the observations for the dimmers as summarized by Drowart et al. [42] in a recent paper related to the mass spectrometric techniques applied to high temperatures:

$$\sqrt{2} < \frac{\sigma_2}{\sigma_1} < 2 \qquad (13)$$

So the total uncertainty on the pressures ratio is about 30%. Consequently, the dimmer molar fraction proposed by Viswanathan and Hilpert at 905 K (melting point) can vary from 5 to 11%. Note that in these mass spectrometric measurements the total ionic intensities (needed to apply the additivity rule for ionization cross sections) associated to one gaseous species include the parent and fragment ions intensities, the later ones being important for the present observed compounds: CsI(g) gives CsI^+ and Cs^+, meanwhile Cs_2I_2 gives Cs_2I^+, Cs_2^+ at least and the assumption of the authors is that Cs^+ and CsI^+ came only from the monomer. This assumption has been put forward because they did not observe any significant change in the ionization efficiency curves. But yet such observation is not very accurate and if this assumption is not sustained, the proportion of dimmer may be underestimated in the gas phase. Besides, Viswanathan and Hilpert did not use their own pressures calibration by mass loss measurements and they used in place Ewing and Stern Knudsen cell mass loss determinations. This fact was not clearly justified in relation with their experimental observations and the authors only admitted that these earlier determinations were more accurate. One can thus conclude that they might have some problems in their mass loss measurements associated with their mass spectrometric experiments. Indeed for such ionic compounds and high volatile gases, different parasitic phenomena can occur at the effusion orifice – surface diffusion along the orifice walls, re-vaporization of the molecular beam as summarized previously in the effusion mass spectrometric methods [42] and recently observed by us in the CsOH(s,l) vaporization [47]–. All these phenomena lead to an increase of the monomer proportion in the observed molecular beam by the mass spectrometer when using a conventional beam sampling [47]. Thus, a lower measured dimmer proportion can be expected in these determinations. Same observation can be done for earlier mass spectrometric determinations by Akishin et al. [38] retained in the Gluskho et al. compilation.

III.4.2. Transport/transpiration methods

Transport/Transpiration methods were used in conjunction with analysis of the quantity of Cs transported with a carrier gas (Ar for example) and finally condensed at the exit of the reactor chamber. In this case – and due to lack of on line gas analysis - the result concerns the total apparent pressure since the original composition of the carrier gas is not exactly known. If the analyzed Cs in the condensate is considered coming from CsI(g) alone, using the gas law equation:

$$p_{app}(Cs)\cdot V_{(Ar)} = n(CsI)\cdot R\cdot T \quad (14)$$

$$p_{app}(Cs) = \frac{n(CsI)\cdot R\cdot T}{V_{(Ar)}} \quad (15)$$

relation in which p_{app} *(Cs*) is the apparent pressure, $V_{(Ar)}$ the argon total volume and *n(CsI)* the total mole number analysed at the condenser. In case of Cs analysis, the total mole number of Cs coming from monomer and dimmer is calculated with the following relation:

$$n_{Cs}^{\ tot} = n(CsI,g) + 2n(Cs_2I_2,g) \quad (16)$$

Since there are 2 moles of Cs per dimmer gas,

$$\frac{p_{app}(Cs)\cdot V_{(Ar)}}{R\cdot T} = \frac{p(CsI)\cdot V_{(Ar)}}{R\cdot T} + \frac{2\,p(Cs_2I_2)\cdot V_{(Ar)}}{R\cdot T} \quad (17)$$

and thus $$p_{app} = p_1 + 2p_2 \quad (18)$$

with p_1 the CsI(g) pressure and p_2 the Cs_2I_2(g) pressure.

In case of trimmer and tetramer in the gaseous phase, taking into account equation like (18) the apparent pressure becomes:

$$p_{app} = p_1 + 2p_2 + 3p_3 + 4p_4 + \ldots \quad (19)$$

Using Glushko et al. (1982) tables, partial pressures of monomer and dimmer have been calculated via the 3rd law of thermodynamics and using equation (18), apparent pressures are deduced and compared to recent studies such as Venugopal et al. (1985) [41] and Cordfunke (1986) [48] as well as earlier Topor (1972) [49] determinations with the same experimental method (transport). Results are presented in figure III-3.

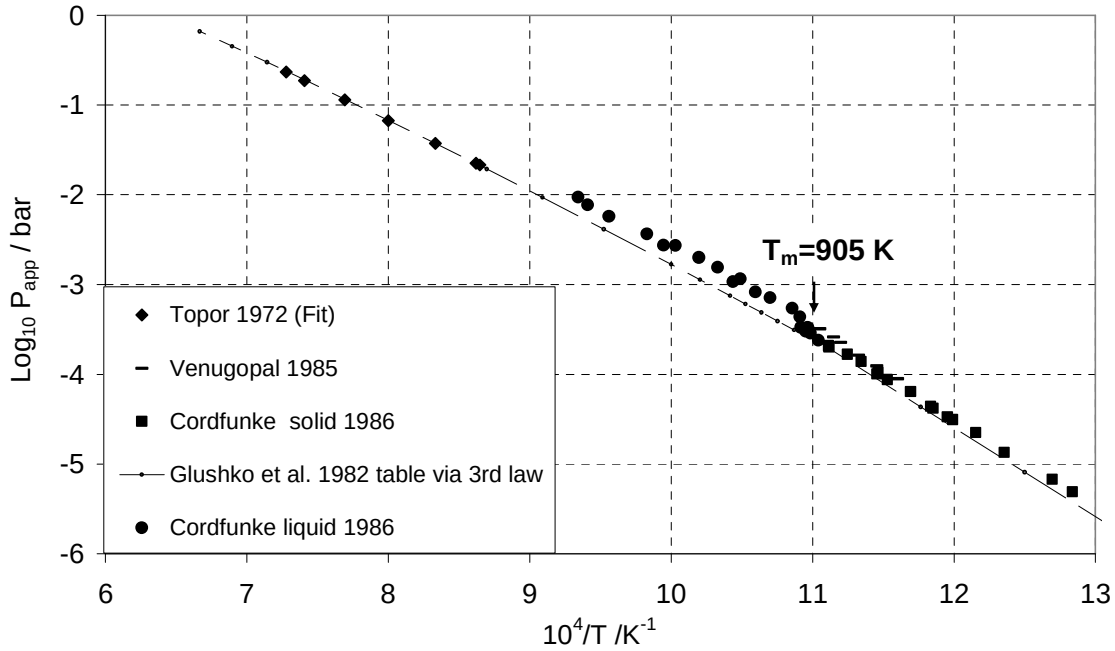

Figure III-3: Apparent pressure determinations over solid and liquid CsI given by different authors using the transport method and comparison with recalculated values from Glushko et al. selected data.

Figure III-3 presents the decimal logarithmic of the apparent pressure of CsI over solid and over liquid as a function of the inverse of temperature given by different authors. Over CsI solid, Glushko et al. data remains slightly lower than the one determined by Cordfunke and Venugopal et al. Above the melting point (T_m = 905 K), Glushko et al. pressures are definitely lower than the one given by Cordfunke over liquid and, finally, at elevated temperatures join the equation proposed by Topor (1972). Indeed, this last agreement corresponds to the Glushko et al. selection at high temperature based on Topor's measurements.

On the other hand, the analysis of Cordfunke's pressure data around the melting point, show an abnormal trend in these data since a step-like is observed. Cordfunke related this fact to a sudden dimmer apparition, an interpretation which can not agree with thermodynamic

behavior –regular increase-. By comparison with Venugopal et al. pressures over the CsI solid, Cordfunke pressures are slightly lower especially close to the melting point and before the step-like. Three main features can explain this sudden increase:

- The difference of pressure can be due to a problem of evaporation rate which might be low because of "retarded" or "hindered" vaporization processes [50, 51]. Consequently, there may be no equilibrium reached over the solid phase and lower pressures are measured. Rothberg et al. [52] determined free vaporization rates and by comparison with equilibrium rates proposed an evaporation coefficient for CsI total pressure $\alpha = 0.36$ in the temperature range 757-772 K - α = p(measured) / p(equilibrium) by definition -. Cordfunke pressures data over CsI solid has been recalculated taking into account of this evaporation coefficient (P_{app}(recalculated) = P_{app}(cordfunke) / 0.36). Results are presented in figure III-4. This correction increases the pressure in the correct direction but seems too important, a feature which is explained because the steady state of vaporization in a transport reactor is not clearly free vaporization: indeed – as already studied for the effusion method [53] – the balance of evaporation and condensation flows at the sample surface increases the apparent net evaporation flow toward the equilibrium value as a function of the steady state flow in the reactor. Further in the experiment, the retarded vaporization observed over solid phase is normally non operating over the liquid phase because the evaporation coefficient is usually 1 for liquids [54] (and pressures are at equilibrium) due to no activation energy barrier for so disordered surfaces. The pressure should thus increase at once at the melting temperature.
- Note that the complex molecules – the dimmer in the present case – are more sensitive to vaporization kinetics due to difficulties in the adsorption stage reactions at the solid surface *i.e.* matching the surface structure to build the adsorbed dimmer before desorption. Considering the retarded vaporization process for the only dimmer, this last might be the responsible molecule of the observed step as proposed by Cordfunke. Thus, considering that the proportion of the dimmer over the solid would be very low (evaporation coefficient ≈ 0 for instance), the pressure step at the melting would be mainly due to the sudden dimmer contribution in the total pressure. the experimental relative difference in apparent pressure between liquid and solid at 905 K is calculated according to the following relation,

$$\frac{p_{app}(s) - p_{app}(l)}{p_{app}(l)} = \frac{\Delta p_{app}}{p_{app}(l)} = 0.32 \qquad (20)$$

Relation in which $P_{app}(s)$ and $P_{app}(l)$ are respectively the apparent pressure over solid and over liquid at 905 K (obtained by least square fits).

The difference in apparent pressure Δp_{app} can be written as following:

$$\Delta p_{app} = (p_1^0 + 2p_2^0)^{liq} - (p_1^0 + 2p_2)^{sol} = 2p_2^0 - 2p_2^{sol} \quad (21)$$

Relation in which p^0_1 and p^0_2 are the standard (pure compound) equilibrium pressures of the monomer and the dimmer at the melting temperature, liq for liquid phase and sol for solid phase. Since the equilibrium is not reached over the solid phase for the dimmer pressure, this pressure can be related to the equilibrium pressure through the evaporation coefficient α by the following relation:

$$p_2^{sol} = \alpha p_2^0 \quad (22)$$

and combining relations (21) and (22),

$$\Delta p_{app} = 2p_2^0 - 2\alpha p_2^0 = 2p_2^0(1-\alpha) \quad (23)$$

and finally relation (20) becomes,

$$\frac{\Delta p_{app}}{p_{app}(l)} = \frac{2p_2^0(1-\alpha)}{(p_1^0 + 2p_2^0)^{liq}} = 0.32 \quad (24)$$

The monomer/dimmer pressure ratio is obtained as,

$$\frac{p_2^0}{p_1^0} = \frac{0.32}{2(1-\alpha-0.32)} \quad (25)$$

For low evaporation coefficients, $\alpha \rightarrow 0$ the ratio dimmer to monomer is at its minimum value, i.e. 0.23, and increases up to 0.28 for $\alpha = 0.1$. As a conclusion, the assumption of no dimmer over the solid phase in the Cordfunke experiments would lead to an estimate of at least 22% of dimmer molar fraction at equilibrium over the liquid at the melting temperature.

- The pressure step may come from temperature determinations. In fact, the necessary evaporation heat associated to the CsI molecules flow swept away by the carrier gas can cool down the vaporizing surface since in a such low temperature range mainly conduction heat tranfer in the solid phase as well as some heat contact resistance between the container and the solid CsI may occur. As the measured temperature is necessarily located between the furnace and the container, the determined pressure is reported to thermocouple temperature and not to the real vaporizing surface. By this way, the author attributes pressure data to the temperature of the liquid phase while these data belong to the temperature of the solid phase. This is the meaning of the 11 K difference observed between the maximum temperature at the step-like (916 K) and the retained melting point (905 K) in the compilations. Cordfunke data in the temperature range 867-916 K were thus corrected using the following relation based on heat transfer relation,

$$T_{corr} = 11 \cdot \left(\frac{T - T_0}{T_{\max} - T_0} \right) \qquad (26)$$

relation in which T_{corr} is the corrected temperature, T the Cordfunke measured temperature, T_0 and T_{max} are respectively the minimum and maximum measured temperature over solid. Corrected data are presented in figure III-4.

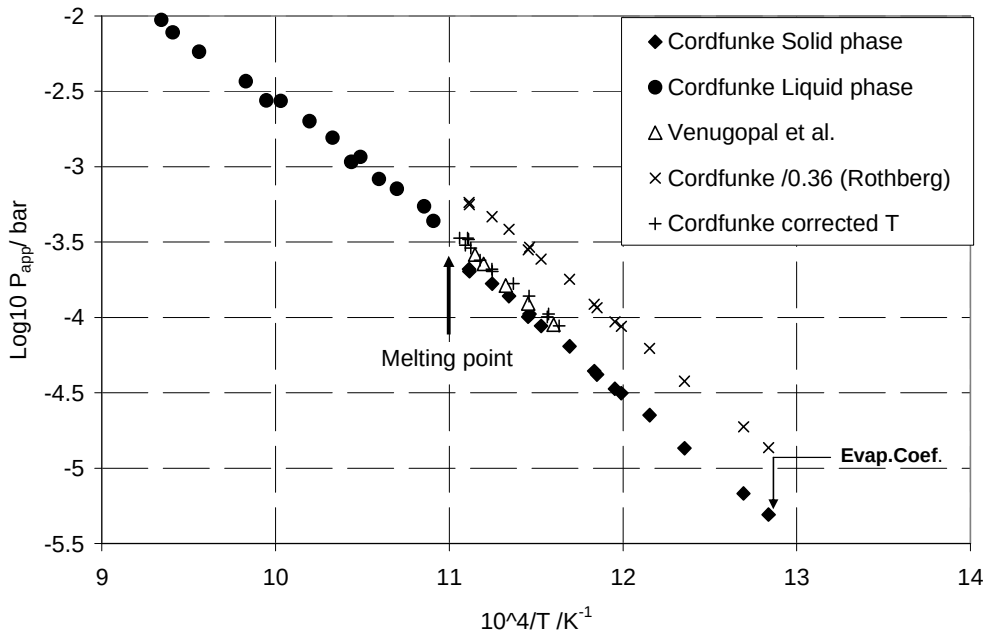

Figure III-4: Corrected data from Cordfunke measured pressures below and close to the melting temperature according to two assumptions: evaporation coefficient and temperature gradients (see text).

According to the general evolution of the data in figure III-4, Cordfunke original pressures data over solid will be thus selected in the temperature range 779-855 K and these last corrected data will be retained in the temperature range 864-904 K. Over liquid, Cordfunke pressures will be used in the temperature range 916-1070 K.

Among the two preceeding above analysis, the second one (temperature gradient) seems likely reliable and we propose to retain the last corrected values.

III.4.3. Total pressure measurements

The total pressure over the liquid phase has been obtained using direct manometric measurements by Deitz (1936) [43], Rodebush-Dixon method by Murgulescu and Topor (1970) [55], boiling point method by Venugopal et al. (1985) [41]. According to these experimental techniques the total (static) measured pressure corresponds to the following relation:

$P_{tot} = p_1 + p_2 + p_3\ldots$ (p_1 for monomer, p_2 for dimmer...) (27)

Comparison between authors data and Glushko et al. calculated total pressures is presented in figure III-5.

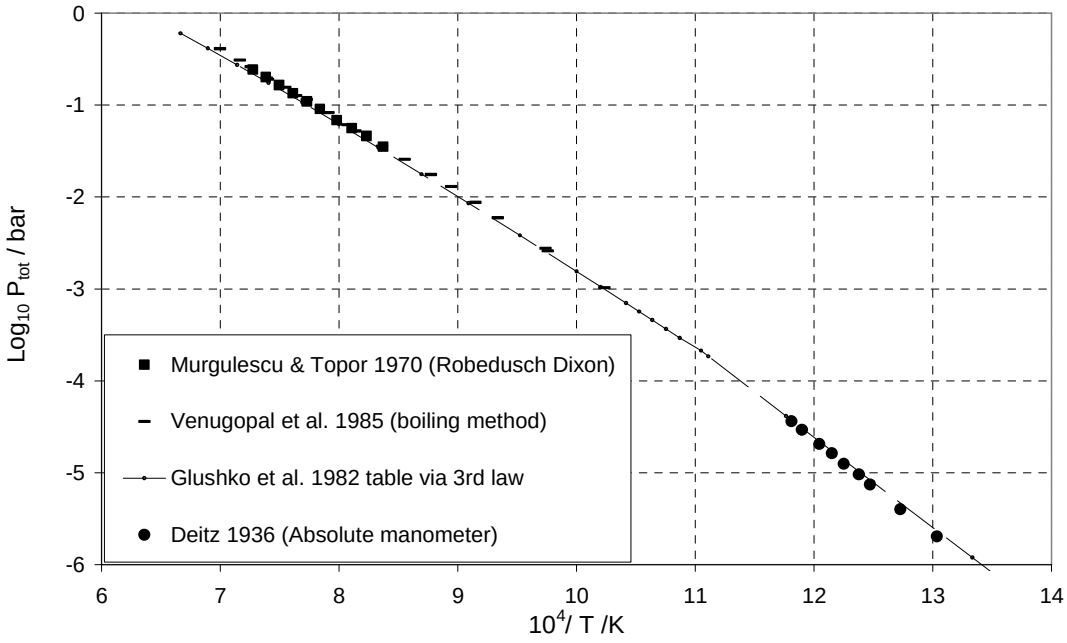

Figure III-5: Total pressure determinations over CsI given by different authors and comparison with Glushko et al. selection.

Glushko et al. total pressures fit very well those proposed by Deitz over solid and are slightly lower than Murgulescu and Topor determinations as well as recent measurements of Venugopal et al. (1985) over CsI liquid at intermediate temperatures.

III.4.4. Discussion

The present comparison of vapour pressure data over CsI(s, or l) was initiated in view of checking the proposed thermodynamic properties for the Cs-I system by the Glushko et al. compilation (1982) [7] against new experimental data for this system. Glushko et al. data in terms of CsI pressures are lower than those proposed by recent measurements of Venugopal et al. (1985) [41] and Cordfunke (1986) [48]. The basic difference between Glushko et al. and later experimental data would be due to different data sources used in the strategy of interpretation of original data:

- The choice of the dimmerization constant K_{dim} for the monomer into dimmer proposed by Glushko et al. (1982) for the reaction 2 CsI(g) = Cs_2I_2(g).
- The choice of the primary enthalpy of vaporization of CsI(g) used by Glushko et al. for the reaction CsI(s) = CsI(g).
- The choice of the melting enthalpy L_f of CsI(s→l) that may change the pressures values over the liquid phase.
- The choice of the heat capacity Cp° of the liquid phase.

Owing to the present differences observed with the preceding Glushko et al. compilation, the present work has been turned up to two principal aims:

- ✓ A better compromise between the selected authors including more recent data
- ✓ Proposition of a new set of thermodynamic data for CsI solid, liquid and gas, more reliable than the Glushko et al. selection.

An optimization of thermodynamic parameters of CsI(s,l) - K_{dim}, vaporization enthalpy, melting enthalpy and heat capacity - is thus necessary with the assumption that the free energy functions $Fef°_T$ of CsI(g) and Cs_2I_2(g) are reliable enough as discussed by Gluskho et al. [7].

III.5. CRITICAL ANALYSIS OF CSI(S,L,AND G) COMPOUNDS THERMODYNAMIC PROPERTIES

III.5.1. Proposition for a new equilibrium constant of dimmerization K_{dim}

The dimmerization constant K_{dim} for the reaction $2CsI(g) = Cs_2I_2(g)$ is related to monomer and dimmer partial pressures p_1 and p_2 according to the following relation:

$$K_{dim} = \frac{p_2}{p_1^2} \quad (28)$$

If the proportion of the dimmer is not correctly evaluated in comparison with the monomer's one, this will have an effect on the dimmerization constant value and consequently in thermodynamic calculations from total pressure or total transport data. So, we have to analyse first the reliability of the selected dimmerization constant K_{dim}.

In literature, depending on the experimental technique, there is a large scatter concerning the fraction of the dimmer $Cs_2I_2(g)$ existing in the gaseous phase over the condensed CsI. The molar fraction of the dimmer x_{dimmer} is calculated according to the following relation:

$$x_{Dimmer} = \frac{p_2}{p_1 + p_2} \quad (29)$$

The dimmer partial pressures can be obtained by combination of two types of measurement: total and apparent pressure measurements, when using the following relations:

$$p_{tot}(measured) = p_1 + p_2 \quad (30)$$

$$p_{app}(transport) = p_1 + 2p_2 \quad (31)$$

p_{tot} is the total measured pressure and p_{app} is the apparent pressure deduced from mass tranport when exploitation of the transported mass is done assuming only one species (the monomer) in the gas phase.

Using equations (30) and (31), the dimmer pressure is deduced as:

$$p_2 = p_{app}(transport) - p_{tot} \quad (32)$$

From the measured total pressure p_{tot} (static methods, or quasi-static ones), the dimmer fraction is thus deduced using relation (29) that becomes,

$$x_{Dimmer} = \frac{p_{app}(transport)}{p_{tot}} - 1 \qquad (33)$$

Independently, mass spectrometric methods also give the vapour composition. Comparison of the different values proposed in literature is displayed in figure III-6.

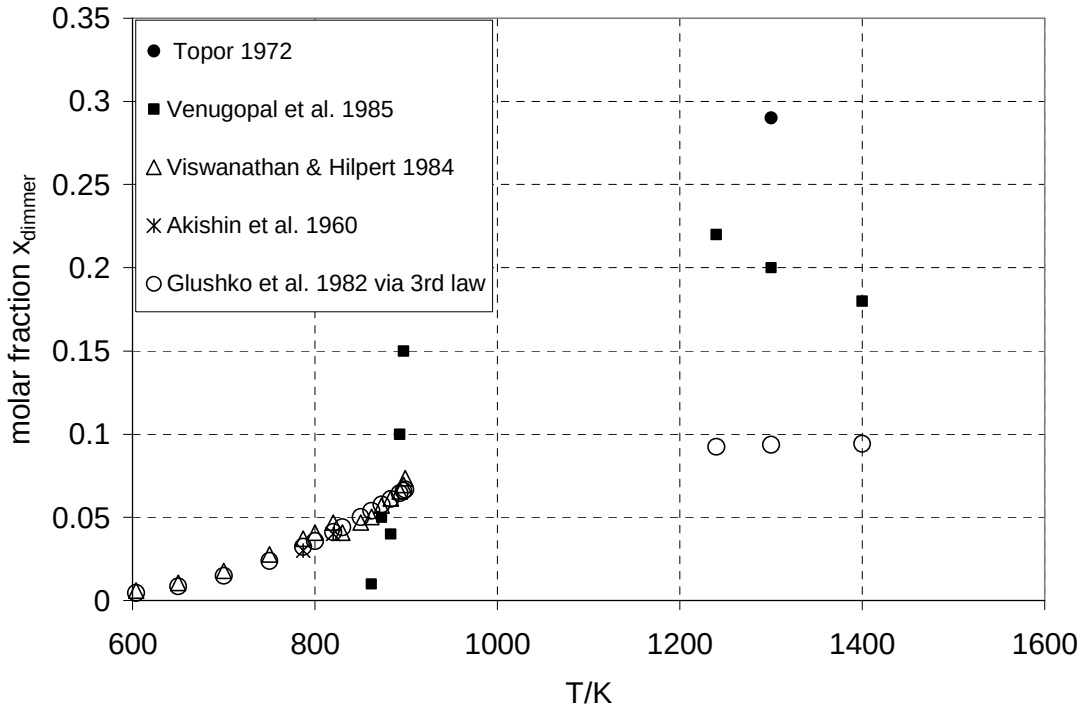

Figure III-6: Calculated Glushko et al. selected dimmer contributions compared to experimental determinations.

This figure shows that the measured dimmer fraction in equilibrium with the condensed phases increases with temperature. Glushko et al. retain a dimmer fraction of 7% at 905 K (melting temperature) based on Akishin et al. [38], Gorokhov [39] mass spectrometric determinations using a double or so-called “Tandem” effusion cell. Values at other temperatures are then recalculated using the Glushko et al. free energy functions.

Viswanathan and Hilpert [40] are in agreement with Glushko et al. in the low temperature range (600-900 K) over the solid phase.

Venugopal et al. [41] values obtained by transport and total pressure measurements below and around the melting point seem to be not accurate enough because the accuracy of their two coupled experimental methods (see relation (33)) becomes of the same order than the dimmer contributions and consequently they are largely scattered or tend to null values.

Conversely, Venugopal et al. values over the liquid phase at high temperature – although quite scatterred - are much higher than calculated ones from Glushko et al., and are in relative agreement with the mean value proposed by Topor [49] at 1300K (x_{dimmer} = 0.29). We have to note that Topor do not propose indivual values but a mean value, probably because there exists also a large scatter. Thus, as in this high temperature range the relative error when using relation (33) becomes smaller, we prefer to select the Topor and Venugopal et al. values.

III.5.2. Equilibrium constant for the dimmerization $2CsI(g)=Cs_2I_2(g)$

Using the dimmer mole fraction mean value 0.25 at 1300 K (from Topor and Venugopal et al.), and knowing their apparent or total pressure at 1300 K, the monomer and dimmer partial pressures p_1 and p_2 have been recalculated and the constant of dimmerization deduced by combining relations (28), (29), (30) and/or (31):

$$K_{\dim}(Venugopal\ et\ al.,1300K) = \frac{p_2}{{p_1}^2} = \frac{0.25 \cdot p_{tot}}{(0.75 \cdot p_{tot})^2} = \frac{0.25}{0.75^2\ p_{tot}} = 3.73 \qquad (34)$$

with total pressure p_{tot} = 0.1191 bar at 1300 K

$$K_{\dim}(Topor,1300K) = \frac{p_2}{{p_1}^2} = \frac{0.2 \cdot p_{app}}{(0.6 \cdot p_{app})^2} = \frac{0.2}{0.6^2\ p^*} = 4.86 \qquad (35)$$

with apparent pressure p_{app} = 0.1143 bar at 1300 K.The mean dimmerization constant value is thus,

$$K_{dim} = 4.295 \pm 0.565$$

Using the 3rd law of thermodynamics, we calculated the enthalpy of dimmerization at 298 K for the reaction $2CsI(g)=Cs_2I_2(g)$:

$$\Delta_{\dim} H^\circ = -RT\,Ln\,K_{\dim} + T\,\Delta Fef \qquad (36)$$

with $\Delta Fef = Fef_T(Cs_2I_2, g) - 2\,Fef_T(CsI, g)$ (37)

the free energy functions being taken from Glushko et al. compilation. The corresponding uncertainty can be obtained according to the following relation:

$$\delta\Delta_{\dim}H^\circ = \left(+ RT\frac{\delta K_{\dim}}{K_{\dim}} \right) + T\frac{\delta\Delta Fef}{\Delta Fef} \quad (38)$$

Relation in which $\delta\Delta_{dim}H$ is the uncertainty on the dimmerization enthalpy, δK_{dim} the uncertainty on the selected dimmerization constant, K_{dim} the dimmerization constant, R the gas contant, T the temperature (1300 K), δΔfef the uncertainty on the CsI (g) and Cs_2I_2(g) free energy functions, and Δfef the free energy function of the dimmerization reaction. Since the Glushko et al. free energy function of CsI(g) and Cs_2I_2(g) are considered accurate:

$$\frac{\delta\Delta Fef}{\Delta Fef} \le 1\% \quad (39)$$

and thus equation (38) becomes :

$$\delta\Delta_{\dim}H^\circ \approx \left(+ RT\frac{\delta K_{\dim}}{K_{\dim}} \right) + 0.01T \quad (40)$$

So finally we propose the selected value,

$$\mathbf{\Delta_{dim}H_{298} = -164.02 \pm 1.43\ kJ.mol^{-1}}$$

Conversely, using the 3rd law of thermodynamics, the constant of dimmerization has been calculated in the temperature range 600-1400 K with the following relation:

$$Ln\,K_{\dim} = (-\Delta_{\dim}H^\circ - T\,\Delta Fef)/RT \quad (41)$$

A fit of the decimal logarithm of the dimmerization constant as a function of the inverse of temperature have been obtained in order to reinterpret literature data:

$$Log_{10}K_{\dim} = \frac{8343}{T(K)} - 5.798 \quad (42)$$

III.5.3. Third law enthalpies for vaporization reaction CsI(s,l)=CsI(g)

The present selection of the dimmerization constant let appear that the monomer pressure is larger than the dimmer one's, and consequently the determination of the vaporization enthalpy of this species is the next important step in the thermodynamic description of the whole vaporization process of the CsI(s, or l) compound. Using 3rd law of thermodynamics, we calculated for each author the monomer enthalpy of vaporization *i.e.* the reaction CsI(s,l) = CsI(g) using the following relations:

$$Kp = \frac{p_1}{\alpha = 1} \quad (43)$$

$$\Delta_{vap} H^{o}_{298} = -RT\, Ln\, p_1 + T\, \Delta Fef \quad (44)$$

$$\Delta Fef_T = Fef_T(CsI, g) - Fef_T(CsI, s, l) \quad (45)$$

relations in which $\Delta_{vap}H_{298}$ is the enthalpy of vaporization, Kp is the equilibrium constant for vaporization, p_1 is the monomer partial pressure, α the activity of CsI (s,l) considered pure and thus equal to 1, T the temperature and Fef is the free energy function tabulated in Glushko et al. compilation.

For each experimental method, the monomer partial pressure p_1 have been calculated taking into account our selected new dimmer contribution (calculation principle in appendix III-B) and the mean third law enthalpy of vaporization of CsI(s,l) per method of measurements has been deduced. Comparison with Glushko et al. selected one is presented in table III-4.

Experimental method	Knudsen effusion	Transport	Total pressure measurements	Glushko et al. selected value
$\Delta_{vap}H_{298}$(CsI,s→g)/ kJ.mol^{-1}	195.07 ± 0.79*	197.19 ± 1.73*	197.21 ± 0.47*	195.78 ± 3*

Table III-4: Enthalpy of sublimation at 298.15 K (mean value) for the reaction CsI(s,l)=CsI(g) calculated for each experimental method and comparison with the selected one of Glushko et al.. The uncertainty is taken as the difference between the mean enthalpy and the maximum or minimum enthalpy value obtained within each experimental method.*

There is about 2 kJ.mol^{-1} difference between the re-calculated CsI enthalpy of vaporization obtained with the Knudsen effusion data reinterpretation (mainly for vapors over the solid phase) and those obtained via transport method or total pressure measurements (mainly over the liquid phase). Although each third law calculation seems consistent per method of measurements, the deduced sublimation enthalpies remain abnormally different when pressure measurements are performed either over the solid CsI(s) or the liquid CsI(l). This difference can be due to the uncertainty in the CsI(l) thermodynamic properties, *i.e.* melting enthalpy $\Delta_m H$ or to the liquid heat capacity C_p^o at less extend.

III.5.4. Selection of the CsI(s,l) monomer enthalpy of vaporization

There is no reason for the observed differences between the 3rd law re-calculated CsI enthalpy of sublimation obtained with the Knudsen effusion data and those obtained via transport method or total pressure measurements when considering the methods themselves since their usual uncertainties are in the same range. For total pressures and for transport method we can estimate $\delta p/p \approx 5$ to 10% (including temperature effects), and for effusion methods $\delta p/p \approx 5$ to 30%, the larger quoted uncertainty range coming from "parasitic" contributions as already analysed for mass spectrometric Knudsen cell coupling [56, 57]. Indeed Glushko et al. preferred to select a dimmer to monomer ratio at 905 K, and then used the total pressure or transport measurements that appear more accurate *(sic).* The origin of the observed differences is thus coming more probably from other selected data, especially those for the liquid phase. The liquid thermodynamic properties are depending on the solid thermodynamic properties through the choice of the melting enthalpy of CsI(l) and the heat capacity of CsI(l), these two quantities being included in the calculated Free Energy Function of the CsI (l) used in the third law analysis of measured pressures over the liquid. Changing the melting enthalpy of CsI(s→l) has a direct effect on the vapour pressure as indicated in figure III-7 meanwhile the change of the liquid heat capacity is of second order impact. Besides, regarding the choice of the monomer vaporization enthalpy – together with the preceding dimmerization enthalpy choice – the deduced pressures over the solid influence the pressure at the melting temperature as sketched in fig. III-7.

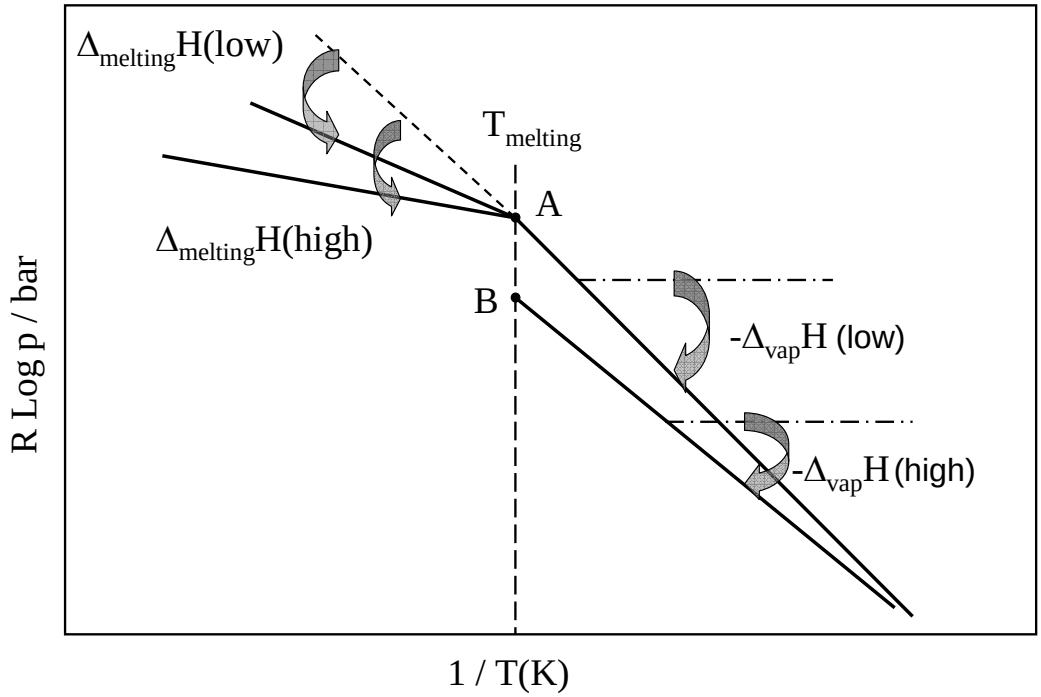

Figure III-7: Influence of the choice of different melting enthalpies and monomer vaporization enthalpies on the vapour pressures of the CsI(s or l) compound.

If the vaporization enthalpy of the monomer is too high (in our case the one deduced from the liquid ≈ 197 kJ.mol^{-1}) the pressures over the solid are too low and do not join the liquid pressures at the melting (point B in fig. III-7), the measured ones being higher (point A in fig. III-7). This is one more reason to explain that the effusion methods give a more reliable value, and indeed the Gluskho et al. selection was performed accordingly to this main analysis. Comparison of recalculated CsI 3rd law enthalpies of vaporization from solid and liquid phases is displayed in figures III-8 and III-9 as a function of the temperature of measurements.

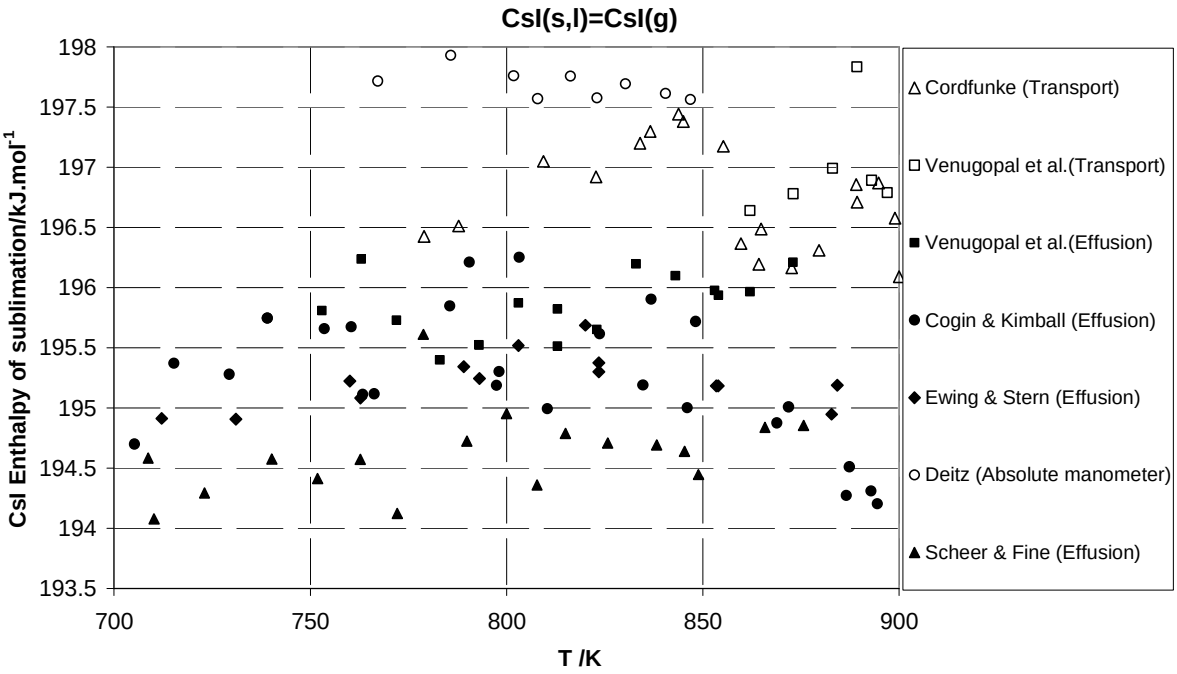

Figure III-8: Third law CsI(g) enthalpies of sublimation calculated from experimental determinations performed over the solid phase as a function of temperature of measurements.

In figure III-8 we observe that results can be divided into two groups of authors: one group corresponds to Knudsen effusion data which seems less scattered and without regular trends. In this case, the mean enthalpy of vaporization varies between 194.66 and 195.86 kJ.mol^{-1}. The second group corresponds to transport and total pressure data. The mean enthalpy of vaporization varies between 196.7 and 197 kJ.mol^{-1}. In comparison to the first group, the enthalpy of sublimation seems less reliable because large scatter is observed especially for transport data reinterpretation (Cordfunke and Venugopal et al.). For this raison, we chose a mean CsI(g) enthalpy of vaporization of the solid phase based on effusion studies,
$\Delta_{sub}H(CsI,g,298.15) = 195.23 \pm 0.63$ kJ.mol^{-1}.

This value corresponds to Sheer and Fine, Ewing and Stern, Cogin and Kimball and Venugopal et al.(effusion method) mean value over CsI solid phase. The other methods more scattered are discarded. The uncertainty is based on the largest deviation between the mean selected vaporization enthalpy and other retained values.

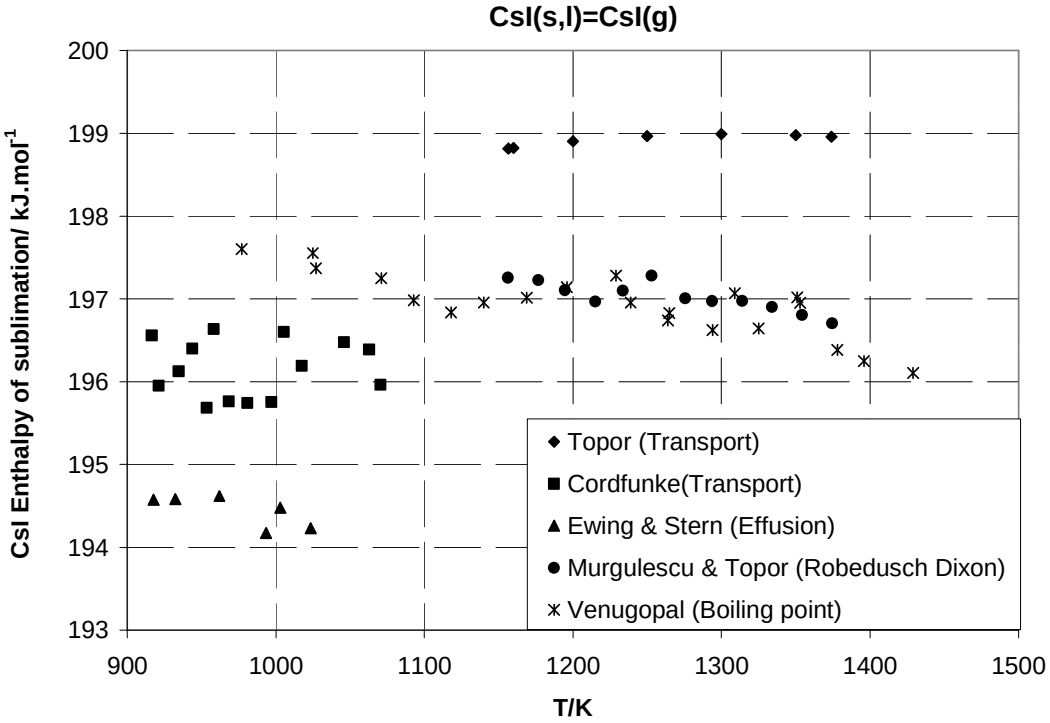

Figure III-9: Third law CsI(g) enthalpy of sublimation calculated from experimental determinations performed over the liquid phase as a function of temperature of measurements.

Figure III-9 presents the CsI(g) 3rd law enthalpy of sublimation obtained from original data over the liquid phase. Results seem very scattered. In fact the enthalpy of vaporization varies between 194.44 and 198.92 kJ.mol^{-1}. Moreover we observe some trends with temperature which can be attributed to errors in Free Energy Function of the reaction – presently for the liquid phase. Since the selected enthalpy of vaporization over solid is closer to the first value (obtained with Ewing and Stern data), we chose it as the mean CsI(l) enthalpy of sublimation over liquid phase and discard the higher values.

Finally, the CsI mean enthalpy of sublimation selected over solid and liquid is thus equal to, $\Delta_{sub}H(CsI,298.15) = 194.83 \pm 4$ kJ.mol^{-1}.

The uncertainty is based on the largest differences between the mean selected vaporization enthalpy and other retained values. Using the retained vaporization enthalpy, we recalculated via the 3rd law of thermodynamics the monomer and dimmer partial pressures as well as the apparent pressures. Results are presented in figures III-10, III-11 and III-12 altogether with experimental data.

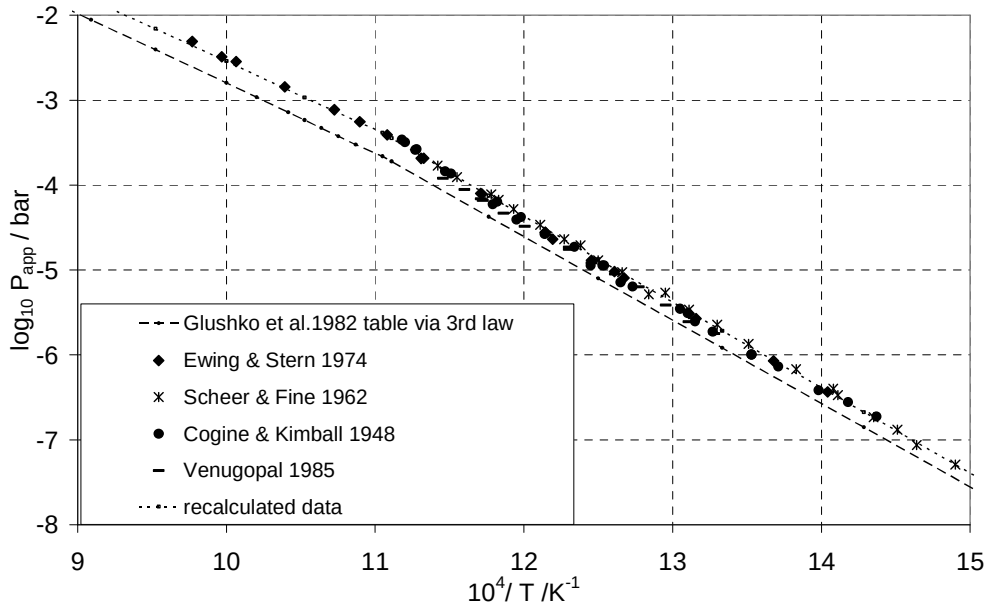

Figure III-10: CsI apparent pressure determinations over solid and liquid given by different authors using the effusion method and comparison with recalculated data using our new dimmerization constant and the selected vaporization enthalpy of the monomer.

With the present selected CsI(s,l) vaporization enthalpy, recalculated data are in good agreement with those determined by different authors over the solid phase.

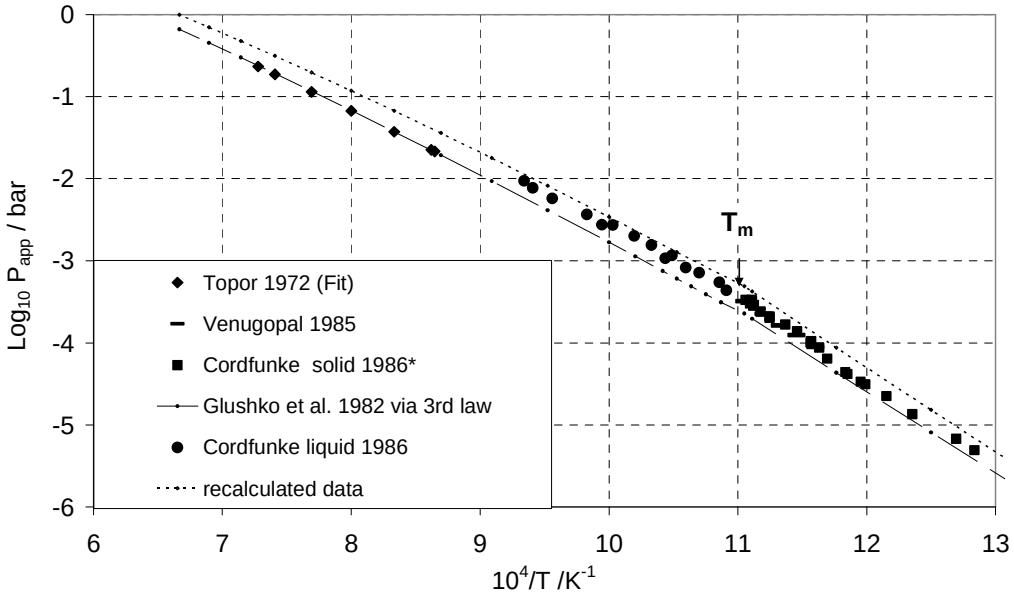

Figure III-11: CsI apparent pressure determinations over solid and liquid given by different authors using the transport method and comparison with recalculated data using our selected dimmerization constant and our selected enthalpy of vaporization for the monomer. Corrected Cordfunke (1986) data as explained in part III-4.2.*

As shown in figure III-11, the present selected CsI(g) enthalpy of vaporization increases the apparent pressures over solid in comparison to Cordfunke and Venugopal et al. and are also slightly higher than Cordfunke above the melting point. Over liquid, recalculated pressures remain slightly higher in comparison to those determined by Cordfunke and join apparently Topor's data at elevated temperature (T > 1600 K).

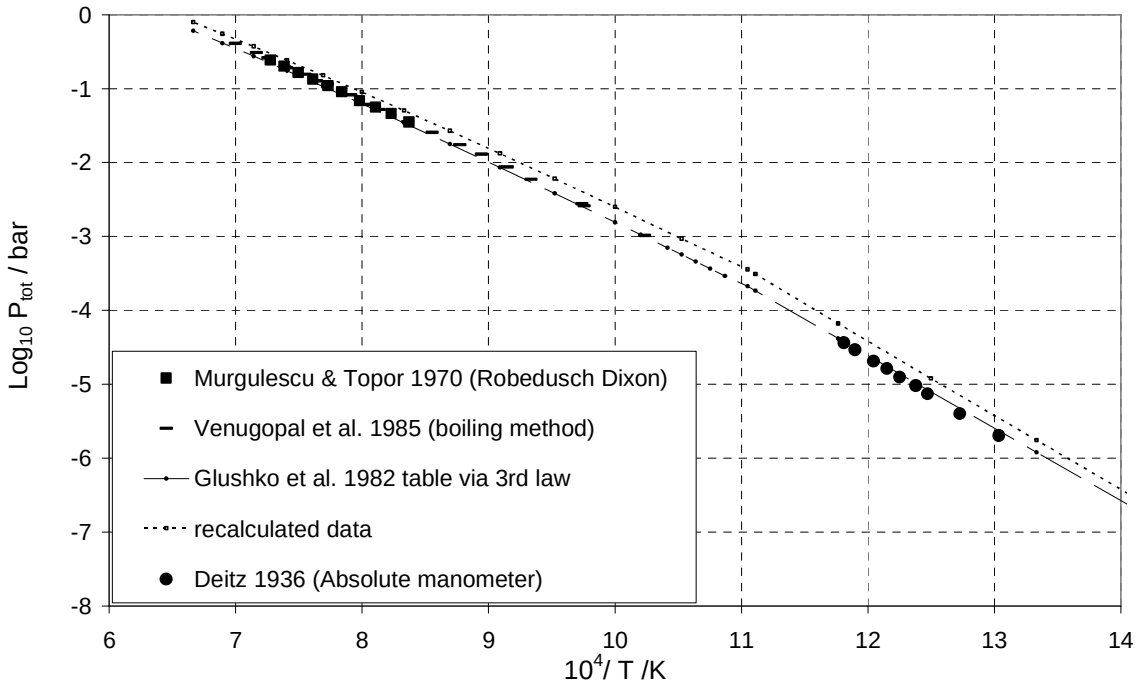

Figure III-12: Total pressure determinations over CsI given by different authors and comparison with recalculated data using our selected K_{dim} and CsI(s,l) enthalpy of vaporization = 194.83 kJ.mol^{-1}

In figure III-12, the recalculated total pressures with the CsI(s,l) selected enthalpy of vaporization are higher than Deitz over solid phase and Venugopal et al. over liquid phase. However, at elevated temperature, the recalculated data tend to join Venugopal et al. determined ones as well as Murgulescu and Topor.

In order to reduce the difference between experimental data and the recalculated data using the present selected CsI(g) enthalpy of vaporization and to find a better compromise between the different experimental methods (Knudsen effusion, transport and total pressure measurements), we propose to select a new CsI(s→l) melting enthalpy rather than keeping the Glushko et al. selected one.

III.5.5. Selection of the melting enthalpy and temperature

Glushko et al. selected value $\Delta_m H$ = 25.65 ± 0.4 kJ.mol^{-1} is a mixed value from Kaylor et al.(25.02 kJ.mol^{-1}) [25] and Smith et al.(25.82 kJ.mol^{-1}) [26] proposed ones. Bousquet and Perachon value (27.61 ± 0.83 kJ.mol^{-1}) [31] was discarded by Glushko et al. because they considered it as too much higher in comparison to other authors. However, conversely to other measurements, Bousquet and Perachon CsI melting enthalpy measurements were done in (quartz) sealed ampoules. Consequently, there is no mass loss due to vaporization and no related heat flow and their determined data should be accurate. So, we choose to retain this melting enthalpy and we obtain a new free energy function for the liquid. Our melting temperature selection is based on Glushko et al. retained one T_m = 905 ± 2 K which we consider accurate enough.

After correction with the new free energy function of the liquid phase, pressures data were recalculated for each experimental method and results are presented in figures III-13, III-14 and III-15.

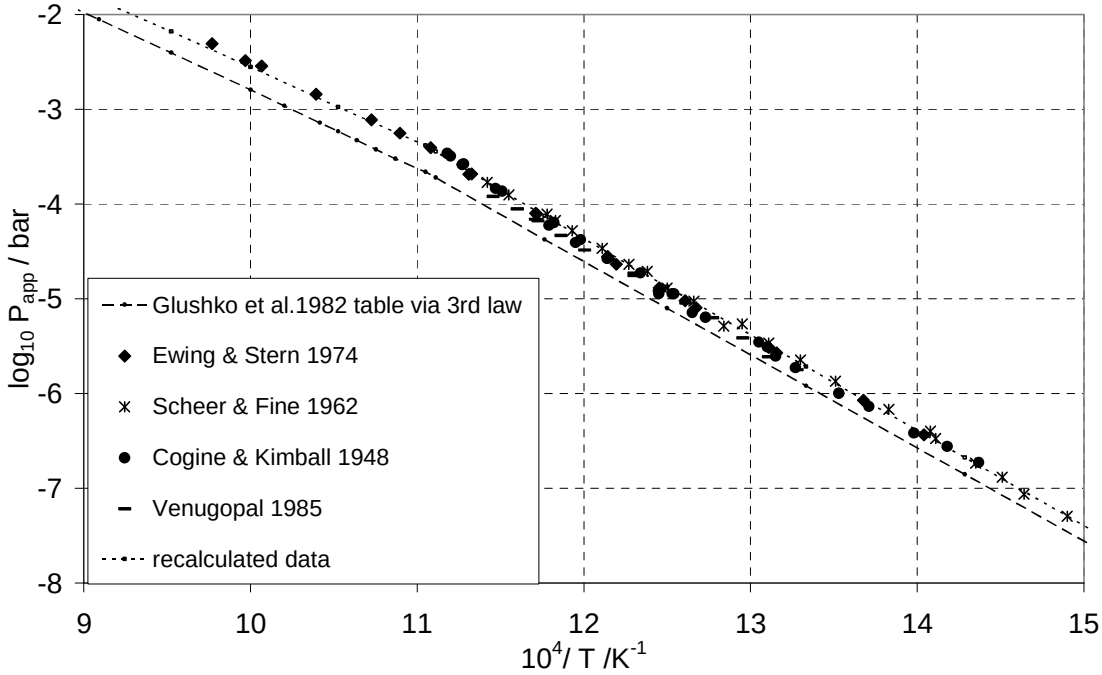

Figure III-13: CsI apparent pressure determinations over solid and liquid given by different authors using the effusion method and comparison with recalculated data after correction of Glushko et al. free energy functions of the liquid phase taking into account of the Bousquet and Perachon CsI(s,l) melting enthalpy.

A slight decrease of pressure is observed especially at elevated temperature. In comparison to figure III-10, there is a relative difference of 13% in term of apparent pressure at 1500 K.

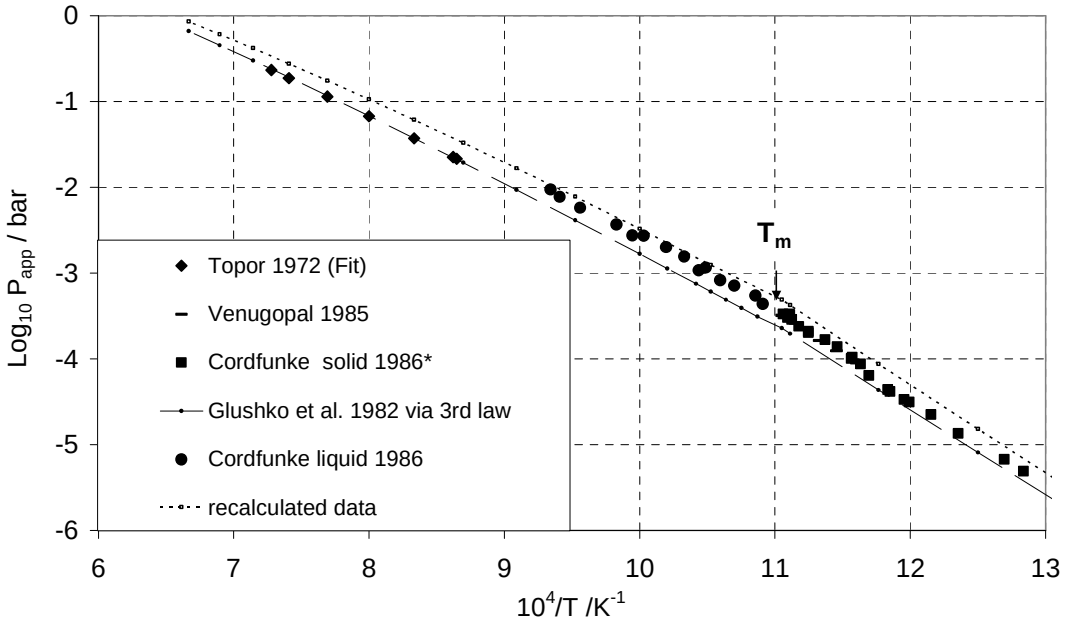

*Figure III-14: Cs (apparent pressure determinations over solid and liquid given by different authors using the transport method and comparison with recalculated data after correction of Glushko et al. free energy functions of the CsI liquid taking into account of the Bousquet and Perachon CsI(s,l) melting enthalpy. * Corrected Cordfunke (1986) data as explained in part III-4.2.*

Same evolution is observed in figure III-14 compared to fig. III-11. In fact, recalculated data become closer to those determined by Cordfunke over the liquid just above the melting temperature. At elevated temperature (1500 K), 13.5 % relative difference in term of apparent pressure is observed.

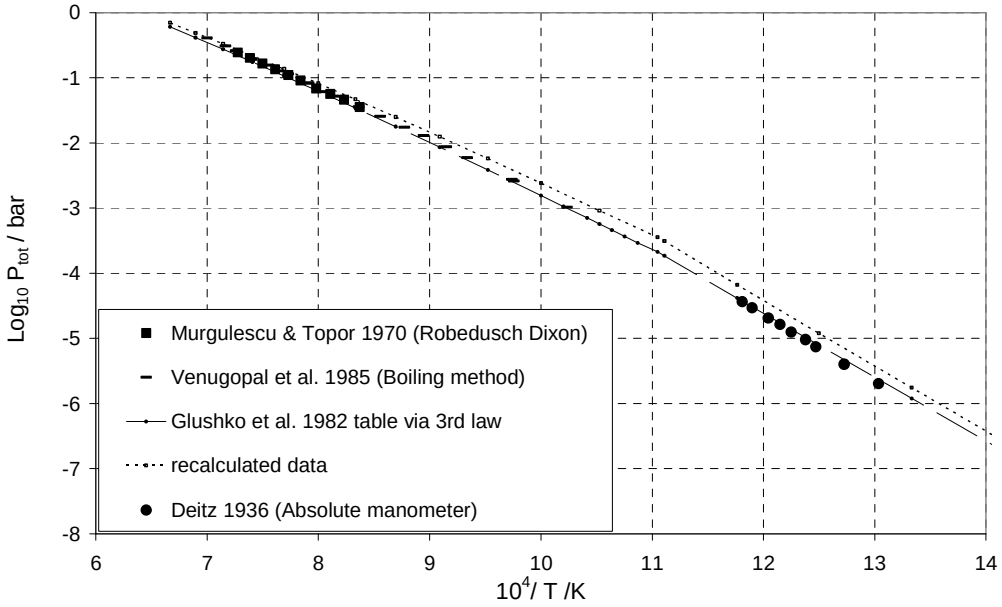

Figure III-15: Total pressure determinations over CsI given by different authors and comparison with recalculated data after correction of Glushko et al. free energy functions of the CsI liquid phase taking into account of the Bousquet and Perachon CsI(s,l) melting enthalpy.

In Figure III-15, new data are closer to Venugopal et al. determined one. Moreover, at elevated temperature (1500 K), a relative difference of 12% in term of total pressure is observed.

We can thus conclude that the correction of the Glushko et al. free energy function for the liquid via the melting enthalpy including Bousquet et al. proposed value improves the first recalculated data set based on the dimmerization constant and sublimation enthalpy (solid). But this improvement does not give enough satisfaction and recalculated pressures do not completely agree with those determined by Topor (transport method). This confirms the fact that the heat capacity Cp° of CsI liquid might have an impact.

III.5.6. CsI(liquid) heat capacity selection

Glushko et al. selected a heat capacity of CsI(l) equal to $C_p°(CsI,l) = 71 \pm 2$ J.K^{-1}.mol^{-1} based on the mean value of Kaylor et al. [25, 26] work over CsI(l) in a narrow temperature range above melting. Besides, Murgulescu and Topor [58] determined a heat capacity value

$C_p°$(CsI,l) = 74.3 $J.K^{-1}.mol^{-1}$. But Glushko et al. discarded this last value because they consider that their temperature range of measurements is not large enough above the melting point. So we propose to test the impact of Murgulescu and Topor value by taking it into account in the free energy function of the liquid already corrected for melting enthalpy. Pressures data were recalculated for each experimental method and results are presented in figures III-16, III-17 and III-18.

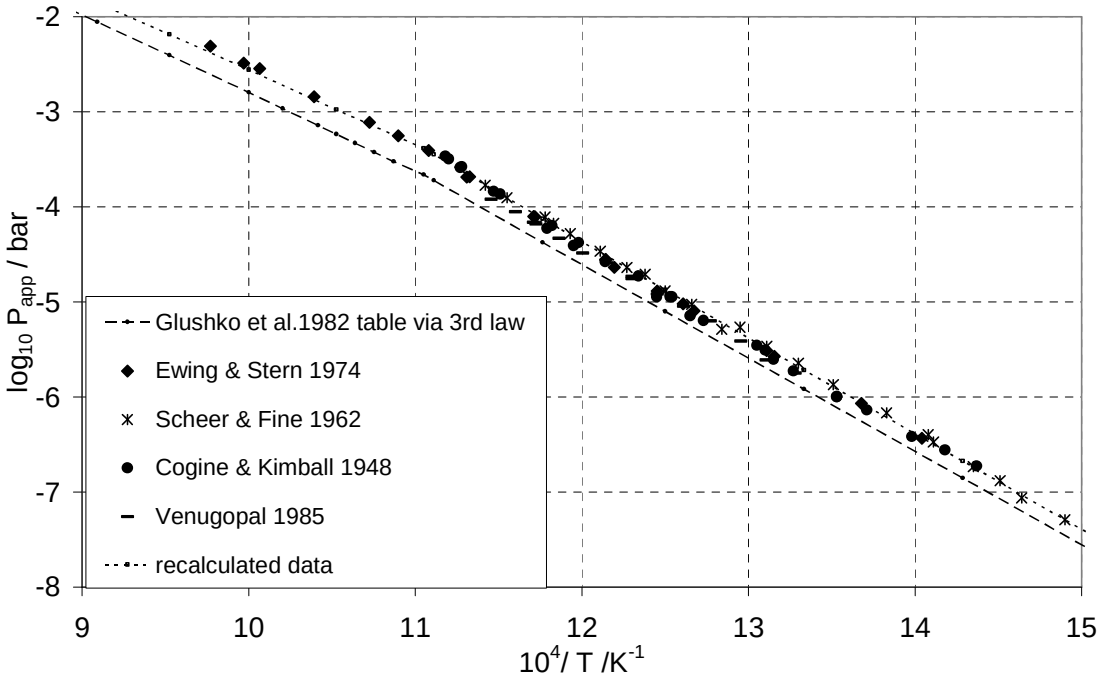

Figure III-16: CsI (apparent) pressure determinations over solid and liquid given by different authors using the effusion method and comparison with recalculated data after correction of Glushko et al. free energy functions of the liquid phase taking into account of the Murgulescu and Topor CsI(l) heat capacity.

In comparison to the preceding results with the melting enthalpy correction (Figure III-13), a slight decrease of pressure is observed: about 5.4% of relative difference (in term of pressure) is observed at 1500K by reference to the experimental data.

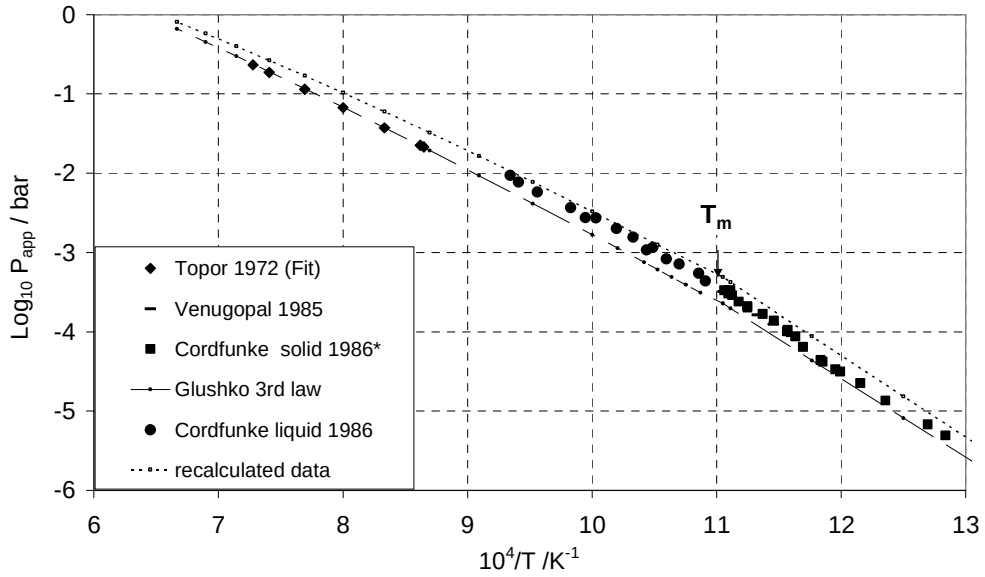

*Figure III-17: CsI (apparent) pressure determinations over solid and liquid given by different authors using the transport method and comparison with recalculated data after correction of Glushko et al. free energy functions for CsI liquid taking into account Murgulescu and Topor CsI(l) heat capacity. * Corrected Cordfunke (1986) data as explained in part III-4.2.*

The heat capacity effect is better observed at elevated temperature, in comparison to previous results (figure III-14) - 6% of relative difference pressure is observed at 1500 K.

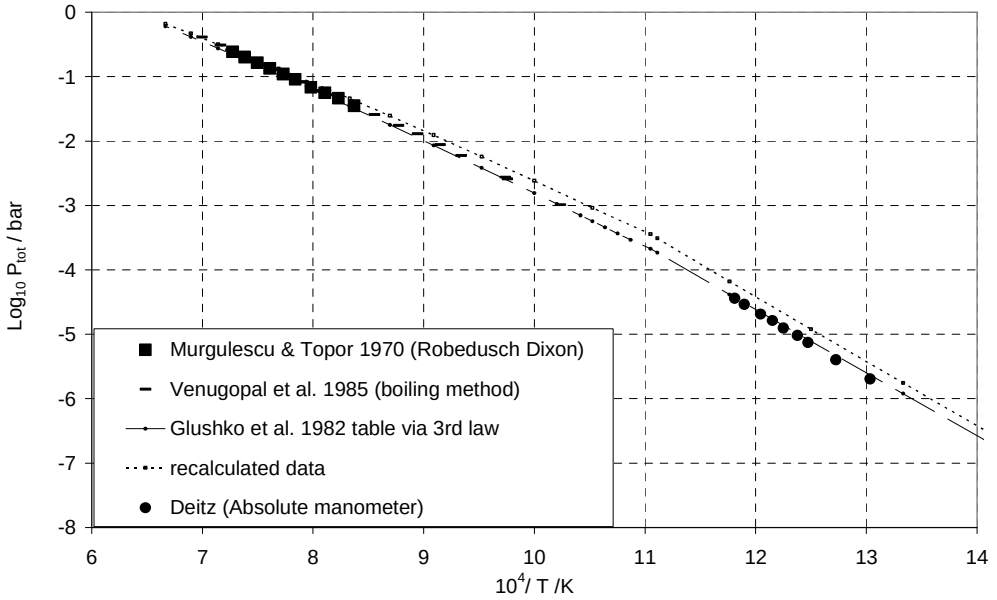

Figure III-18: Total pressure determinations over CsI given by different authors and comparison with recalculated data after correction of Glushko et al. free energy functions of the CsI liquid phase taking into accountof the Murgulescu and Topor CsI(l) heat capacity.

Total pressure data in comparison to those obtained after melting enthalpy correction show about 5% decrease at 1500 K. We can thus conclude that the choice of this heat capacity improves the final coherence of the CsI vaporization data.

III.6. CONCLUSIONS

The present work was initiated in view of checking the presently retained thermodynamic data for the Cs-I system in SGTE data bank [9] (coming from the Glushko et al. compilation (1982) [7]) against new experimental data for this system. We observe that:

- Numerous mass spectrometric observations of CsI vaporization showed that the gaseous phase is composed by the monomer CsI(g), dimmer $Cs_2I_2(g)$, trimmer $Cs_3I_3(g)$ and tetramer $Cs_4I_4(g)$.
- Glushko et al. thermodynamic data concerning the enthalpy of formation of CsI(s), the free energy functions of CsI(s), CsI(g), $Cs_2I_2(g)$ are accurate enough to be retained.
- The heat capacity of the solid has been improved.
- The new selected constant of dimmerization for the reaction $2CsI(g) = Cs_2I_2(g)$ warranties a good compromise between recent data obtained using different experimental methods in comparison to Glushko et al. retained ones and thus represents more reliably the real dimmer fraction in the vapour phase (dimmer mole fraction at 1300 K equal to 0.25). The corresponding proposed enthalpy of dimmerization is,

$$\mathbf{\Delta_{dim}H(CsI,298.15K) = -164.025 \pm 1.43\ kJ.mol^{-1}}$$

- The resultant selected enthalpy of vaporization of the reaction CsI(s,l) = CsI(g):

$$\mathbf{\Delta_{sub}H(CsI,298.15K) = 194.83 \pm 4\ kJ.mol^{-1}}$$

Comparison of this sublimation enthalpy between Glushko et al., Cordfunke and Konings (1990) [11] and Barin (1993) [59] is presented in table III-5.

Authors	$\Delta_f H$ CsI(s,298.15K) /kJ.mol^{-1}	$\Delta_{sub} H$ CsI(298.15K) /kJ.mol^{-1}	$\Delta_f H$ CsI(g,298.15K) /kJ.mol^{-1}
Glushko et al. (1982) [7]	-348.10 ± 0.18	195.78 ± 3	-152.32 ± 3
Cordfunke & Konings (1990) [11]	-348.13 ± 0.51	193.8 ± 2	-154.3 ± 2.1
Barin (1993) [59]	-346.603*	194.703*	-151.90*
This work	-348.10 ± 0.18	194.83 ± 4	-153.27 ± 4.2
* no given uncertainty			

Table III-5: CsI retained thermodynamic data compared to earlier compilations.

Contrarily to Glushko et al., the monomer sublimation enthalpy selected by Cordfunke and Konings didn't take into account of the dimmer contribution in the 3rd law calculations. Moreover, the criteria for the selection of this value are not justified although all the published values are relatively scattered. Consequently, the value for the dimmer is also impacted.

Barin (1993) CsI thermodynamic data references are based on NBS tables (1982) [22], JANAF [60] and Pankratz (1984) [61] issued from calorimetric measurements. By comparison with Glushko et al. compilation, there is about 2 kJ.mol^{-1} difference for the CsI(s) enthalpy of formation due to iodine dissolution enthalpy. We selected Glushko et al. proposed one in agreement with Cordfunke and Koning [11].

In this work, the selected enthalpy of vaporization is closer to Barin's one. This selected value is based on older works enriched by new measurements of vapour pressures, dealing mainly with the solid phase vaporization. The difference with Glushko et al. selected one is due to the fact that our choice is based on the selection of original data rather than calculation of a mean value.

Combining the enthalpy of sublimation with the enthalpy of formation of CsI(s) gives the enthalpy of formation of CsI (g) monomer. The differences between thermodynamic tables and our selected value for the enthalpy of formation of CsI gas comes mainly from the enthalpy of formation of CsI solid.

As the vapour pressures over the CsI liquid phase are systematically underestimated from thermodynamic tables, we propose a new melting enthalpy as well as a new heat capacity for the liquid based on experimental determinations. In table III-6, original selected experimental pressures are compared with recalculated pressures from the retained thermodynamic properties in this work.

Authors		T range/ K	% $\frac{P(\exp)-P(slt)}{P(slt)}\cdot 100$	% $\frac{P(\exp)-P(Glu)}{P(Glu)}\cdot 100$
Effusion Knudsen Method	Venugopal et al. [41]	753 - 873	-27 / -14	+20 / +47
	Cogin & Kimball [46]	695 - 894	-27 / +15	+25 / +112
	Ewing & Stern [45]	712 - 902	-18 / +5	+43 / +95
		917 - 1023	-12 / +18	+84 / +100
	Scheer & Fine [44]	671 - 875	-17 / +15	+38 / +89
Transport Method	Cordfunke [48]	779 - 904	-42 / -20	+16 / +70
		916 - 1070	-38 / -6	+42 / +77
	Topor [49]	1156 - 1374	-41 / -29	-2 / +10
	Venugopal et al. [41]	862 - 897	-35 / -31	+36 / +46
Total pressure measurements	Murgulescu & Topor [55, 62]	1156 - 1374	-7 / -21	+11 / +41
	Venugopal et al. [41]	977 - 1429	-36 / -3	+4 / +25

Table III-6: relative differences in total pressures between experimental data, Glushko et al. tables and the present selected values as recalculated from the retained thermodynamic properties. P(exp): experimental pressures, P(slt): recalculated pressures from our selection, P(Glu): Glushko et al.selected pressures.

Table III-6 shows that selected data reproduce the experimental pressures better than Glushko et al. over the solid phase and liquid phase. Over the liquid phase Glushko et al. proposed data are only in agreement with Topor pressures obtained by transport method.

By combining the enthalpy of dimmerization and the enthalpy of formation of CsI(g), the enthalpy of formation of Cs_2I_2(g) is: $\Delta_fH(Cs_2I_2,298.15K) = -470.56 \pm 10$ kJ.mol^{-1}

Summary of retained data to be stored in thermodynamic data bank is presented in table III-7.

CsI (s,l)	Authors	**Proposition for new data**
$Cp°_{298.15}$(s) (J.K^{-1}.mol^{-1})	Glushko et al. (fit) [63] T range: 298.15 - 905 K	61.09898 - 3.997402 10^{-2}T+ 5.493041 10^{-5}T^2-1.416414 10^5T^{-2}
$\Delta_fH_{298.15}$ (kJ.mol^{-1})	Glushko et al. [7]	-348.14 ± 0.18
$S°_{298.15}$ (J.K^{-1}mol^{-1})	Glushko et al. [63]	122.20
$T_{melting}$ (K)	Glushko et al. [7]	905 ± 2
$\Delta_{melting}H$ (kJ.mol^{-1})	**Bousquet and Perachon [31]**	**27.61 ± 0.83**
$Cp°_{298.15}$(l) (J.K^{-1}.mol^{-1})	**Murgulescu and Topor [58]**	**74.3**

CsI (g)	Authors	**Proposition for new data**
$Cp°_{298.15}$(g) (J.K^{-1}.mol^{-1})	Glushko et al. (fit) [63]	37.99146 - 1.193445 10^{-4}T + 5.384526 10^{-7}T^2-5.189732 10^4T^{-2}
$S°_{298.15}$ (J.K^{-1}mol^{-1})	Glushko et al. (ref. 1 bar)[63]	275.283
Δ_fH_{298} (kJ.mol^{-1})	**This work**	**-153.27 ± 4.2**

Cs_2I_2 (g)	Authors	**Proposition for new data**
$Cp°_{298.15}$(g) (J.K^{-1}.mol^{-1})	Glushko et al. [63]	83.14328 + 6.384707 10^{-7}T - 8.062363 10^{-11}T^2 -4.147424 10^4T^{-2}
$S°_{298.15}$ (J.K^{-1}mol^{-1})	Glushko et al. (ref.1 bar) [63]	431.181
Δ_fH_{298} (kJ.mol^{-1})	**This work**	**-470.56 ± 10**

Table III-7: Retained thermodynamic data of CsI(s,l), CsI(g) and Cs_2I_2(g).

Using the selected thermodynamic properties of Cs-I system, CsI(g) and Cs_2I_2(g) vapour pressures have been calculated and presented in figures III-19, III-20

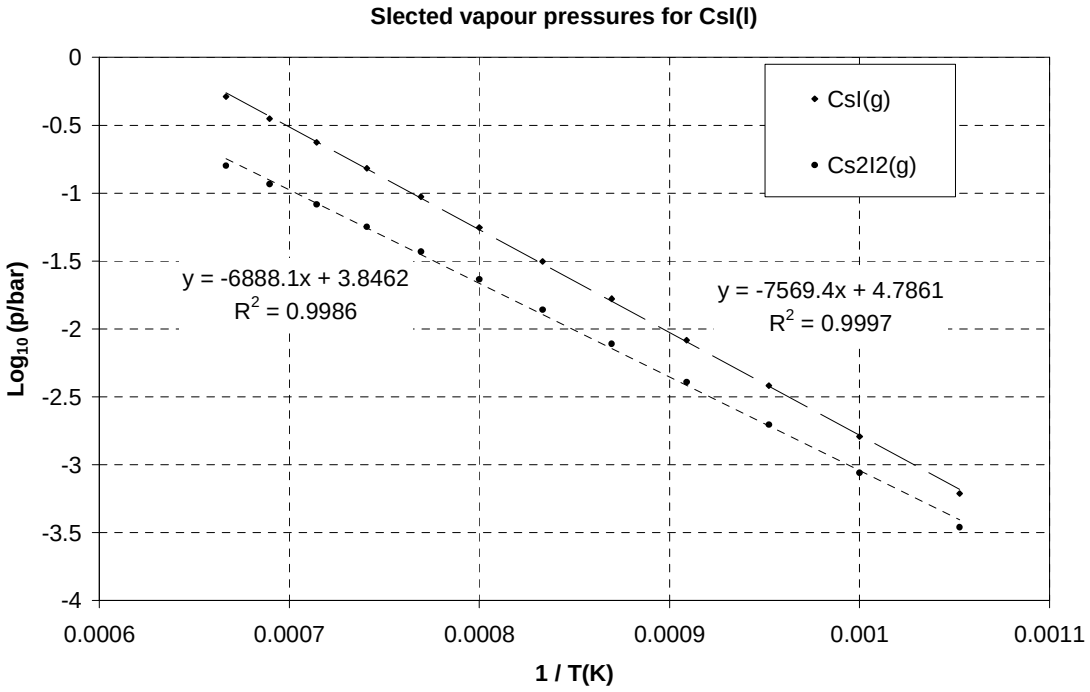

Figure III-19: CsI(g) and Cs_2I_2(g) selected pressures liquid phase

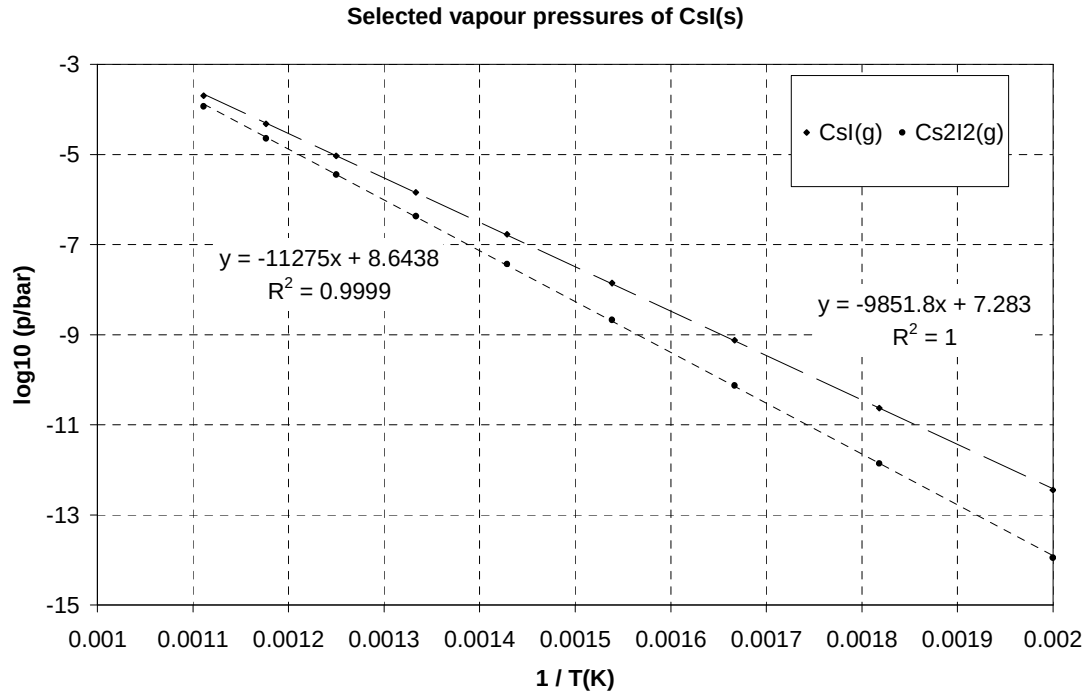

Figure III-20: CsI(g) and Cs_2I_2(g) selected pressures over solid phase

REFERENCES

[1] A.Auvinen, K.E.J.Lehtinen, J.Enriquez, J.K.Jokiniemi, and R.Zillacus, "Vaprisation Rates of CsOH and CsI in Conditions Simulating a Severe Nuclear Accident," J. Aerosol Sci., Vol. 31 (No 9), 2000, pp. 1029-1043.

[2] J.McFarlane, J.C.Wren, and R.J.Lemire, "Chemical Speciation of Iodine Source Term to Containment," Nucl. Techn., Vol. 138, 2002, pp. 162-178.

[3] A.Alonso, S.Fernandez, J.M.Buron, and J.V.Lopez, "Analysis of the Kinetic Behaviour of Iodine and Caesium Isotopes in the Primary Circuit of LWR's During Severe Fuel Damage Accidents", Nuclear Sicence and Technology, EUR13791, 1991, Madrid, 84 p.

[4] J.C.Cummings, R.M.Elrick, and R.A.Sallach, "Status Report on The Fission-Product Research Program", Sandia National Laboratories, NUREG-CR-1820, 1982, New Mexico, 10 p.

[5] L.Brewer and E.Brackett, "The Dissociation Energies of Gaesous Alkali Halides," Chem. Rev., Vol. 61, 1961, pp. 425-432.

[6] R.C.Feber, "Thermodynamic data for selected Gas Impurities in the Primary coolant of High-Temperature Gas-Cooled Reactors", Los Alamos Scientific Laboratory. LA-NUREG, N° 6635, 1977, 1977, New Mexico 87545, 26 p.

[7] V.P.Glushko, L.V.Gurvich, G.A.Bergman, I.V.Veits, V.A.Medvedev, G.A.Khachakuruzov, and V.S.Yungman, "Thermodynamics of Individual Substances", Part 2, Vol. IV, Nauka, Moscow, 1982, pp. 492-495.

[8] E.H.P.Cordfunke and G.Prins, "The Thermochemical Properties of Caesium Iodine.I-Thermodynamic Functions of Solid CsI," J. Thermochimica Acta, Vol. 90, 1985, pp. 169-176.

[9] SGTE, Scientific Group Thermodata Europe*: www.sgte.org;*

[10] A.T.Dinsdale, "SGTE Data for Pure Elements," CALPHAD, Vol. 15 (No 4), 1991, pp. 317-425.

[11] E.H.P.Cordfunke and R.J.M.Konings, "Thermochemical Data for Reactor Materials and Fission Products", Elsevier Science Publishers B.V., Amsterdam, 1990, pp. 111-119.

[12] P.E.Blackburn and C.E.Johnson, "Mass Spectromety Studies of Fission Product Behavior. II- Gas phase species in the CsI-CsOH system," J. Nucl. Mater., Vol. 154, 1988, pp. 74-82.

[13] V.B.Parker, "Thermal Properties of aqueous uni-univalent electrolytes", National Bureau of Standard 2, D.C., 20402, 1965, Washignton, 66 p.

[14] N.Beketov and W.Beketov, Z. Anorg. Chem., Vol. 40, 1904, pp. 355.

[15] M.Forcrand, "Thermochimie.-Etude thermochimique de quelques composés binaires des métaux alcalins et alcalino-terreux," CR. Acad. Sci., Vol. 152, 1911, pp. 27-31.

[16] M.Forcrand, "Recherche sur les Sels Haloides et les Oxydes des Métaux Alcalins et Alcalino-Terreux," Ann. Chim. Phys., Vol. 24 (8), 1911, pp. 256-282.

[17] V.G.Tsvetkov and I.B.Rabinovitch, "The isotopic effects on the enthalpy of solution," Zh. Fiz. Khim., Vol. 43, 1969, pp. 1213.

[18] R.L.Montgomery, R.A.Melaugh, Ch.Lau, G.H.Meier, R.T.Grow, and F.D.Rossini, "Enthalpies of Solution of Some Salts in Water," J. Chem. Eng. Data, Vol. 23 (No 3), 1978, pp. 245-249.

[19] J.Thourey and G.Perachon, "Enthalpies de Dissolution des Halogenures de Rubidium et Cesium dans les Solutions Aqueuses d'Acides Halogenes Correspondants," J. Thermochimica Acta, Vol. 39, 1980, pp. 243-252.

[20] J.D.Cox, D.D.Wagman, and V.A.Medvedev, "CODATA Recommended key values for thermodynamics", Hemisphere Pub. Corp., New York, 1989, pp. 271 p.

[21] C.E.VanderZee and M.E.Sprengel, "The standard molar enthalpies of formation of I^- (aq) and HI(g) at 298.15 K," J. Chem. Thermodyn., Vol. 15, 1983, pp. 869-879.

[22] NBS, "National Bureau of Standards, Washington," Tech. Note Vol., 1981, pp. 270-8.

[23] Z.Morlin, "Phase transformation of thin caesium iodide layers at low temperatures," Acta Cristallogr., Vol. Sect. B27, 1971, pp. 2493-2494.

[24] A.R.Taylor, T.E.Gardner, and D.F. Smith, "Thermodynamic properties of cesium chloride and cesium iodide from 0° to 300°K", U.S. Bur. Mines. Rept Invest., N. 6157, 1963, Washington, 7 p.

[25] C.E.Kaylor, G.E.Walden, and D.F.Smith, "High Temperature Heat Content and Entropies of Cesium Chloride and Cesium Iodide," J. Am. Chem. Soc., Vol. 64, 1960, pp. 276-278.

[26] D.F.Smith, C.E.Kaylor, G.E.Walden, J. A.R.Taylor, and J.B.Grayle, "Construction, Calibration and Operation of Ice Calorimeters", Bur. Mines Rep. Invest., 5832, 1961, Washington, 20 p.

[27] Y.Takahashi and Y.Kohsaka, "Heat Capacity and Enthalpy of Cesium Iodide from 300 to 830 K," J. Nucl. Mater., Vol. 130, 1985, pp. 109-114.

[28] M.Sorai, H.Suga, and S.Seki, "Thermal Properties of Alkali Halide Crystals with the CsCl-type Structure," Bull. Chem. Soc. Jpn, Vol. 41, 1968, pp. 312-321.

[29] B.J.Marshall and J.R.Kunkel, "Heat Capacity and Elastic Constants of CsI at Low Temperatures," J. Appl. Phys., Vol. 40, 1969, pp. 5191-5192.

[30] CODATA, "Recommended key values for thermodynamics", 1977.

[31] J.Bousquet, G.Perachon, and J.C.Remy, "Mesures calorimétriques des chaleurs de fusion des iodures de sodium, potassium, rubidium et caesium," Bull. Soc. Chim (Fr.), Vol., 1967, pp. 238-239.

[32] K.Sommermeyer, "New Spectra for Gaseous Alkali Halides and Their Interpretation," Z. Phys., Vol. 56, 1929, pp. 548-562.

[33] E.M.Bulewicz, L.F.Philipes, and T.M.Sugden, "Determination of Dissociation Constants and Heats of Formation of Simple Molecules by Flame Photometry," Trans. Faraday Soc., Vol. 57, 1961, pp. 921-931.

[34] A.G.Gaydon, "Dissociation Energies and Spectra of Diatomic Molecules", 3, Chapman and Hall LTD, London, 1968, pp. 269.

[35] J.Berkowitz, "Photoionization of High-Temperature Vapors. V. Cesium Halides, Chemical Shift of Autoionization," J. Chem. Phys., Vol. 50 (No 8), 1969, pp. 3503-3512.

[36] K.P.Huber and G.Herzberg, "Molecular spectra and molecular structure. IV. Constants of Diatomic molecules", Van Nostrand Reinhold Company, New York, 1979.

[37] T.-M.R.Su and S.J.Riley, "Alkali halide photofragment spectra. I. Alkali iodide bond energies and excited state symmetries at 266 nm," J. Chem. Phys., Vol. 71, 1979, pp. 3194-3202.

[38] P.A.Akishin, L.N.Gorokhov, and L.N.Sidorov, "A Mass-Spectrometric Study of Cesium Halides," Dokl. Akad. Nauk. SSSR trans. p 1001-1004 of Phys. Chem. Sec, Vol. 135 (No 1), 1960, pp. 113-116.

[39] L.N.Gorokhov, "thesis", Moscow University, Moscow 1972.

[40] R.Viswanathan and K.Hilpert, "Mass Spectrometric Study of the Vaporization of Cesium Iodide and Thermochemistry of (CsI)2(g) and (CsI)3(g)," J. Phys. Chem., Vol. 88, 1984, pp. 125-131.

[41] V.Venugopal, R.Prasad, and D.D.Sood, "Vaporisation Thermodynamics of Caesium Iodide and Caesium Chromate," J. Nucl. Mater., Vol. 130, 1985, pp. 115-121.

[42] J.Drowart, C.Chatillon, J. Hastie, and D. Bonnell, "High-Temperature Mass Spectrometry: Instrumental Techniques, Ionisation Cross-Sections, Pressure

Measurements, and Thermodynamic Data," J. Pure Appl. Chem., Vol. 77, 2005, pp. 683-737.

[43] V.Deitz, "The Vapor Pressure of Potassium Chloride and Cesium Iodide Crystals," J. Chem. Phys., Vol. 4, 1936, pp. 575-580.

[44] M.D.Scheer and J.Fine, "Entropies, Heats of Sublimation and Dissociation Energies of the Cesium Halides," J. Chem. Phys., Vol. 36 (6), 1962, pp. 1647-1653.

[45] C.T.Ewing and K.Stern, "Equilibrium Vaporization Rates and Vapor Pressures of Solid and Liquid Sodium Chloride, Potassium Chloride, Potassium Bromide, Cesium Iodide and Lithium Fluoride," J. Phys. Chem., Vol. 78 (No 20), 1974, pp. 1998-2005.

[46] G.E.Cogin and G.E.Kimball, "The Vapor Pressures of Some Alkali Halides," J. Chem. Phys., Vol. 16 (No 11), 1948, pp. 1035-1048.

[47] F.Z.Roki, M.N.Ohnet, C.Chatillon, and D.Jacquemain, "Thermodynamic study of the CsOH(s,l) vaporization by high temperature mass spectrometry," J. Chem. Thermodyn., Vol. 40, 2008, pp. 401-416.

[48] E.H.P.Cordfunke, "Thermodynamic Properties of CsI. II. Vapour Pressures and Thermochemical Properties of CsI(g) and Cs_2I_2(g)," J.Thermochimica Acta, Vol. 108, 1986, pp. 45-55.

[49] L.Topor, "Thermodynamic study of alkali halide vapors in equilibrium with the liquid phase," J. Chem. Therm., Vol. 4, 1972, pp. 739-744.

[50] G.M.Rosenblatt, "in Evaporation from Solids: Treatise on Solid-State Chemistry VI, Surfaces", N.B. Hannay, 1976, New York, pp. 165-239.

[51] R.C.Paul and J.L.Margrave, "in The caracterization of High-Temperature Vapors. Chapter 6: Free-Evaporation and Effusion Technique", J.L. Margrave, 1967, John Willey, New York, pp. 130-151.

[52] G.M.Rothberg, M.Eisenstadt, and P.Kusch, "Free Evaporation of Alkali Halide Crystals," J. Chem. Phys., Vol. 30 (No 2), 1959, pp. 517-527.

[53] M.Heyrman and C.Chatillon, "Kinetic Steady-States in Knudsen Effusion Cells," Electochem. Soc. proceeding, Vol. 2003-16, 2003, pp. 503-514.

[54] G.M.Pound, "Selected Values of Evaporation and Condensation Coefficients for Simple Substances," J. Phys. Chem. Ref. Data, Vol. 1 (No 1), 1972, pp. 135-145.

[55] I.G.Murgulescu and L.Topor, "L'association Moléculaire des Iodures Alcalins en Phase Gazeuse," Rev. Roum. Chim., Vol. 15, 1970, pp. 997-1004.

[56] M.Tmar and C.Chatillon, "Refinement of the vapor pressures in equilibrium over the InP and InAs compounds by mass spectrometry," J. Chem. Thermodynamics, Vol. 19, 1987, pp. 1053 -1063.

[57] P.Morland, C.Chatillon, and P.Rocabois, "High Temperature Mass Spectrometry Using the Knudsen Effusion Cell. I-Optimization of Sampling Constaints on the Molecular Beam," J. High Temp. & Mat. Sci., Vol. 37, 1997, pp. 167-187.

[58] I.G.Murgulescu and L.Topor, "Heat Capacities in Molten Alkaline Halides," Rev. Roum. Chim., Vol. 22, 1977, pp. 683-689.

[59] I.Barin, "Thermochemical Data of Pure Substances, Part I", 1993, pp. 457.

[60] M.W.Chase, J., "NIST-JANAF Thermochemical Tables," J. Phys. Chem. Ref. Data,, Vol. Fourth Edition, Part I, 1998.

[61] L.B.Pankratz, "Thermodynamic Properties of Halides", Vol. bulletin 674, U.S. Bur. Mines Washignton, 1984, pp. 175-176.

[62] I.G.Murgulescu and L.Topor, "Thermodynamical Data Of Molten Rubidium and Cesium Halides from Vapour Pressure Determinations," Rev. Roum. Chim., Vol. 12, 1967, pp. 1077-1083.

[63] V.P.Glushko, L.V.Gurvich, G.A.Bergman, I.V.Veits, V.A.Medvedev, G.A.Khachakuruzov, and V.S.Yungman, "Thermodynamics of Individual Substances", Part 2, Vol. IV, Nauka, Moscow, 1982, 558 p.

[64] C.T.Ewing and K.Stern, "Vaporisation Kinetics of Solid and Liquid Silver, Sodium Chloride, Potassium Bromide, Cesium Iodide and Lithium Fluoride," J. Phys. Chem., Vol. 79 (19), 1975, pp. 2007-2017.

APPENDIX III-A

Table III-A1: Cesium Iodide investigations using different experimental methods such as Knudsen effusion, transport/transpiration methods……

Knudsen Effusion Method					
Authors & references	Samples	*Cell & Material*	T (K) range	Determined data	Observations
Deitz (1936) [43]	CsI	Knudsen/mass loss Quartz cell	789-815	Apparent vapor pressure	-No variation of pressure with orifice size within a factor of 10 (α =1)
Cogin and Kimball (1948) [46]	CsI	Knudsen effusion with Thermoionisation of the molecular beam Ag cell $s/S=5.10^{-3}$ (C=1)	910-700	Log p(bar) = 11193/T +8.845 + 2.5 log1000/T	analysis of the thermal ionisation yield (>0.99)
M.D. Scheer and J. Fine (1962) [44]	CsI	-Ag effusion cell detection by thermoionisation ($\sum$Cs+) $s*C/S=1.29\ 10^{-3}$	671-807	$S°_{298.15}$ CsI = 109.934 $J.K^{-1}.mol^{-1}$ Δ_{sub} H (298.15 K) CsI = 202.73 $kJ.mol^{-1}$ $D°_{298.15}$ CsI = 318.934 $kJ.mol^{-1}$ CsI(s) = CsI(g)	-Distance orifice-detector equivalent to 1m: possibility of elimination of molecules in the free path. -according to Venugopal et al. dimmer contribution < 1% at T<862 K -3rd law recalculated by Cordfunke (1986)
C. T.Ewing and K. H.Stern (1974) [45]	CsI	Knudsen effusion cell/thermobalance Pd cell sealed with Gold paste. Orifice diameter: 1/32,			-continuous mass loss -no pressure difference observed with orifice diameter (α =1) -ratio monomer/dimmer from Topor used to calculate the monomer pressure which is 20%

		1/16, 3/32 inch			lower than Scheer and Fine
C. T.Ewing and K. H.Stern (1975) [64]	CsI single crystal (different phase)	-Free evaporation/ thermobalance -boat cemented with Ag paste on graphite	700	$\alpha_{CsI(g)} = 0.88$ $\Delta_{sub} H$ (700 K) CsI = 187.9 kJ.mol^{-1}	The pressure decreases from equilibrium when the temperature increases. We attribute this anomaly to the freezing of the surface due to high flow rate. Indeed for LiF the pressure of which is lower, this behaviour is not observed.
V.Venugopal et al. (1985) [41]	CsI (s) 99.95%	-Knudsen effusion graphite cell sC(=1)/S = 0.0025	753-862	results are coupled with those obtained from transpiration method	-mass loss
Transpiration/ Transport Method					
L. Topor (1972) [49]	CsI	Transpiration method	1300	Combining total pressure(quasi-static) and mass transport: Dimmer mole fraction: $x_d = 0.29$ at 1300 K	-Mass gain of the condenser -Calculation of partial pressures of monomer and dimmer by combination with preceding Rodebush-Dixon total pressure determination.
V.Venugopal et al. (1985) [41]	CsI(l)	-Transpiration (quartz vessel) with Ar carrier gas	862-887	CsI(s) $Log_{10}P(kPa) = (7.59 \pm 0.12) - 0.00113T(K) - (10301 \pm 95)/T(K) - 21088/T^2(K) + 1.13\log_{10}T(K)$ CsI(l) CsI(s)=CsI(l) $\Delta_{sub}H°_{298} = 193.1 \pm 0.6$ kJ.mol^{-1} (3rd law)	- Dimeric species <1% up to 873K -Dimmer proportion increases from 1 to 15% at the melting temperature -Smoothed pressure for transpiration experiment -Fef of Feber for CsI solid and gas

Cordfunke (1986) [48]	CsI	Transportation method And Compilation	Tm=903.5 (calorimetry)	Log10 p(CsI)/atm = (-9550±79)/T +(6.945±0.093) $\Delta_{sub}H°_{298.15}(CsI)$ = 193.1± 0.1 kJ.mol^{-1} ($\sum P= p_{monomer}+2p_{dimmer}$) *Dimmer fraction*: x_d = (18.6 ± 1.8)% at 912 K Log10 p(Cs_2I_2)/atm = (-7587±530)/T +(4.19±0.54) $\Delta_{sub}H°_{298.15}(Cs_2I_2)$ = 229.9± 1.0 kJ.mol^{-1} $\Delta_fH°_{298.15}(CsI,g)$ = -155.0± 0.2 kJ.mol^{-1} $\Delta_fH°_{298.15}(Cs_2I_2,g)$ = -466.4± 1.1 kJ.mol^{-1}	Cordfunke didn't take into account the presence of the dimmer below the melting point.
Total pressure measurements					
Deitz (1936) [43]	CsI	Absolute manometer (magnetic balance)	747-847	$\Delta_{sub}H$ = 198.7 kJ.mol^{-1} Log p(bar)=-10360/T + 7.793 (Combining Knudsen & manometer measurements)	Works like a valve attached to a magnetic balance
I.G.Murgulescu and L. Topor (1967) and (1970) [55, 62]	CsI dryed at 378 K during 24h Quartz cell degasing under vaccum at 373 K for 24h before introduction of Ar	Quasi-static Rodebush-Dixon Method	1156-1374	CsI(l)=CsI(g)+Cs_2I_2(g)+... logP(atm)= -9483.9/T - 3.5235log T + 17.320	Direct Measurement of Total pressure
V.Venugopal et al. 1985[41].	CsI (s) 99.95%	Boiling point temperature (quartz vessel)	977-1430	$Log_{10}P_2$ (kPa)=(28.42 ±0.41)-(9986±415)T(K)-6.56log_{10}T(K) $\Delta_{sub}H°_{298.15}(CsI)$ = 196.8 ± 1.6 kJ.mol^{-1}	Dimmer fraction evaluated from total pressure(boiling data) and mass transport in the temperature range 1240-1400 K

				$\Delta_{sub}H°_{298.15}$ (Cs_2I_2)= 227.2 ± 2.3 kJ.mol^{-1} (3rd law) $\Delta_{diss}H°_{298.15}$ (Cs_2I_2,g) = 166.4 ± 3.9 kJ.mol^{-1} $\Delta_fH°_{298.15}$(CsI) = -154.2 ± 1.6 kJ.mol^{-1} $\Delta_fH°_{298.15}$ (Cs_2I_2)= -474.9± 2.3 kJ.mol^{-1}	2nd and 3rd law didn't not agree due to "in consistencies in thermodynamic data" (sic)

APPENDIX III-B

Monomer and dimmer pressures calculations

- Knudsen effusion method

The combination of relations (6) $p_{app} = p_1 + \sqrt{2}\, p_2$ and (24) $K_{\dim} = \frac{p_2}{{p_1}^2}$, gives a 2nd degree equation:

$$\sqrt{2} K_{\dim} {p_1}^2 + p_1 - p_{app} = 0$$

$$\Delta = 1 + 4\sqrt{2} K_{\dim} p_{app}$$

$$p_1 = \frac{-1 + \sqrt{\Delta}}{2\sqrt{2} K_{\dim}}$$

$$p_2 = \frac{p_{app} - p_1}{\sqrt{2}}$$

Relations in which K_{dim} is the constant of dimmerization, p_1, p_2 and p_{app} are respectively the partial monomer and dimmer pressures and the apparent pressure.

- Transport/transpiration Methods:

The combination of relations (18) $p_{app} = p_1 + 2 p_2$ and (24) $K_{\dim} = \frac{p_2}{{p_1}^2}$, gives the following 2nd degree equation:

$$2 K_{\dim} {p_1}^2 + p_1 - p_{app} = 0$$

$$\Delta = 1 + 8 K_{\dim} p_{app}$$

$$p_1 = \frac{-1 + \sqrt{\Delta}}{4 K_{\dim}}$$

$$p_2 = \frac{p_{app} - p_1}{2}$$

- Total pressure measurements

The combination of relations (23) $P_{tot} = p_1 + p_2$ and (24) $K_{\dim} = \frac{p_2}{p_1^2}$, gives a 2nd degree equation:

$$K_{\dim} p_1^2 + p_1 - P_{tot} = 0$$

$$\Delta = 1 + 4K_{\dim} P_{tot}$$

$$p_1 = \frac{-1 + \sqrt{\Delta}}{2K_{\dim}}$$

$$p_2 = P_{tot} - p_1$$

relations in which P_{tot} is the total measured pressure.

CHAPTER IV

THERMODYNAMICS OF THE CSI-CSOH GAS PHASE SYSTEM

IV.1. INTRODUCTION

In the Cs-I-O-H quaternary system, the pseudo-binary CsI-CsOH system is a section of high thermodynamic stability. Thus, phases belonging to this section may be formed rapidly in any cooling processes. These phases might be gas – like mixtures of CsI and CsOH gaseous molecules including monomers and dimmers or complex molecules – or liquid and solids that could be basic components of aerosols. In case of gas – liquid mixtures, the reactions at the liquid surface are usually very fast meanwhile the gas-solid reactions may be "retarded" (or "hindered"). Further, in the condensation processes, the phase diagram of the CsI-CsOH system is an important tool to understand the mechanisms of condensation and the production of liquid droplets or solid aerosols. The complex gaseous phase of the Cs-I-O-H system was observed by High Temperature Mass Spectrometry (HTMS) when vaporizing CsI-CsOH(l) mixtures. It was found that the molecule $Cs_2IOH(g)$ is extremely stable. This feature is not surprising because such gaseous mixed molecules having an ionic character such as $BOHF_2$, $B(OH)_2F$ [1] and Na_2OHCl [2] have been already observed.

IV.2. EARLIER WORKS

First, mixed molecules in the gas phase chemistry of ionic bonds molecules have been already suspected by Schoonmaker and Porter (1960) [2] namely in equilibrium with {NaOH-NaCl} condensed mixtures. The authors observed by mass spectrometry some anomalous increase in the mass spectrum of Na_2OH^+ ion intensity. According to them, this effect would not be consistent with an increase in $Na_2O_2H_2(g)$ concentration resulting from thermodynamic activity changes, but may be explained by postulating the existence of $Na_2OHCl(g)$ which can dissociate into Na_2OH^+ by the electron impact. Later, Blackburn and Johnson [3] observed the same feature for the gas phase in equilibrium with {CsOH-CsI} mixtures, and proposed the existence of a new molecule, i.e. the $Cs_2IOH(g)$ molecule.

IV.2.1. Blackburn and Johnson (1988) preceding study

Blackburn and Johnson [3] performed a mass spectrometric vaporization study of CsI-CsOH mixtures, and observed an abnormal proportion of ions corresponding to the dimmers, namely Cs_2I^+ and Cs_2OH^+ when compared to pure compounds vaporization. Indeed, the dimmers proportions in equilibrium with a liquid mixture have to decrease with composition compared to the pure compounds since their proportions are related to the activity in the liquid phase according for instance to the following vaporization relations:

$CsOH(liq.) + CsOH(g) = Cs_2O_2H_2(g)$ with $K_1(T) = \frac{p(Cs_2O_2H_2)}{a(CsOH)\,p(CsOH)}$ (1)

and

$CsI(liq.) + CsI(g) = Cs_2I_2(g)$ with $K_2(T) = \frac{p(Cs_2I_2)}{a(CsI)\,p(CsI)}$ (2)

The equilibrium constants depend only on temperature. At a fixed temperature, the dimmer to monomer ratio is thus directly related to the activity. Using a regular liquid solution for CsI-CsOH system, Blackburn and Johnson show that for solutions with small CsI or CsOH contents the dimmers pressures respectively $Cs_2I_2(g)$ or $Cs_2O_2H_2(g)$ should decrease strongly and therefore the pertaining ions Cs_2I^+ or Cs_2OH^+ can come only from another molecule.

Their experimental observations have been explained by the presence of another gaseous species whose ionization gives the same ions. This feature is directly related to the only dissociative ionization processes observed for such gaseous molecules. These kind of ionization patterns are observed for molecules with a tendency to strong ionic bonds: in case of halides [4] it is due to electronic affinity energy for the halide quite equal to the ionization energy of the metal. Consequently, the main ionization processes observed by mass spectrometry are only dissociative ionizations as,

$Cs_2O_2H_2(g) + e^- \rightarrow Cs_2OH^+(g) + OH(g) + 2\,e^-$ (3)

$Cs_2IOH(g) + e^- \rightarrow Cs_2OH^+(g) + I(g) + 2\,e^-$ (4)

$Cs_2I_2(g) + e^- \rightarrow Cs_2I^+(g) + I(g) + 2\,e^-$ (5)

$Cs_2IOH(g) + e^- \rightarrow Cs_2I^+(g) + OH(g) + 2\,e^-$ (6)

Besides at very low energies of the ionizing electrons (< 5 to 10 eV), the occurrence of ion pair formation can not be discarded according to the process for instance:

$Cs_2IOH\ (g) + e^- \rightarrow Cs_2OH^+(g) + I^-\ (g) + e^-$ (7)

But yet the I^- production (or OH^-) can not be observed directly at the same time with the mass spectrometer when observing the positive ions since their deviation in the magnetic analyser is the reverse and these ions are lost. Moreover, in terms of total ion currents, for this process the ionization cross section becomes negligible at higher electron energies where positive ions are monitired quantitatively. For pure compounds vaporization, we remind that the ions CsI^+ and $CsOH^+$ were attributed [3, 5, 6] to the only adiabatic ionization of the monomers CsI(g) and CsOH(g).

Blackburn and Johnson observed first that the measured Cs_2I^+ ion when vaporizing "low CsI concentrations" (sic) corresponds to the only $Cs_2I_2(g)$ dimmer ionization. For low CsOH concentrations (molar fractions from 0.135 to 0.053) the calculated proportion of the dimmer coming from the monomer CsOH(g) - measured when monitoring the ionic intensity of $CsOH^+$ - was much lower than the measured one deduced from the total ionic intensity of Cs_2OH^+. The excess (18-fold higher) was attributed to the new mixed molecule $Cs_2IOH(g)$.

As a conclusion of their study, Blackburn and Johnson,

- Propose the existence of a new molecule $Cs_2IOH(g)$ whose stability is more important than the one of the two basic dimmers of pure components in the gaseous phase.
- Propose a main dissociative ionization process leading to the only Cs_2OH^+ ion.
- Second and third law calculations are presented for the equilibrium constant of the main reaction

  $CsI(g) + CsOH(g) = Cs_2IOH(g)$ (8)

  but yet the thermodynamic functions ($C°p$, $S°_T$, $Gef\ °_T$) for the new molecule are not presented and only a rough estimate of the entropy is done at the mean experiment temperature.
- Determine the liquid interaction coefficient from partial pressure evolution of the monomer CsOH(g) as a function of composition in an isothermal run using the mass loss of CsOH controlled by effusion.

Finally, Blackburn and Johnson performed thermodynamic calculations with a molar fraction x(CsI) = 0.1 that corresponds to a total concentration of iodine in agreement with nuclear released gases under severe accident. They concluded that CsICsOH(g) will increase the iodine concentration in the vapor and in the iodine release from the containment by as much as a factor of two compared with CsI(g) and Cs_2I_2 (g) alone (sic).

IV.2.2. Analysis of Blackburn and Johnson Thermodynamic data

From the original data of Blackburn and Johnson, and our selected values for vaporization of pure compounds (this work), the different partial vapor pressures were calculated at 950 K – *i.e.* over the liquid phase – as displayed in figure IV-1.

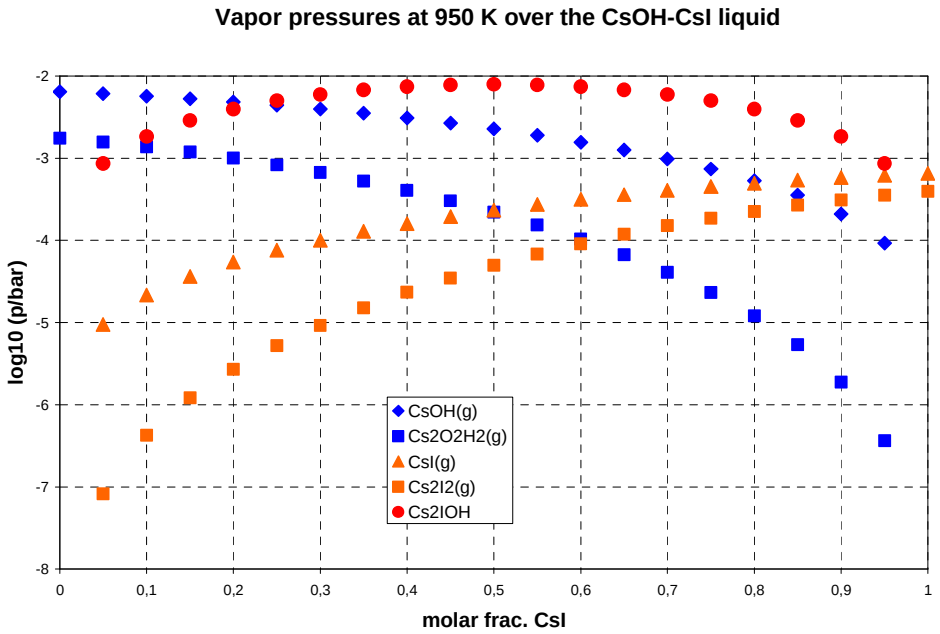

Figure IV-1: Vapor pressures in equilibrium with the CsI-CsOH liquid mixtures at 950 K as calculated from our selected data for the pure compounds CsOH (chapter II) and CsI (Chapter III) and the proposed thermodynamic data for the liquid mixture and the $Cs_2IOH(g)$ molecule by Blackburn and Johnson (1988).

The main feature is that the new molecule $Cs_2IOH(g)$ is more important than the pure dimmers within practically the whole composition domain. Moreover, this new molecule remains the main gas component for molar fractions x(CsI, liq) > 0.3. According to these data

- and following the conclusions of Blackburn and Johnson – the molecule $Cs_2IOH(g)$ can transport iodine in excess in case of:

- a rapid kinetics of formation from a dissociated original gas phase,
- low total iodine initial concentrations compared to Cesium

In order to understand the condensation of vapors as well as gas-liquid reactions, the vaporization behavior of CsI-CsOH mixtures must be analyzed since the condensation phenomena are the reverse according to the micro-reversibility principle [7] for chemical elementary reactions. Two main ways for this analysis are presented, - (1) the vaporization flows are analyzed in terms of liquid composition evolution due to distillation, - (2) the impact of reference choice on the stability of the $Cs_2IOH(g)$ molecule.

1) Vaporization of liquid CsI-CsOH mixtures is analyzed with or without the new molecule. This permits to determine if complete distillation till a final residue of pure CsI can be produced as observed by Blackburn and Johnson in their isothermal experiment for the interaction coefficient determination. For this purpose, the effusion flow is calculated in terms of CsOH or CsI molecular flows according to the Hertz-Knudsen equation. For the molecular flow of CsOH per unit time the relation is,

$$F(CsOH)=\frac{sC}{\sqrt{2\pi R}}\left[\frac{p(CsOH)}{\sqrt{M(CsOH)}}+\frac{2\,p(Cs_2O_2H_2)}{\sqrt{2\,M(CsOH)}}+\frac{p(Cs_2IOH)}{\sqrt{M(CsOH)+M(CsI)}}\right]. \quad (9)$$

Same relation is written for CsI. M is the molar mass of the effused species, p the partial pressure, s and C the cross section and the Clausing coefficient of the effusion orifice, and R the gas constant. The molar fraction named Y (composition) of the effused – vaporized flow is,

$$Y(CsOH)=\frac{F(CsOH)}{F(CsOH)+F(CsI)}. \quad (10)$$

These molar fractions of the effused flow – taking or not into account the new molecule – are compared to those of the liquid X(CsOH) in figure IV-2. If occurring, a congruent composition (azeotropic composition) corresponds to

X(CsOH, liq.) / Y(CsOH) = 1 (11)

and consequently no further evolution of the liquid composition can occur at this azeotropic composition due to vaporization.

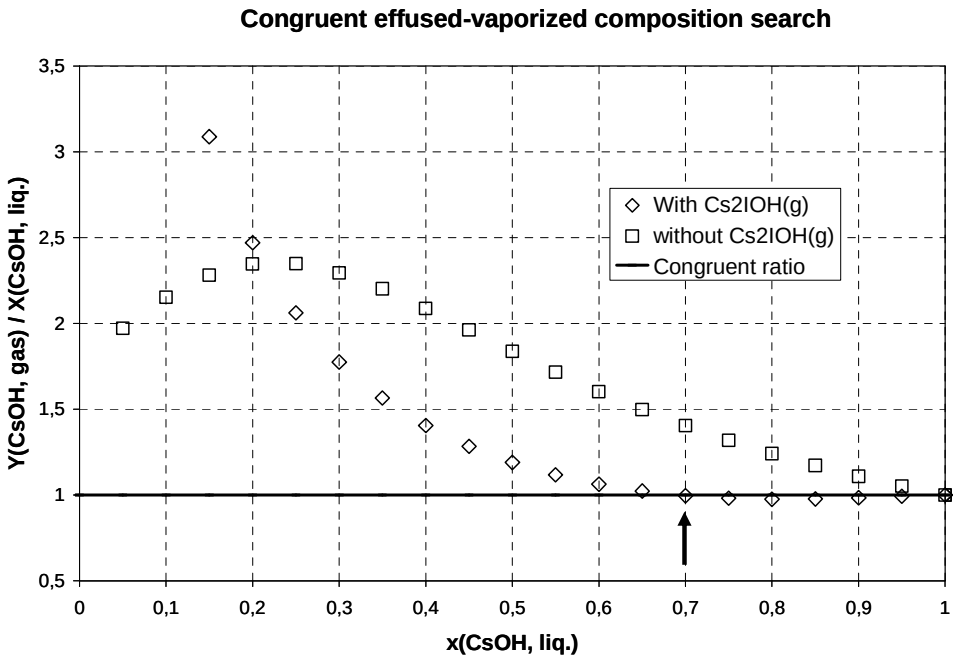

Figure IV-2: Test for congruent composition in the vaporization of CsI-CsOH liquid phase when taking or not into account the $Cs_2IOH(g)$ molecule as proposed by Blackburn and Johnson. The arrow shows the congruent composition attained only when taking into account the new molecule.

We observe in figure IV-2 that without taking into account the new molecule, the molecular vaporization flow is always richer with CsOH than the liquid. Complete distillation can be obtained leading to a CsI(l, or s) residue. Conversely, with the new molecule, there is a congruent composition at x(CsOH, liq.) ≈ 0.7.

In order to understand the composition evolution directions by vaporization losses, the nature of the azeotropic (congruent vaporization) stability [8, 9] has to be known. This stability is related to the nature of the molecular flow extremum at the congruent composition. In figure IV-3 the total molecular flow is displayed and the congruent composition corresponds to a maximum of the molecular flow when taking into account the new molecule.

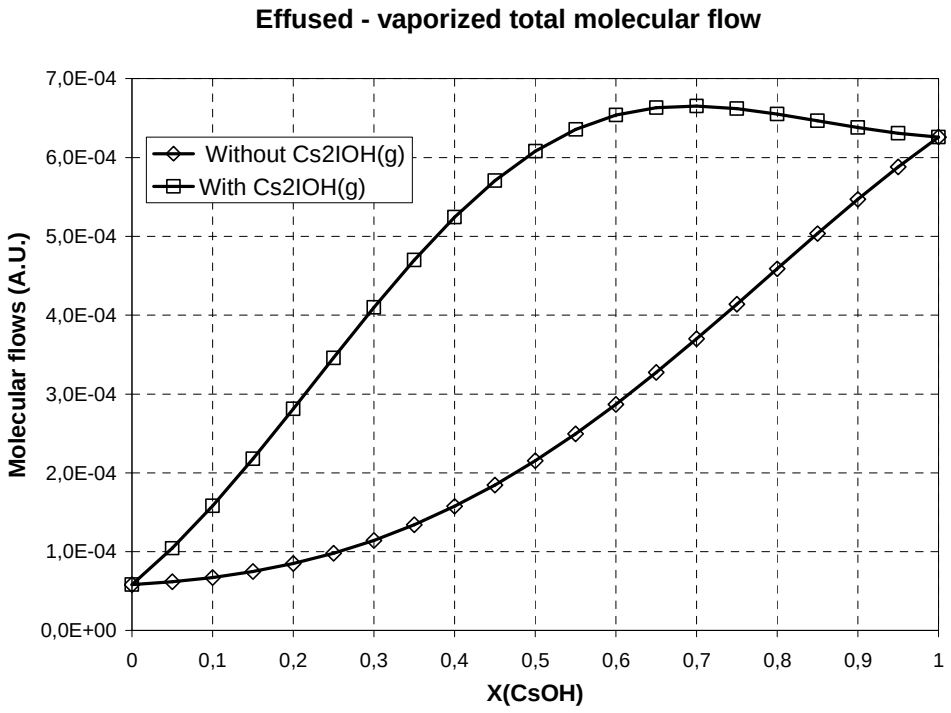

Figure IV-3: Calculated total molecular flow vaporizing from CsI-CsOH liquid mixtures according to our pure compounds selected pressures (chapter II and III) and thermodynamic data from Blackburn and Johnson for the liquid phase and the new $Cs_2IOH(g)$ molecule.

This property means that the azeotropic composition is not stable: whatever the chosen composition is, each side of the congruent one, it will move away from the azeotropic composition by vaporization mass loss:

- for initial X(CsOH,liq.) > 0.7 , the gas is less richer with CsOH than the liquid and the liquid composition becomes enriched with CsOH till pure CsOH(l),
- for X(CsOH,liq.) < 0.7 the gas losses mainly CsOH and the liquid composition becomes depleted with CsOH and goes to pure CsI(l). Reversely, in condensation processes the maximum flow (or pressure under atmospheric conditions) is in fact an "activation pressure like barrier" for creating different liquid compositions. This characteristic property is directly related to the partial pressure of the new $Cs_2IOH(g)$ molecule which is likely at its maximum value for X(CsOH) $\approx$ X(CsI) $\approx$ 0.5 (fig. IV-1). In the Blackburn and Johnson experiments, starting from x(CsOH) $\approx$ 0.135, and whatever the presence of $Cs_2IOH(g)$ is, the gas flow would have been richer with CsOH than the liquid, and the liquid should have been depleted with CsOH and consequently enriched with CsI. This evolution was effectively observed in their isothermal run (table 5 in [3]). The final composition is close to pure CsI. But yet, no

CsOH rich compositions have been tested in order to check the real influence of this new molecule.

2) Pressures of the new $Cs_2IOH(g)$ molecule were determined by Blackburn and Johnson using the equilibrium constant of reaction (8). In their calculation they subtract the proportion of Cs_2OH^+ coming from $Cs_2O_2H_2(g)$ by using their CsOH(g) measured pressures and their dimmerization constant. Because their own dimmerization constant determined for the $Cs_2O_2H_2(g)$ molecule is largely different from the one measured and selected in our previous works (chapter II) [5] or in JANAF tables [10], Their dimmer proportion is about 1/10 to 1/100 lower than the retained one and consequently the proportion of Cs_2OH^+ ion attributed by Blackburn and Johnson to the new molecule is over- evaluated.. Causes for these lower dimmer measured pressures over pure CsOH(l) can come at least from two different factors: - (i) a non controlled mass discrimination in the quadrupole filter, or – (ii) parasitic molecular flows coming from flow out of CsOH(l) on external surfaces around the effusion orifice as observed by us in the vaporization of pure CsOH(l) [5]. In order to correct the Blackburn and Johnson values (table 5 in [3]), new $Cs_2IOH(g)$ pressures have been recalculated from our selection of the dimmerization constant (chapter II). The final relation for calculating the real *(p_2(corr.))* dimmer pressure values is:

$$p_2(corr.) = p_2(Blackburn\ \ Calc.) \times \left[\frac{\exp\left[\frac{17001.4}{T} - 14.1482\right]}{\exp\left[\frac{18574}{T} - 19.08\right]} \right] \qquad (12)$$

relation in which the subscripts 2 account for the dimmer of CsOH, *p_2 (Blackburn Calc.)* is taken as the original calculated dimmer pressure in Blackburn and Johnson [3] as well as the dimmerization constant naperian logarithm (denominator term). The numerator is the equilibrium constant from our selected values (see chapter II). Original values are presented in table IV-1, altogether with the corrected values for the $Cs_2IOH(g)$ pressures.

T/K	p/bar $Cs_2O_2H_2$ from Total Cs_2OH^+	p/bar CsOH Blackburn CsOH	p/bar $Cs_2O_2H_2$ Blackburn Calc.	ratio. $Cs_2O_2H_2$ Blackburn Meas/Calc.	p/bar $Cs_2O_2H_2$ Our Calc.	ratio $Cs_2O_2H_2$ Meas.Black/ Our Calc.	p/bar Cs_2IOH Blackburn	p/bar Cs_2IOH Our Calc.*	p/bar CsI Blackburn
809	4.05E-06	7.52E-05	2.31E-07	17.5	4.58E-06	0.88	7.15E-06	-5.34E-07	2.97E-05
839	6.47E-06	9.43E-05	1.60E-07	40.4	3.40E-06	1.90	1.18E-05	3.07E-06	1.18E-04
876	5.06E-06	9.70E-05	6.67E-08	75.9	1.54E-06	3.29	9.33E-06	3.52E-06	2.32E-04
888	6.16E-06	1.12E-04	6.64E-08	92.0	1.57E-06	3.93	1.14E-05	4.59E-06	2.99E-04
918	7.78E-06	1.60E-04	6.89E-08	112.9	1.72E-06	4.52	1.44E-05	6.06E-06	4.27E-04
925	9.63E-06	1.59E-0	5.81E-08	165.7	1.47E-06	6.55	1.79E-05	8.16E-06	5.98E-04
926	9.99E-06	1.46E-04	4.83E-08	206.8	1.23E-06	8.15	1.86E-05	8.76E-06	7.79E-04
927	7.86E-06	1.22E-04	3.25E-08	241.8	8.26E-07	9.52	1.46E-05	7.03E-06	8.17E-04
927	6.08E-06	8.54E-05	1.60E-08	380.0	4.07E-07	14.95	1.13E-05	5.67E-06	6.88E-04

*Table IV-1. Comparison of $Cs_2O_2H_2(g)$ and $Cs_2IOH(g)$ pressures as determined by Blackburn and Johnson and our corrected values taking into account our selected values for the equilibrium constant of the dimmerization reaction 2 CsOH(g) = $Cs_2O_2H_2(g)$ (see chapter II). Meas. : measured, Calc. : calculated, * our calculation takes into account the corrected dimmer pressure*

As the selected value for the dimmerization constant leads to higher pressure values for the dimmer, our correction decreases the contribution of the mixed molecule in the measured Cs_2OH^+ ionic intensity. Thus the ratio Measured/Calculated for the dimmer $Cs_2O_2H_2(g)$ decreases soundly. At 809 K (due to activity of CsOH), the new molecule contribution becomes too small to be detected (negative value). Indeed Blackburn and Johnson quoted that the best conditions to observe the new molecule is for lower concentrations (either CsOH or CsI). The new second law equilibrium constant for reaction (8) is calculated from Table IV-1 and presented, compared to the Blackburn and Johnson original one in figure IV-4:

$$\ln K_p \text{ (reaction (8))} = 10805 / T(K) - 7.2638 \qquad (13)$$

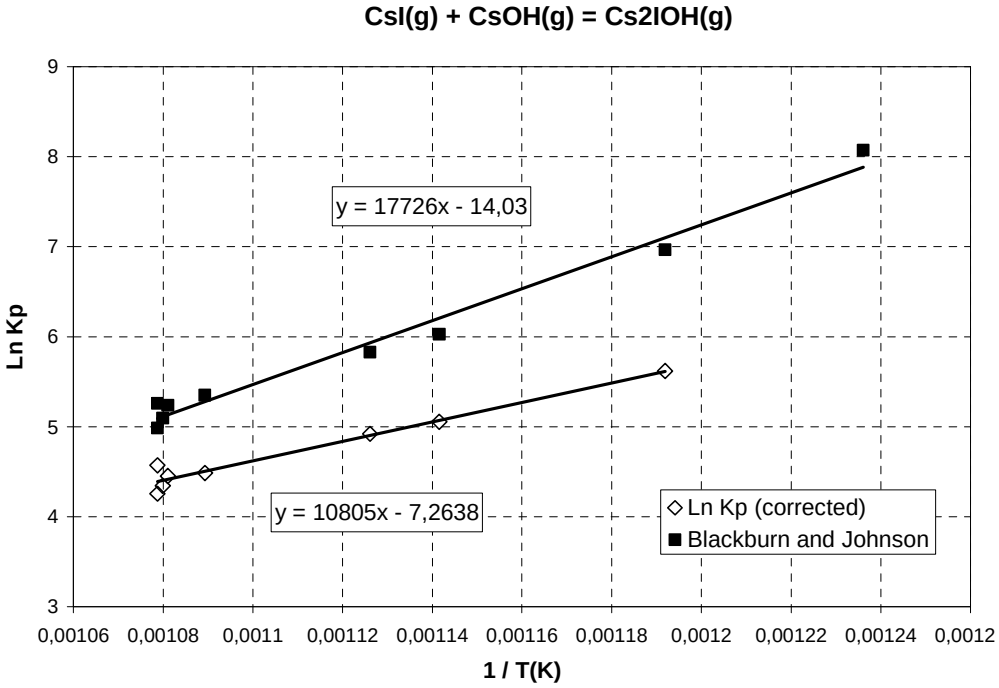

Figure IV-4: Comparison of the equilibrium constant naperian logarithm for the reaction CsI(g) + CsOH(g) = $Cs_2IOH(g)$ from original Blackburn and Johnson work and the present correction taking into account our selected thermodynamic values for the CsOH(g) and its dimmer (this work, chapter II).

As a conclusion of the present analysis, it appears that the new molecule proposed by Blackburn and Johnson is effectively present in the vapor phase of the CsOH-CsI system, but the proposed stability of this molecule is overrated. For a better understanding of the exact role of this molecule in the transport of iodine, thermodynamic functions have to be evaluated in order to facilitate thermodynamic previsions and reliable temperature extrapolations.

IV.3. PRESENT MASS SPECTROMETRIC VAPORISATION DATA

From the Blackburn and Jonhson [3] determined interaction coefficient for the liquid phase, and assuming no solubility in the solid phases, the phase diagram of the CsI-CsOH system is calculated as presented in figure IV-5 using the Factsage software. The present analyzed compositions and temperature ranges are presented in this figure and compared to the one analyzed by Blackburn and Johnson.

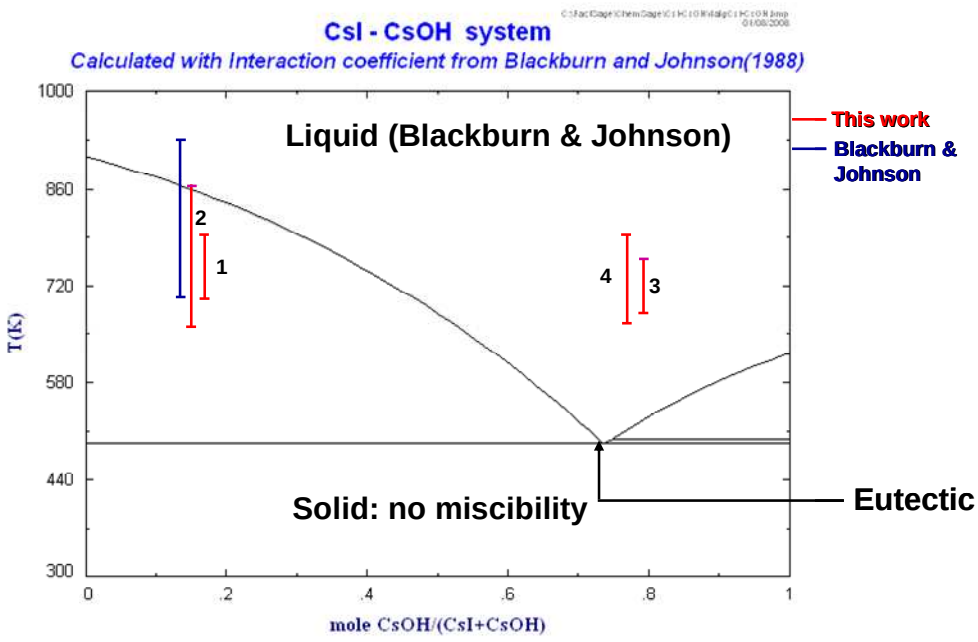

Figure IV-5: Calculated phase diagram from liquid data proposed by Blackburn and Johnson and our selection for the pure compounds (chapter II and III). 1: CsOH-CsI-01s, 2: CsOH-CsI-02s, 3: CsOH-CsI-03s, 4: CsOH-CsI-04s experimental runs.

IV.3.1. Sample preparation

Two different compositions have been prepared directly in pure Ni crucibles (part of the Knudsen cell). Same Ni cells has been already used in the preceding CsOH vaporization study [5]. The preparation method is the one already applied for preparing pure CsOH(s or l) by water distillation [5] when heating slowly under primary vacuum. The known mass of the pure CsOH(s) residue staying in the Ni crucible is then loaded with a known amount of pure CsI(s) beforehand degazed at 423 K under primary vacuum. The mixture in the Ni crucible is then heated in a quartz ampoule under primary vacuum till melting.

The use of a Pyrex (borosilicate) ampoule allows the visual observation of the prepared mixtures melting behavior. It is to notice that the melting point of CsI-CsOH mixture rich in CsOH has been observed at about 473 K and during cooling, the sample became vitreous at about 438 K. After cooling and crystallization, the crucible and its lid are weighted, stored in a desiccant atmosphere and/or loaded in the mass spectrometer. The sample weight loss during the mass spectrometric experiment is known by weighting the “crucible+lid+sample” before and after each experiment. In two experiments we observed a partial creeping

(overflow) of liquid along the effusion orifice or at the junction crucible-lid. This residual liquid film on external surfaces of the crucible and the lid was cleaned carefully with water and alcohol cotton stem in order to evaluate if necessary some corrections to the effusion genuine mass loss. The four experiments are summarized in table IV-2 with comments.

Material cell	**Experience label**	**Initial composition/ mol %**		**T range/ K**	**(s C)/S**	**Observations after HTMS experiments**
		CsOH	CsI			
Ni[a]	CsI-CsOH-01s	17.0	83.0	699-809	$7.1\ 10^{-3}$	- slight sticking of the crucible and its lid to the external envelope - no flow out detected - some vapor deposits on the first field aperture. -white color sample
	CsI-CsOH-02s	14.7	85.3	657-863		Same observations as CsI-CsOH-01s
Ni[a]	CsI-CsOH-03s	79.0	21.0	676-753	$7.1\ 10^{-3}$	-flow out around the effusion orifice and the crucible lid, - sticking of the crucible to the external envelope, - vapor deposit on the internal part of the lid, - green-blue color of the sample (Ni interaction?) -field aperture of the restricted collimation has been rapidly clogged
	CsI-CsOH-04s	76.8	23.2	666-804		-Same observations as CsI-CsOH-03s but contrarily to preceding run the temperature was increased slowly in order to avoid the partial clogging of the field aperture.

Table IV-2. Sample behavior after each experimental run in a pure Ni effusion cell.

The ratio (sC)/S –as mentioned table IV-2- represents the ratio of effective effusion cross-section (sC) versus vaporization section (S cell cross section) that characterizes equilibrium conditions in the cell (see Chapter II).

The effusion orifice alignment along the ionization chamber axis (restricted collimation axis) is performed by moving the effusion cell furnace in two X and Y directions orthogonal to this axis. The analysis of the mass spectrometric response as a function of the cell position (see chapter II) has been checked for each run at low and high temperature. For CsI-CsOH-01s and 02s runs (CsI rich) the scanning profile in X and Y directions didn't show any surface diffusion or flow out anomaly in comparison with what was observed during CsOH vaporization (Appendix IV-A). For run CsI-CsOH-03s, the scanning profile in X and Y directions showed that it becomes slightly sharper when temperature increases (Appendix IV-

A). This confirms the fact that some surface diffusion flow is occurring. But yet, this feature was not so important as observed during CsOH vaporization. In the next run CsI-CsOH-04s, this slight change when temperature increase was no longer observed because the temperature increase was better managed in order to prevent from any partial and rapid clogging of the field aperture as was occuring in the preceding run (CsI-CsOH-03s). For this reason, no mass loss correction is needed to take into account this parasitic phenomenon (surface diffusion) and we further considered that CsI-CsOH-03s run will be discarded because it was not very well managed in term of temperature sequences.

IV.3.2. Ionization processes and gas phase composition

The ionization efficiency curves could evidence different adiabatic and dissociative ionization processes, but the complexity of the gaseous phase as well as the lack of independent information about the activities of the components did not allow the direct determination of the apparition of the mixed molecule via the parent ion Cs_2IOH^+ which is not detected in the spectrum. Consequently, ionic intensity ratios were the only way to analyze the vapor composition.

The main ionic intensity observed during CsI and CsOH compounds vaporization corresponds to the ion Cs^+. Taking into account the proportions measured at 20-24 V ionizing electron voltage for the pure compounds vaporization, the total measured ionic intensity of Cs^+ coming from the CsI(g) and CsOH(g) in the gas phase should be,

$$I(Cs^+) = 4 \cdot I(CsI^+) + 8.7\ I(CsOH^+) \qquad (14)$$

The factor 4 comes from our specific experiments performed with pure CsI(s) in agreement with Lelik et al. [11] mass spectrometric work, and 8.7 is the mean factor as measured in our preceding vaporization work of pure CsOH(l) [5]. The above formula results are compared to experimental results when vaporizing CsI-CsOH mixtures in figure IV-6.

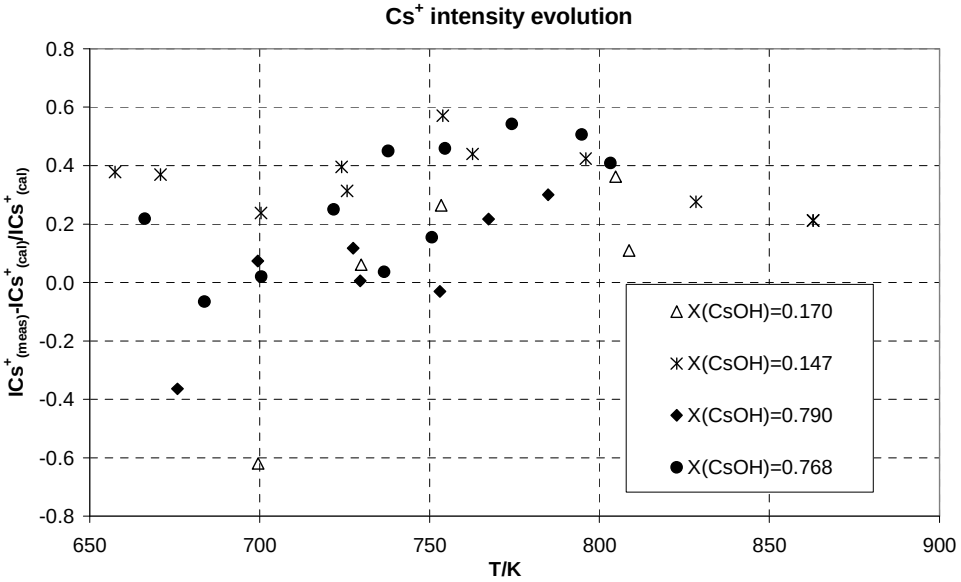

Figure IV-6: Relative values for the comparison of measured ionic intensity of Cs^+ (at 20-24 V) with the attended ionic intensity of Cs^+ as calculated from the monomer ions $CsOH^+$ and CsI^+. (Meas.) Measured Cs^+ intensity and (cal.) for calculated Cs^+ intensity

We observe – except for a few data – that the measured Cs^+ ionic intensity is in relative excess by 0 to 60%. This excess clearly can come only from a new molecule in the gas phase.

Among the different vaporization reactions, reactions (1) and (2) are called "isomolecular" reactions regarding to the gas phase, and these reactions are often used since the mass spectrometric sensitivity cancels as for instance for reaction (1) :

$$K_1(T)\,a(CsOH) = \frac{p(Cs_2O_2H_2)}{p(CsOH)} = \frac{I(Cs_2OH^+)T}{I(CsOH^+)T} \times \frac{G(\sigma\gamma f)_{CsOH^+}}{G(\sigma\gamma f)_{Cs_2OH^+}} = \frac{I(Cs_2OH^+)}{I(CsOH^+)} \times \frac{(\sigma f)_{CsOH^+}}{(\sigma f)_{Cs_2OH^+}} \qquad (15)$$

and for our mass spectrometer ($\gamma = 1$) [5],

$$\frac{I(Cs_2OH^+)}{I(CsOH^+)} = K_1(T)\,a(CsOH) \times \frac{(\sigma f)_{Cs_2OH^+}}{(\sigma f)_{CsOH^+}} \qquad (16)$$

Thus, the total ionic intensities ratio coming from the parent molecules is directly proportional to the activity, assuming that the different determinations have been performed at the same ionization potential in order to fix the ionization cross section ratio. As the activity of CsOH or CsI in the mixtures has to decrease monotonically with respectively CsOH or CsI composition, activity trends have to be observed according to relation (16) for the present ionic intensity ratios if no new molecule contribute to the observed ions coming

from the dimmers ionization. The right term can be recalculated from known equilibrium constant selected values, and with the estimation of (total) ionization cross sections ratio equal to ½. Another way is to compare directly the ionic intensities ratios with those measured over the pure compounds. Figures IV-7 and IV-8 present the measured intensity ratios respectively of $Cs_2OH^+/CsOH^+$ and Cs_2I^+/CsI^+ for different CsI-CsOH mixtures

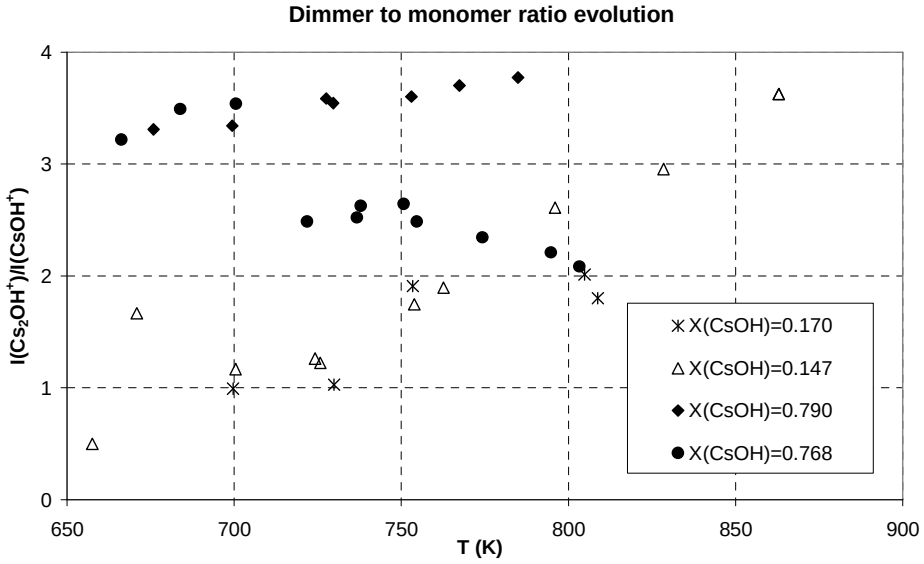

Figure IV-7: Evolution of $Cs_2OH^+/CsOH^+$ total intensity ionic ratio in the CsOH-CsI system as a function of temperature for different CsOH mole fractions.

For CsOH (fig. IV-7) ionic intensity ratio trends (at constant temperature) agree with thermodynamic evolution of the activity with composition. But yet we observe that for the two x(CsOH) low content the ratios or related activities are within the same range. This feature may be related to the phase diagram shape and can indicate that we are in a diphasic domain, CsI(s or solution) in equilibrium with a liquidus according to our calculated phase diagram (fig. IV-5). However, at higher temperatures and for an homogenous liquid phase, the activity should increase with composition increase. If we fit independently each run values, we can observe that (apart for run CsI-CsOH-04s, x(CsOH)=0.768) all activity trends converge and there is no evolution with composition. This fact let suppose a major contribution from a new molecule which perturbs our system.

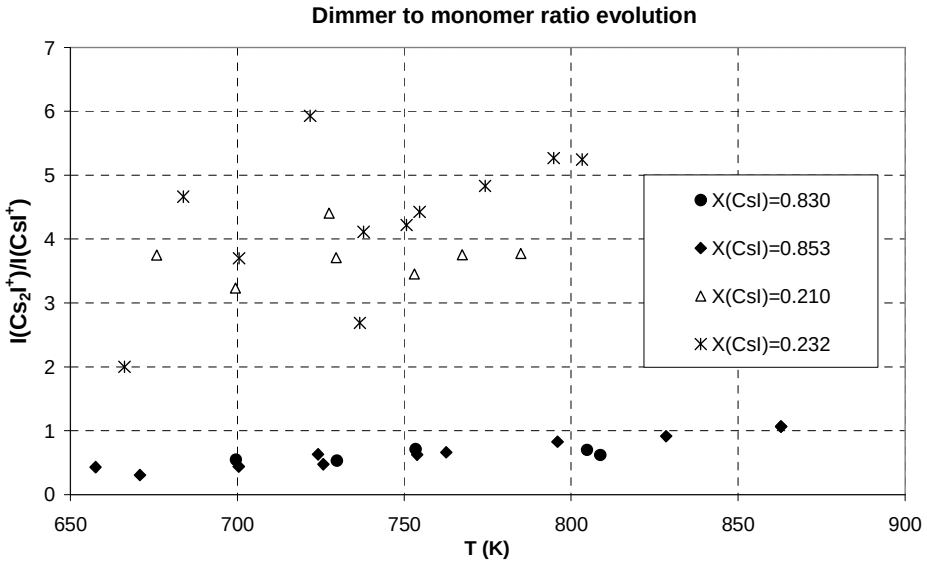

Figure IV-8: Evolution of the Cs_2I^+/CsI^+ total ionic intensity ratio as a function of temperature for different CsI molar fractions.

For CsI (fig. IV-8), trends are clearly in the reverse direction as attended by thermodynamics: activity must decrease with composition decrease and vice versa. Since for lower concentrations the vapor pressures of CsI gases should become lower and probably quite non detectable for the dimmer, this feature let suppose that the ions Cs_2I^+ or CsI^+ have a significant contribution from a new molecule.

IV.3.3. Vapor pressure determinations

The calibration method is the same as applied for the CsOH vaporization study [5]:

- Total ionic intensity associated to one parent molecule is obtained by addition of all ionic intensities of the formed ions: for $Cs_2O_2H_2(g)$ the ions $Cs_2OH^+ + Cs_2O^+ + Cs_2^+$, for CsOH(g) the ions $Cs^+ + CsOH^+$, for $Cs_2I_2(g)$ the ions $Cs_2I^+ + Cs_2^+$, for CsI(g) the ions $Cs^+ + CsI^+ + I^+$
- Different original contributions for common ions (Cs^+ and Cs_2^+) are calculated on the basis of the ratios as measured when vaporizing the pure compounds [5, 6, 11].
- Dimmer to monomer total ionization cross sections ratio is taken equal to 2 [12].

IV.3.3.1. Calculations assuming no new species in the gas phase

Calculations of partial pressures from measured ionic intensities are first applied assuming there is no new species in the gaseous phase. So doing, all mass loss during the experiment is attributed to effusion of the only CsOH(g), $Cs_2O_2H_2$(g), CsI(g) and Cs_2I_2(g) vapors. Experimental vapor pressures for CsOH(g) and $Cs_2O_2H_2$(g) are displayed in figures IV-9 and IV-10.

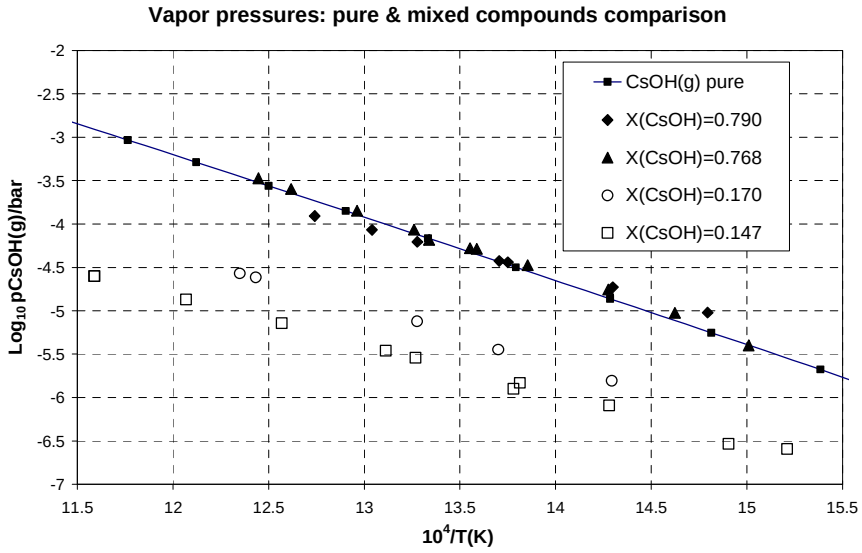

Figure IV-9: Experimental vapor pressure of CsOH(g) in equilibrium with different CsI-CsOH mixtures and comparison with our selected vapor pressure for the pure CsOH compound (this work, chapter II)

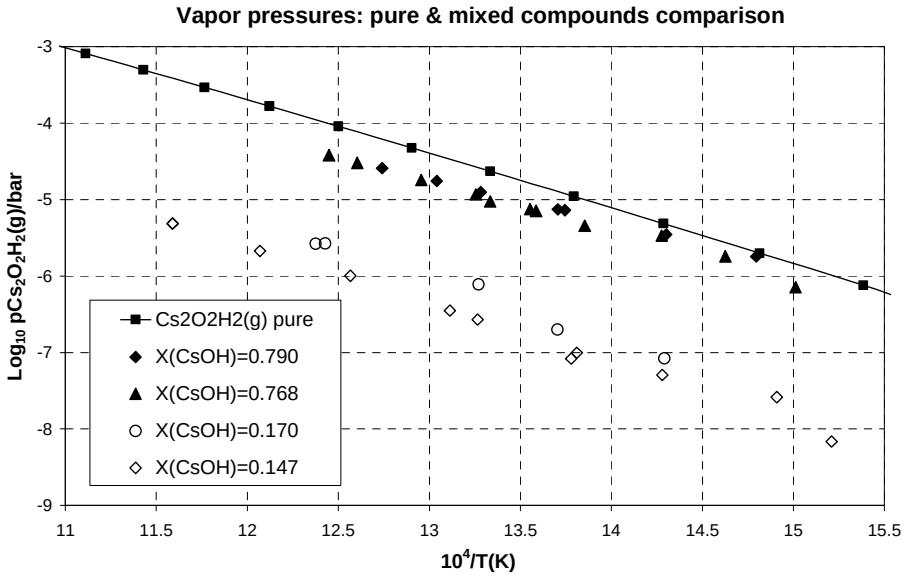

Figure IV-10: Experimental vapor pressure of $Cs_2O_2H_2$(g) in equilibrium with different CsI-CsOH mixtures and comparison with our selected vapor pressure for the pure CsOH compound (this work, Chapter II).

In figure IV-9 and IV-10, the partial pressures respectively of CsOH(g) and $Cs_2O_2H_2$(g) decrease when the CsI content increases, according to the evolution of the CsOH activity, but yet the CsOH rich samples give practically the same pressure than pure compound (activity = 1). We can conclude in different ways: - (i) the activity decrease may be too small for these concentrations close to pure compound and thus pressures would be included within our experimental uncertainty, - (ii) an excess mass loss is due to a new species and taking it into account in the calibration increases the pressures, or - (iii) there is a fragment ion contribution from the dimmer or other molecule with major ionic intensity, *i.e.* $CsOH^+$ although preceding studies did not mention this feature. Experimental vapor pressures for CsI(g) and Cs_2I_2(g) are displayed in figures IV-11 and IV-12.

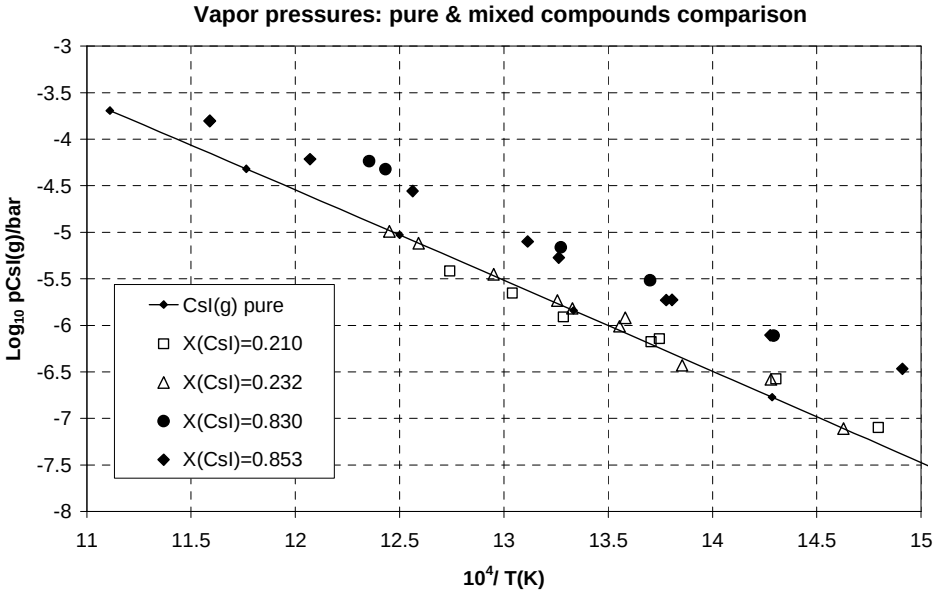

Figure IV-11: Experimental vapor pressure of CsI(g) in equilibrium with different CsI-CsOH mixtures and comparison with our selected vapor pressure for the pure CsI compound.(this work, chapter III)

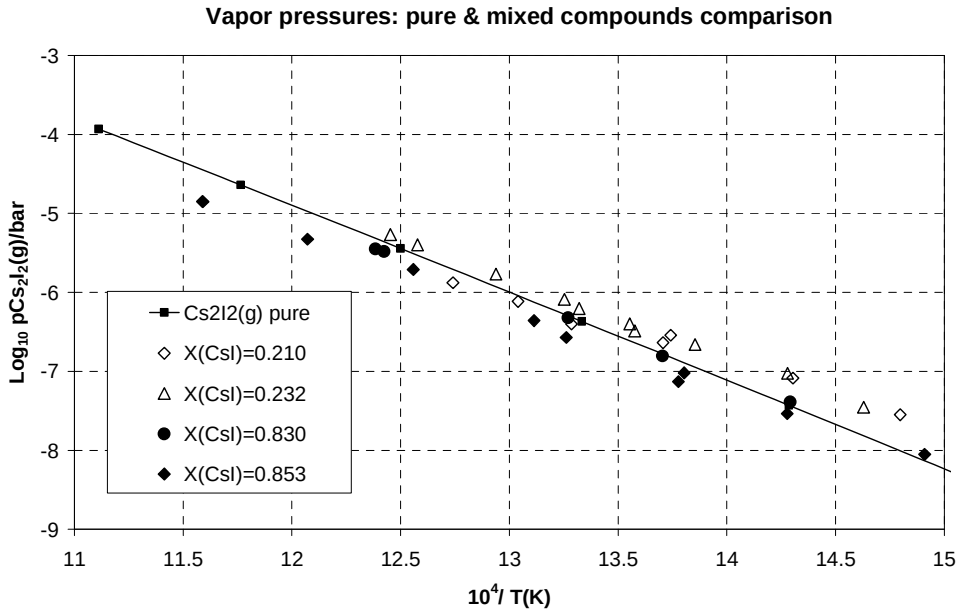

Figure IV-12: Experimental vapor pressure of $Cs_2I_2(g)$ in equilibrium with different mixtures CsI-CsOH and comparison with our selected vapor pressure for the pure CsI compound.(this work, chapter III)

Figure IV-11 shows that vapor pressures of CsI(g) are always equal or greater than those for the pure compound, meanwhile for the dimmer (figure IV-12), the vapor pressures are scattered but distributed around the pure compound vapor pressure. Clearly, these values show trends contrarily to thermodynamic evolution and we can conclude: - (i) for CsI^+ either an extra contribution of CsI^+ ions or an excess of mass loss which is more sensitive on this smaller vapor pressure value compared to CsOH(g), - (ii) for Cs_2I^+ ions clearly an extra contribution in the ionic intensities compared to the only dimmer of CsI.

A last check is done by comparison of the measured dimmer pressures and the calculated ones from the measured monomers and our selected dimmerization equilibrium constants as retained in our preceding compilations (this work chapter II and III). As the dimmerization constant do not depend on the concentrations but only on temperature, differences can evidence fragment ions contributions. Figures IV-13 and IV-14 display this comparison as a function of the inverse of temperature over a liquid at low CsOH concentrations.

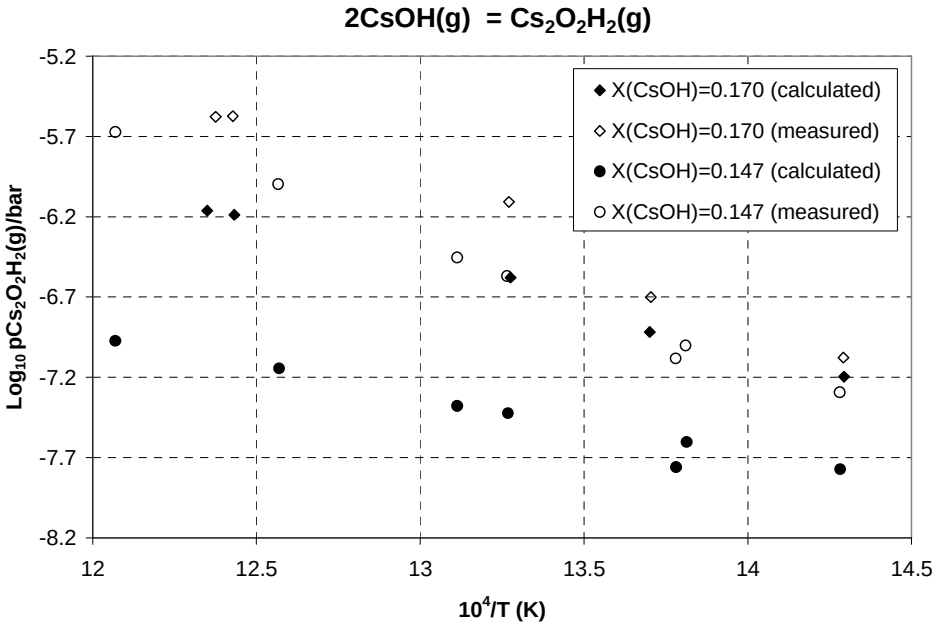

Figure IV-13: Experimental vapor pressures of $Cs_2O_2H_2(g)$ in equilibrium with a CsI-CsOH mixture at low CsOH concentration and comparison with the pressure calculated from the experimental CsOH(g) pressure in the same experiment and our selected dimmerization equilibrium constant.

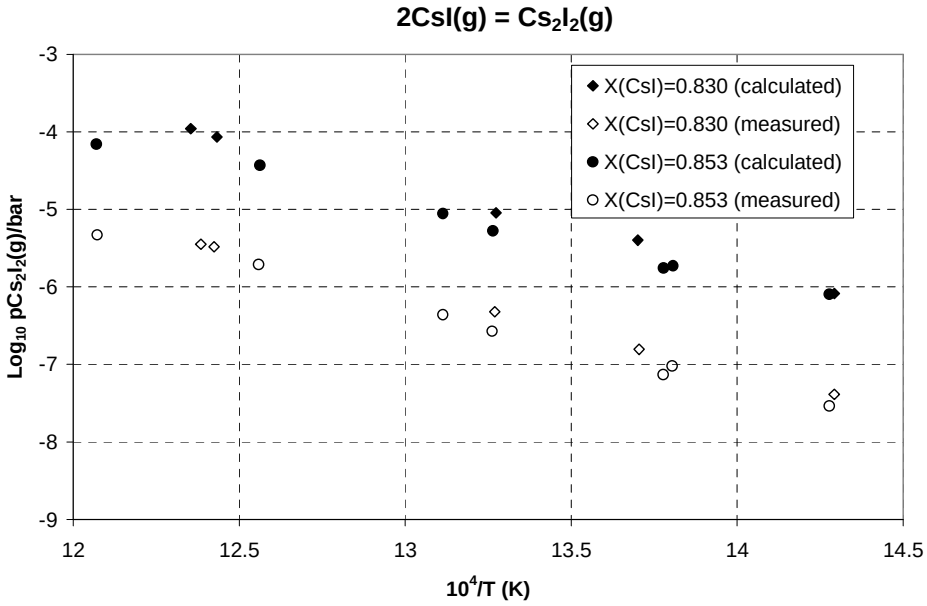

Figure IV-14: Experimental vapor pressures of $Cs_2I_2(g)$ in equilibrium with a CsI-CsOH mixture at low CsOH concentration and comparison with the pressure calculated from the experimental CsI(g) pressure in the same experiment and our selected dimmerization equilibrium constant.

Figure IV-13 shows an excess of measured Cs_2OH^+ ions, - measured pressures over the calculated ones - meanwhile for Cs_2I^+ (fig. IV-14), the reverse is observed - feature that can

be obtained only from an excess of CsI^+ ions compared to Cs_2I^+ ions - . In the case of rich CsOH concentrations, the reverse is observed as illustrated in figures IV-15 and IV-16.

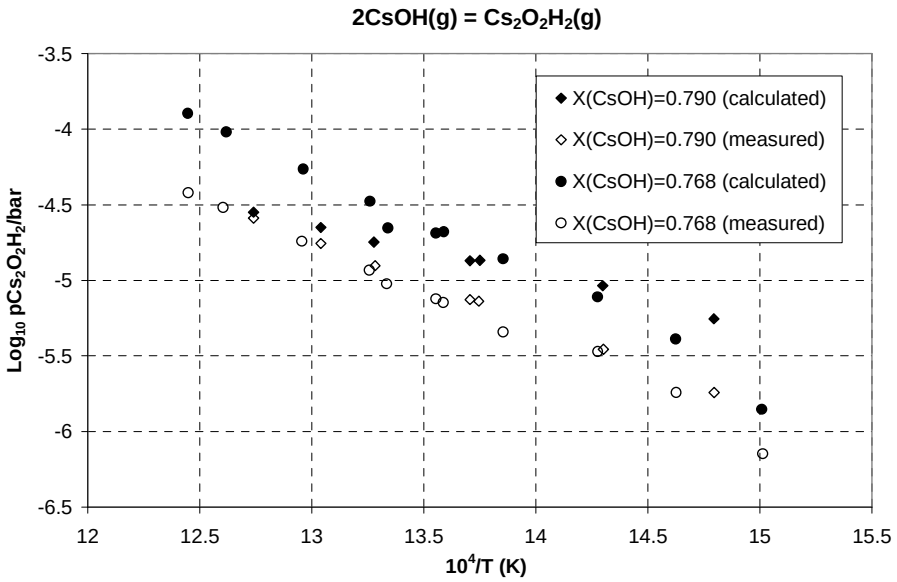

Figure IV-15: Experimental vapor pressures of $Cs_2O_2H_2(g)$ in equilibrium with a CsI-CsOH mixture rich with CsOH and comparison with the pressure calculated from the experimental CsOH(g) pressure in the same experiment and our selected dimmerization equilibrium constant.

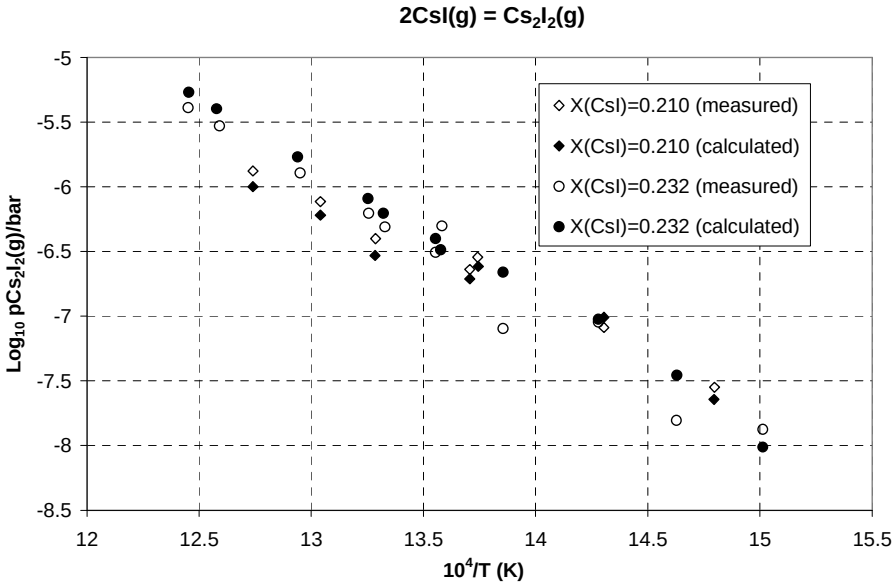

Figure IV-16: Experimental vapor pressures of $Cs_2I_2(g)$ in equilibrium with a CsI-CsOH mixture rich with CsOH concentration and comparison with the pressure calculated from the experimental CsI(g) pressure in the same experiment and our selected dimmerization equilibrium constant.

In figure IV-16, the excess of Cs_2I^+ ions seems very small. This means that the mixed molecule produces less Cs_2I^+ ions than Cs_2OH^+ ions as already observed by Blackburn and

Johnson and an excess of $CsOH^+$ ions is also produced. We have to keep in mind that the parent ions contributions coming from the monomers vary also as a function of composition of the liquid phase due to activity variations, and the above check can evidence different contributions in the spectrum when using different concentrations. The present results clearly imply that the new molecule also produce $CsOH^+$ and CsI^+ fragment ions.

IV.3.3.2 Calculations assuming a new species in the gas phase

The above analysis of ionic intensities ratios and comparison with those of pure compounds vaporization as well as the quantitative interpretation of experiments without occurrence of the new molecule (previous paragraph) show that the $Cs_2IOH(g)$ exists and has a dissociative ionization according to at least five processes leading to the Cs_2OH^+, Cs_2I^+, Cs^+, $CsOH^+$ and CsI^+ fragment ions. The two first ions could not be detected altogether for the same mixture or gaseous composition due to interferences with the ionization of the dimmers, Cs^+ is always present, meanwhile $CsOH^+$ and CsI^+ fragment ions overlap with parent monomers and their detection depends on the composition.

Preceding results indicate that our experimental results have to take into account the mixed molecule as proposed by Blackburn and Johnson [3]. As already performed by Blackburn and Johnson, we first calculated the real contribution of Cs_2OH^+ or Cs_2I^+ coming from the dimmers via our selected values for the dimmerization constants and the monomer intensities. Then the remaining measured intensities are attributed to the ionization of the only $Cs_2IOH(g)$ molecule. Such calculations can be performed for the only case where measured intensities of the like dimmers ions are above the calculated ones, *i.e.* those presented in figures IV-13 and IV-16. Calibration of the mass spectrometer is then performed using mass loss of the samples but taking into account the whole set of molecules in the gas phase, *i.e.* adding the $Cs_2IOH(g)$ contribution to the mass loss meanwhile estimating its total ionization cross section according to the additivity rule [12]: $\sigma(Cs_2IOH) = \sigma(CsOH) + \sigma(CsI)$. This calculation gives different final condensed phase concentrations that the ones obtained when the mixed molecule is ignored as displayed in table IV-B1 (appendix IV-B).

The present retained ionic intensities calculated from the only Cs_2OH^+ or Cs_2I^+ ions and not from the total ionic intensities produced by the complete ionization process of the molecule give necessarily lower vapor pressures for $Cs_2IOH(g)$. This is due to the fact that the estimate

of the ionization cross sections according to the additivity rule operates for total ionization cross section. But yet such calculations can be compared directly with Blackburn and Johnson ones, calculated with the same assumptions. Vapor pressures for the $Cs_2IOH(g)$ molecule are presented in figure IV-17 as a function of the inverse of temperature for all experiments where either Cs_2OH^+ or Cs_2I^+ excess intensities are detected depending on the concentration of the condensed phase.

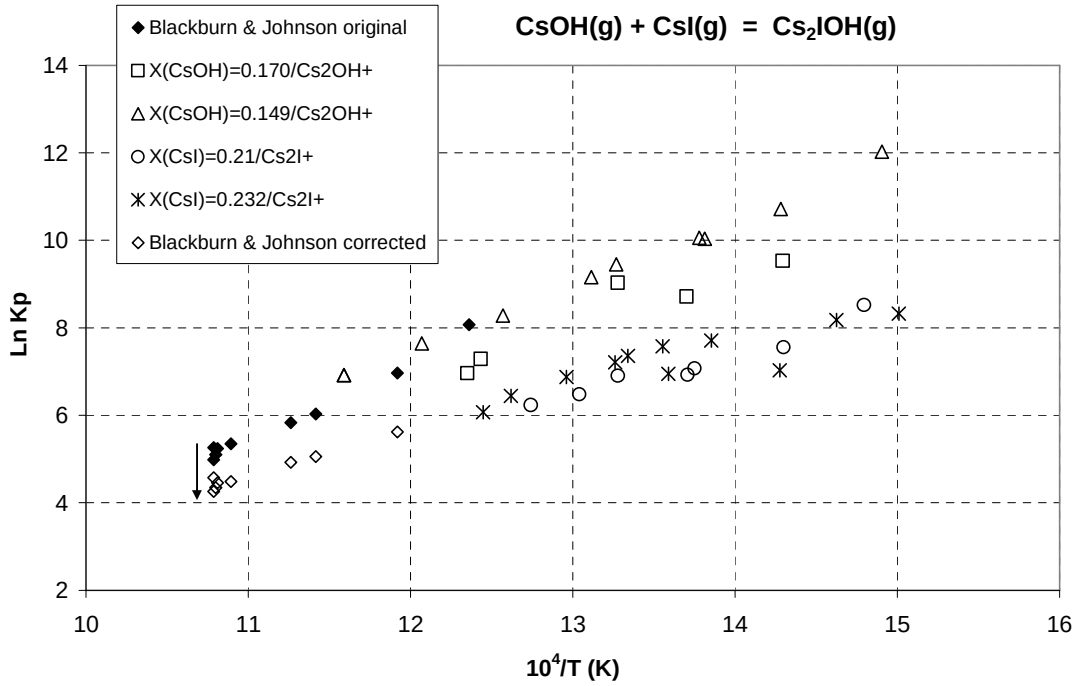

Figure IV-17: Experimental equilibrium constant for the reaction CsOH(g) + CsI(g) = $Cs_2IOH(g)$ as determined using the only Cs_2OH^+ ionic intensity from $Cs_2O_2H_2(g)$ and Cs_2I^+ ionic intensity from $Cs_2I_2(g)$ as measured when vaporizing different CsI-CsOH mixtures and comparison with Blackburn and Johnson original data with the Cs_2OH^+ ion. Blackburn and Johnson data have been corrected according to our selected value for the CsOH dimmerization constant (see text).

Calculated pressures from Cs_2OH^+ intensities presented in figure IV-17 show that we agree reasonably with those proposed by Blackburn and Johnson starting from the same ion.

Same calculations were then performed taking into account the excess of Cs^+ ion *i.e.* with $\{Cs_2OH^+ + Cs^+\}$ or $\{Cs_2I^+ + Cs^+\}$ total ionic intensities (those Cs^+ coming from CsOH and CsI being calculated from relation (14)). So doing, from the same mass loss each experiment gives new final and initial compositions (Appendix IV-B). The calculated pressures of $Cs_2IOH(g)$ increase as presented in figure IV-18. and the pressures scatter slightly decreases. Our experimental pressures become above those from Blackburn and Johnson.

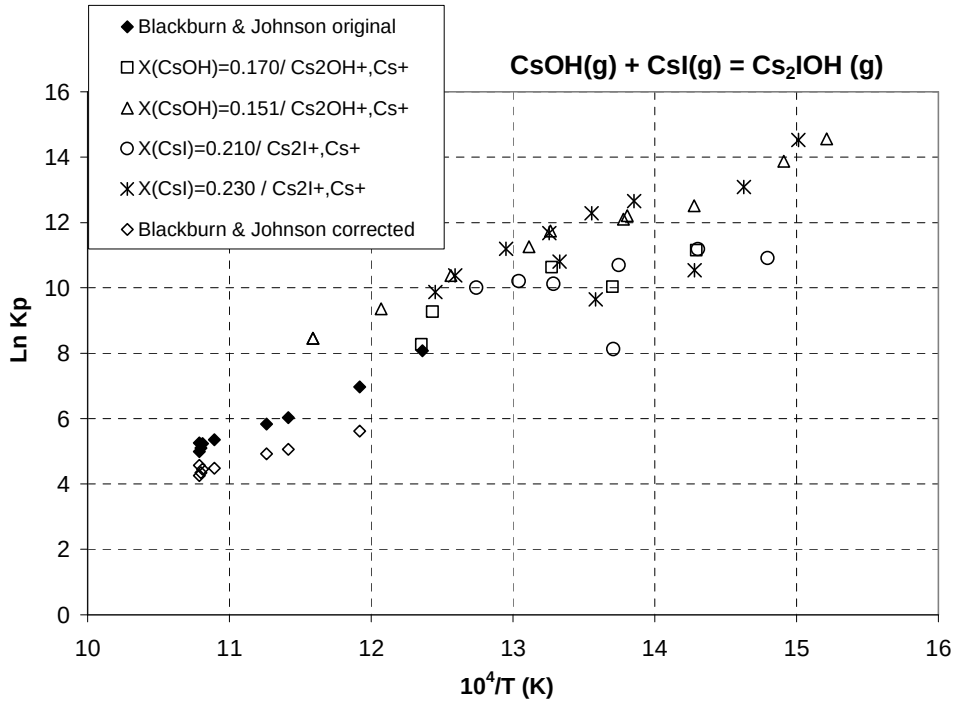

Figure IV-18: Experimental equilibrium constant for the reaction CsOH(g) + CsI(g) = $Cs_2IOH(g)$ as determined using the only ($Cs_2OH^+ + Cs^+$) or ($Cs_2I^+ + Cs^+$) ionic intensities when vaporizing different CsI-CsOH mixtures and comparison with Blackburn and Johnson original and corrected data (see text).

Discrepancies between the present determinations and those of Blackburn and Johnson concerning the equilibrium constant may come from the pressures of the monomers or an over-evaluated monomer's ions due to the above quoted contribution from dissociative ionization of the new molecule. Comparison between our monomers vapor pressures with those published for similar liquid compositions is presented in figures IV-19 and IV-20.

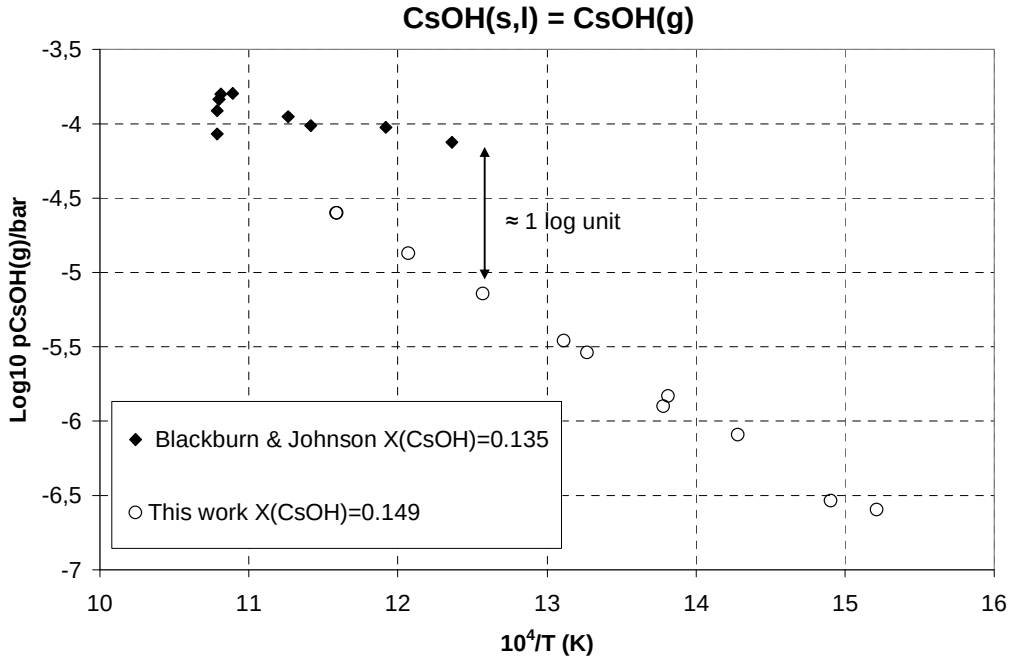

Figure IV-19: Comparison of our experimental vapor pressures of CsOH(g) in equilibrium with CsOH-CsI mixtures at low CsOH concentrations with Blackburn and Johnson values. Note the pressure drop of these last values when temperature increases due to CsOH losses.

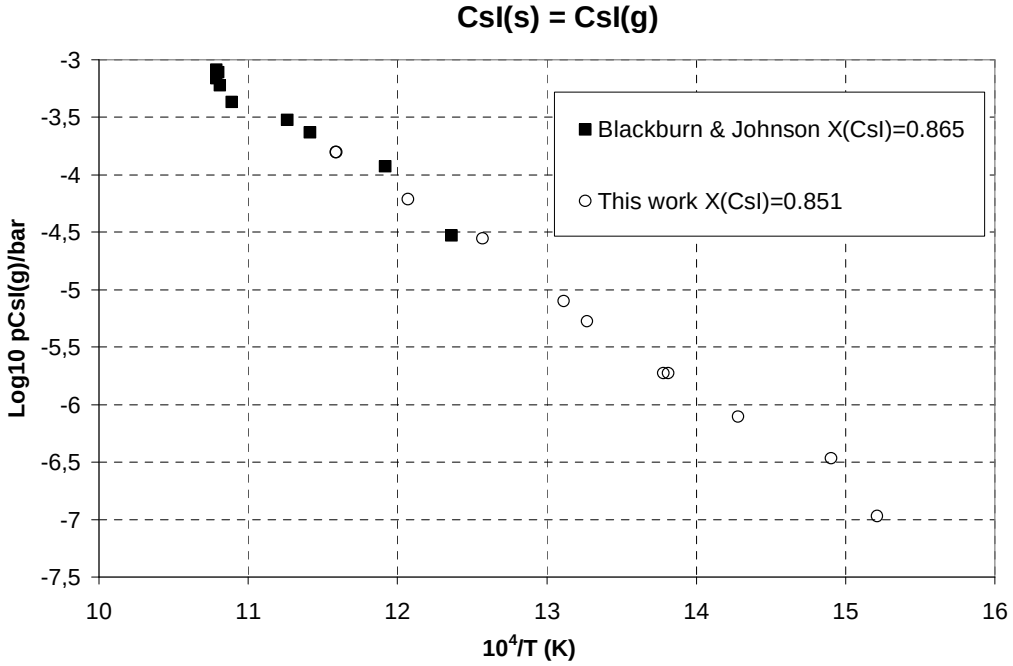

Figure IV-20: Comparison of our experimental vapor pressures of CsI(g) in equilibrium with CsOH-CsI mixtures at low CsOH concentrations with Blackburn and Johnson values. Note the pressure increase of these last values when temperature increases due to CsI enrichment

Contrarily to CsOH(g), the agreement is good for CsI(g). We believe that Blackburn and Johnson largely over evaluated the CsOH(g) pressure – not only due to the already mentioned experimental difficulties from surface diffusion or overflow (see chapter II) – but also because the dimmer pressure was considered as negligible. In fact their initial monomer pressures were about a factor 10 higher above us. So, decreasing their CsOH(g) pressures to our values, the equilibrium constant for reaction (7) will increase significantly as presented in figure IV-21.

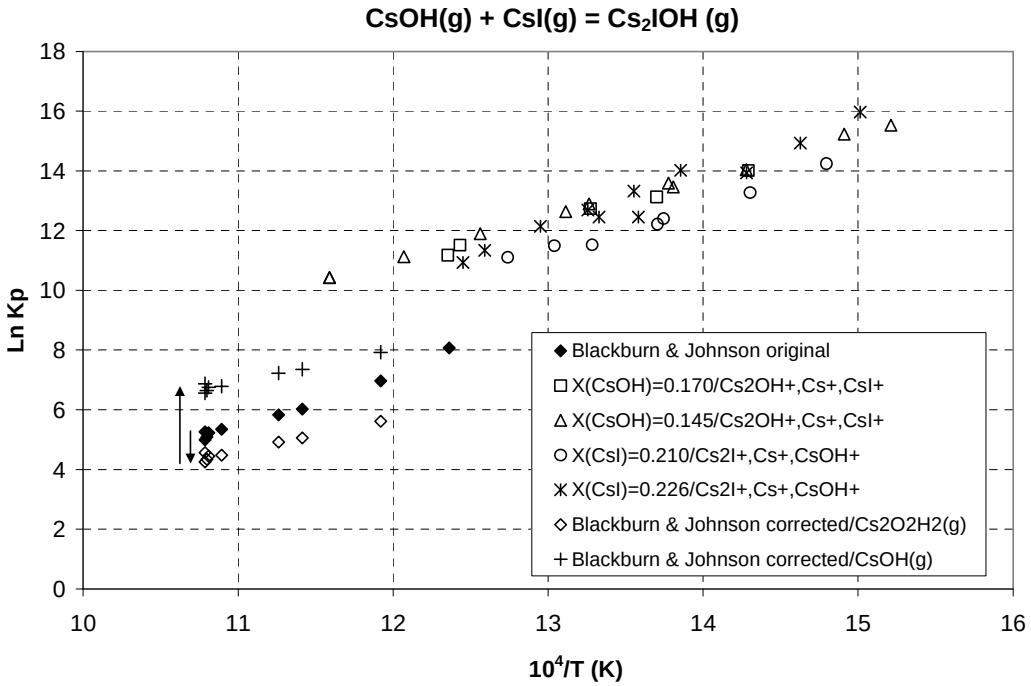

Figure IV-21: Experimental equilibrium constant for the reaction CsOH(g) + CsI(g) = $Cs_2IOH(g)$ as determined using the sum (Cs_2OH^+ + Cs^+ + CsI^+) ionic intensities and the sum (Cs_2I^+ + Cs^+ + $CsOH^+$) when vaporizing different CsI-CsOH mixtures and comparison with Blackburn and Johnson original and corrected data.

In order to take into account the contribution of the CsI^+ and $CsOH^+$ fragment ions in the total ionic intensity coming from $Cs_2IOH(g)$ ionization, we calculated these contributions from figures IV-14 and IV-15 respectively. Conversely to the first calculation for the dimmers contributions, we fix the dimmer intensity – considered coming mainly from the dimmers and with too small contributions from the mixed molecule - and we recalculated the true monomer pressures. Finally the new proposed equilibrium constant for reaction (8) is presented in figure IV-21. Determined pressures logically increase due to total considered intensities, but also become more consistent whatever the liquid composition is. This feature

is in agreement with thermodynamics since the gaseous phase equilibrium constant does not depend on liquid composition. Remaining difference with the double corrected values of Blackburn and Johnson (from selected $Cs_2O_2H_2$(g) and monomer pressure) comes from the only retained dimmers ions in their study that under-evaluates the real pressure of the mixed molecule since the different contributions from fragment ions are important.

A least square fit of all our data for reaction (8) in figure IV-21 gives the second law values,

$$\ln K_p = \frac{14611}{T} - 6.8822 \qquad (657 < T/K < 863) \qquad (17)$$

Considering the different successive corrections in order to take into account the total ionization process of the Cs_2IOH(g) molecule, total uncertainty for this second law is difficult to evaluate correctly. Indeed, the overlap of ions coming from different molecular origins can probably have or not a significant impact depending on internal compensations as a function of temperature and compositions.

IV.4. THERMODYNAMIC FUNCTIONS OF THE CS_2IOH(G) MOLECULE

Heat capacity (Cp°), entropy (S°_T) and free energy functions (Gef or Fef) for the present molecule can be calculated from the “so-called” molecular parameters of the molecule, i.e. its geometry, its vibration modes and its fundamental electronic state. As the structure of the molecule has not yet been studied, these molecular parameters have to be estimated. For complex molecules, molecular constants can often be estimated by analogy with those of closely related known species. Trends along rows and columns in the periodic table of elements assist in selecting the more probable molecular parameters and geometry. Simple rules [13, 14] help in estimating interatomic distances and vibrational frequencies for which approximate values can also be calculated with the central force or the valence force [15] approximations (see chapter I for Fef calculation).

IV.4.1. Structure of the molecule

By analogy with the two dimmers $Cs_2I_2(g)$ and $Cs_2O_2H_2(g)$, we stated that the molecule is linked by ionic type bonds and its minimum energy as a function of the structure can be calculated according to the Pauling's model for molecules of the family Alkaline-Halogen as NaCl, and its dimmer, etc...[16, 17]. Dimmers of this family - as for example Cs_2I_2 - have been evaluated according to this model by Milne and Cubicciotti [18]. The structure of those ionic molecules is planar, and the shape according to ionic bonds is square or lozenge. For hetero-cationic dimmers the lozenge becomes slightly deformed. The ionic bond in the diatomic gaseous molecules is described by the addition of two potential energies, one Colombian attractive energy, and one repulsive energy according to the following relation [18],

$$E = -\frac{z^2 e^2}{r} + \beta \frac{B_0 e^2 (r_+ + r_-)^{n-1}}{r^n} \qquad (18)$$

Where E the potential energy, r distance of separation of the two ions (anion and cation), z the ion charge (+1 or -1), e the charge of the electron, β a constant, B_0 a constant such that $nB_0=0.291$, , r_+ and r_- constants characteristic of the ions and equal to their crystal radii, n a constant characteristic of the alkali halide which is deduced by derivation of this relation relative to *r* (the distance between the two ions). The minimum of the energy corresponds to the experimental equilibrium distance r_e for the gaseous molecule:

$$r_e = (r_+ + r_-)(n B_0)^{1/(n-1)} \qquad (19)$$

It has been observed that a change of 1 in the *n* value contribute to 0.05 Å in the r_e value.
The extension of the model to dimmers has been previously done by Milne and Cubicciotti and the basic relation becomes for pure dimmers,

$$E(M_2X_2) = 4\frac{Z_M Z_X e^2}{a} + \frac{Z_M^2 e^2}{c} + \frac{Z_X^2 e^2}{d} + 4\beta_+^- B_0 e^2 \frac{(r_M + r_X)^{n-1}}{a^n} + \beta_+^+ B_0 e^2 \frac{(2r_M)^{n-1}}{c^n} + \beta_-^- B_0 e^2 \frac{(2r_X)^{n-1}}{d^n} \qquad (20)$$

Relation in which β is a constant : 1 for univalent cation – anion interaction, 1.25 for cation-cation, and 0.75 for anion-anion, Z the ion charge (+1 or -1), e the charge of the electron, B_0 a constant = 0.291/n and n= (n_M + n_X) , $2n_M$ or $2n_X$ from table I in [18], a , b , c and d are the inter atomic distances as defined in figure IV-22.

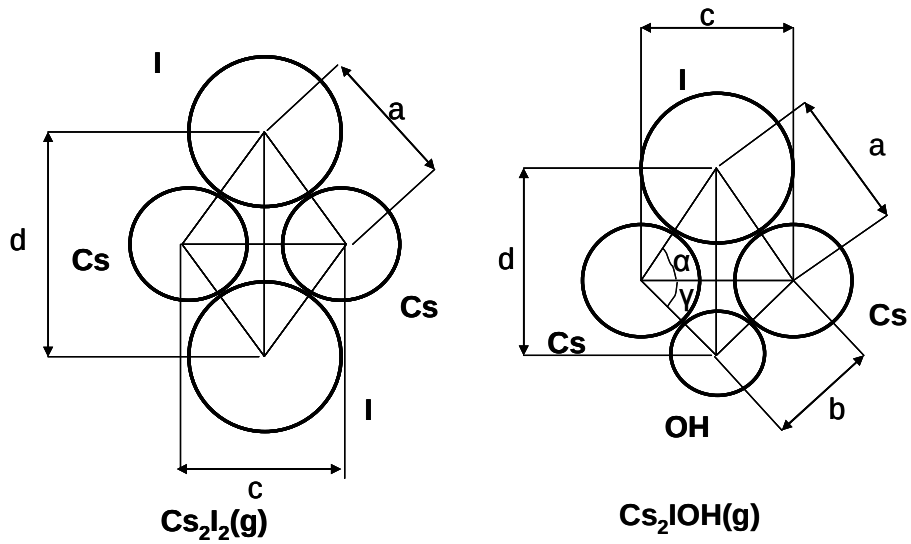

Figure IV-22: $Cs_2I_2(g)$ and Cs_2IOH (g) molecular geometries and their defined inter-atomic distance.. α is the I-Cs-Cs angle, γ is the Cs-Cs-OH angle.

Our calculations were tested by comparison with the previous estimates of Milne and Cubicicotti and with the retained values by Glushko et al. [19] also deduced from ionic modeling for the Cs_2I_2 molecule. Figure IV-23 shows results of our calculations. The minimum of the potential energy (note that this minimum is quite flat) is obtained for the a, c and d distances. Comparison with earlier works is presented in table IV-3.

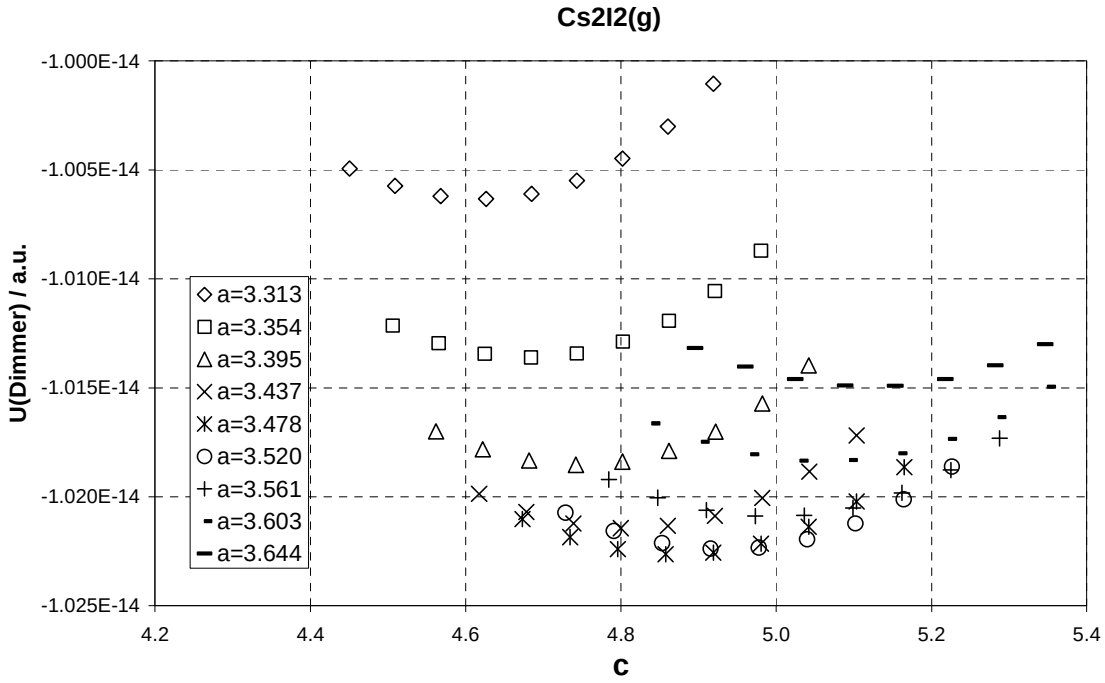

Figure IV-23: $Cs_2I_2(g)$ ionic model results and its minimum potential energy

Authors	r_e /Å (monomer)	a (Å)	c (Å)	d (Å)	Angle α (°)	Angle γ (°)	Moment of Inertia $I_A I_B I_C$ (cgs)
Milne and Cubicciotti [18]	-------	3.49	4.91	4.96	44.7	44.7	$3.625\ 10^{-110}$
Feber [20] (based on Krasnov et al.[21])	-------	3.548	-------	-------	49 ± 5	49 ± 5	$3.969\ 10^{-110}$
Glushko et al. (1982) [19]	3.3152	3.54	-------	-------	49 ± 5	49 ± 5	$3.9\ 10^{-110}$
Present work	-------	3.478	4.919	4.919	45.4	45.4	$3.472\ 10^{-110}$

Table IV-3. Calculations of equilibrium inter-atomic distances for the $Cs_2I_2(g)$ molecule using ionic bond modeling for the inter-atomic cation-anion, cation-cation and anion-anion interactions.

The equilibrium distance for the Cs-I bond in the monomer is slightly enlarged in the dimmer by ≈ 0.16 to 0.22 Å due to relaxation of the dimmer structure. Our calculations in comparison with those of literature (Gurvich et al. [19]) lead to similar results and the resulting moment of inertia give differences for free energy function which is within ± 0.5 J. $K^{-1}.mol^{-1}$ at 1000 K.

For the mixed molecule $Cs_2IOH(g)$, the constants of the model associated to the Cs-OH bond have to be evaluated by comparison with the known equilibrium distance (r_e) in the CsOH(g) molecule using relation (19). As the OH^- ion is considered as a single entity, the distance Cs-OH at equilibrium (r_e) is obtained from Gurvich et al. selected parameters for the Cs-O-H bonds, and r(Cs-OH) = r(Cs-O) + r(O-H)/2 = 2.403 + 0.92/2 = 2.463 Å. Using the OH^- ionic radius equal to 1.32 Å [22], the best constants are B_0 (Cs-OH)= 0.320 and n(OH) = 2.40 and n(Cs-OH) = n(Cs) + n(OH) = 4.1+2.4 = 6.5 bond that give the minimum of energy as shown in figure IV-24.

The above optimized data are used for the calculation of the molecular parameters a, b, c, d (Fig. IV-22) of the molecule $Cs_2IOH(g)$ according to the following relation based on relation (20):

$$E(Cs_2IOH) = 2\cdot\frac{Z_{Cs}Z_{OH}e^2}{b} + 2\cdot\frac{Z_{Cs}Z_Ie^2}{a} + \frac{{Z_{Cs}}^2e^2}{c} + \frac{Z_{OH}Z_Ie^2}{d} + 2\cdot\frac{\beta_+^-B_{0Cs-I}e^2((r_{Cs}+r_I)^{(n_{Cs}+n_I-1)})}{a^{n_{CsI}}}$$
$$+ 2\cdot\frac{\beta_+^-B_{0Cs-OH}e^2((r_{Cs}+r_{OH})^{(n_{Cs}+n_{OH}-1)})}{b^{n_{Cs}+n_{OH}}} + \frac{\beta_+^+B_{0Cs-Cs}e^2((2r_{Cs})^{(2n_{Cs}-1)})}{c^{2n_{Cs}}} + \frac{\beta_-^-B_{0I-OH}e^2((r_I+r_{OH})^{(n_I+n_{OH}-1)})}{d^{n_I+n_{OH}}}$$

(20-bis)

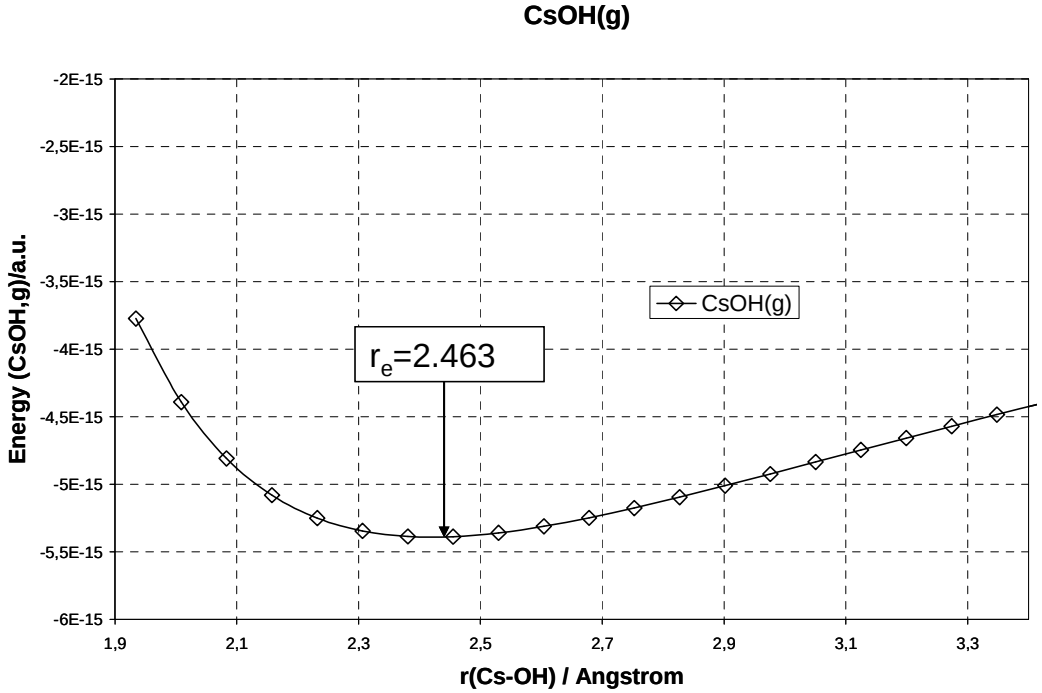

Figure IV-24: CsOH(g) ionic model results and its minimum potential energy located for r_e=2.463 Å.

A preliminary test is done when calculating the dimmer $Cs_2O_2H_2$(g). Calculated distances according to figure IV-25 are compared to retained values by Gurvich et al. [23] in table IV-4. The resulting moment of inertia in comparison with Gurvich et al. ionic model $Cs_2(OH)_2$(g) and real model $Cs_2O_2H_2$(g) give differences for free energy function which is within ± 8.6 J. K^{-1}.mol^{-1} at 1000 K. This large uncertainty in comparison with Cs_2I_2(g) (1.1 J. K^{-1}.mol^{-1} at 1000 K) is due to the fact that $Cs_2O_2H_2$(g) molecular parameters are not well known in literature contrarily to Cs_2I_2(g). Besides, better values for hydroxides could be obtained by a complete analysis similar to the one performed by Pauling for halides [16, 17].

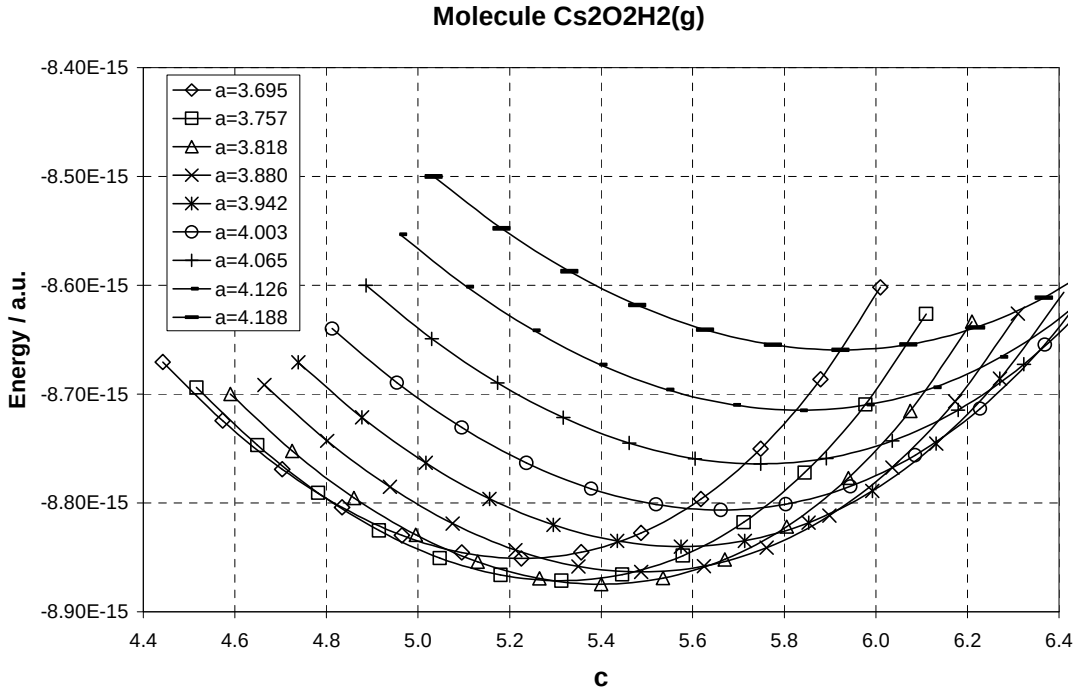

Figure IV-25: $Cs_2O_2H_2(g)$ ionic model results and its inter-atomic distance optimization for a minimum potential energy

Authors & molecules	r_e /Å (monomer)	a (Å)	b (Å)	c (Å)	d (Å)	Angle α (°)	Angle γ (°)	Moment of Inertia $I_AI_BI_C$ (cgs)
Gurvich et al. [23] $Cs_2O_2H_2(g)$		2.62 (Cs-O)						$5.2\ 10^{-112}$
Gurvich et al. $Cs_2(OH)_2(g)$ ionic model	2.463 (Cs-OH)	3.105	b = a	4.39	4.39	45	45	$1.39\ 10^{-111}$
Present work $Cs_2(OH)_2(g)$ ionic model	2.463 (Cs-OH)	3.818	b = a	5.4	5.4	45	45	$4.81\ 10^{-111}$
Present work $Cs_2IOH(g)$	3.3152 (Cs-I) 2.463 (Cs-OH)	3.512	2.65	4.2	4.406	53.3	37.6	$6.001\ 10^{-111}$

Table IV-4. Calculations of equilibrium inter-atomic distances for the $Cs_2O_2H_2(g)$ and $Cs_2IOH(g)$ molecules using ionic bond modeling for the inter-atomic cation-anion, cation-cation and anion-anion interactions.

Calculation of the inertia products $I_AI_BI_C$ is performed from [24] using the Cartesian coordinates (in Å) with the origin at the c-d crossing (fig. IV) for the atoms in $Cs_2IOH(g)$ which are,

$$Cs(1)\begin{cases} x = -2.1 \\ y = 0 \\ z = 0 \end{cases} \qquad I\begin{cases} x = 0 \\ y = a\sin\alpha = 2.816 \\ z = 0 \end{cases}$$

$$(OH)\begin{cases} x = 0 \\ y = b\sin\gamma = -1.617 \\ z = 0 \end{cases} \qquad Cs(2)\begin{cases} x = 2.1 \\ y = 0 \\ z = 0 \end{cases}$$

The molar masses are: M_{Cs} = 132.9054 M_I = 126.9045 M_{OH} = 17.007 (g.mol^{-1})

Figure IV-26 displays the potential energy of the $Cs_2IOH(g)$ molecule from which distances a, b, c and d are extracted and presented in table IV-4.

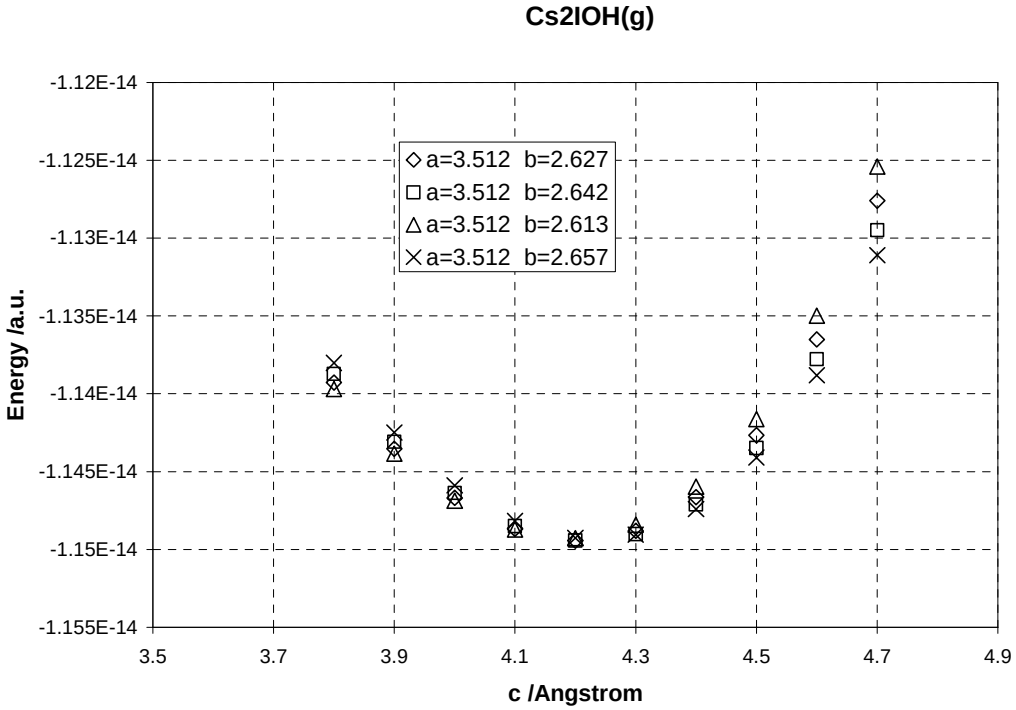

Figure IV-26: $Cs_2IOH(g)$ ionic model results and its minimum potential energy

Note that the c and d distances (Cs-Cs and I-OH, respectively) calculated with the ionic model are very close to those calculated by addition of each bond Cs-I and Cs-O as taken in the pure dimmers and imposing the angle $\alpha+\gamma = 90°$ in place of the present 90.9°. The resulting small differences in the interatomic distances – about 0.01 Å - lead to quite identical values for the products $I_AI_BI_C$ (for $Cs_2I_2(g)$ molecule) and are within the estimates uncertainties.

IV.4.2. Molecular vibrations

Facing the lack of spectroscopic information, the vibration frequencies have to be estimated. Starting from those of the pure dimmers, the shift of the frequencies are roughly estimated when postulating that the force constants – namely stretching, angular deformation and torsion deformations - for the Cs-I and Cs-OH bonds or I-Cs-I angles etc.....keep the same values and applying the general force constant relation [15],

$$\omega_i = \frac{1}{2\pi}\sqrt{\frac{k_i}{\mu}} \qquad (21)$$

in which μ is the reduced mass calculated from,

$$\frac{1}{\mu} = \frac{1}{m_1} + \frac{1}{m_2} + \frac{1}{m_3} + \frac{1}{m_4} \qquad (22)$$

m_i being the masses of the two Cs and I atoms forming the square or lozenge basic structure and the OH entities, k_i the force constant associated to the present vibration mode. Although this relation applies theoretically only for each atom in the molecule associated with particular force constants for each bond (like stretching) or associated bonds (like angular deformation), these estimates have been applied to each normal vibration as known in the pure dimmers. The "global" force constants for the dimmers are thus calculated for every normal mode corresponding to the basic structure as shown in table IV-5. The force constant (k_{Cs2IOH}) for the mixed dimmer is calculated from the mean value of the two pure dimmers. The normal vibration frequencies are deduced from the reduced mass of the mixed dimmer (relations (21) and (22)). The three vibration normal modes associated to the O-H bond are taken equal to those in the $Cs_2O_2H_2$(g) molecule. All vibration frequencies are presented in table IV-6. Each of these vibration frequencies (3N-6 = 9) is not degenerated. (N is the number of atoms in the molecule)

Vibration Frequencies /cm^{-1}	Molecules		Force constants / Arb.Units			Vibration Frequencies Cs_2IOH/cm^{-1}
	Cs_2I_2 [25]	$Cs_2O_2H_2$ [23]	k(Cs_2I_2)	k($Cs_2O_2H_2$)	k(Cs_2IOH)	
ω_1	89	235	1.69 E-17	2.60 E-17	2.14 E-17	167
ω_2	44	113	4.12 E-18	6.01 E-18	5.07 E-18	81
ω_3	62	185	8.18 E-18	1.61 E-17	1.21 E-17	126
ω_4	25	85	1.33 E-18	3.40 E-18	2.37 E-18	55
ω_5	82	227	1.43 E-17	2.43 E-17	1.93 E-17	158
ω_6	90	272	1.72 E-17	3.48 E-17	2.60 E-17	184
ω_7		280				280
ω_8		275				275
ω_9		3700				3700

Table IV- 5. Vibration frequencies of pure Cs_2I_2(g) and $Cs_2O_2H_2$(g) and estimated ones for the mixed molecule.

IV.4.3. Other molecular parameters

The symmetry number is σ = 2, the electronic ground state is Σ state for such a saturated molecule (ε_0 = 0 and the ground state statistical weight g_0 = 1) and no excited molecular states are postulated (see chapter I). The molar mass of CsICsOH is equal to 0.4097223 kg.mol^{-1}.

IV.4.4. Thermodynamic functions

Thermodynamic functions – namely $C°_p$, $S°_T$ and Free energy functions (Gef or Fef), referred either to 0 K or 298.15 K - are calculated based on the harmonic oscillator and rigid rotator approximation for an ideal polyatomic molecule by using the Janaf formulae [14] and the present molecular parameters. Results are presented in table IV-6.

T(K)	Cp (J.K^{-1}.mol^{-1})	H(T) - H(0) (J.mol^{-1})	H(T) - H(298) (J.mol^{-1})	S(T) (J.K^{-1}mol^{-1})	- Gef(0) (J.K^{-1}mol^{-1})	- Gef(298) (J.K^{-1}mol^{-1})
298.15	95.742	23074.940	0.000	405.727	328.333	405.727
300	95.789	23252.106	177.166	406.319	328.812	405.728
400	97.474	32926.457	9851.517	434.139	351.823	409.510
500	98.304	42719.400	19644.460	455.988	370.549	416.699
600	98.822	52577.104	29502.164	473.959	386.331	424.789
700	99.243	62480.652	39405.712	489.225	399.967	432.931
800	99.658	72425.569	49350.629	502.504	411.972	440.815
900	100.095	82412.973	59338.033	514.267	422.697	448.335
1000	100.554	92445.243	69370.303	524.836	432.391	455.466
1100	101.024	102524.106	79449.166	534.442	441.238	462.215

1200	101.493	112650.044	89575.103	543.252	449.377	468.607
1300	101.950	122822.322	99747.382	551.394	456.916	474.666
1400	102.385	133039.262	109964.322	558.966	463.938	480.420
1500	102.796	143298.550	120223.609	566.044	470.511	485.895
1600	103.179	153597.509	130522.569	572.690	476.692	491.114
1700	103.533	163933.310	140858.369	578.956	482.525	496.098
1800	103.859	174303.109	151228.169	584.883	488.048	500.868
1900	104.158	184704.152	161629.211	590.507	493.294	505.439
2000	104.432	195133.827	172058.886	595.857	498.290	509.827
2100	104.682	205589.697	182514.756	600.958	503.058	514.046
2200	104.911	216069.513	192994.573	605.833	507.620	518.108
2300	105.120	226571.217	203496.277	610.501	511.992	522.025
2400	105.311	237092.931	214017.991	614.979	516.191	525.805
2500	105.486	247632.952	224558.012	619.282	520.229	529.459
2600	105.647	258189.737	235114.797	623.422	524.119	532.994
2700	105.794	268761.891	245686.951	627.412	527.871	536.417
2800	105.929	279348.152	256273.212	631.262	531.495	539.736
2900	106.054	289947.379	266872.439	634.982	535.000	542.957
3000	106.168	300558.540	277483.600	638.579	538.393	546.084

Table IV-6: Thermodynamic functions for the $Cs_2IOH(g)$ molecule

The free energy functions as presented in table IV-7 are either referred to 0 or 298.15 K according to the general formulae:

$$Gef(0) = -\frac{G_T^\circ - H_0^\circ}{T} \qquad or \quad Gef(298.15) = -\frac{G_T^\circ - H_{298.15}^\circ}{T} \tag{23}$$

in which Gef and H° are respectively the free energy function and the enthalpy, G°_T the Gibbs energy and T the temperature.

These thermodynamic functions are then used in the third law calculations of the reaction enthalpies at 298.15 K, meanwhile the enthalpy increments (H_T-H_{298}) are used in second law calculations of the reaction enthalpies at 298.15K.

IV.5. SECOND AND THIRD LAW ANALYSIS

Second and third law calculations have been performed for each successive ion contribution to the ionic intensity of the $Cs_2IOH(g)$ in order to evaluate the impact on the resulting enthalpy for the measured reaction (8),

$CsOH(g) + CsI(g) = Cs_2IOH(g)$

as presented in the appendix IV-C. The agreement between second and third laws is neither obtained. This feature is quite certainly related to the increasing uncertainty on the successive

addition of fragment ions contributions as well as to the narrow temperature range for derivation. Moreover the deconvolution into fragment ion contributions is performed with the assumption of constant contributions whatever the temperature is. Any relative evolution with temperature of the different ionization channel efficiencies may contribute to build larger trends in second law results more than in third law results.

As already observed when displaying ln K_p versus 1/T, trends of third law enthalpy as a function of the temperature become smaller when the different ion contributions are taken into account. This observation confirms our ions selection issued from the $Cs_2IOH(g)$ molecule. The whole set of results is presented in table IV-7 altogether with Blackburn and Johnson [3] results as recalculated with our free energy function for $Cs_2IOH(g)$ and corrected for same references for CsOH(g) and its dimmer.

Run label This work	Temperature range /K	$\Delta_rH°_{298.15}$ / (kJ.mol^{-1})	
		2nd law	3rd law
CsI-CsOH-01s	699-809	-119.6 ± 6.7	-171.9 ± 3.0
CsI-CsOH-02s	657-863	-119.9 ± 2.0	-173.2 ± 4.8
CsI-CsOH-03s	676-753	-130.7 ± 8.7	-165.3 ± 2.0
CsI-CsOH-04s	666-804	-155.5 ± 11.1	-170.9 ± 2.1
Blackburn & Johnson [3]	Temperature range /K	$\Delta_rH°_{298.15}$ / (kJ.mol^{-1})	
		2nd law	3rd law
Original data	809-927	- 151.5 ± 7.5	-151.7 ± 1.0
$Cs_2O_2H_2(g)$ corr		- 94.1 ± 7.3	-144.9 ± 1.8
CsOH(g) corr		- 94.0 ± 7.3	-162.2± 2.4

Table IV-7: Second and third law enthalpy calculations and their standard deviation for the reaction CsOH(g) + CsI(g) = $Cs_2IOH(g)$ and comparison with earlier results from Blackburn and Johnson [3] referred to our selected references for the CsOHg) and CsI(g) molecules.

Difference as observed in third laws between the present work and the previous Blackburn and Johnson one comes mainly from the set of fragment ions choice, our choice is in favor of increasing $Cs_2IOH(g)$ partial pressure. Considering the observed trends in third law results, we propose to retain the mean value of the three experiments labeled 01, 02 and 04s. Experiment labeled 03s has been discarded because of the encountered problems during temperature increase (see part IV-3-2): The standard enthalpy of reaction is thus equal to: $\Delta_rH°_{298.15}$ = - 172 ± 12.0 (kJ.mol^{-1}). The rather large uncertainty takes into account: -(i) the assumption of compensation of the errors (standard deviation) $\sqrt{((3^2+4.8^2+2.1^2)/3)}$= ± 3.5

kJ.mol^{-1}, -(ii) the difficulties in deconvolution of the fragment ions origin, -(iii) the uncertainty in $Cs_2IOH(g)$ free energy functions calculations and which can be evaluated from the mean value of pure dimmers at 1000 K to be about ± 5 kJ.mol^{-1} ($\delta fef(Cs_2I_2)$+ $\delta fef(Cs_2O_2H_2)/2$). The total uncertainty can be estimated to ± 12 kJ.mol^{-1}. From our selected values for the formation enthalpies of CsI(g) (-153.27 ± 4.2 kJ.mol^{-1}) and CsOH(g) (-252.7 ± 4 kJ.mol^{-1}) , we propose the following standard formation enthalpy for the $Cs_2IOH(g)$ molecule:

$$\mathbf{\Delta_f H°_{298.15} = -577.97 \pm 13\ (kJ.mol^{-1})}$$

The uncertainty is calculated with the assumption of errors compensation $\sqrt{(4.2^2+4^2+12^2)} = \pm$ 13 kJ.mol^{-1}

IV.6. CONCLUSION AND PERSPECTIVES

The present mass spectrometric work contributed to detection of new gaseous molecules in the mixed gaseous phase of the CsOH-CsI system. Results show the presence of one mixed molecule $Cs_2IOH(g)$ that contributes to excess ions in the ionization of gaseous phase molecules in equilibrium over {CsOH-CsI} mixtures. The present work confirms the proposed Blackburn and Johnson mixed molecule.

The whole ionization pattern of this molecule has been analyzed using a set of different compositions for the vaporizing condensed phase combined with earlier selection of the dimmerization constants for the pure dimmers $Cs_2O_2H_2(g)$ and $Cs_2I_2(g)$ in the gas phase. This analysis revealed that five fragment ions are produced in the ionization process: Cs_2OH^+, Cs_2I^+, Cs^+, $CsOH^+$, and CsI^+. Due to other ion contributions coming from either the monomers or the pure dimmers, four of these ions can be measured altogether at the same time in the gas phase, depending on the condensed phase composition. This new feature leads to increase the partial pressures of the $Cs_2IOH(g)$ molecule in equilibrium with the mixed condensed phase {CsOH-CsI} as proposed earlier by Blackburn and Johnson [3].

Second and third law analysis of the gas phase reaction $CsOH(g) + CsI(g) = Cs_2IOH(g)$ were performed on the basis of Knudsen cell mass loss calibration of the mass spectrometer and using estimates of the free energy function for the $Cs_2IOH(g)$ molecule based on the ionic

bond modeling proposed by Pauling [16, 17]. Standard formation enthalpy of the $Cs_2IOH(g)$ molecule is proposed to be: $\Delta_f H°_{298.15}$= -577.97 ± 13 (kJ.mol^{-1}).

Finally, the following data are proposed for the mixed molecule $Cs_2IOH(g)$

Cs_2IOH (g)	**Proposed Data**
$Cp°_{298.15}(g)$ (J.K^{-1}.mol^{-1})	1.0021 10^2 – 2.6989 10^{-3}T + 3.3782 10^{-6}T^2 -3.5238 10^5T^{-2} (298.15-1100 K)
	94.2117 + 7.5428 10^{-3}T – 1.2156 10^{-6}T^2 - (1100-2500 K)
	96.4175 + 5.4823 10^{-3}T – 7.4433 10^{-7}T^2 - (2500-3000 K)
H(T)-H(0) (J.mol^{-1})	23074.94
$S°_{298.15}$ (J.K^{-1}mol^{-1})	405.73
$Gef°_{298.15}$ (J.K^{-1}mol^{-1})	455.47 at 1000 K
$\Delta_f H°_{298.15}$ (kJ.mol^{-1})	-577.97 ± 13

Table IV-8: Retained thermodynamic data of $Cs_2IOH(g)$

REFERENCES

[1] R.F.Porter and W.P.Sholette, "Stabilities of Gaseous Boroxine and Its Fluoro Derivatives," J. Chem. Phys., Vol. 37, 1962, pp. 198-199.

[2] R.C.Schonnmaker and R.F.Porter, "Mass Spectrometric Study of High Temperature Reactions of $H_2O(g)$ and HCl(g) with Na_2O and Li2O[1a,b] " J. Phys. Chem, Vol. 64, 1960, pp. 457-461.

[3] P.E.Blackburn and C.E.Johnson, "Mass Spectrometry Studies of Fission Product Behavior. II- Gas phase species in the CsI-CsOH system," J. Nucl. Mater., Vol. 154, 1988, pp. 74-82.

[4] R.I.Reed, "Ion Production by Electron Impact", Academic Press, New York, 1962, 242 p.

[5] F.Z.Roki, M.N.Ohnet, C.Chatillon, and D.Jacquemain, "Thermodynamic study of the CsOH(s,l) vaporization by high temperature mass spectrometry," J. Chem. Thermodyn., Vol. 40, 2008, pp. 401-416.

[6] R.Viswanathan and K.Hilpert, "Mass Spectrometric Study of the Vaporization of Cesium Iodide and Thermochemistry of (CsI)2(g) and (CsI)3(g)," J. Phys. Chem., Vol. 88, 1984, pp. 125-131.

[7] J.C.Slater, "Introduction to ChemicalPhysics", McGraw-Hill Book Company, 1963, 521 p.

[8] M.Heyrman, G.Brethomé, A.Pisch, and C.Chatillon, "Thermodynamics of the Al-C-O Ternary system. II. High-Temperature Mass Spectrometric Study of the Vaporization of the Alumina-Graphite System," J. Elect. Soc., Vol. 153 (10), 2006, pp. J107-J115.

[9] I.Prigogine, R.Defay, and D.H.Everett, "Chemical Thermodynamics, Chapt. XXVIII & XXIX", Longmans, London, 1965.

[10] M.W.Chase, J., "NIST-JANAF Thermochemical Tables", Fourth Edition, J. Phys. Chem. Ref. Data, Part II, 1998, pp. 977-996.

[11] L.Lelik, G.Sajo, K.Vass-Balthazar, and O.Kaposi, "High Temperature Mass Spectroscopic Investigation of The Formation of Homo and Heterocomplexes in The Equilibrium Vapour Over Sodium Iodide and Ceasium Iodide," J.Acta Chimica Hungarica, Vol. 113 (1), 1983, pp. 61-74.

[12] J.Drowart, C.Chatillon, J. Hastie, and D. Bonnell, "High-Temperature Mass Spectrometry: Instrumental Techniques, Ionisation Cross-Sections, Pressure Measurements, and Thermodynamic Data," J. Pure Appl. Chem., Vol. 77, 2005, pp. 683-737.

[13] J.L.Margrave, "The characterization of high temperature vapors", Chapter 13, John Wiley & sons, New York, 1967, pp. 359-424.

[14] M.W.Chase, J., "NIST-JANAF Thermochemical Tables", Fourth Edition, J. Phys. Chem. Ref. Data, Part I, 1998, 957 p.

[15] G.Herzberg, "Molecular Spectra and Molecular Structure. II: Infrared and Raman Spectra of Polyatomic Molecules", Chapter II, D. Van Nostrand Company New York, 1960.

[16] L.Pauling, "The Nature of The Chemical Bond and The Structure of Molecules and Crystals, Chapt. 13", ed. 3, Cornel University Press, New York, 1960, pp. 504-562.

[17] L.Pauling, "A Simple Theoretical Treatment of Alkali Halide Gas Molecules", in Proc. National Academy of Sciences India, 1956, California Institute of Technology, pp. 1-19.

[18] T.A.Milne and D.Cubicciotti, "Calculation of the Energies of Gaseous Alkali Halide Dimer Molecules," J. Chem. Phys., Vol. 29 (N°4), 1958, pp. 846-851.

[19] V.P.Glushko, L.V.Gurvich, G.A.Bergman, I.V.Veits, V.A.Medvedev, G.A.Khachakuruzov, and V.S.Yungman, "Thermodynamics of Individual Substances", Part 2, Vol. IV, Nauka, Moscow, 1982, pp. 492-495.

[20] R.C.Feber, "Thermodynamic data for selected Gas Impurities in the Primary coolant of High-Temperature Gas-Cooled Reactors", Los Alamos Scientific Laboratory, LA-NUREG, N° 6635, 1977, 1977, New Mexico 87545, 26 p.

[21] K.S.Krasnov, V.G.Solomonik, and E.V.Morozov, "Thermodynamic Functions and The Molecular Parameters of Rhumbic Dimer Molecules of Alkali Metal Halides," Teplofiz. Vys. Temp. (Engl. Transl.) Vol. 10, 1972, pp. 682-686.

[22] R.D.Shannon, "Revised Effective Ionic Radii and Systematic Studies of Interatomic Distances in Halides and Chalcogenides," Acta. Cryst., Vol. A32, 1976, pp. 751-767.

[23] L.V.Gurvich, L.N.Gorokhov, G.A.Bergman, V.S.Iorish, V.Ya.Leonidov, and V.S.Yungman, "Thermodynamic Properties of Alkali Metal Hydroxides

Part II. Potassium, Rubidium, and Cesium Hydroxides," J. Phys. Chem. Ref. Data, Vol. 26 (4), 1997, pp. 1031-1109.

[24] J.O.Hirschfelder, "Simple Method for Calculating Moment of Inertia," J. Chem. Phys., Vol. 8, 1940, pp. 431.

[25] V.P.Glushko, L.V.Gurvich, G.A.Bergman, I.V.Veits, V.A.Medvedev, G.A.Khachakuruzov, and V.S.Yungman, "Thermodynamics of Individual Substances", Part 2, Vol. IV, Nauka, Moscow, 1982, pp. 473.

APPENDIX IV-A

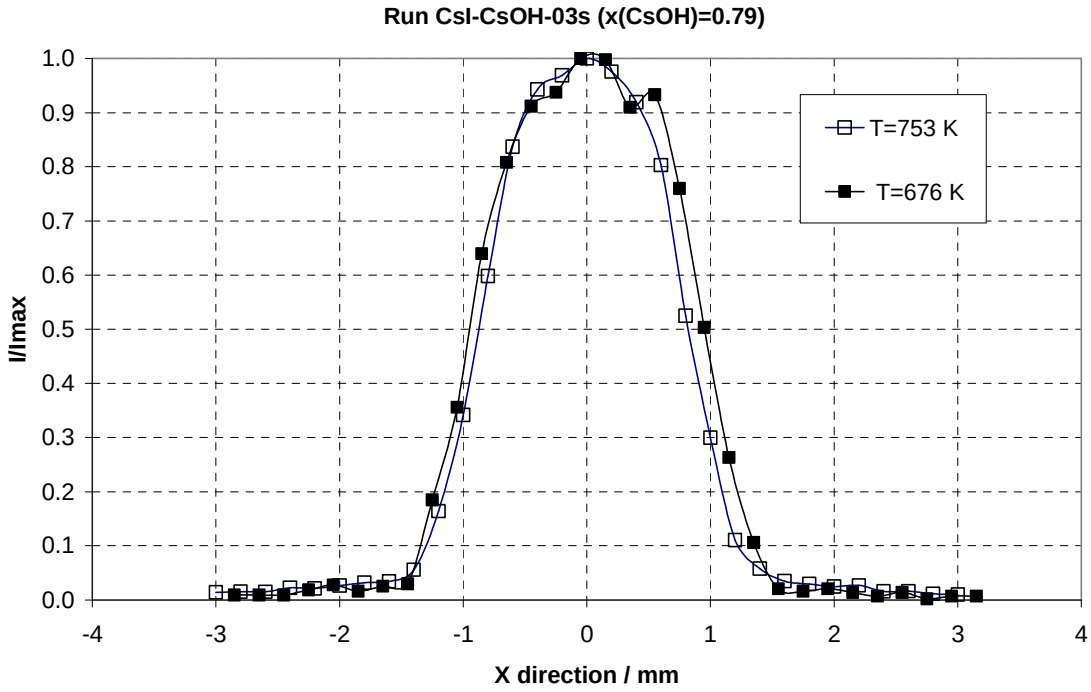

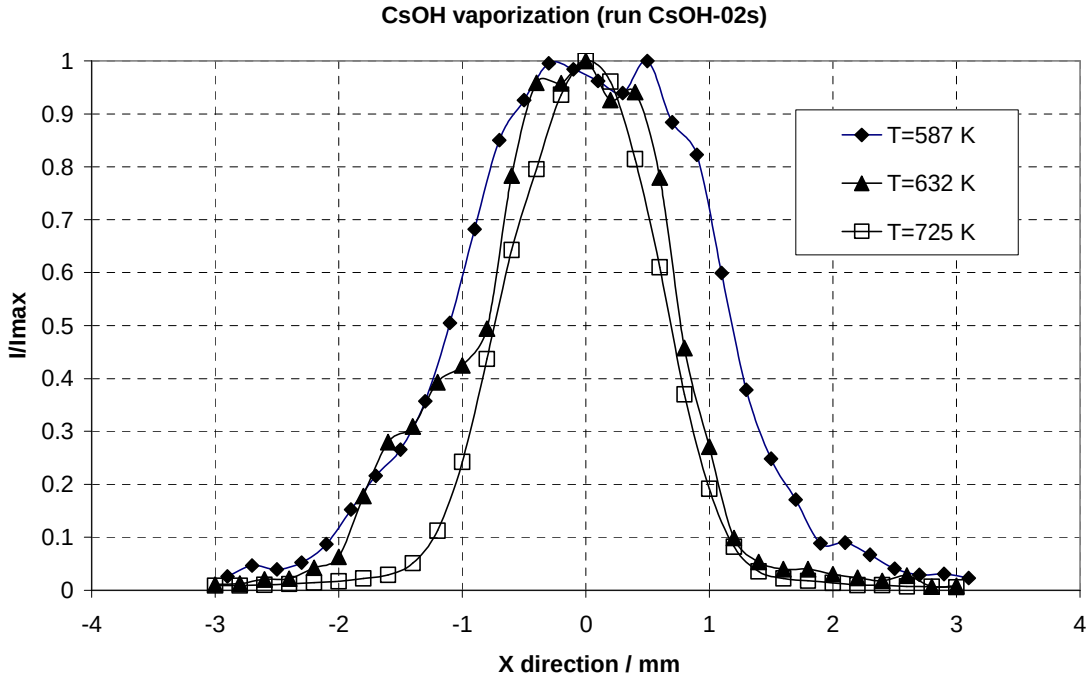

Figure IV-A1: Normalized registration of Cs^+ ion intensity during scanning of the position of the effusion orifice of the Nickel cell containing: (a) CsOH-CsI mixture (0.79% CsOH molar fraction), (b) CsOH pure sample vaporization (chapter II).

APPENDIX IV-B

Table IV-B1. Sample composition before and after each run as deduced from mass loss of the sample(crucible+lid+sample) and according to different assumptions for the ions issued from the $Cs_2IOH(g)$ molecule.

Run label	**Sample CsI-CsOH (mixed molecule not taken into account)**							
	Initial mass/g		**Initial composition/ mol %**		**Mass loss/g**		**Final composition/ mol %**	
	CsOH	CsI	CsOH	CsI	CsOH	CsI	CsOH	CsI
CsI-CsOH-01s	0.3068	2.5956	17.0	83.0	0.0610	0.1180	14.7	85.3
CsI-CsOH-02s	0.2463	2.4776	14.7	85.3	0.0673	0.3977	13.0	87.0
CsI-CsOH-03s	3.4990	1.6197	79.0	21.0	0.4394	0.0156	76.8	23.2
CsI-CsOH-04s	3.0590	1.6041	76.8	23.2	0.6868	0.0322	72.3	27.7
Run label	**Sample CsI-CsOH (Cs_2IOH= Cs_2OH^+ or Cs_2I^+)**							
	Initial mass/g		**Initial composition/ mol %**		**Mass loss/g**		**Final composition/ mol %**	
	CsOH	CsI	CsOH	CsI	CsOH	CsI	CsOH	CsI
CsI-CsOH-01s	0.3068	2.5956	17.0	83.0	0.0558	0.1180	14.9	85.1
CsI-CsOH-02s	0.2510	2.4770	14.9	85.1	0.0670	0.3977	13.3	86.7
CsI-CsOH-03s	3.4990	1.6197	79.0	21.0	0.4394	0.0145	76.8	23.2
CsI-CsOH-04s	3.0596	1.6052	76.8	23.2	0.6867	0.0291	72.3	27.7
Run label	**Sample CsI-CsOH (Cs_2IOH = Cs_2OH^+ + Cs^+ or Cs_2I^+ + Cs^+)**							
	Initial mass/g		**Initial composition/ mol %**		**Mass loss/g**		**Final composition/ mol %**	
	CsOH	CsI	CsOH	CsI	CsOH	CsI	CsOH	CsI
CsI-CsOH-01s	0.3068	2.5956	17.0	83.0	0.0510	0.1080	15.1	84.9
CsI-CsOH-02s	0.2558	2.4877	15.1	84.9	0.0667	0.3962	13.5	86.5
CsI-CsOH-03s	3.4990	1.6197	79.0	21.0	0.4050	0.0133	77.0	23.0
CsI-CsOH-04s	3.0940	1.6064	77.0	23.0	0.5730	0.0243	73.4	26.6
Run label	**Sample CsI-CsOH (Cs_2IOH = Cs_2OH^+ + Cs^+ + CsI^+ or Cs_2I^+ + Cs^+ + $CsOH^+$)**							
	Initial mass/g		**Initial composition/ mol %**		**Mass loss/g**		**Final composition/ mol %**	
	CsOH	CsI	CsOH	CsI	CsOH	CsI	CsOH	CsI
CsI-CsOH-01s	0.3068	2.5956	17.0	83.0	0.0573	0.0395	14.5	85.5
CsI-CsOH-02s	0.2494	2.5561	14.5	85.5	0.1158	0.2830	9.2	90.8
CsI-CsOH-03s	3.4990	1.6197	79.0	21.0	0.3270	0.0145	77.4	22.6
CsI-CsOH-04s	3.1720	1.6052	77.4	22.6	0.4242	0.0263	75.1	24.9

APPENDIX IV-C

Second and third law calculations performed with different assumptions for the ions produced by the molecule $Cs_2IOH(g)$ when analyzing the reaction

$CsI(g) + CsOH(g) = Cs_2IOH(g)$

Table IV-C1: Second and third law enthalpy calculations for the reaction $CsOH(g) + CsI(g) = Cs_2IOH(g)$ from the only $\{Cs_2OH^+ + Cs_2I^+\}$ ionic intensities summation as measured coming from the $Cs_2IOH(g)$ molecule.

Run label	Temperature range K	$\Delta_r H°_{298\ K}$ / (kJ.mole^{-1})	
		2nd law	3rd law
CsI-CsOH-01s	699-809	-109.5 ± 21.5	-145.4 ± 3.0
CsI-CsOH-02s	657-863	-127.4 ± 2.5	-151.6 ± 2.1
CsI-CsOH-03s	676-753	-88.1 ± 9.7	-133.5 ± 2.5
CsI-CsOH-04s	666-804	-64.8 ± 11.4	-135.2 ± 4.4

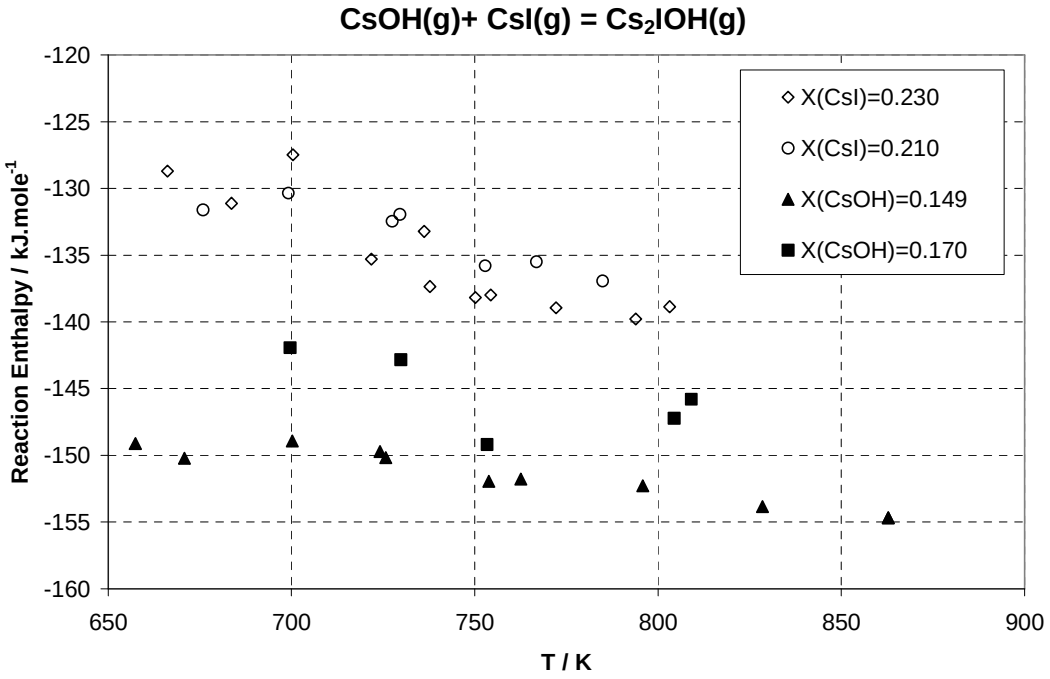

Figure IV-C1: Third law enthalpy calculations for the reaction $CsOH(g) + CsI(g) = Cs_2IOH(g)$ from the only $\{Cs_2OH^+ + Cs_2I^+\}$ ionic intensities summation as measured coming from the $Cs_2IOH(g)$ molecule as a function of the temperature.

Table IV-C2: Second and third law enthalpy calculations for the reaction CsOH(g) + CsI(g) = $Cs_2IOH(g)$ from the only {Cs_2OH^+ + Cs_2I^+ + Cs^+} ionic intensities summation as measured coming from the $Cs_2IOH(g)$ molecule.

Run label	Temperature range K	$\Delta_r H°_{298\,K}$/ (kJ.mol^{-1})	
		2nd law	3rd law
CsI-CsOH-01s	699-809	-104.7 ± 30.4	-155.3 ± 4.4
CsI-CsOH-02s	657-863	-137.2 ± 5.0	-163.7 ± 2.5
CsI-CsOH-03s	676-753	-46.1 ± 48.5	-152.4 ± 7.9
CsI-CsOH-04s	666-804	-116.4 ± 35.0	-161.2 ± 6.6

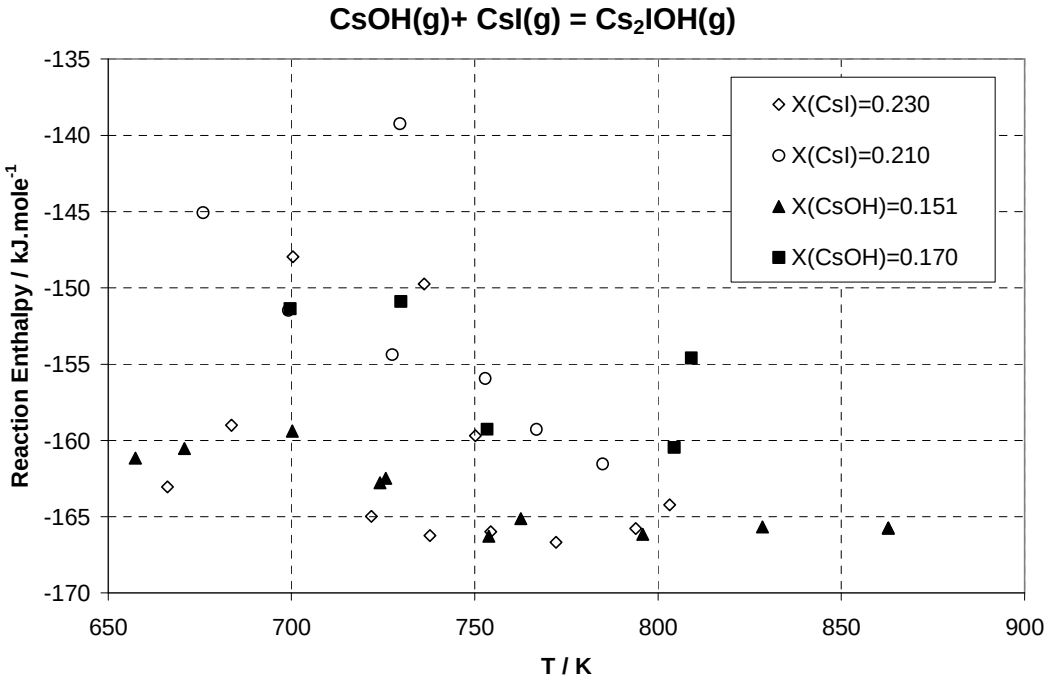

Figure IV-C2: Third law enthalpy calculations for the reaction CsOH(g) + CsI(g) = $Cs_2IOH(g)$ from the only {Cs_2OH^+ + Cs_2I^+ + Cs^+} ionic intensities summation as measured coming from the $Cs_2IOH(g)$ molecule as a function of temperature.

Table IV-C3: Vapor pressures of gaseous species in equilibrium as measured taking into account the total ionization processes for each gaseous species. For the molecule $Cs_2IOH(g)$ the total ionic intensity is the summation of the {Cs_2OH^+ + Cs_2I^+ + Cs^+ + $CsOH^+$ or CsI^+} ionic intensities determined after discarding other contributions.

Run: CsI-CsOH-01s

T/K	p CsOH(g) /bar	p CsI(g) /bar	p Cs_2IOH /bar	RT Ln Kp	Δfef / $J.K^{-1}.mol^{-1}$	$\Delta_rH°_{298}$ /$kJ.mol^{-1}$
699.65	1.606E-06	2.208E-07	4.305E-07	8.150E+04	-123.605	-167.976
753.40	7.783E-06	1.916E-06	5.033E-06	7.974E+04	-122.980	-172.390
729.83	3.666E-06	8.469E-07	1.551E-06	7.962E+04	-123.254	-169.578
809.08	2.766E-05	1.580E-05	3.124E-05	7.519E+04	-122.348	-174.183
804.45	2.503E-05	1.295E-05	3.253E-05	7.703E+04	-122.399	-175.495

Run: CsI-CsOH-02s

T/K	p CsOH(g) /bar	p CsI(g) /bar	p Cs_2IOH /bar	RT Ln Kp	Δfef / $J.K^{-1}.mol^{-1}$	$\Delta_rH°_{298}$ /$kJ.mole^{-1}$
700.28	1.405E-06	4.621E-07	8.123E-07	8.175E+04	-123.597	-168.298
657.42	4.397E-07	6.848E-08	1.669E-07	8.488E+04	-124.085	-166.451
670.78	5.049E-07	1.965E-07	4.093E-07	8.496E+04	-123.935	-168.089
724.12	2.542E-06	1.198E-06	2.134E-06	8.104E+04	-123.320	-170.334
725.72	2.184E-06	1.118E-06	1.949E-06	8.200E+04	-123.302	-171.482
753.83	4.978E-06	3.386E-06	6.669E-06	8.078E+04	-122.975	-173.482
795.82	1.244E-05	1.612E-05	2.945E-05	7.872E+04	-122.496	-176.206
828.53	2.320E-05	3.579E-05	5.655E-05	7.666E+04	-122.136	-177.858
862.87	4.330E-05	9.293E-05	1.353E-04	7.478E+04	-121.777	-179.856
862.85	4.326E-05	9.293E-05	1.353E-04	7.478E+04	-121.777	-179.859
762.60	5.980E-06	4.811E-06	8.857E-06	8.013E+04	-122.874	-173.832

Run: CsI-CsOH-03s

T/K	p CsOH(g) /bar	p CsI(g) /bar	p Cs_2IOH /bar	RT Ln Kp	Δfef / $J.K^{-1}.mol^{-1}$	$\Delta_rH°_{298}$ /$kJ.mole^{-1}$
675.87	6.375E-06	8.013E-08	7.841E-07	8.004E+04	-123.878	-163.769
699.18	1.252E-05	2.674E-07	1.940E-06	7.714E+04	-123.610	-163.567
727.50	2.424E-05	7.215E-07	4.252E-06	7.502E+04	-123.281	-164.702
752.85	4.166E-05	1.237E-06	5.195E-06	7.211E+04	-122.986	-164.705
784.90	8.262E-05	3.856E-06	2.107E-05	7.243E+04	-122.619	-168.678
766.85	5.707E-05	2.238E-06	1.252E-05	7.328E+04	-122.825	-167.463
729.60	2.510E-05	6.697E-07	3.387E-06	7.409E+04	-123.256	-164.018

Run: CsI-CsOH-04s

T/K	p CsOH(g) /bar	p CsI(g) /bar	p Cs_2IOH /bar	RT Ln Kp	Δfef / $J.K^{-1}.mol^{-1}$	$\Delta_rH°_{298}$ /$kJ.mole^{-1}$
666.15	2.249E-06	4.484E-08	8.727E-07	8.847E+04	-123.987	-171.066

683.67	5.340E-06	7.034E-08	1.142E-06	8.485E+04	-123.789	-169.482
700.37	9.902E-06	2.363E-07	2.641E-06	8.115E+04	-123.596	-167.717
721.80	1.896E-05	3.355E-07	7.749E-06	8.410E+04	-123.347	-173.129
736.23	2.919E-05	1.088E-06	8.134E-06	7.623E+04	-123.179	-166.922
750.22	3.717E-05	1.376E-06	1.316E-05	7.771E+04	-123.017	-169.996
754.37	4.872E-05	1.668E-06	2.645E-05	7.961E+04	-122.969	-172.376
772.18	8.031E-05	3.206E-06	4.808E-05	7.793E+04	-122.763	-172.723
793.92	1.428E-04	6.883E-06	8.296E-05	7.488E+04	-122.517	-172.145
803.20	1.905E-04	9.261E-06	9.846E-05	7.299E+04	-122.413	-171.312
737.80	2.977E-05	8.833E-07	1.594E-05	8.168E+04	-123.161	-172.548

Table IV-C4: Second and third law enthalpy calculations for the reaction CsOH(g) + CsI(g) = $Cs_2IOH(g)$ from the whole set of {Cs_2OH^+ + Cs_2I^+ + Cs^+ + $CsOH^+$ or CsI^+} ionic intensities summation as measured coming from the $Cs_2IOH(g)$ molecule after discarding other contributions.

Run label	Temperature range K	$\Delta_rH°_{298\ K}$/ (kJ.mol^{-1})	
		2nd law	3rd law
CsI-CsOH-01s	699-809	-119.6 ± 6.7	-171.9 ± 3.0
CsI-CsOH-02s	657-863	-119.9 ± 2.0	-173.2 ± 4.8
CsI-CsOH-03s	676-753	-130.7 ± 8.7	-165.3 ± 2.0
CsI-CsOH-04s	666-804	-155.5 ± 11.1	-170.9 ± 2.1

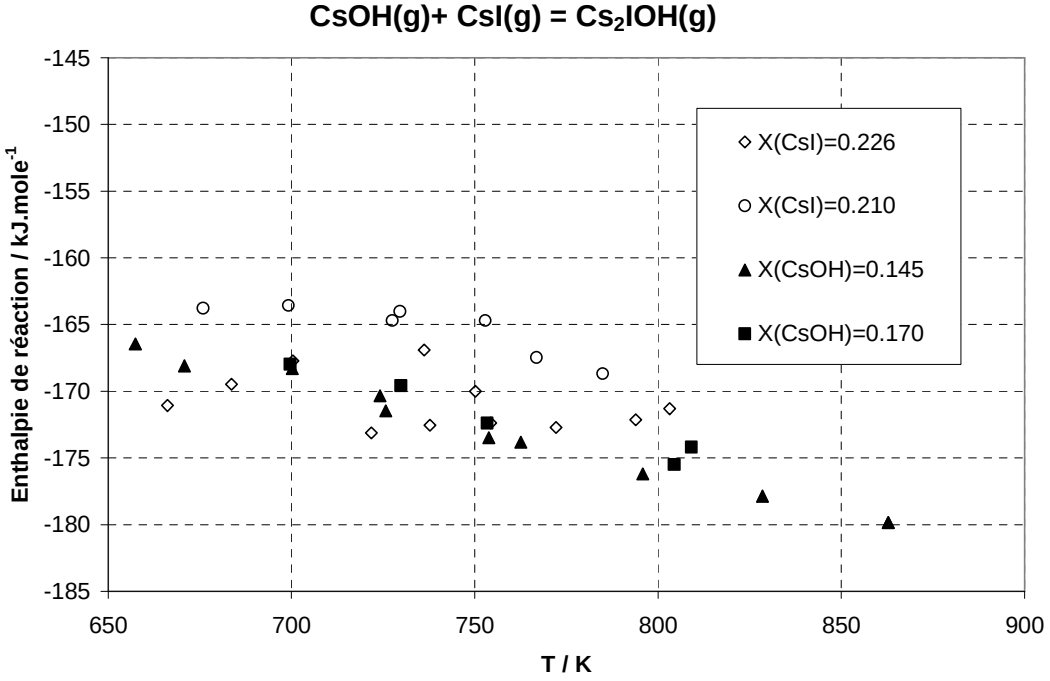

Figure IV-C3: Third law enthalpy calculations for the reaction CsOH(g) + CsI(g) = $Cs_2IOH(g)$ from the whole {Cs_2OH^+ + Cs_2I^+ + Cs^+ + $CsOH^+$ or CsI^+ } ionic intensities summation as measured coming from the $Cs_2IOH(g)$ molecule as a function of temperature.

Table IV-C5: Second and third law enthalpy calculations for the reaction CsOH(g) + CsI(g) = $Cs_2IOH(g)$ from the only {Cs_2OH^+} ionic intensities as measured by Blackburn and Johnson coming from the $Cs_2IOH(g)$ molecule. The free energy function used in the calculations is the one selected in this work (for corrected values, see text).

Blackburn & Johnson	Temperature range K	$\Delta_rH°_{298\ K}$/ (kJ.mol^{-1})	
		2nd law	3rd law
Original data	809-927	- 151.5 ± 7.5	-151.7 ± 1.0
$Cs_2O_2H_2(g)$ corr		- 94.1 ± 7.3	-144.9 ± 1.8
CsOH(g) corr		- 94.0 ± 7.3	-162.2± 2.4

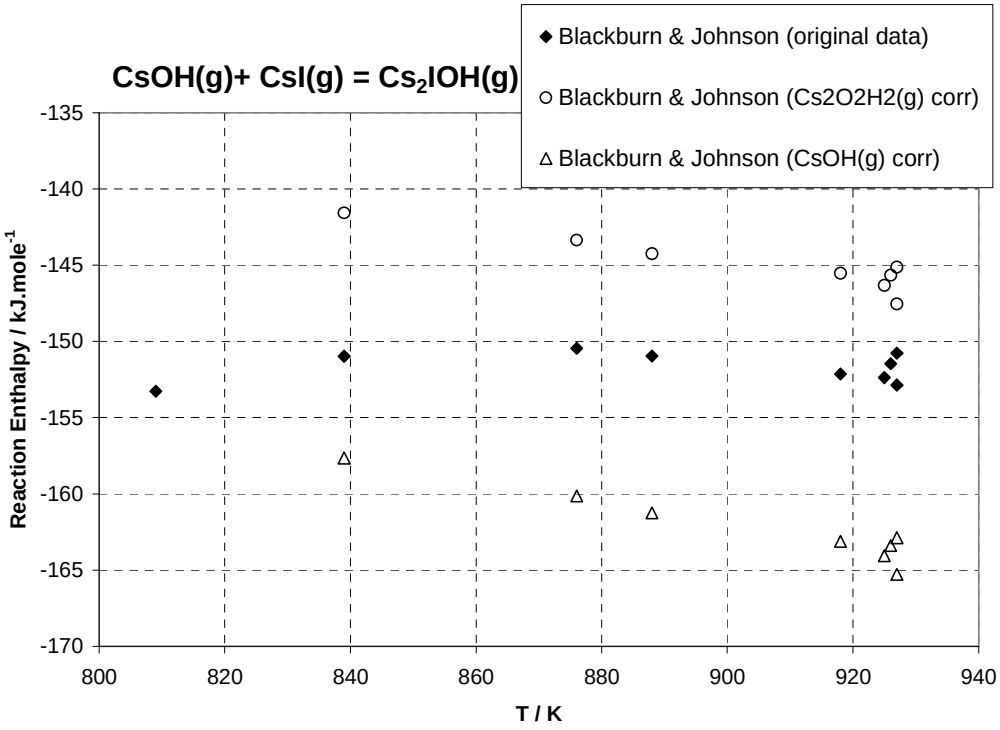

Figure IV-C4: Blackburn and Johnson third law enthalpy calculations for the reaction CsOH(g) + CsI(g) = $Cs_2IOH(g)$ from the only Cs_2OH^+ ionic intensities as measured coming from the $Cs_2IOH(g)$ molecule as a function of temperature. Calculations are performed with our selected free energy function for the $Cs_2IOH(g)$ molecule.

CHAPTER V

BUILDING AND TESTING THE CHIP THERMO-KINETIC REACTOR

V.1. INTRODUCTION

The iodine at the exhaust of the nuclear reactor's core under severe accident is in principle in a dissociated state due to temperature effect before introduction into the primary coolant circuit where a break can occur. The "dissociated" state corresponds to temperature range 1800-2300 K and pressures about 2 to 80 bar depending on the type of the accident. Breaks at the hot leg occur between 1000 and 1300 K approximately. Till now two different approaches were used to understand or simulate the iodine transport - (I) either experiments of transport under conditions of pressure and temperature close to those of the break (high temperature), - (II) or thermodynamic calculations. This last approach is supposed to give – for conditions where all the chemical species would be known – all the molecules responsible for iodine transport especially by association with other components. The transport experiments - provided with adequate detectors when possible - give quantitative assessments of iodine transport in vapour or aerosol form but do not inform about the mechanisms. Important differences between thermodynamic calculations and transport experiments lead to many important questions about the chemical kinetics role in the primary cooling circuit especially during the short transient time - about one to some 10 s.

In parallel with a noticeable improvement of the basic thermodynamic data of the molecules and solutions in the system {Cs-I-O-H}, it was decided to test the behaviour of the gaseous molecules (vapours) under conditions as close as possible to those at the hot leg break. The most universal detector of vapour pressures being a mass spectrometer coupled to an effusion cell, we chose to build a complex reactor called the "CHIP Thermokinetic reactor" reproducing some chemical steps close to those of the break and ending with an effusive stage corresponding to conditions close to the break at high temperature. This effusive stage is the one analysed by the mass spectrometer. The CHIP reactor will have to be flexible in term of geometry, temperature as well as flow capabilities for different gaseous species. It is important that the CHIP reactor could warranty both the conditions close to equilibrium and after modifications, the conditions of kinetic studies far-away from equilibrium.

Molecules and vapours corresponding to the complex systems resulting from the severe nuclear accident – such as {Cs-I-O-H} system (first simplified studied system)- are for one part condensable vapours (CsOH, $Cs_2O_2H_2$, CsI, Cs_2I_2, etc…) which in principle are easily analyzed by using a suitable effusion cell, but for another part gases (H_2) or high volatile

vapours (H_2O, HI, I_2, I, HIO…) which are difficult to analyze. This feature explains the few numbers – or the lack - of mass spectrometric studies of this kind of volatile molecules. The mass spectrometer of SIMaP/CNRS (French National Scientific Research Center in Grenoble) was selected to be associated to the CHIP reactor for the following reasons:

- A great sensitivity of detection - dynamic range of 10^6-10^7 depending on the observed species nature.
- A high resolution - about 800% to 10% valley - to separate almost and completely all the observed species.
- The ionization chamber is cooled by direct contact with liquid-nitrogen to prevent any re-vaporization of molecular high volatile gaseous species that have entered into the ionization chamber for analysis [1].
- An accurate 2D-positioning system of the effusion cells (effusion orifice) (accuracy ± 0,05 mm) which is independent of the reactor [2]
- A sampling system of the molecular beam sampling called “restricted collimation” which discards definitively any surface contributions (re - evaporation, surface diffusion phenomenon, …) [3].
- A shutter of the molecular beam which is reliable not only for condensable vapours but also for the detection of “permanent” gases (H_2, Ar…) and for high volatile vapours (HI, I_2, H_2O…) [3].
- Reactor’s and “ions source” housings are well insulated and equipped of large pumping capacities, respectively 1300 and 800 l/s which correspond to 900 and 450 l/s in the location where the molecules are produced and ionized.

The practice since 1968 of thermodynamic studies on “difficult” gaseous phases as well as the development of precise differential measurements of partial pressures using a multiple effusion cells were a determining factor to associate a specific reactor to this mass spectrometer [4] rather than installing a mass spectrometer on a reactor built separately.

V.2. CONSTRUCTION OF THE CHIP REACTOR: PRELIMINARY CONDITIONS

A description of the CHIP 4-stages thermo-kinetic reactor was given in Chapter I. The complementary study presented in this report based on flow calculations was pursued to determine the working conditions of the CHIP reactor in terms of input pressures and flows and to be able to calibrate the HTMS in each experiment using the carrier gas.

V.2.1. Molecule sources

We were forced to use an independent injection line by element with a neutral carrying gas (Argon) to impose no beforehand reactions between elements in a dissociated form and to control the quantity of each element of the studied system (iodine, cesium, H_2/H_2O ratio). Each line was provided with a suitable source. The dissociation of the elements and their mixing will be obtained by a rise of temperature - part which we describe as cracking cell (or cracker). To be closen to severe accident conditions, this part of the reactor must be common to all the elements. Thus, the various selected sources which converge towards the cracking cell are:

- For iodine: a flow of Argon on crystal bed of iodine immersed in a thermostated bath (regulated from 253 to 400 K) and outside of the mass spectrometer.
- For cesium: a flow of Argon on a liquid bath of CsOH(l). The presence of excess water in the accidental vapours conditions makes low probability to find Cs(g) dissociated from other molecules different than CsOH (g) or CsI (g). We chose to use the CsOH vapour as source of Cesium. The first stage of CHIP reactor will consist of the vaporization of CsOH (l), between 800 and 1000 K under Argon flow.
- For H_2 and H_2O: an Argon flow more or less rich in H_2 (up to 100%) and which can be supplied with H_2O vapour by a micro pump coupled to an evaporator (Bronkhorst system). This system is placed outside the mass spectrometer.

The different gas input lines are heated at 430 K up to the reactor and can be pumped under for vacuum (0.5 bar) in order to avoid any iodine or H_2O condensation.

V.2.2. Gas flow and vapours conditions in CHIP reactor

At the reactor's exhaust, effusion flows correspond to molecular flow conditions i.e. $\approx 10^{-4}$ bar maximum for millimetric orifices (standard diameter = 2 mm in our case). This corresponds in the upstream of the reactor (for only one gas line) to a flow of 0.1 to 1 Ncm^3.mn (N for normal conditions, *i.e. 298 K and 1 bar).* Such a flow is in extreme cases even lower than those for usual working of flowmeters under atmospheric inlet pressure. In the absence of lost derived flows, it will be necessary to consider lines with reduced pressure inferior to 1 bar (1 to 600 mbar as we will calculate further). These lines can be considered only if welded materials or tight bounded parts with gaskets are used. So, the stages called "high pressure" will have to be limited to temperatures and compatible materials to warranty no leaks.

The pressure change, *i.e.* going from high pressure to low pressure - in the absence of capillary solutions as used in catalysis chemistry for less reactive gases like CO, CO_2, O_2 and H_2O - will have to be assumed by using small orifices or diaphragms (nozzles of 50 μm are the standard minimum available) as it is used in the flowmeters technology. The use of such orifices makes it possible to go from a viscous flow regime to a molecular regime. In this last case, the containers do not require any welded junction, but only rectified contact surfaces which ascertains a very small leakage rate. Consequently, it is possible to use refractory materials in the cracking zone.

The spectrometric measurement conditions in the last stage called "condenser" because it must be cooled to simulate the hot leg break temperature (1000-1300 K), require beginning the experiments with isothermal conditions - A quasi-identical temperatures of cracking and condenser cells-. The flow regime in the cracker and condenser zones being molecular and temperatures being high, these two stages will be built using identical or compatible refractory materials by stacking carefully the adjusted parts.

The gas and vapours circuits in the CHIP reactor are presented in figure V-1 where we define also the zones of expected temperatures. On the basis of this architecture, gas flows will be calculated in the following paragraph in order to obtain the ranges of upstream pressures, the knowledge of which must make it possible to control and know the value of related effusion flows. This value will be used for the mass spectrometer calibration based on the carrier gas (Argon). This kind of operation was often attempted but no calibration was published today. For this reason, we particularly studied the architecture and the design of the inlet gas lines,

which have never been described with accuracy in the case of effusion cells provided with gas introduction for solid – vapours interactions. We must also specify that such objective requires imperatively avoiding any parallel flow either because of leaks or lost by an additional pumping - as it is practiced with a capillary system - in order to carry all the introduced gas up to the final effusion orifice stage.

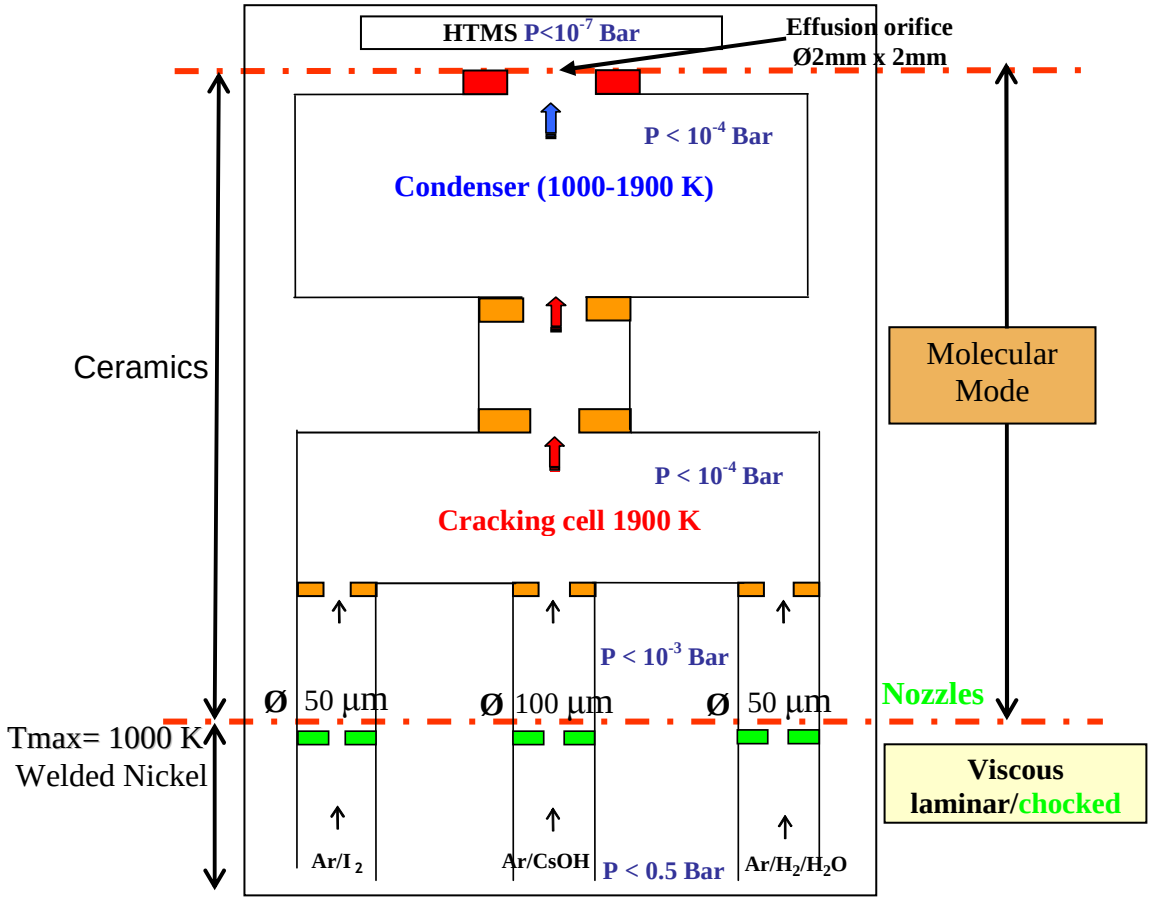

Figure V-1: Scheme of the flow-paths in the thermo-kinetic reactor CHIP

V.2.3. Choice of materials and corrosion conditions

The design of the lines was not only defined according to the laws governing the gas flow regime but also by taking into account the building capabilities and the available materials.

The "high pressure" sections have to assume a temperature range between 430 K and higher temperatures than the CsOH(l) source temperature i.e. 1000 K. We choose as pure Nickel material because this metal can be welded and keep interesting mechanical properties until

1300 K. Moreover, it is compatible chemically with CsOH and according to thermodynamics predictions, it should not have any reaction with iodine and it is not easily oxidized by the H_2/H_2O mixtures in the conditions of the CHIP study. The first two stages of the CHIP reactor including the 3 gas introduction pipes, the CsOH source and the injection nozzles are built with Nickel and were ascertained without vacuum leaks by Helium spectrometry. The two other stages of the reactor working under molecular vacuum – cracker cell and condenser - as well as their connections (tubes) are made of ceramics (dense and pure alumina 99.7%). If necessary, certain parts could be built with other ceramics more resistant to corrosion (Zirconium oxide, Hafnium oxide). Tantalum was eliminated because the oxygen potential of the H_2/H_2O mixtures would lead to the formation of oxides of Ta when temperature decreases in the condenser.

From the chemical or physicochemical reactivity point of view, we are faced to two major problems:

- For the high pressure lines, CsOH has an important wetability that we hope to limit by using a specific upper wall container design. Concerning iodine, the presence of a thin layer of metal iodides or iodide oxides on the walls can generate “transient flows” after storage effects.
- For low pressure and high temperature sections, the formation of iodide gases like AlI(g),…or iodide oxides like AlOI(g) by interactions with the material would be possible. In fact, such compounds exist for chlorides. These vapours will be analysed by mass spectrometry as well as those of the studied system. If their presence is limited to steady-state pressures, this will not affect the experiments, but requires taking them into account in the chemical balance. The measurement of non-steady-state pressures for such species would mean that the walls undergo a continuous attack by spallation.

V.3. CALCULATION OF GAS AND VAPOURS FLOW MODES IN THE CHIP REACTOR

V.3.1. Flow regimes

A gas flow in a tube is characterized by three regimes: molecular regime, transition regime, or viscous regime. To determine the flow regime in a tube we calculate the Knudsen number Kn as explained in Chapter I.

Starting from pressure of a rarefied gas and by increasing it, we can define the various regimes in the CHIP reactor with three modes: molecular one, viscous laminar or transition flow regime.

- ***Molecular mode***

For the low pressures corresponding to the cracking-condenser section, the flow regime is molecular and we will apply the Hertz-Knudsen relation for each orifice corrected by its Clausing coefficient (or probability of transmission) that characterizes the tubular section according to the method suggested by Santeler [5]. This regime is limited to a maximum pressure of about 10^{-4} bar for a diameter of 1 mm approximately. The flow is expressed in moles per second, and the length of the orifice is corrected to an equivalent length:

$$\frac{dN}{dt} = \frac{1}{1 + 3l_{eq}/8r} \times \frac{p\,s}{\sqrt{2\pi MRT}} \qquad (1)$$

$$\frac{l_{eq}}{l} = 1 + \frac{1}{3 + 3l/7r} \qquad (2)$$

dN/dt: molar flow in mole.s^{-1}, p: pressure in Pa, s: tube section in m^2, M: molar mass of the considered gaseous species in g.mole^{-1}, R: constant of inert gas, T: temperature in K, l_{eq}: equivalent length in m, l: tube length in m and r: tube radius in m.

The uncertainty in this relation proposed by Santeler is within 0.015 to 0.6 % for l/r ratios of 0.1 to 1000 with a maximum of 0.6 % corresponding to l/r = 6.

- ***Viscous flow regime***

For high pressures for a Knudsen number Kn > 80 the flow regime is viscous laminar. It can become turbulent when increasing the pressure. We checked according to ref. [6] that in the CHIP reactor case the turbulent flow was never reached due to small needed matter flows. The laminar viscous regime is defined by the Hagen-Poiseuille relation (in case of gases the relation is given by Henry [6]) but this relation is not correct when the exit of the tube (or nozzle) performs under vacuum because of chocked effect, known also as sonic mode - Instead of correcting the relation of Hagen-Poiseuille by using equivalent lengths for the tube, we preferred to use the method of Santeler [7] who shares the nozzle (or an unspecified tube) into laminar flow in the tube and a choked exit. When increasing the pressure, the flow becomes defined in a prevalent way by the choked flow at the exit: this feature is the usual operating mode of the flowmeters. Santeler considers two flow regimes across the tube with three pressures: p_0 upstream pressure (isotropic due to large volume), p_1 pressure at the end of the pipe just before the exit, and p_2 downstream pressure after the chock (isotropic conditions due to large volume). This relation is accurate in case there is no restriction of the vein gas at the tube entry. For this reason, Santeler proposes a corrective coefficient C_0 often slightly less than 1. Henry explains this coefficient by the slip of the molecules along the wall. In fact to avoid the constriction of the vein gas at the entry or a turbulent whirl, it is necessary to avoid right angles (i.e. to favour conical or round shape at the entry. What is done when machining the nozzles by electro-erosion is well-suited). So, the use of these relations and an adequate realization allow evaluating the gas flow within a few percents.

The flow in a small tube with an orifice at the exit can be presented as follows:

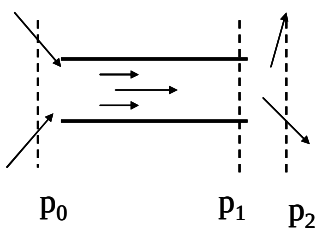

p_0 : upstream pressure (at the entry of the tube), p_1 : pressure at the end of the tube in the orifice section and p_2 : downward pressure towards the cracking cell ($p_2 << p_0, p_1$)

The flow at the orifice under chocked regime *i.e.* "sonic" is calculated according to the following relation:

$$F(volume) = \pi r^2 p_1 \left[\frac{\gamma RT}{M} \times \left(\frac{2}{\gamma+1} \right)^{\frac{\gamma+1}{\gamma-1}} \right]^{1/2} = Cp_1 \quad (3)$$

r: orifice radius; p_1: pressure at the exit of the orifice; $\gamma = C°_p/C°_v$: heat capacities ratio at constant pressure and volume; and C: constant for chocked regime.

The relation between the volume flow and molar flow is:

$$F(molar) = \frac{F(volume)}{RT} \quad (4)$$

The viscous laminar flow in a tube is calculated according to Hagen-Poiseuille relation:

$$F(conduit, volume) = \frac{\pi r^4}{16\eta l}\left(p_0^2 - p_1^2\right) = K\left(p_0^2 - p_1^2\right) \quad (5)$$

R and l are respectively the radius and the length of the tube (m), p_0 : upstream pressure (Pa), p_1 : pressure in the orifice (Pa), η : coefficient of viscosity of the gas versus function of temperature, K: constant for viscous regime.

The combination of the two equations (3 and 5) gives the viscous laminar choked flow:

$$F(volume) = \frac{C^2}{2K}\left[\left(1 + \left(\frac{2Kp_0}{C} \right)^2 \right)^{1/2} - 1 \right] \quad (6)$$

According to Santeler, the condition for chocked flow is that the downward pressure has to be small enough compared to the inward pressure:

$$\frac{p_2}{p_1} < \left[\frac{2}{(\gamma+1)} \right]^{\gamma/(\gamma-1)} \quad (7)$$

This limit depends on the gas nature via $\gamma = C°_p/C°_v$. The difference $C°_p$-$C°_v$ = R for any species and at each temperature.

For monoatomic species: $C°_v = 5/2\ R$ + Electronic contribution (depending on T). In this case, $\gamma = 5/3$. For diatomic or polyatomic gases, vibrational and electronic contributions are negligible when the vibration frequencies and the first electronic level are far enough from the ground state in comparison with the temperature. In this case $C°_v = 5/2\ R$ and $\gamma = 7/5$.
Thus, critical ratio p_2/p_1 is equal to 0.48 for monoatomic species, and 0.53 for polyatomic species.

- ***Transition flow regime***

For intermediate pressures, the regime is called transition and it is calculated with a combination of the two others - molecular and viscous laminar - using a percentage of each mode. For the attribution of the percentage, we used the relation of DeMuth and Watson [8] based on the Knudsen number because this relation has a physical meaning. For any tube (or nozzle), we will calculate the percentage on the basis of the average pressures in the tube ($(p_0+p_1)/2$). Indeed DeMuth and Watson proposed their relation based on experiments undertaken with pressure ratios (downstream/upstream) from 0.7 to 0.9 i.e. without chock effect, which corresponds to the inner pipe pressure ranges of the CHIP reactor (this condition is systematically checked during calculations). Moreover, the interpretation of DeMuth and Watson experiments was done in the central zone of transition for the simple reason that the limits of the transition zone are rather not well defined because the junctions to each regime are asymptotic. These limits, fixed here at 3 and 80, depend in fact on the authors who studied the transition.

$$F_{trans} = F_{mol} + (F_{vis} - F_{mol})(1 - C_a^{-Kn}) \quad or \quad F_{trans} = F_{mol} C_a^{-Kn} + F_{vis}(1 - C_a^{-Kn}) \qquad (8)$$

relation in which $C_a = 1.05$ and $Kn = 2r/\lambda$, F_{trans}: transition flow, F_{mol}: molecular flow, F_{vis}: viscous flow, C_a: experimental constant measured by DeMuth and Waston [8], Kn: Knudsen number, r: tube radius and λ: mean free path.

Molecular and laminar flows are calculated according to previous formulas, as if each mode operated alone in the pipe.

V.3.2. Calculation tests for the nozzles

The test of flows produced by different regimes was done with argon at 1100 K (functioning temperature for the nozzles). Calculations were carried out with an exit maintained under vacuum pressure sufficiently low to prevent any back flow. This ensures a maximum of flow that will be compared with the maximum acceptable in the effusion orifice for the mass spectrometer measurement. In this way, we ensure the operation of the nozzle at the exit in a choked mode, the unique mode which allows a non return of the molecules in the pipe. Real flow (fig. V-2) presented by dashed lines corresponds to calculation with transition flow equation which ensures a description of the whole range of pressures. With low input pressures, the flow is similar to the only flow in molecular regime meanwhile at higher pressures the flow joins that proposed by Santeler (laminar + chocked combination). In figure V-2, we observe also the difference between the Hagen-Poiseuille relation and the Santeler relation taking into account the chocked regime at the orifice. This difference increases with the diameter of the tube (fig. V-3). The calculated flows show the operating zones of the nozzles but do not give any information about the conditions related to the connecting tube with the cracking cell and the pressure at the entrance of the cracking cell which should not exceed the pressure of the molecular regime ≈ 10^{-4} bar. In the next chapter, we answered to this questioning.

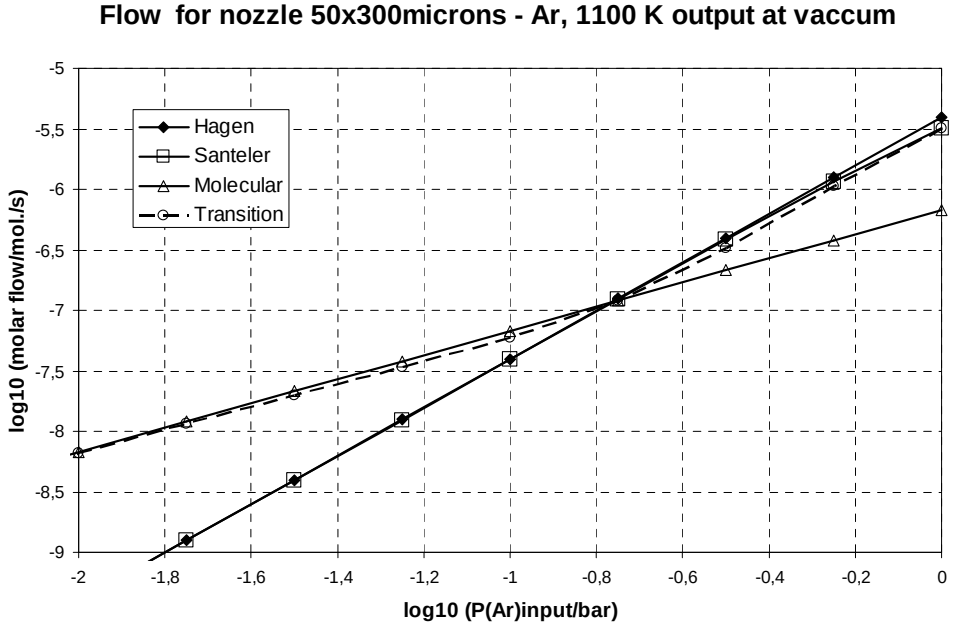

Figure V-2: Decimal logarithm of the calculated molecular flow for different regimes with a 50 μm diameter nozzle, the one fitting the Iodine/Ar and H_2/H_2O/Ar lines.

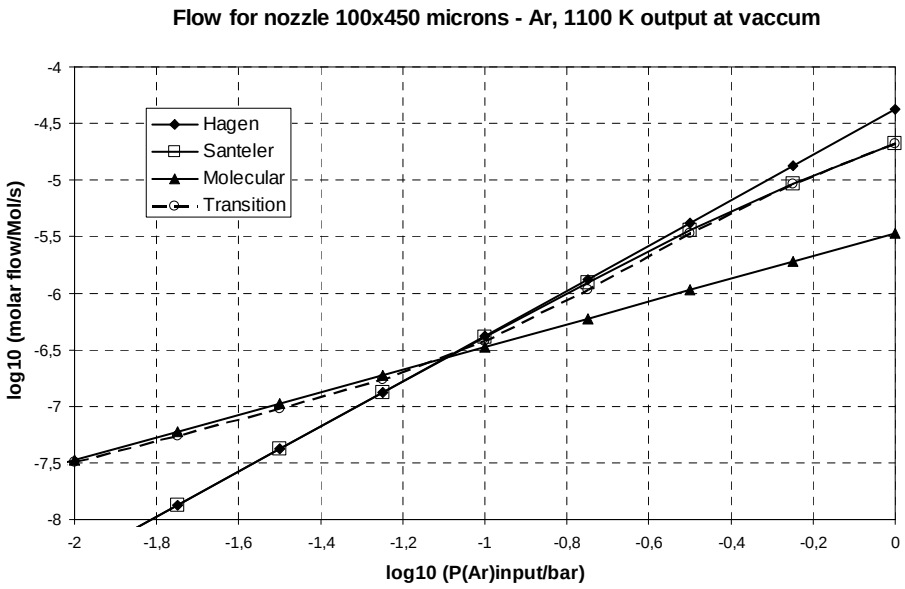

Figure V-3: Decimal logarithm of the calculated molecular flow for different regimes with a 100 µm diameter nozzle, case of CsOH/Ar line.

V.3.3. Calculation of the source lines upstream pressure range

To calculate the upstream pressures, we start by fixing a downstream pressure value and a temperature in the cracking cell which corresponds to a known effusion vapours flow at the exit of the CHIP reactor (fig. V-4).

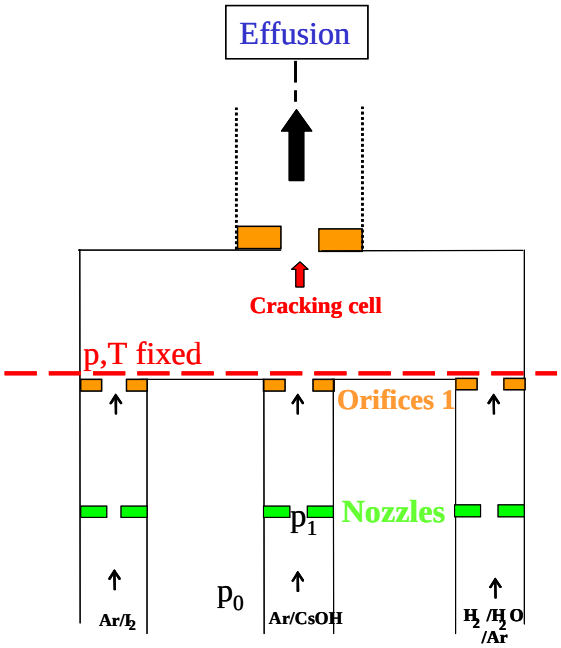

Figure V-4: pressures lines in CHIP reactor

The total argon pressure is imposed in the cracking cell once receiving the three introduction sources gas lines, but the flow calculated from each line must correspond to a certain proportion of this pressure. The molar conductance in the tube 1 (connecting tube between a nozzle and the cracker) which has a temperature gradient is calculated as explained further for the connection cracker-condenser, and for the viscous mode by application of a mean temperature viscosity. The different calculated pressures for each section - tube of connection 1 and orifice 1 for introduction in the cracking cell - and for IG line (Iodine Generator line) are presented in fig. V-5.

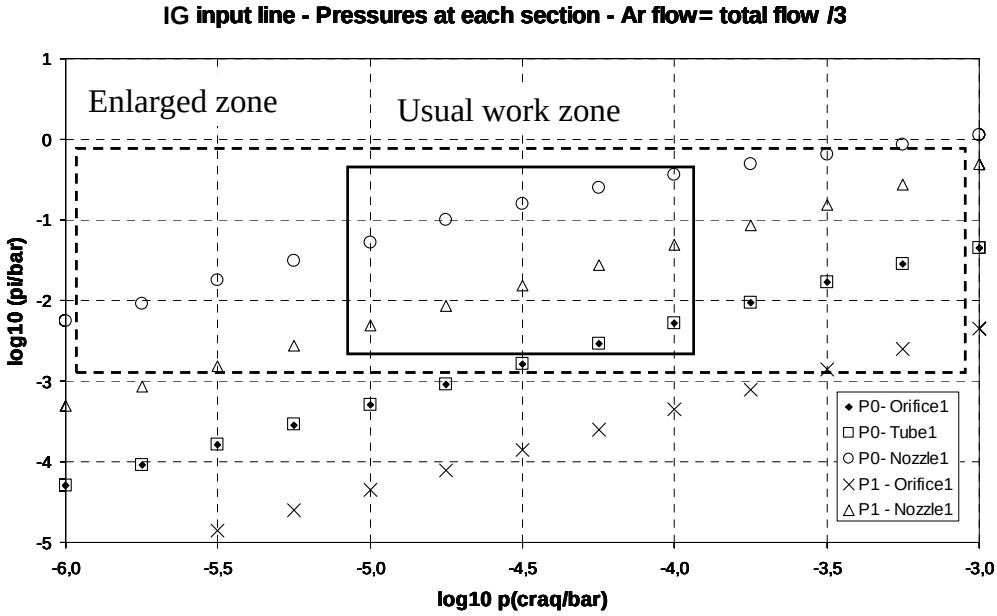

Figure V-5: Pressures calculation in different sections: from IG line (Iodine/Ar), the nozzle1 (50 μm diameter), connection tube (Tube1, 12 mm diameter) and orifice 1 of introduction in the cracking cell (orif1, 30 μm diameter). Calculation is carried out with a flow in the line equal to 1/3 total flow at the cracking cell exit.

This calculation reveals a working area for the upstream pressures of argon about some mbar to approximately 500 mbar for pressures at the cracker's entry between 10^{-5} and 10^{-4} bar.
Extreme conditions can also be defined which will depend on two limits:

- a maximum limit corresponds to higher effusion pressures which will be limited by the spectrometer pumping capacities.
- a minimum limit corresponds to carrier gas pressures inferior or equal to 1 mbar which presents no interest since we can alternately and more easily dilute a vapour in argon

by decreasing its source temperature or by decreasing its flow at the mass flow regulator when starting the experiment (case of H_2O and H_2).

In order to evaluate the regime in the nozzle of 50 μm diameter, fig. V-6 presents pressures at the nozzle level, the Knudsen number and various zones regimes. We observe that the working mode corresponding to the conditions calculated in the previous figure is the transition regime with a predominant viscous laminar-chocked regime, which ensures in principle no backwards flows of the vapours in the input gas lines.

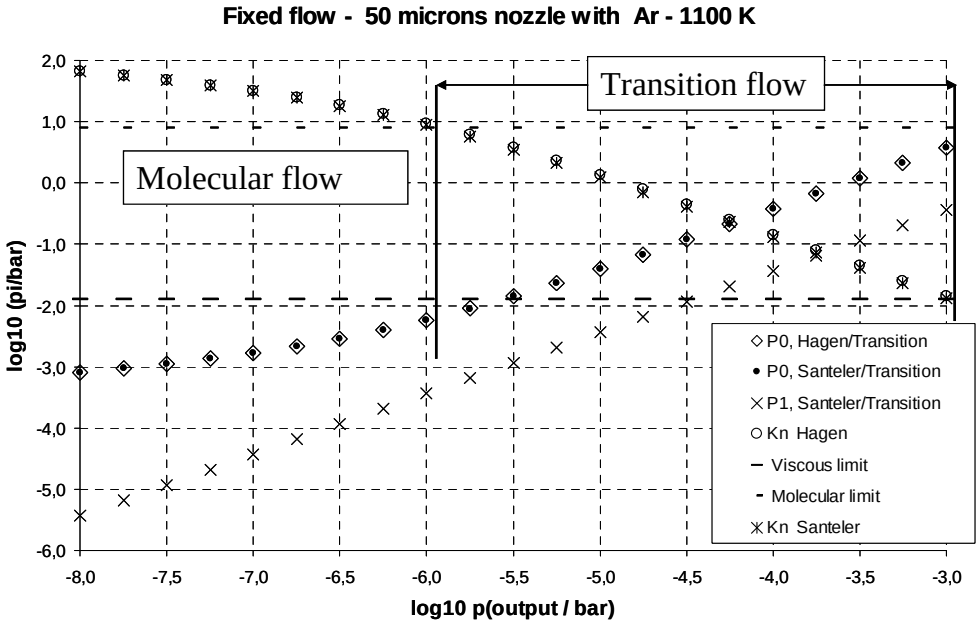

Figure V-6: Calculated pressures in the nozzle (50 μm), and flow regime as a function of the pressure in the cracking cell's entrance.

A way to test the existence of no backwards flow in the nozzles consists of comparing the influence of the cracker's total pressure on the upstream pressure of the nozzle when the flow of this one corresponds either to this total pressure or to a small proportion of this pressure. We chose for example to supply all the cracking cell pressure with one nozzle and with only 1/10 of this pressure, the rest being ensured by the other nozzles. Results are presented in figure V-7.

There is a difference of a factor 10 in the cracking cell pressures between the two flows for the same upstream pressure. This difference corresponds exactly to the difference in term of argon's pressures coming from the nozzle. For example a nozzle providing 1/10 of total cracker's pressure 10^{-4} bar corresponds exactly to a nozzle providing the total flow for a

cracker functioning at 10^{-5} bar of total pressure. The upstream pressures ratio calculated for the same partial pressures due to the nozzle is about 1 ± 0.001.

This confirms that the cracker's total pressure does not influence the flow mode of the nozzles working in the chocked mode regime.

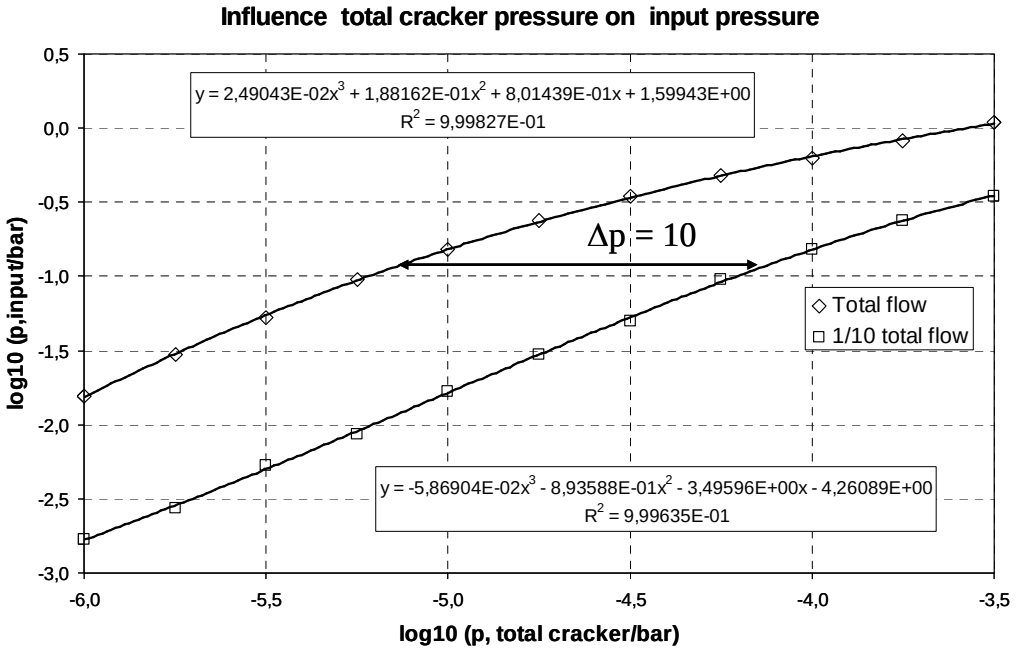

Figure V-7: Upstream Argon pressure necessary to supply a nozzle of 50 microns which provides total or one part (1/10) of the total cracking cell pressure.

V.3.4. Calculation of molecular flow between the cracking cell and the condenser

The objective is to know the exact pressure at the condenser exit – effusion pressure which is recorded by the mass spectrometer – as a function of the pressure in the cracker's entry which is imposed and known by the gas lines via the nozzles. The temperatures of the different sections and their geometry define the molecular conductance between the cracker's entry and condenser's exit according to the following relations:

- The conductance in molecular regime for a cylindrical tube between 0 →1 levels is defined as following:

$$C_{om}^{0} = \frac{1}{1 + 3l_{eq}/8r} \times \frac{\pi r^{2}}{\sqrt{2\pi MRT}} \qquad (9)$$

- The exchanged flow between the two levels 0 and 1 with pressures p_0 and p_1 :

$$F_0 = C_{om}^0 \times (p_0 - p_1) \tag{10}$$

This flow is always directed towards the effusion orifice, consequently the pressure $p_0 > p_1$. For a non isothermal tube, the conductance - with a linear temperature gradient - is calculated from the basic formulae [8, 9], by integration [10] according to a linear temperature gradient:

$$C_{om} = \frac{1}{1+3l_{eq}/8r} \times \frac{3}{2} \times \frac{\pi r^2}{\sqrt{2\pi MR}} \times \frac{\sqrt{T_0}+\sqrt{T_1}}{T_0+\sqrt{T_0T_1}+T_1} \tag{11}$$

N.B. Further calculations using a simplified formula replacing the temperature factor by the mean temperature showed a variation of calculated pressures less than 1%, which is less than the total uncertainty.

For all the sections existing between the cracker and the condenser, we use the equations of the steady state flow in the reactor:

$$p_0 - p_1 = \frac{F_0}{C_0}$$

$$p_1 - p_2 = \frac{F_1}{C_1}$$

.....

$$p_i - p_{i+1} = \frac{F_i}{C_i} \tag{12}$$

.....

$$p_{n-1} - p_n = \frac{F_{n-1}}{C_{n-1}}$$

$$p_n - 0 = \frac{F_n}{C_n} = \frac{F_{eff}}{C_{eff}}$$

The flow is constant at steady state $F_0=F_1\ldots=F_{eff,}$ *and* p_0 is the pressure at the cracker's entrance, F_{eff} *the recorded effused flow by the mass spectrometer* ($p_{eff} = p_n$), and thus we can conclude:

$$p_0 = p_{eff}\left[1 + C_{eff}\left(\sum_{i=0}^{i=n-1}\frac{1}{C_i}\right)\right] \tag{13}$$

$$\log_{10}(p_{eff}) = \log_{10}(p_0) + Cte$$

In fact, this relation corresponds to in series conductances calculation. The cracker-condenser sections will be close to equilibrium if the intermediate conductances (term in brackets) are

large ($\sum 1/C_i$ small) by comparison with the conductance of the effusion orifice. In our configuration of quasi-equilibrium, figure V-8 gives the relation between the cracker's pressures and the condenser under isothermal conditions.

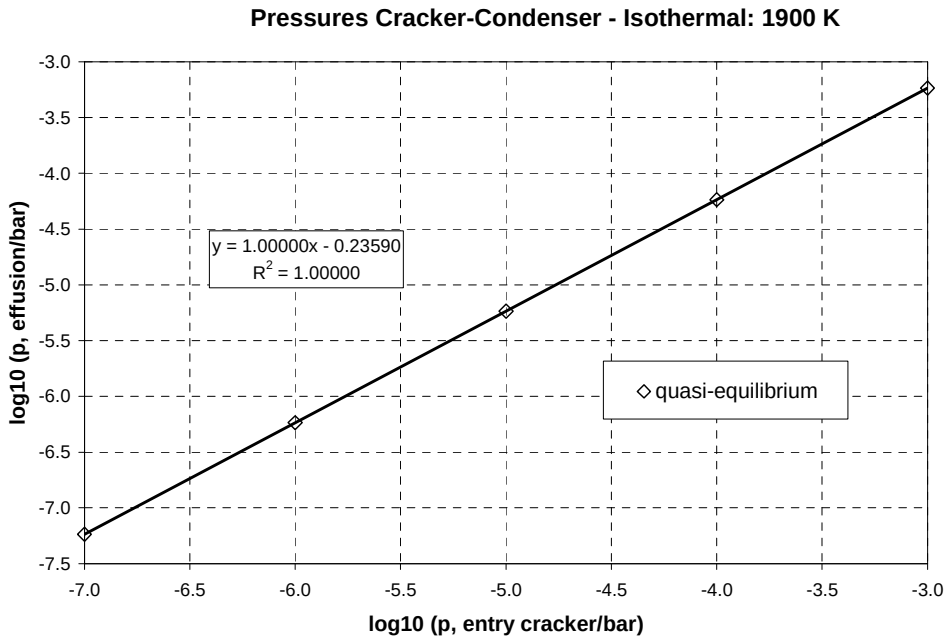

Figure V-8: Relation between cracker and condenser argon pressures and configuration of quasi-equilibrium in the CHIP reactor.

The present configuration known as quasi-equilibrium corresponds to condenser working conditions as close as possible to equilibrium conditions in the cracking cell, while keeping all the intermediate baffles (fig. V-9). The purposes of these baffles are to mix the different injection gases and to obtain an homogenous temperature in the cell. In the present case with the same diameter for the two intermediates orifices between the cracker and the condenser cells *(4 mm diameter, 4mm length),* the effusion pressure is 58% of the cracking cell pressure, which presents a pressure diminution of a factor 2 approximately at same temperature in the whole assembly.

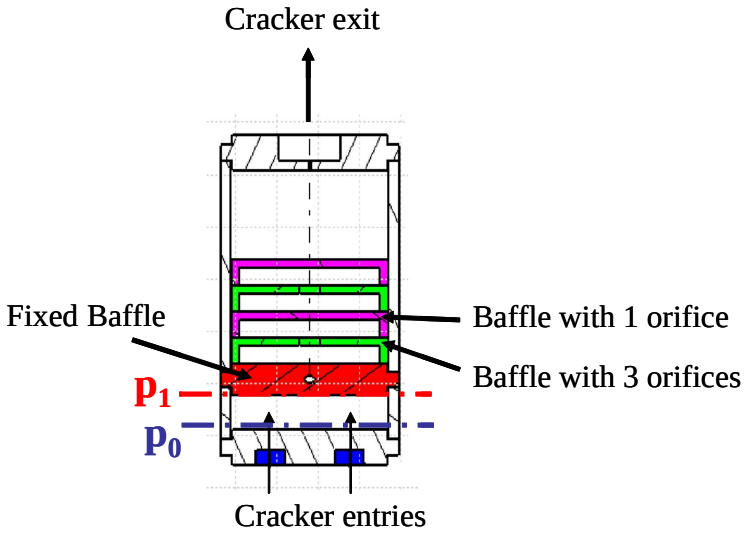

Figure V-9: Cracking cell composed of, firstly, one fixed baffle with 1 central orifice (in red) and, secondly, series of baffles with 1 and 3 orifices respectively (in green and purple).

V.3.5. Pressure at effusion from known gas pressure in the introduction line

By associating the calculated configurations of the two previous sub-chapters, we obtain a direct relation between the upstream pressure in the gas line and the one corresponding to effusion for argon only coming from this line. Results of calculation for IG line (Iodine/Ar) and CsOH/Ar line are presented in figures V-10 and V-11.

Working zones - in term of input pressures in the CHIP reactor lines - are presented on the basis of the maximum effusion flow corresponding to condenser pressures of 10^{-4} bar, and the minimum regulated pressure (between 5 and 10 mbar) in the input lines. These results are quasi-identical to those obtained only with the nozzles, which is consistent since the nozzles were designed to limit flows in the CHIP reactor.

These results allowed fixing the components of the gas lines as well as the assemblies of these components as a function of a vacuum source (primary pump), pressure gauges and/or flowmeters which will operate with pressures lower than the atmospheric pressure. This working mode also requires that the lines must be designed like vacuum lines: a test of the lines using Helium is necessary before each experiment to check the airtightness.

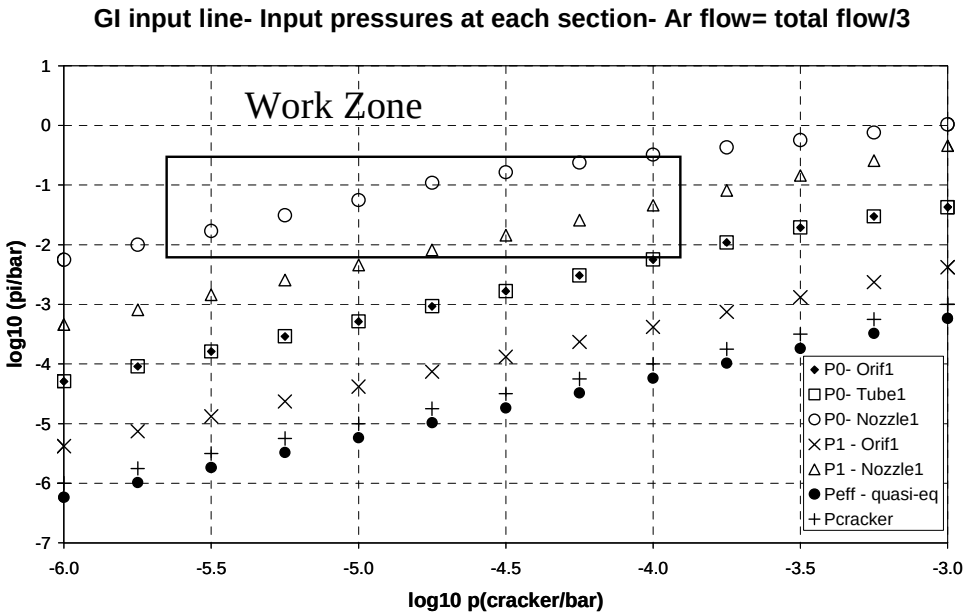

Figure 10: Upstream pressures (p_0- nozzle 1, 50μm diameter), intermediate pressures and effusion pressures as a function of total pressure at the entrance of the cracking cell for IG line (Iodine in Ar) assuming 1/3 of the total Argon flow in the CHIP reactor under isothermal conditions (1900 K) for the last two stages (cracking cell and condenser).

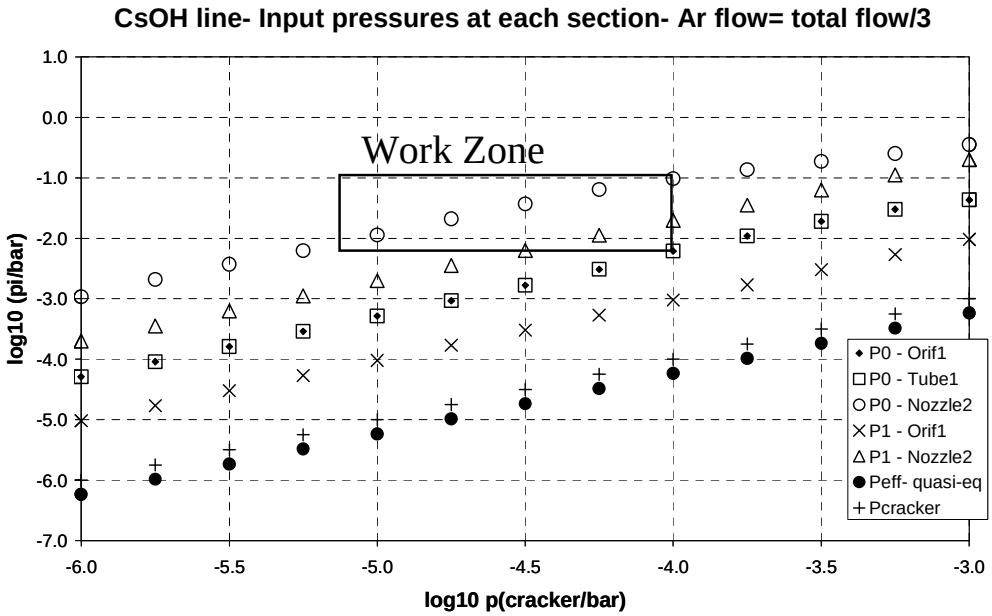

Figure V-11: Upstream pressures (p_0-nozzle 2, 100μm diameter), intermediate pressures and effusion pressures as a function of the total pressure at the entrance of the cracking cell for CsOH line alone assuming 1/3 the total flow in the CHIP reactor under isothermal conditions (1900 K) for the last two stages (cracking cell and condenser).

V.4. FLOW PARAMETRISATION FOR SPECTROMETRIC EXPERIMENTS

The flow calculation of the gas lines allows firstly to configure their architecture and to dimension their pressure gauges and flowmeters, but must also permit to calibrate the mass spectrometer at each time during the experiments by referring to total Argon pressure which can be monitored by the mass spectrometer. By this way, we are able to know at any time the pressure of the other gaseous species or vapours through their ionic intensities ratio to Argon intensity. In a conventional effusion cell, the presence of an inert reference or the total mass loss of the sample during the experiment allows this calibration. In the configuration of an effusion cell with gas introduction, the inert carrier gas has a role of an inert reference and our objective is to use it like an additional way of calibration because the usual methods may be limited in their application depending on the investigated system.

During the CHIP reactor experiments, the lines pressures are recorded as well as the sources temperatures (Iodine and CsOH) and the proportions of argon, H_2O and hydrogen vapours. These measurements would allow knowing at any time the flow of each element - Ar (total), Iodine, Cesium, H_2O and H_2 - which flow in the high leak-tightness CHIP reactor. These flows will be analyzed at the effusion with the mass spectrometer. As argon is so far the major species – but this will not be always the case - it is important to deduce a relation between each upstream pressures and those resulting from the cracking cell because the temperature are fixed - at least during one experiment - from the introduction lines to cracking cell. The effusion pressure will be then easily calculable via the geometry and the temperatures of the condenser during measurements: the geometry does not change during one experiment but the condenser temperature varies. Consequently, the calculation must be made for each point of measurement once interpreting the mass spectrometric results. (a specific program has been developed).

Each line will introduce a known quantity of gas into the cracking cell, and concerning argon that will imply that each line gives a partial pressure in the cracking cell, the total pressure will be the addition of the partial pressures. Taking into account no backwards effects in the nozzles for chocked regime, the previous calculations give the relation between upstream pressures and pressures in the cracker's entrance. Results are presented in figures V-12 to V-14 for argon, H_2 and H_2O. Each species is supposed alone in the line, using a nozzle of

50µm diameter. The large observed differences are mainly due to the Knudsen number which included the molecules diameter and modifies the transition zone noticeably. Another difference comes from the factor $\gamma = C°_p/C°_v$ which is different for a monoatomic and diatomic gas. The pressures at the effusion orifice - calculable for each experimental determination - will be in the same proportion even if the gases have different molar masses. In fact, there is compensation in the relation which permits to calculate the total molar conductance (relation (9)) of the cracking cell–condenser assembly.

This kind of calculation dedicated to the experimental results interpretation can be performed - with a rigorous way – only for a major species as the inert carrier gas, Ar. It could also be used for other major species like H_2 or H_2O, if they are not consumed in the chemical reactions which will occur between the cracker and the condenser in a significant way. If not, the atomic balance will be more difficult to establish for all produced species which have different molar mass. The relative calibration compared to argon is thus very important.

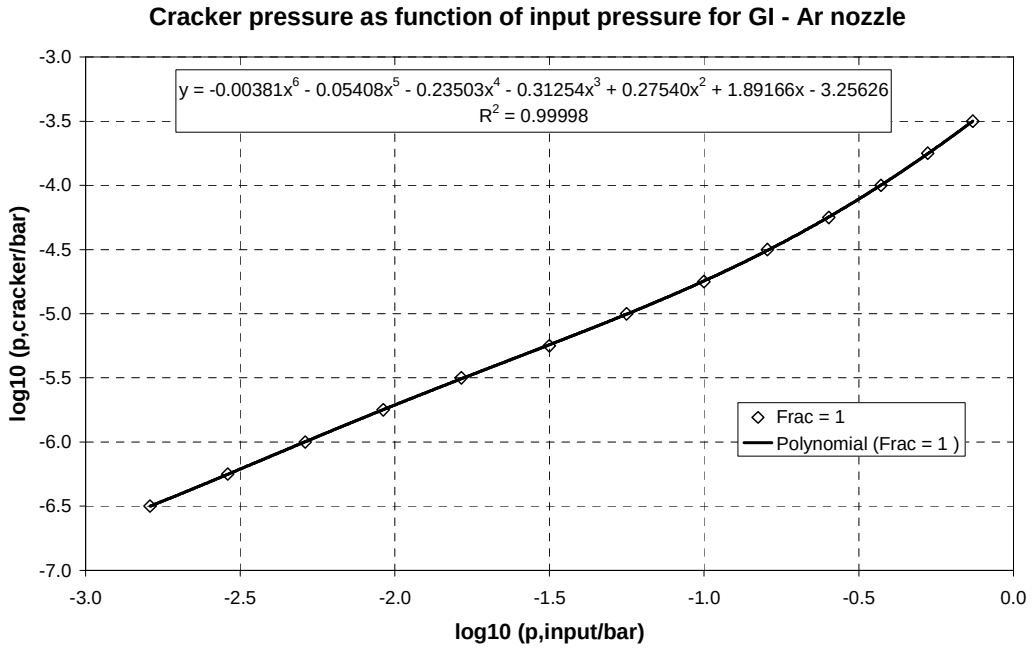

Figure V-12: Cracking cell pressures calculation as a function of the upstream pressure for Ar alone.

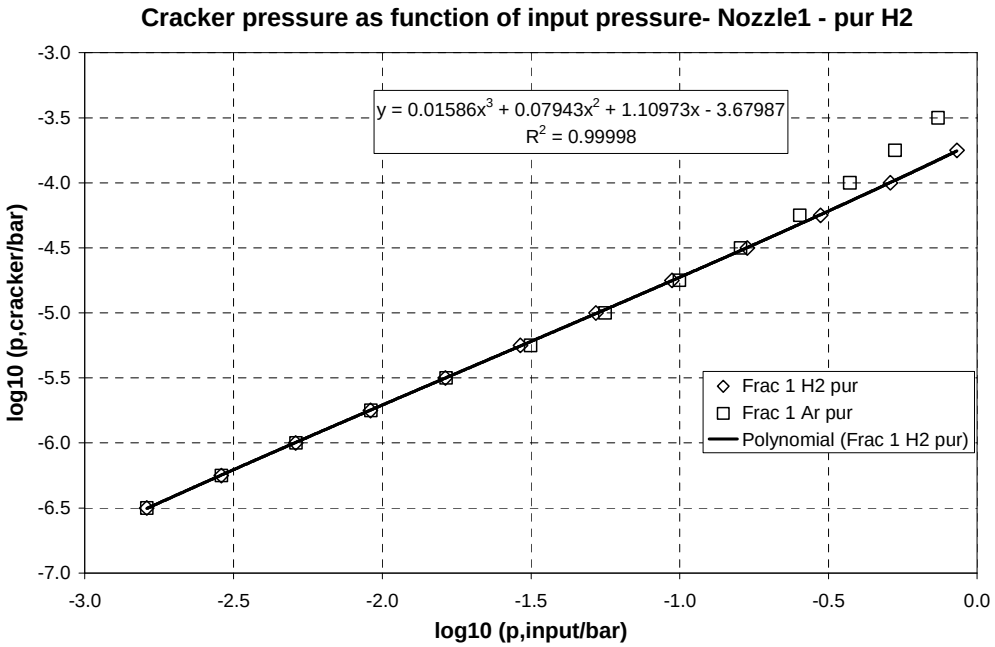

Figure V-13: Cracking cell pressures calculation as a function of the upstream pressure for H_2 alone.

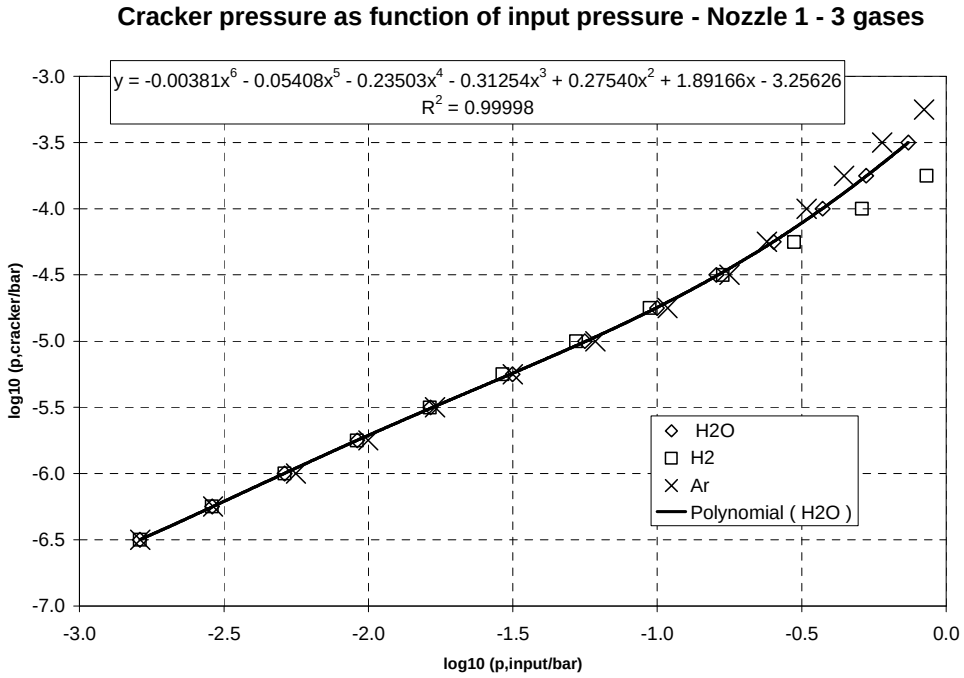

Figure V-14: Cracking cell pressures calculation as a function of the upstream pressure for the three gases: Ar, H_2 and H_2O. The fit corresponds to the H_2O curve.

The smoothing of the relation between the upstream and downstream pressures provides a way of calculation of cracking cell pressure at the entrance which is imposed by each input

line (recorded pressures). The further correction to obtain the effusion pressure will be deduced for each determination as a function of the condenser temperature via the conductance calculations in molecular flow regime.

As intermediate conclusions:

- The pressures of Ar, H_2 and H_2O in the cracking cell are calculated for each line using nozzles of 50 microns (Iodine and H_2/H_2O lines, respectively) and 100 microns (CsOH line). Summing the 3 injection lines gives the total pressure in the cracking stage (non measurable and essential pressure for the calibration of the mass spectrometer).
- The molar conductance of the cracking cell – condenser section allows determining the pressure of argon in the effusion cell.
- The program developed in Visual BASIC (Excel software, see Appendix V-A) necessary to fix the working conditions of the CHIP reactor in terms of input pressures and flows operate correctly and all the relations used in the program were controlled.
- Relations were established to evaluate pressure of effusive iodine gaseous species or vapours from HTMS measurements.
- The viscosity constants were smoothed for each pure component. Calculation of the mixtures (for high contents) and the impact of the composition in the viscous mode flow have to be tested.
- Gamma Constant ($\gamma = C°_p/C°_v$) for argon, monoatomic and diatomic species (considered here as air) are stored apart for H_2O which has to be calculated taking into account the impact of the chocked regime.

V.5. THERMAL TEST OF THE CHIP REACTOR

For kinetics study, the vapors issued from the cracker travels through a connecting tube toward the condenser zone that have to be cooler. The interpretation of the condenser pressure results as measured by the mass spectrometer in terms of kinetic laws will depend on the temperature gradient in this tube and consequently this gradient must be known. For this reason the first tests were thermal tests aimed to,

- The knowledge of the minimum condenser temperature that can be reached for any cracker temperature.
- The knowledge of the temperature gradient existing in the connecting tube.

The conception of the CHIP reactor allows regulation of temperature using an isothermal mode for each reactor's stage separately. The cracker and condenser cells can be linked through a large temperature gradient between the two zones. Cooling between each stage – in order to avoid excessive heat flow exchange - is done by using a special water cooled "sol". The device is fitted with several thermocouples (a whole set of 15 standard TC type B and K) allowing measurements in the walls – lateral, bottom and top - of each reactor's stages (see Appendix V-B). Thermal behaviour tests (fig. V-15) showed that it is possible to maintain a cracking of the vapors at 1900 K with a condenser temperature varying from 900 to 1900 K. Results show that for a cracking temperature of 1800 K, the condenser temperature can be decreased down to 850 K – temperature largelly in agreement with the hot leg assigned one.

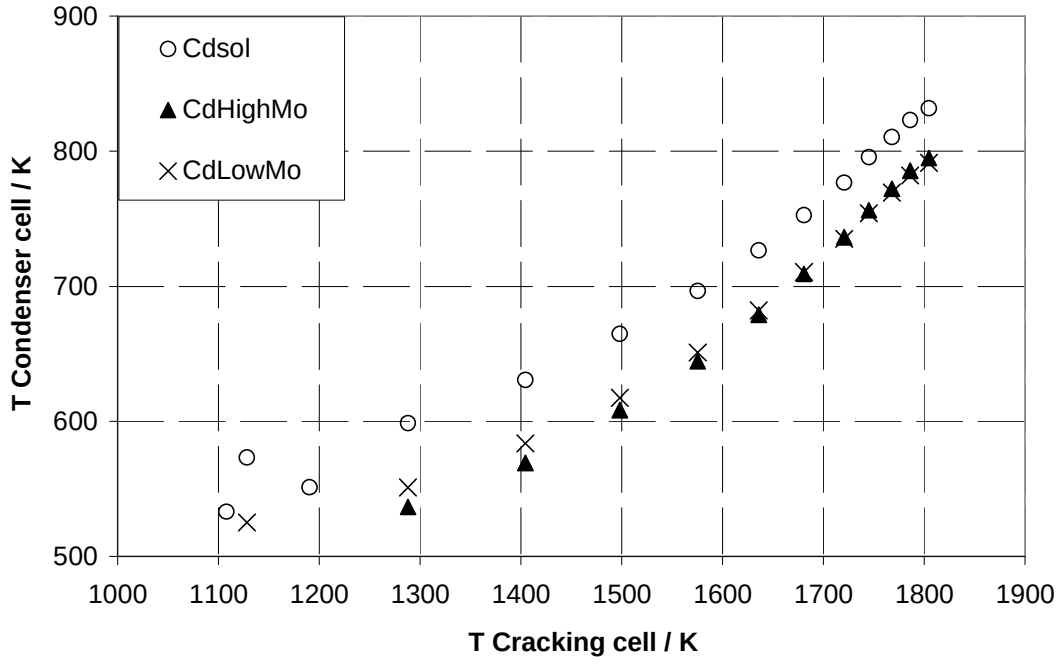

Figure V-15: Influence of cracking cell temperature on condenser temperature when this last device is not heated. Its temperature is thus the minimum one's that can be reached for any cracker temperature. Cdsole: thermocouple on the condenser sole, CdHighMo and CdLowMo: two thermocouples in the condenser wall envelope made in Mo, one at the top, one near the bottom.

In a special series of experiments, the intermediate zone were fitted with two thermocouples introduced in special holes drilled in the connecting tube – the thermocouples being then bent inside the tube. Temperature measurements show that when the thermal mode of the two stages (cracker and condenser) is isothermal, a cold point occurs in the innner volume of the connecting tube. Consequently, there is a risk of vapours condensation at this level. This cold point disappears when the temperature of the condenser decreases. Different thermal shields with different shapes – radial discs or cylindrical tubes and combination of the two - have been tested. The best device shows that from 1900 K down to 1350-1300 K for the condenser temperature there exists a cold zone [11]. Below, the temperature gradient displays a form which has been fitted as a function of the condenser temperature – the cracker temperature being kept at 1900 K for further experiments with vapors. A last version named “diabolo” has been calculated to enlarge this useful temperature zone by thermal simulation of the CHIP reactor (work performed at the engineering service of DPAM/IRSN).

Finally, we have to quote that in terms of kinetic simulation, the influence of the thermal gradient will be less important for a connecting tube with short transit time, that is the case when using a large orifice at the cracker exit meanwhile the condenser entrance orifice is decreased. So doing the expansion of the vapors will occur mainly in the condenser zone.

V.6. POSITIONNING TEST OF CHIP REACTOR

The detection of the only genuine effused gaseous species is a prerequisite of the method in order to warranty the accuracy of the measured vapor pressures. This is important particularly for high volatile species - as I(g), I_2(g), HI(g)... – that come also from multiple surface vaporizations once effused in the furnace housing. These surface vaporizations can become more important than the genuine effusion flow as detected. In order to avoid these parasitic phenomena, we use a so called “restricted collimation device” (see Chap. II).

The effusion orifice alignment along the ionization chamber axis - that is the restricted collimation axis - is performed by moving the effusion cell furnace in two X and Y directions orthogonal to this axis as explained in Chapter II. As the CHIP reactor is made of discs and tubes pilled altogether, the mechanical assembly may be not necessarilly stable. Positionning tests for the CHIP reactor have been performed under Ar carrier gas and when varying the temperature of the cracking cell (fig. V-16) and scanning in X and Y directions.

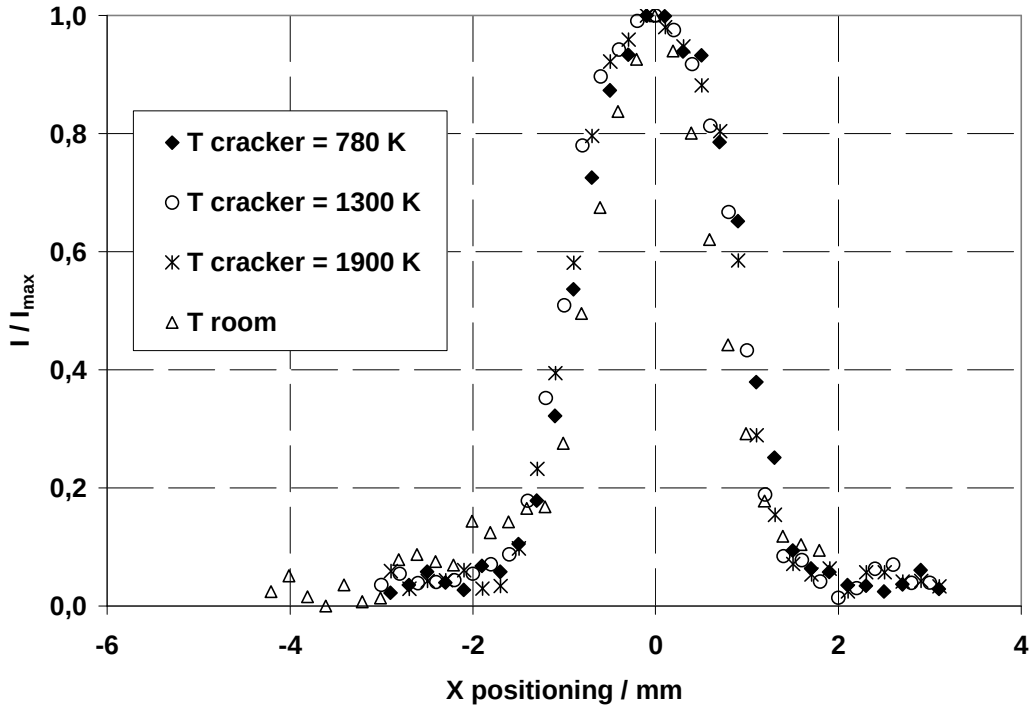

Figure V-16: X axis scanning of the CHIP reactor effusion orifice position under Ar flow when varying the cracking cell temperature.The ion Ar^+ is monitored at mass 40.

Orifice effusion positioning must be precise (± 0,025 mm) and reproducible during the experiment whatever the temperature is. It can be checked constantly during the experiment at each temperature ramp in order to warranty the detection of the only molecules coming from the effusion cell and not from parasitic phenomena such as surface vaporizations around the effusion orifice. In figure V-16, different Ar flow can be distinguished as detected by the ions source: - (i) at the top of the peak, the ion source sighting is perfectly inside the effusion orifice, - (ii) far away when there is no signal, the ion source sighting is outside the effusion orifice and beyond the thermal shields, - (iii) and at the basis of the peak, the configuration is intermediate: part of the signal comes from the cell and another from outside surface vaporizations just around the effusion orifice edge on external surface of the condenser (see chapter II). The perfect superposition of the different scans warranty the correct positionning of the effusion orifice along the detection axis whatever is the temperature and movement.

V.7. PRESSURE CALIBRATION TESTS OF THE CHIP REACTOR

One main problem in mass spectrometry is to obtain partial pressures from ionic intensities as reported to one gaseous species. This operation is only possible using special calibration procedures that depend on the kind of reactor. In the present case, our aim – and the only solution - is to report any vapor pressure measurement to the Ar carrier gas pressure. The Ar gas pressure at the condenser is in principle calculated from input pressures as explained in this chapter. In order to check the present adequacy of the experimental device architecture with our calculations, special calibration experiments were performed.

Calibration tests of the CHIP reactor have been performed either with Ar gas or with Ar gas by reference to Ag melting point (T_m = 1234 K) and Ni melting point (T_m = 1726 K) using an alumina crucible placed in the condenser. These tests were aimed to:

- check our Mass Spectrometer response when each input line (with Ar) is working separately or all together,
- check the proportionality of each line – (i) against its input pressure, - (ii) against each others,
- calibrate the reactor using as reference the melting point of a pure compound (Ag and Ni). This will make it possible also to calibrate the temperature measurements as well as the thermocouples accuracy.
- compare the measured intensities (or pressures) with those obtained according to flow calculations (see first part of this chapter).

V.7.1. Check of the mass spectrometer response for each injection line

The control of our mass spectrometer response was done for Ar/CsOH and Ar/I_2 lines by varying the Ar pressure of the checked line separately. Ar/H_2/H_2O line was not tested at that time due to a defectious pressure sensor. An example of results is presented in figure V-17.

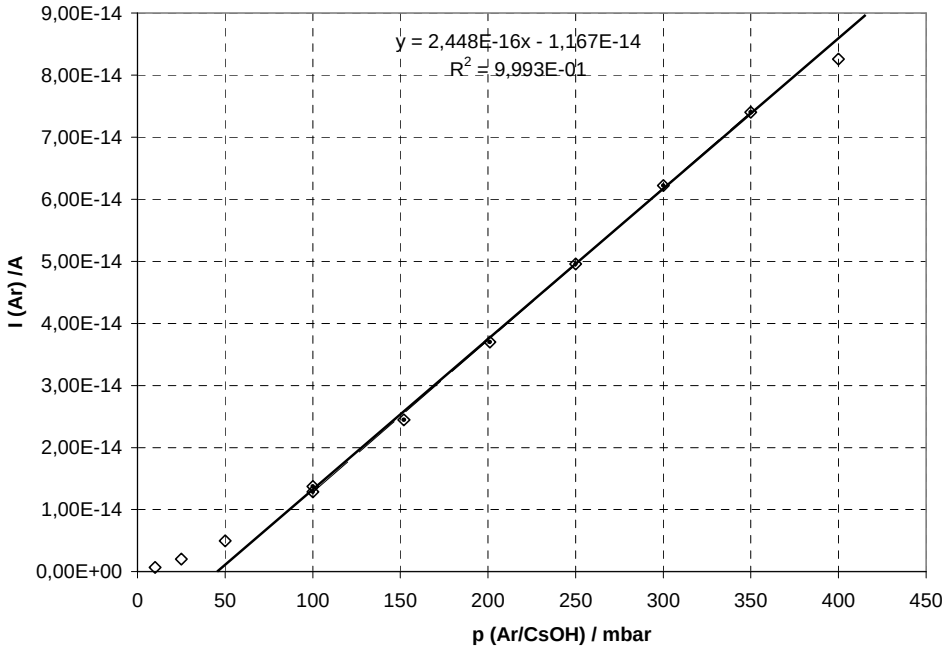

Figure V-17: test of Ar/CsOH line using argon gas. Ionic intensity of Ar^+ as a function of the input pressure at the nozzle. Other lines: $Ar/H_2/H_2O$ line constant at 100 mbar (without any input flow because of a defectious pressure sensor) and Ar/I_2 line off (the nozzle is clogged).

Figure V-17 displays the total measured intensity of Ar (observed by the mass spectrometer) as function of the input Ar pressure in the Ar/CsOH line. Results show that the measured intensities are proportional to introduced pressures from 100 to 350 mbar. Above this value, the intensities evolution doesn't respect the proportionality to the input pressure values. As calculations showed, for pressures more than 400 mbar, the transition regime would be attained in the tube just after the nozzles, and below 50 mbar, the flow regime is no more chocked at the nozzles exit: these results seem correct, and the conclusion is that the Ar/CsOH line must be used in the 100 – 350 mbar range. Same features with pure Ar were observed previously with Ar/I_2 and the useful pressure range is 50 - 600 mbar due to smaller diameter of the nozzle.

The $Ar/H_2/H_2O$ line was tested later and results are shown in fig. V-18. We observed at that time that the nozzle is clogged, probably due to oxydation at high temperature (1100 K) in previous experiments. The clogging was confirmed by special post experimental He leak tests.

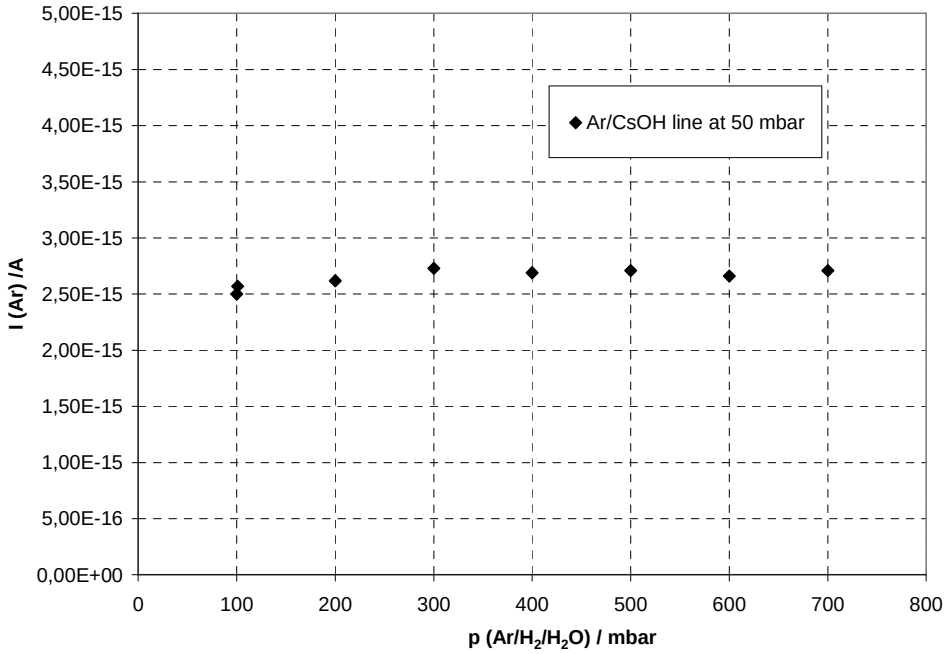

Figure V-18: test of Ar/H_2/H_2O line: mass spectrometric response as a function of the input pressure using pure argon. Other lines: Ar/CsOH line input pressure is constant at 50 mbar and the Ar/I_2 line is off.

The check of the Ar/I_2 nozzle working was performed first with Ar then with Ar and iodine (1 mbar I_2 in 100 mbar Ar carrier gas). During this last experiment, Ni reacted with I_2 to form NiI_2(s) that clogged the nozzle after two hours working at about 1100 K: regular decrease of the I^+ signal, then disappearance. The CHIP reactor was set at 1500 K for the cracker and condenser, and the mass spectrometer detected first the only I(g) and Ar gaseous species (no I_2(g) was observed at ion I_2^+). In order to regenerate the nozzle, several tests using water, nitric acid diluted in water and finally HF / HNO_3 mixtures (4% HF, 20% HNO_3 as used for stainless steel passivation) deposited on the nozzle plate lead to the (partial?) elimination of the passive iodide layer. This fact was confirmed during further Ar/I_2 test as shown in figure V-19.

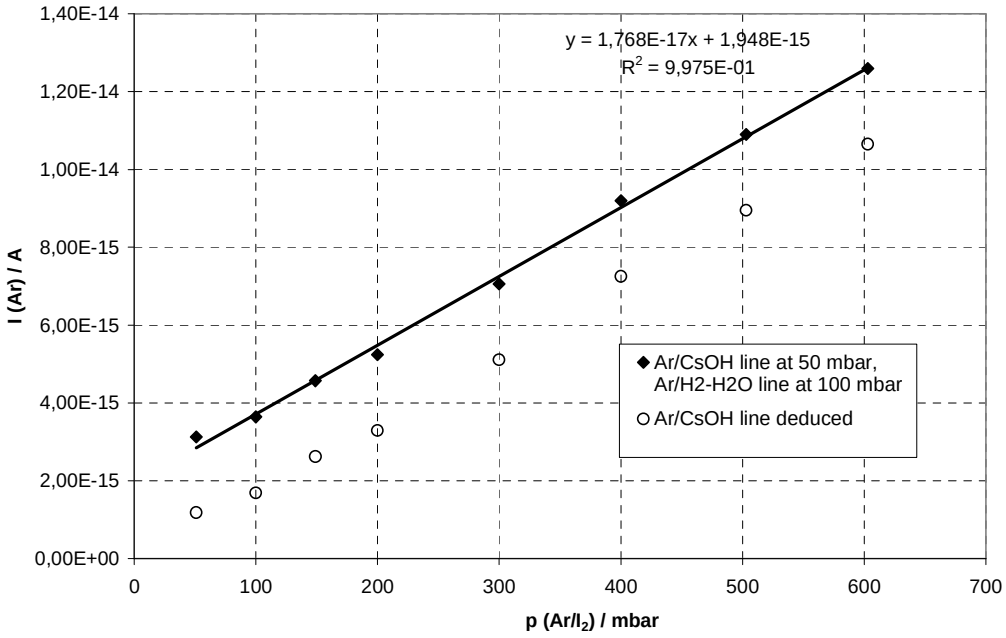

Figure V-19: test of Ar/I_2 line: response of the mass spectrometer as a function of the input argon gas pressure. Other lines: Ar/CsOH line input pressure is maintained constant at 50 mbar and the Ar/H_2/H_2O line off (clogged).

This figure presents the total measured Ar intensity (coming from the two lines) when increasing the input Ar pressures of the Ar/I_2 line. The Ar/CsOH line input pressure is maintained constant at 50 mbar and Ar/H_2/H_2O line at 100 mbar for safety (but without any input flow since this nozzle is clogged). As shown in the calculations of the CHIP reactor, due to the chocked regime at the nozzles, the measured intensities of Ar are the sum of each nozzle contributions. So, the Ar/CsOH contribution is evaluated at null Ar/I_2 flow (at the Y axis) and removed from the total measurements to give the only Ar/I_2 contribution as displayed in figure V-19. The evolution of the registered pressure of Ar at the condenser show, - (i) for the only Ar/I_2 nozzle, a signal quasi proportional to the input pressure in the 50 to 600 mbar input pressure range, with a yield slightly lower than attended: for instance, between 50 and 500 mbar, the ionic intensity is multiplied by 9 instead of 10 attended from calculations, - (ii) for the full pressure that corresponds to the two working nozzles, the measured pressure for 500 mbar input pressure is 3.66 times the one measured at 50 mbar meanwhile the calculated value is 5.48.

Comparison between experimental pressure and calculated evolutions shows that there is probably some leak in the CHIP reactor device in the molecular regime, i.e. after the nozzles. In principle the total flow regime in the CHIP reactor – including the leaks - should be a

steady state at least during an experiment. This steady state can change any time the reactor is taken off from the mass spectrometer, due to mechanical re-positioning of the numerous parts.

V.7.2. Calibration tests with pure components at their melting temperature

The pressure p_i of any gaseous species existing in the condenser can be related at any time to the pressure of Ar p_{Ar} when reporting the ionic intensity of this species I_i^+ to the one of the Ar carrier gas I_{Ar}^+ at the same time, provided that the Ar pressure is known. Using the spectrometric relation:

$$p_i S_i = I_i T \tag{14}$$

relation in which I_i is the measured ionic intensity of ion i, p_i the partial pressure of its original molecule in the cell, T temperature in the cell and S_i is the sensitivity given by the general relation:

$$S_i = G\eta\sigma_i(E)\gamma_i f_i \tag{15}$$

where G is a geometrical factor related to the solid angle for molecular beam sampling defined by the ionization chamber aperture and the effusion orifice, η is the extraction and transmission efficiency of the formed ion in the mass spectrometer (for our ion source and magnetic η = constant whatever is the measured ion), $\sigma_i(E)$ is the ionization cross-section at the electron energy E, γ_i is the efficiency of the ion detector (for our discriminated pulse-counting detection $\gamma_i = 1$ whatever is the measured species i), f_i is the isotopic abundance of the detected ion that is calculated exactly for any atomic composition of each ion.

$$\frac{p_{Ar}}{p_i} = \frac{I_{Ar}T}{A\sigma_{Ar}f_{Ar}} \cdot \frac{A\sigma_i f_i}{I_i T} = \frac{I_{Ar}}{I_i} \cdot \frac{\sigma_i f_i}{\sigma_{Ar} f_{Ar}} \tag{16}$$

$$p_{Ar} = p_i \cdot \frac{I_{Ar}}{I_i} \cdot \frac{\sigma_i f_i}{\sigma_{Ar} f_{Ar}} \tag{17}$$

I_{Ar} and I_i are measured, the ionization cross section can be either calculated or estimated from atoms (see appendix V-C), the isotopic abundance of each gas is calculated exactly from the atoms. Any p_i pressure can be related to a known Ar pressure, or reversely any p_{Ar} pressure can be calculated from a well known p_i at a temperature such as the melting point using relation (17).

From literature the melting temperatures of Ag and Ni are respectively 1234 K and 1726 K, and pressures are well known. The observation of the melting plateau of each pure compound was done several times during an experiment by increasing and decreasing temperature around the melting range. This will able us also to calibrate the thermocouple readings. Figure V-20 presents an example of evolution of Ag measured intensities once decreasing the temperature of the condenser.

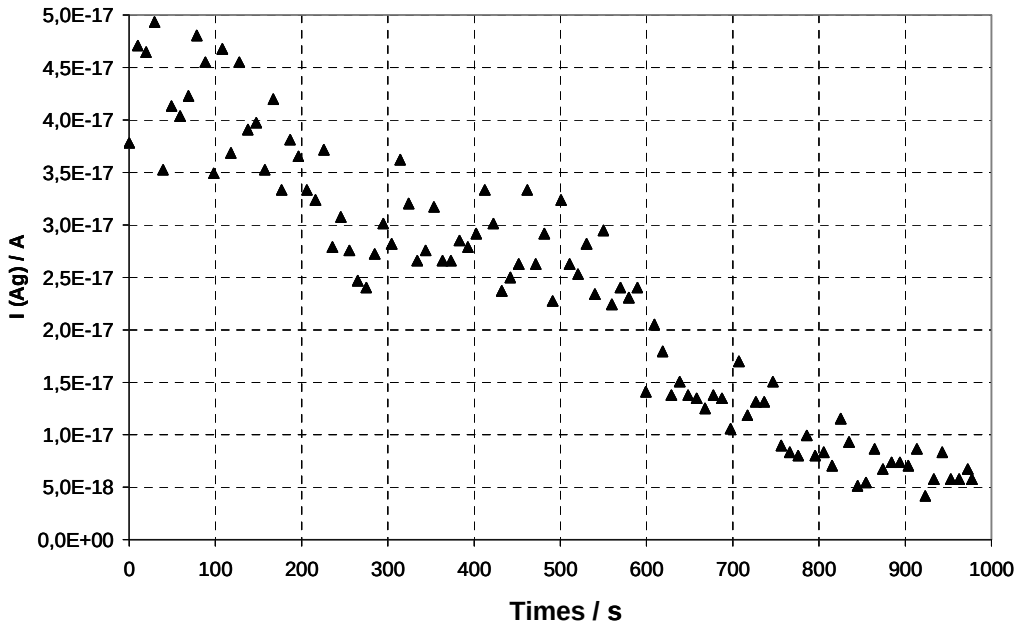

Figure V-20: Observed melting temperature of a Ag sample when decreasing the temperature of the condenser cell.

The solid-liquid phase change appears clearly as a plateau in measured intensities as function of time. Monitoring altogether the thermocouples (CdHighMo and CdLowMo in the condenser wall envelope), obtained melting temperatures for Ag and Ni are presented in table V-1. The results showed that a correction have to be applied to measured temperatures (+ 5.4 K for Ag and + 7 K for Ni).

Label run	compound	Melting point /K (mean value)	Theoretical value/K	Comments
Chip22-09-08	Ag	---------	1234	Melting point not well observed during run
Chip23-09-08		1228.6		Correction to be applied to our measured temperatures +5.4 K
Chip25-09-08	Ni	1719	1726	Correction to be applied to our measured temperatures +7 K

Table V-1: Observed melting temperatures of pure compounds Ag and Ni and comparison with values from literature.

V.7.3. Ar pressures at the melting temperatures

Using the known thermodynamic properties of Ag and Ni at the melting point in term of pressure and enthalpy of vaporization $\Delta_{vap}H$ [12],

$Tm_{(Ag)}$ = 1234 K
$\Delta_{vap}H_{(Tm)}$ (Ag solid) = 277.12 kJ.mol^{-1}
$\Delta_{vap}H_{(Tm)}$ (Ag liquid) = 265.83 kJ.mol^{-1}
$p_{(Ag)}$ = 3.78 10^{-6} bar

$Tm_{(Ni)}$ = 1726 K
$\Delta_{vap}H_{(Tm)}$ (Ni solid) = 417.42 kJ.mol^{-1}
$\Delta_{vap}H_{(Tm)}$ (Ni liquid) = 399.944 kJ.mol^{-1}
$p_{(Ni)}$ = 4.13 10^{-6} bar

The products Ln(IT) have been calculated over solid and liquid phases according to the following relations:

$$Ln(IT) = a \cdot \frac{1}{T} + b \qquad (18)$$

With $a = \frac{\Delta_{vap}H_T^{\circ}}{R}$. (R the gas constant) (19)

Scaling the relation at the true melting temperature, the obtained results are presented and compared with our measured intensities for each temperature plateau both sides of the melting temperature in figures V-21 and V-22.

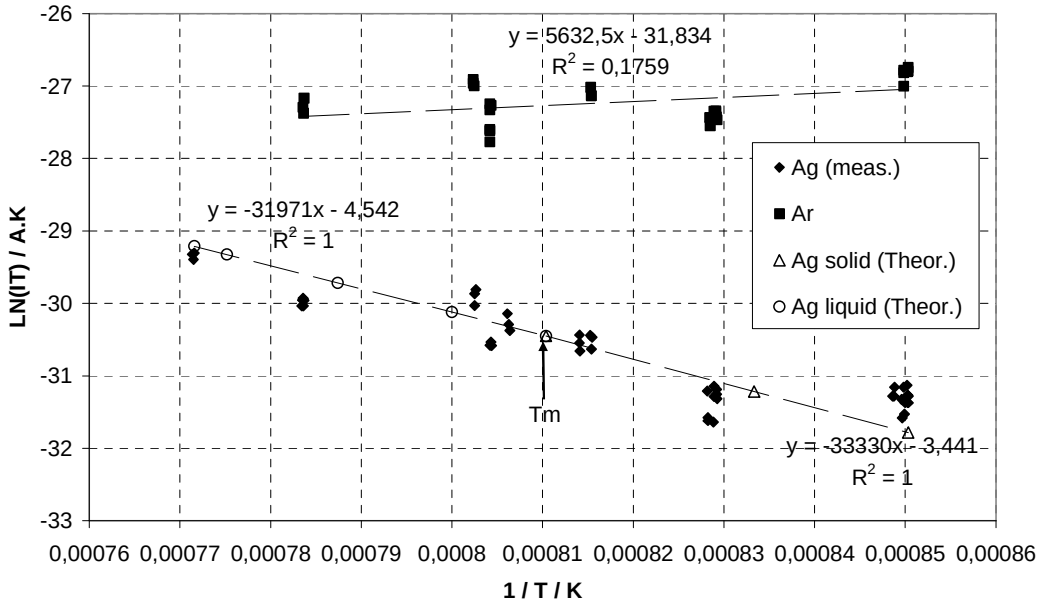

Figure V-21: Comparison between our measured ionic intensities of Ag^+ and those calculated from literature over liquid and solid phases. (meas.): our measured intensities scaled at the melting, (Theor.): data calculated from literature and scaled at the melting temperature. (Note that our measurements are abnomalously scattered due to problems in the ion source supply)

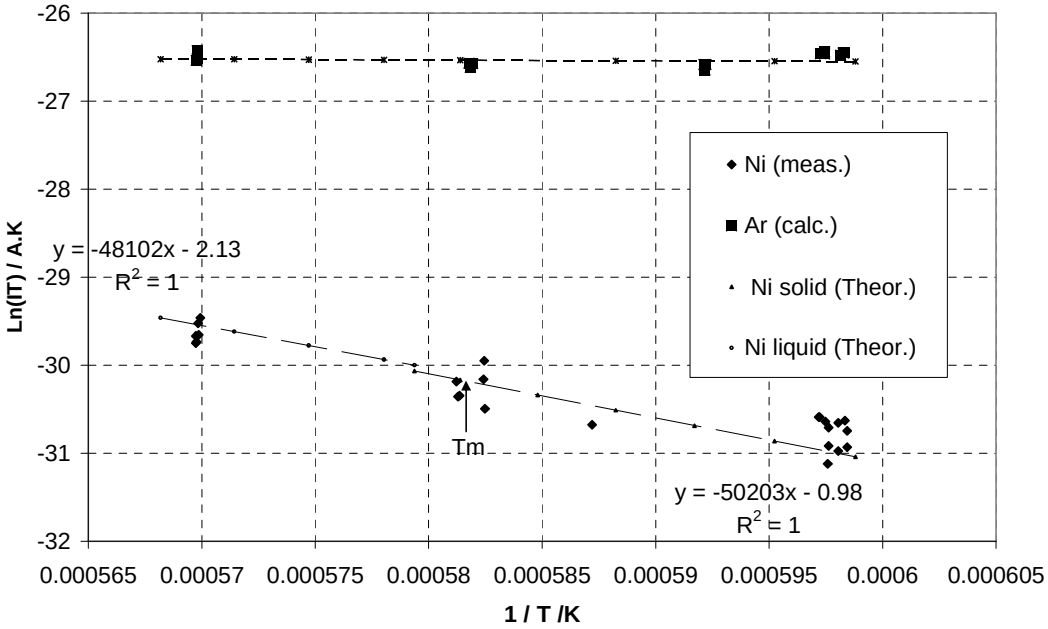

Figure V-22: Comparison between our measured ionic intensities of Ni^+ and those calculated from literature over liquid and solid phases. (meas.): our measured intensities scaled to the melting intensity, Ni (Theor.): data calculated from literature scaled at the melting temperature. Ar (Calc.): data calculated according to relation (22).

Results show that our measured IT products evolutions for our two references Ag and Ni are in general agreement with those obtained using the known thermodynamic properties around the melting temperatures. Ionic intensities of Ar – not detected at the melting temperatures due to the only monitoring of the Ag and Ni plateaus – are presented in the same figures. Then, the values for Ar^+ intensities at the melting temperatures are deduced.

The evolution with temperature of Ar intensities can be evaluated from the constant flow maintened in the CHIP reactor, the input pressures at any nozzle being maintained constant. In terms of effused flows, this means that according to the Hertz-Knudsen relation and for two different temperatures T_1 and T_2 of the condenser,

$$\frac{p_1}{\sqrt{T_1}} = \frac{p_2}{\sqrt{T_2}} \tag{20}$$

and using the basic mass spectrometric relation,

$$\frac{I_1^+ T_1}{\sqrt{T_1}} = \frac{I_2^+ T_2}{\sqrt{T_2}} \tag{21}$$

finally,

$$I_1^+ = I_2^+ \sqrt{\frac{T_2}{T_1}} \tag{22}$$

An example of application of this relation for Ar intensities taking as reference the melting temperature ($T_2 = T_{melting}$) has been drawn in figure V-22. The observed evolution of Ar intensities as a function of temperature agrees with the attended one.

Considering the calibration of Ar pressures as refered to pressures at the melting temperature, relation (17) becomes for exemple for Ag,

$$p_{Ar}(meas.) = p_{Ag}(T_{melting}) \frac{\sigma_{Ag}\ f_{Ag}}{\sigma_{Ar}\ f_{Ar}} \frac{I_{Ar}^+}{I_{Ag}^+} \tag{23}$$

In this relation the Ag pressure at melting is known, the ionisation cross sections calculated as proposed by Drowart et al. [4] at the measurement potential and the isotopic abundance known. More details about factors as used in relation (23) are presented in V-C and V-D. Table V-2 summarizes our determined experimental pressures of Ar as refered to the Ag and Ni melting pressures. Conditions of measurements are also presented as well as the calculated values for the Ar pressure at the condenser from the known input pressures at the nozzles. The experimental pressures are both sides of the calculated ones, and the difference is more

pronounced when the input pressure at the Ar/I_2 line is high. This feature suggests that either leaks are existing in the molecular stage of the reactor, or the Ar/I_2 nozzle is not totally clear of corrosion products. Both explanations are also plausible. However, a post experimental careful analysis of the junctions between the free tubes and the cracker revealed some large mechanical clearance. This feature may be a short circuit for Ar gas flows which is more pronounced in the case of one line working at higher pressures. In this case, the relative difference between calculated and experimental pressures is larger.

Experiment label	Sample $T_{melting}$ Melting pressure	Ar total experimental Pressure	Temperature and input conditions:	Ar calculated pressure (bar)
CHIP 23-09-08	Pure Ag 1234 K $3.78\ 10^{-6}$ bar	**$9.1\ 10^{-5}$ bar**	$T_{nozzles}$ = 1045 K $T_{cracker}$ = 1770 K $T_{condenser}$ = 1234 K Ar/I_2=0.632 bar Ar/CsOH=0.050 bar	 $4.49\ 10^{-4}$ bar $4.91\ 10^{-5}$ bar Total (meas.) **$4.98\ 10^{-4}$ bar**
CHIP 25-09-08	Pure Ni 1726 K $4.135\ 10^{-6}$ bar	**$1.5\ 10^{-4}$ bar**	$T_{nozzles}$ = 1012 K $T_{cracker}$ = 1853 K $T_{condenser}$ = 1726 K Ar/I_2=0.0994 bar Ar/CsOH=0.051 bar	 $2.47\ 10^{-5}$ bar $6.30\ 10^{-5}$ bar Total (meas.) **$8.77\ 10^{-5}$ bar**

Table V-2. Comparison of the Ar experimental pressures at the condenser as refered by calibration to the Ag and Ni melting pressures with the calculated pressures from the known input pressures at the nozzles. The only two lines Ar/I_2 and Ar/CsOH operated (see text). In the last column, calculations take into account of each line contribution, and experimental pressures have to be compared to the total measured pressure of Ar.

Moreover, although accurate knowledge of the nozzles initial dimensions was established, these tests show that keeping these dimensions in a corrosive environment is essential for

further accurate calibrations of any gaseous species by reference to Ar pressures at the condenser.

For the present device the two calibration runs show that the real pressure of Ar cannot be known within ± 80% using the relation,

$$\frac{\delta p}{p} = \frac{p_{meas.} - p_{calc.}}{p_{calc.}} \qquad (24)$$

This uncertainty is related for one part to the mechanical structure that allows some leaks and for another part to the carrier gas regime for Ar that have been intentionally chosen close to the Knudsen limits. Indeed, for these conditions increasing the Ar pressure at constant temperature showed effectively a decrease of the Ag pressure that can be attributed to collisions in the molecular beam – light atoms "push" away the heavy ones –. This feature is to be analyzed in the future as a function of total pressure in order to set up better conditions for mass spectrometric analysis when decreasing the Ar pressure in the CHIP reactor.

V.8. CONCLUSIONS AND PERSPECTIVES

The present CHIP reactor has been built for two main purposes, - (i) give a diagnostic of molecules that undergo kinetic limitations within temperature and time conditions similar to a severe nuclear accident in the hot branch of the primary cooling circuit, - (ii) determine kinetic constants for the main reactions that show kinetic limitations in the homogeneous gas phase issued from the accident. Owing to the real challenge of such new and specific research and due to technical difficulties related to Iodine chemistry, the present work was circumvented to the calculation, the construction and the qualification tests of the CHIP reactor.

Flow calculations were performed in order to – (i) first propose a design of the device compatible with the monitoring of very small flows, equal to Knudsen flows, - (ii) second allow calculations of carrier gas pressures as a function of input pressures in view of mass spectrometric calibrations. The retained structure combines gas introduction with a chocked regime and matter flow at high temperature in the molecular regime.

The CHIP reactor device was built in collaboration with the engineering service of DPAM/IRSN in order to afford the complexity of the mechanical structure in a very demanding mass spectrometric environment: Ultra High Vacuum (≈ 10^{-6} to 10^{-8} mbar), accuracy of the mechanical positioning (± 0.05mm) of the final effusion orifice, high temperature (from room temperature up to 1900 K), four stages furnace and limited space in the mass spectrometer. Owing to the numerous constraints, the present device is complex, and probably will become simpler when all possible tests will be completed. This "simplifying" step will improve certainly the intrinsic performances as checked in this study.

The present tests of the CHIP reactor showed that for:

1-Thermal behaviour:

- The condenser temperature, starting from 1800 K can be decreased down to 800 K for a constant cracker temperature at 1800 K.
- The temperature gradient between cracker and condenser has been evaluated combining experimental determinations and thermal simulations. A cold point exists at high temperature, but in the 800 to 1300 K range for the condenser this cold point disappears. Improvements are possible up to 1400 K when using a special combination of radial and cylindrical thermal shields between the cracker and the condenser.

The working temperature range of the condenser is thus fully compatible with the expected hot leg temperature and the temperature gradient is known in this working range. Note that the influence of the temperature uncertainty on this gradient has a non negligible impact on further kinetic studies and minimization of this impact can be done when using a transfer tube working in quasi-equilibrium state once the input and output orifices are well managed.

2- Mechanical behaviour:

- The positioning of the ultimate orifice – the effusion orifice – along the axis of the mass spectrometric ion source worked satisfactorily at any temperature and allows correct measurements of the useful molecular beam (source of molecules).
- The locking of the reactor position by a wedge is not entirely satisfactory because this way of fixing the position may be a cause for gas leaks.

For future experiments, the mechanical equilibrium positioning of the reactor should be reached and complementary tests should be performed in order – (i) to improve the reliability of the different parts piled up – (ii) to clearly evaluate the leak flow relative value as compared to effusion flow.

3- Chemical and flow behaviour:

- The clogging of the nozzles due to corrosion by pure iodine at a pressure of 1 mbar occured in the range of desired input flow values.
- A clogging by oxides occured also when vacuum conditions are not good enough in the nozzles.
- Argon condenser pressure calculations from known input pressures do not reproduce accurately (uncertainty is about ± 80%) those obtained by calibration with Ag and Ni pressures at the melting temperature.

Further progresses are underground using new materials after preliminary tests performed at IRSN. Besides, the chemical behaviour of the high temperature stage of the reactor could not be ascertained since pure iodine input could not be done a long time enough. Special tests performed at IRSN showed that the reaction of Iodine with alumina seems weak, but in further mass spectrometric experiments search for aluminium iodides or oxo-iodides should be done. Tentative of pressure calibrations with pure known components – Ag and Ni - for the Ar pressure in the condenser as analyzed by the mass spectrometer showed large uncertainties. Note that kinetic effects will be effectively detected for molecules produced with very slow rate processes when evaluated relatively to this large uncertainty: this evaluation must be performed via simulation of the flow regime in the CHIP reactor (as done at the modelling service of DPAM/IRSN) taking into account the flow regime with reactions at equilibrium as a reference since the only pressure detected is not a direct parameter to judge the reality of kinetic effects.

As a perspective, the present state of the reactor allows the diagnostics of the chemical behaviour of simple systems – as for exemple Cs(g) + I(g) recombination starting from CsI vaporization and cracking, or the addition of H_2 for observation of the production HI(g) – but probably not the evaluation of kinetic constants due to the lack of reproducibility and accurate calibrations. For further kinetic studies, improvements of the mechanical, thermal and chemical behaviour of the CHIP reactor have to be undertaken, probably with a most simple

device able to reduce the uncertainty within a range of ± 30% as usual in mass spectrometry when run with convenient calibrations.

REFERENCES

[1] M.Tmar and C.Chatillon, "Refinement of the vapor pressures in equilibrium over the InP and InAs compounds by mass spectrometry," J. Chem. Thermodynamics, Vol. 19, 1987, pp. 1053 -1063.

[2] M.Heyrman, C. Chatillon, H. Collas, and J.-L. Chemin, "Improvements and new capabilities for the multiple Knudsen cell device used in high temperature mass spectrometry," Rap. Comm. Mass Spectrom., Vol. 18, 2004, pp. 163 -174.

[3] P.Morland, C.Chatillon, and P.Rocabois, "High Temperature Mass Spectrometry Using the Knudsen Effusion Cell. I-Optimization of Sampling Constaints on the Molecular Beam," J. High Temp. & Mat. Sci., Vol. 37, 1997, pp. 167-187.

[4] J.Drowart, C.Chatillon, J. Hastie, and D. Bonnell, "High-Temperature Mass Spectrometry: Instrumental Techniques, Ionisation Cross-Sections, Pressure Measurements, and Thermodynamic Data," J. Pure Appl. Chem., Vol. 77, 2005, pp. 683-737.

[5] D.J.Santeler, "New Concepts in Molecular Gas Flow," J. Vac. Sci. Technol, Vol. A4, 1986, pp. 338-343.

[6] R.P.Henry, "Cours de Science et Technique du vide", Livre I, Tome II, Soc. Franç. Vide, Paris, 1968, pp. 1-21.

[7] D.J.Santeler, "Exit loss in viscous tube flow," J. Vac. Sci. Technol, Vol. A 4 (3), 1986, pp. 348-352.

[8] S.F.DeMuth and J.S.Watson, "Prediction of flow rates trough an orifice at pressures corresponding to the transition between molecular and isentropic flow," J. Vac. Sci. Technol. , Vol. A 4, 1986, pp. 244-347.

[9] J.Delafosse and G.Mongodin, "Les calculs de la technique du vide", Ed.: la société Française des Ingénieurs et Techniciens du vide, 1961.

[10] P.Violet, "private communication during a PhD work", INP, Grenoble, 2008.

[11] B.Simondi-Teisseire, "Seventh half-yearly Progress Report of the Source Term Program N°80," DPAM-SEREA-2008-250, Vol., pp. 14-17.

[12] R.Hultgren, P.D.Desai, D.T.Hawkins, M.Gleiser, K.K.Kelley, and D.D.Wagman, "Selected Value of the Thermodynamic Properties of the Elements", American Society for Metals, Ohio, 1973.

APPENDIX V-A

This program in visual basic is used in Excel software. It permits calculation of Ar pressures at the entry of the cracking cell and condenser for input data (temperature and pressures of introduction of each line) corresponding to run CHIP230908-test with Ar in the condenser.

```
Public Reff, Leff, Leffeq, Rorif1, Rtub1, Rtub2, P0, P1, P2, R, P, Theta, Z, L1, M
Public Rbuse1, Rbuse2, Lbuse1, Lbuse2, Lbuse1eq, Lbuse2eq
Public Lmbuse1, Lmbuse2, Lmbuse3, Lmorif1, Lmtub1
Public Kbvis1, Kbvis2, Korif1, Ktub1, Etabuse, Etatub1, Etaorif1
Public Pst, Ptub1e, Ptub1s, Ptub2e, Ptub2s, Ptub3e, Ptub3s
Public Cbchoc1, Cbchoc2, Cbmol1, Cbmol2, Ctub1, Corif1, Cchocorif1, Cchocorif2, Gamma, Choc
Public Cbaf14, Cbaf13, Cbaf34, Cbaf33, Cbafint4, Cbafint3, Centre4, Centre3, Ccraq, Ceff, Ccond, Corif3,
Ctub2, Corif2, Cbaffix4, Cbaffix3, Ctot
Public Qsant, Qeff, Qchoc, Qchocvis, Qhag, Qtran, QtranS, Qmolbuse1, Qmolbuse2, Qmolbuse3, Clbuse1,
Clbuse2, Clbuse3, Kn1, Kn2, Kn3
Public Tbuse, Tcraq, Ttub1, Ttub2, Teff, T, T0, Clbuse, Rg, Kn, Delta, Nav, Ca, Pcraq, Qcraq, Peff
**************************************************************************
Sub variables()    'Ensemble des constantes et variables intermédiaires à calculer avant de lancer les programmes.
Pi = 4 * Atn(1)
'Dimensions en MKSA'
Pst = 100000
Rg = 8.3145
Viscosité     'défini les constantes reliées à une espèce Masse, eta...choc...
'M = 0.04    'Masse en kg pour Ar(g) est defini dans le sous prog. viscosité Mar'
'Delta = 2.9 * 10 ^ -10 ' Delta est défini dans Viscosité
Nav = 6.02252 * 10 ^ 23
Ca = 1.05  'cste de De Muth pour régime de transition'

Reff = 0.001  'en m' rayon de l'orifice d'effusion
Leff = 0.002  'en m' longueur
Leffeq = Leff * (1 + 1 / (3 + (3 * Leff) / (7 * Reff))) 'longueur equivalente orifice - correction de Santeler
Claus = 1 / (1 + (3 * Leffeq) / (8 * Reff)) 'coefficient de Clausing de l'orifice d'effusion

Rcond = 0.019  'en m' rayon du condenseur
Lcond = 0.038  'en m' sans les baffles
Lcondeq = Lcond * (1 + 1 / (3 + (3 * Lcond) / (7 * Rcond))) 'longueur equivalente orifice - correction de
Santeler
Clauscond = 1 / (1 + (3 * Lcondeq) / (8 * Rcond)) 'coefficient de Clausing

Rorif3 = 0.002  'en m' orifice entrée condenseur = sortie craq.
Lorif3 = 0.004  'en m'
Lorif3eq = Lorif3 * (1 + 1 / (3 + (3 * Lorif3) / (7 * Rorif3))) 'longueur equivalente orifice - correction de
Santeler
Clausorif3 = 1 / (1 + (3 * Lorif3eq) / (8 * Rorif3)) 'coefficient de Clausing de l'orifice3

Rtub2 = 0.006  'en m' tube de transfert entre craqueur et condenseur
Ltub2 = 0.0725  'en m'
Ltub2eq = Ltub2 * (1 + 1 / (3 + (3 * Ltub2) / (7 * Rtub2))) 'longueur equivalente orifice - correction de Santeler
Claustub2 = 1 / (1 + (3 * Ltub2eq) / (8 * Rtub2)) 'coefficient de Clausing

Rorif2 = 0.002  'en m' orifice sortie craqueur
Lorif2 = 0.004  'en m'
```

```
Lorif2eq = Lorif2 * (1 + 1 / (3 + (3 * Lorif2) / (7 * Rorif2))) 'longueur equivalente orifice - correction de
Santeler
Clausorif2 = 1 / (1 + (3 * Lorif2eq) / (8 * Rorif2)) 'coefficient de Clausing de l'orifice2

Rcraq = 0.019  'en m' rayon du craqueur
Lcraq = 0.0495  'en m'
Lcraqeq = Lcraq * (1 + 1 / (3 + (3 * Lcraq) / (7 * Rcraq))) 'longueur equivalente orifice - correction de Santeler
Clauscraq = 1 / (1 + (3 * Lcraqeq) / (8 * Rcraq)) 'coefficient de Clausing

Rbaffix = 0.003  'en m' rayon de la baffle fixe à 3 trous
Lbaffix = 0.0125  'en m'
Lbaffixeq = Lbaffix * (1 + 1 / (3 + (3 * Lbaffix) / (7 * Rbaffix))) 'longueur equivalente orifice - correction de
Santeler
Clausbaffix = 1 / (1 + (3 * Lbaffixeq) / (8 * Rbaffix)) 'coefficient de Clausing en sortie de baffle fixe

Rbaf1 = 0.0025  'en m' rayon de la baffle mobile à 1 trou
Lbaf1 = 0.005  'en m'
Lbaf1eq = Lbaf1 * (1 + 1 / (3 + (3 * Lbaf1) / (7 * Rbaf1))) 'longueur equivalente orifice - correction de Santeler
Clausbaf1 = 1 / (1 + (3 * Lbaf1eq) / (8 * Rbaf1)) 'coefficient de Clausing en sortie de baffle mobile

Rbaf3 = 0.0015  'en m' rayon de la baffle mobile à 3 trous
Lbaf3 = 0.005  'en m'
Lbaf3eq = Lbaf3 * (1 + 1 / (3 + (3 * Lbaf3) / (7 * Rbaf3))) 'longueur equivalente orifice - correction de Santeler
Clausbaf3 = 1 / (1 + (3 * Lbaf3eq) / (8 * Rbaf3)) 'coefficient de Clausing en sortie de baffle fixe

Rbafint = 0.017  'en m' rayon de l'espace inter-baffles
Lbafint = 0.003  'en m'
Lbafinteq = Lbafint * (1 + 1 / (3 + (3 * Lbafint) / (7 * Rbafint))) 'longueur equivalente orifice - correction de
Santeler
Clausbafint = 1 / (1 + (3 * Lbafinteq) / (8 * Rbafint)) 'coefficient de Clausing en sortie de baffle fixe

Rentre = 0.017  'en m' rayon de l'espace d'entrée cond. ou craqueur = amont de la baffle fixe
Lentre = 0.003  'en m'
Lentreeq = Lentre * (1 + 1 / (3 + (3 * Lentre) / (7 * Rentre))) 'longueur equivalente orifice - correction de
Santeler
Clausentre = 1 / (1 + (3 * Lentreeq) / (8 * Rentre)) 'coefficient de Clausing

Rorif1 = 0.0003  'en m' orifice entrée craqueur
Lorif1 = 0.004  'en m'
Lorif1eq = Lorif1 * (1 + 1 / (3 + (3 * Lorif1) / (7 * Rorif1))) 'longueur equivalente orifice - correction de
Santeler
Clausorif1 = 1 / (1 + (3 * Lorif1eq) / (8 * Rorif1)) 'coefficient de Clausing de l'orifice1

Rtub1 = 0.00445  'en m' tube de transfert entre buses et craqueur
Ltub1 = 0.067  'en m'
Ltub1eq = Ltub1 * (1 + 1 / (3 + (3 * Ltub1) / (7 * Rtub1))) 'longueur equivalente orifice - correction de Santeler
Claustub1 = 1 / (1 + (3 * Ltub1eq) / (8 * Rtub1)) 'coefficient de Clausing

        'Rbuse = 0.000025 '(en m)rayon buse à définir dans les sous progammes
Rbuse1 = 0.000025 ' (en m) rayon buse de l'iode et H2/H2O
Lbuse1 = 0.0003 '(en m) longueur buse
Lbuse1eq = Lbuse1 * (1 + 1 / (3 + 3 * Lbuse1 / (7 * Rbuse1))) 'longueur equivalente buse1
Clbuse1 = 1 / (1 + (3 * Lbuse1eq) / (8 * Rbuse1)) ' coefficient Clausing sortie buse1
Rbuse2 = 0.00005 ' (en m) rayon buse du CsOH
Lbuse2 = 0.00045 '(en m) longueur buse
Lbuse2eq = Lbuse2 * (1 + 1 / (3 + 3 * Lbuse2 / (7 * Rbuse2))) 'longueur equivalente buse2
Clbuse2 = 1 / (1 + (3 * Lbuse2eq) / (8 * Rbuse2)) ' coefficient Clausing sortie buse2
        'Eta0 = 0.0000229     'viscosité Ar à 300°K MKSA'
        'depend des temperatures à définir dans les sous programmes
```

```
Ceff = Claus * Pi * Reff ^ 2 / ((2 * Pi * M * Rg * Teff) ^ (1 / 2)) ' conductance orifice effusion en flux moleculaire (moles/s)
Ccond = Clauscond * Pi * Rcond ^ 2 / ((2 * Pi * M * Rg * Teff) ^ (1 / 2))          'volume condenseur
Corif3 = Clausorif3 * Pi * Rorif3 ^ 2 / ((2 * Pi * M * Rg * Teff) ^ (1 / 2))       'orifice 3 entrée condenseur
'conductance intégrée sur gradient de T
'Ctub2 = (Claustub2 * (3 / 2) * (Pi * Rtub2 ^ 2) / ((2 * Pi * M * Rg) ^ (1 / 2))) * (((Tcraq ^ (1 / 2)) + (Teff ^ (1 / 2))) / (Teff + (Tcraq ^ (1 / 2)) * (Teff ^ (1 / 2)) + Teff)) 'tube liaison craqueur - condenseur
'conductance fixe à T moyen
Ctub2 = (Claustub2 * (Pi * Rtub2 ^ 2) / ((2 * Pi * M * Rg * Ttub2) ^ (1 / 2)))
Corif2 = Clausorif2 * Pi * Rorif2 ^ 2 / ((2 * Pi * M * Rg * Tcraq) ^ (1 / 2))      'orifice 2 sortie condenseur
Ccraq = Clauscraq * Pi * Rcraq ^ 2 / ((2 * Pi * M * Rg * Tcraq) ^ (1 / 2))         'volume craqueur
Cbaffix4 = Clausbaffix * Pi * Rbaffix ^ 2 / ((2 * Pi * M * Rg * Teff) ^ (1 / 2))   'baffle fixe pour l'étage 4 condenseur'
Cbaffix3 = Clausbaffix * Pi * Rbaffix ^ 2 / ((2 * Pi * M * Rg * Tcraq) ^ (1 / 2))  'baffle fixe pour l'étage 3 craqueur'
Cbaf14 = Clausbaf1 * Pi * Rbaf1 ^ 2 / ((2 * Pi * M * Rg * Teff) ^ (1 / 2))        'baffle mobile 1 orifice
Cbaf13 = Clausbaf1 * Pi * Rbaf1 ^ 2 / ((2 * Pi * M * Rg * Tcraq) ^ (1 / 2))       'baffle mobile 1  orifice
Cbaf34 = 3 * Clausbaf3 * Pi * Rbaf3 ^ 2 / ((2 * Pi * M * Rg * Teff) ^ (1 / 2))    'baffle mobile 3 orifices
Cbaf33 = 3 * Clausbaf3 * Pi * Rbaf3 ^ 2 / ((2 * Pi * M * Rg * Tcraq) ^ (1 / 2))   'baffle mobile 3 orifices
Cbafint4 = Clausbafint * Pi * Rbafint ^ 2 / ((2 * Pi * M * Rg * Teff) ^ (1 / 2))   'espace inter baffles mobiles étage 4
Cbafint3 = Clausbafint * Pi * Rbafint ^ 2 / ((2 * Pi * M * Rg * Tcraq) ^ (1 / 2))  'espace inter baffles mobiles étage 3
Centre4 = Clausentre * Pi * Rentre ^ 2 / ((2 * Pi * M * Rg * Teff) ^ (1 / 2))      'espace entrée - baffle fixe étage 4
Centre3 = Clausentre * Pi * Rentre ^ 2 / ((2 * Pi * M * Rg * Tcraq) ^ (1 / 2))     'espace entrée - baffle fixe étage 3
Corif1 = Clausorif1 * Pi * Rorif1 ^ 2 / ((2 * Pi * M * Rg * Tcraq) ^ (1 / 2))      'orifice d'entrée dans le craqueur
'conductance selon formules L. Michelutti sur intégration volumique'
'Ctub1 = (Claustub1 * Pi * Rtub1 ^ 2 / ((2 * Pi * M * Rg) ^ (1 / 2))) * ((Tcraq - Tbuse) / 2 * 1 / (Tcraq ^ (3 / 2) - Tbuse ^ (3 / 2)))
'conductance des tubes 1 sur intégration molaire (notre calcul)'
'Ctub1 = (Claustub1 * (3 / 2) * (Pi * Rtub1 ^ 2) / ((2 * Pi * M * Rg) ^ (1 / 2))) * (((Tcraq ^ (1 / 2)) + (Tbuse ^ (1 / 2))) / (Tcraq + (Tcraq ^ (1 / 2)) * (Tbuse ^ (1 / 2)) + Tbuse))
'conductance des tubes 1 fixe à T moyen
Ctub1 = Claustub1 * (Pi * Rtub1 ^ 2) / ((2 * Pi * M * Rg * Ttub1) ^ (1 / 2))
'Choc
'Choc = 200
Choc = (Gamma * Rg / M * (2 / (Gamma + 1)) ^ ((Gamma + 1) / (Gamma - 1))) ^ (1 / 2) 'coeff à multiplier par racine de T
Cbchoc1 = Choc * ((Tbuse) ^ (1 / 2)) * (Rbuse1 ^ 2) * Pi / (Rg * Tbuse) 'Conductance choquée sortie buse en moles/s
Cbchoc2 = Choc * ((Tbuse) ^ (1 / 2)) * (Rbuse2 ^ 2) * Pi / (Rg * Tbuse) 'Conductance choquée sortie buse en moles/s
Cchocorif1 = Choc * ((Tcraq) ^ (1 / 2)) * (Rorif1 ^ 2) * Pi / (Rg * Tcraq) 'Conductance choquée sortie orifice1 en moles/s
Cbmol1 = Clbuse1 * Pi * (Rbuse1 ^ 2) / ((2 * Pi * M * Rg * Tbuse) ^ (1 / 2)) 'conductance moleculaire sortie buse en moles/s
Cbmol2 = Clbuse2 * Pi * (Rbuse2 ^ 2) / ((2 * Pi * M * Rg * Tbuse) ^ (1 / 2)) 'conductance moleculaire sortie buse en moles/s

Kbvis1 = Pi * (Rbuse1 ^ 4) / (16 * Etabuse * Lbuse1) / (Rg * Tbuse) 'conductance visqueuse buse en moles/s
Kbvis2 = Pi * (Rbuse2 ^ 4) / (16 * Etabuse * Lbuse2) / (Rg * Tbuse) 'conductance visqueuse buse en moles/s
Korif1 = Pi * (Rorif1 ^ 4) / (16 * Etaorif1 * Lorif1) / (Rg * Tcraq) 'conductance visqueuse orifice1 en moles/s
Ktub1 = Pi * (Rtub1 ^ 4) / (16 * Etatub1 * Ltub1) / (Rg * Ttub1) 'conductance visqueuse tube1(GI) en moles/s
Lmbuse1 = Rg * Tbuse / (2 ^ (1 / 2) * Pi * Delta ^ 2 * Nav) 'libre parcours moyen (en m) = Lm / P (en Pa)'
Lmbuse2 = Rg * Tbuse / (2 ^ (1 / 2) * Pi * Delta ^ 2 * Nav) 'libre parcours moyen (en m) = Lm / P (en Pa)'
Lmorif1 = Rg * Tcraq / (2 ^ (1 / 2) * Pi * Delta ^ 2 * Nav) 'libre parcours moyen (en m) = Lm / P (en Pa)'
Lmtub1 = Rg * ((Tcraq + Tbuse) / 2) / (2 ^ (1 / 2) * Pi * Delta ^ 2 * Nav) 'libre parcours moyen (en m) = Lm / P (en Pa)'
Lmeff = Rg * Teff / (2 ^ (1 / 2) * Pi * Delta ^ 2 * Nav) 'libre parcours moyen (en m) = Lm / P (en Pa)'
```

```
End Sub
*************************************************************************
Sub Condenseur() 'calcul écoulement moléculaire craqueur-condenseur à partir de la
'pression à l'entrée craqueur Pcraq'
Tbuse = 1045 'K
Tcraq = 1770
Teff = 1234    ' T condenseur
Ttub1 = (Tbuse + Tcraq) / 2
Ttub2 = (Tcraq + Teff) / 2
variables

K = 0
J = 0
Worksheets("feuil5").Cells(1 + J, 1 + K).Value = "Pcraq(bar)"
Worksheets("feuil5").Cells(1 + J, 2 + K).Value = "Ctot"
Worksheets("feuil5").Cells(1 + J, 3 + K).Value = "Ceff"
Worksheets("feuil5").Cells(1 + J, 4 + K).Value = "Peff"
Worksheets("feuil5").Cells(1 + J, 5 + K).Value = "log Pcraq/bar"
Worksheets("feuil5").Cells(1 + J, 6 + K).Value = "log Peff/bar"
Worksheets("feuil5").Cells(1 + J, 7 + K).Value = " Peff/Pcraq"
Worksheets("feuil5").Cells(1 + J, 8 + K).Value = "Qeff"


For I = 2 To -2 Step -1
'Pcraq = 10  ' Pcraq entrée craqueur en Pa

Pcraq = 10 ^ I ' Pcraq entrée craqueur en Pa

Ctot = 1 / Centre3 + 1 / Cbaffix3 + 3 / Cbafint3 + 1 / Cbaf13 + 2 / Cbaf33 + 1 / Ccraq
Ctot = Ctot + 1 / Corif2 + 1 / Ctub2 + 1 / Corif3
Ctot = 1 / Ctot + 1 / Centre4 + 1 / Cbaffix4 + 3 / Cbafint4 + 1 / Cbaf14 + 2 / Cbaf34 + 1 / Ccond
Ctot = 1 / Ctot
Peff = Pcraq / (1 + Ceff / Ctot)
Qeff = Peff * Ceff

J = J + 1
Worksheets("feuil5").Cells(1 + J, 1 + K).Value = Pcraq / Pst
Worksheets("feuil5").Cells(1 + J, 2 + K).Value = Ctot
Worksheets("feuil5").Cells(1 + J, 3 + K).Value = Ceff
Worksheets("feuil5").Cells(1 + J, 4 + K).Value = Peff / Pst
Worksheets("feuil5").Cells(1 + J, 5 + K).Value = Log(Pcraq / Pst) / Log(10)
Worksheets("feuil5").Cells(1 + J, 6 + K).Value = Log(Peff / Pst) / Log(10)
Worksheets("feuil5").Cells(1 + J, 7 + K).Value = Peff / Pcraq
Worksheets("feuil5").Cells(1 + J, 8 + K).Value = Qeff

Next I

End Sub
*************************************************************************
Sub ligneGI() ' buse 1 (50 microns) avec un seul tube de liaison pour toute  buse
'= tub1 et pression craqueur imposée '
L = 0
K = 0
J = 0
Tbuse = 1045 'K
Tcraq = 1770
Teff = 1234
Ttub1 = (Tbuse + Tcraq) / 2
Ttub2 = (Tcraq + Teff) / 2
variables
```

```
K = 0
Worksheets("feuil3").Cells(1 + J, 1 + K).Value = "P0"
Worksheets("feuil3").Cells(1 + J, 2 + K).Value = "P0sant"
Worksheets("feuil3").Cells(1 + J, 3 + K).Value = "P0mol"
Worksheets("feuil3").Cells(1 + J, 4 + K).Value = "Qmol"
Worksheets("feuil3").Cells(1 + J, 5 + K).Value = "Qsant"
Worksheets("feuil3").Cells(1 + J, 6 + K).Value = "Qcraq"
Worksheets("feuil3").Cells(1 + J, 7 + K).Value = "QtranS"
Worksheets("feuil3").Cells(1 + J, 8 + K).Value = "test"
Worksheets("feuil3").Cells(1 + J, 9 + K).Value = "P1"
Worksheets("feuil3").Cells(1 + J, 10 + K).Value = "Kn"

K = 12
Worksheets("feuil3").Cells(1 + L, 1 + K).Value = "Orif-1"
Worksheets("feuil3").Cells(1 + L, 4 + K).Value = "Tube-1"
Worksheets("feuil3").Cells(1 + L, 7 + K).Value = "Buse-1"
Q = K + 9
Worksheets("feuil3").Cells(1 + L, 1 + Q).Value = "Orif-1"
Worksheets("feuil3").Cells(1 + L, 4 + Q).Value = "Tube-1"
Worksheets("feuil3").Cells(1 + L, 7 + Q).Value = "Buse-1"
L = L + 1
Worksheets("feuil3").Cells(1 + L, 1 + K).Value = "P2/Pa"
Worksheets("feuil3").Cells(1 + L, 2 + K).Value = "P1/Pa"
Worksheets("feuil3").Cells(1 + L, 3 + K).Value = "P0/Pa"
Q = K + 9
Worksheets("feuil3").Cells(1 + L, 1 + Q).Value = "Log P2/bar"
Worksheets("feuil3").Cells(1 + L, 2 + Q).Value = "Log P1/bar"
Worksheets("feuil3").Cells(1 + L, 3 + Q).Value = "Log P0/bar"
K = K + 3
Worksheets("feuil3").Cells(1 + L, 1 + K).Value = "P2/Pa"
Worksheets("feuil3").Cells(1 + L, 2 + K).Value = "P1/Pa"
Worksheets("feuil3").Cells(1 + L, 3 + K).Value = "P0/Pa"
Q = K + 9
Worksheets("feuil3").Cells(1 + L, 1 + Q).Value = "Log P2/bar"
Worksheets("feuil3").Cells(1 + L, 2 + Q).Value = "Log P1/bar"
Worksheets("feuil3").Cells(1 + L, 3 + Q).Value = "Log P0/bar"
K = K + 3
Worksheets("feuil3").Cells(1 + L, 1 + K).Value = "P2/Pa"
Worksheets("feuil3").Cells(1 + L, 2 + K).Value = "P1/Pa"
Worksheets("feuil3").Cells(1 + L, 3 + K).Value = "P0/Pa"
Q = K + 9
Worksheets("feuil3").Cells(1 + L, 1 + Q).Value = "Log P2/bar"
Worksheets("feuil3").Cells(1 + L, 2 + Q).Value = "Log P1/bar"
Worksheets("feuil3").Cells(1 + L, 3 + Q).Value = "Log P0/bar"
Worksheets("feuil3").Cells(1 + L, 4 + Q).Value = "Log Pcraq/bar"
Worksheets("feuil3").Cells(1 + L, 5 + Q).Value = "Log Peff/bar"

'calcul de la conductance entre craqueur et condenseur
Ctot = 1 / Centre3 + 1 / Cbaffix3 + 3 / Cbafint3 + 1 / Cbaf13 + 2 / Cbaf33 + 1 / Ccraq
Ctot = Ctot + 1 / Corif2 + 1 / Ctub2 + 1 / Corif3
Ctot = 1 / Ctot + 1 / Centre4 + 1 / Cbaffix4 + 3 / Cbafint4 + 1 / Cbaf14 + 2 / Cbaf34 + 1 / Ccond
Ctot = 1 / Ctot
K = 0
For I = 2 To -3 Step -0.25
'les pressions sont calculées en Pa'
'Pcraq = 10 'Pa'
Pcraq = 10 ^ I 'Pa'
'Peff = 10 ^ (Log(Pcraq) / Log(10) - 0.2359)
'Qcraq = (Pcraq * Corif2) / 3 'même flux dans chacune des 3 lignes'
```

```
Peff = Pcraq / (1 + Ceff / Ctot)   'calcule la Peff et le Qeff (flux) correspondant à Pcraq
Qeff = Peff * Ceff
Qcraq = Qeff
Ptub1s = Qcraq / Corif1 + Pcraq
P2 = Pcraq
P1 = Qcraq / Cchocorif1
'P0sant = (Qcraq * (1 / Korif1 + Qcraq / (Cchocorif1 ^ 2))) ^ (1 / 2) 'élimination de P1'
P0sant = (Cchocorif1 / (2 * Korif1)) * ((2 * Korif1 * Qcraq / (Cchocorif1 ^ 2) + 1) ^ 2 - 1) ^ 1 / 2
P0mol = (Qcraq / Corif1) + P2
'Résolution de la transition avec Santeler dans l'orifice 1'*****************************
J = J + 1
If P0mol > P0sant Then
P0max = P0mol * 1.2
P0min = P0sant * 0.9
Else
P0max = P0sant * 1.1
P0min = P0mol * 0.9
End If
pas = (P0max - P0min) / 10
Line1:
For P0 = P0min To P0max Step pas
Qsant = (Cchocorif1 ^ 2 / (2 * Korif1)) * ((1 + (2 * Korif1 * P0 / Cchocorif1) ^ 2) ^ (1 / 2) - 1) ' débit buse+choc
en moles/s'
Lmoyen = Lmorif1 / ((P1 + P0) / 2)
Kn1 = Lmoyen / (2 * Rorif1)  'attention DeMuth definit Kn à l'inverse
Qmol = Corif1 * (P0 - P2)
'QtranS = Qsant * (1 - Ca ^ -Kn1) + Qmol * (Ca ^ - Kn1) formule DeMuth
QtranS = Qsant * (1 - Ca ^ (-1 / Kn1)) + Qmol * Ca ^ (-1 / Kn1)  'inversion du Kn
Test = QtranS - Qcraq
J = J + 1
Worksheets("feuil3").Cells(1 + J, 1 + K).Value = P0
Worksheets("feuil3").Cells(1 + J, 2 + K).Value = P0sant
Worksheets("feuil3").Cells(1 + J, 3 + K).Value = P0mol
Worksheets("feuil3").Cells(1 + J, 4 + K).Value = Qmol
Worksheets("feuil3").Cells(1 + J, 5 + K).Value = Qsant
Worksheets("feuil3").Cells(1 + J, 6 + K).Value = Qcraq
Worksheets("feuil3").Cells(1 + J, 7 + K).Value = QtranS
Worksheets("feuil3").Cells(1 + J, 8 + K).Value = Test
Worksheets("feuil3").Cells(1 + J, 9 + K).Value = P1
Worksheets("feuil3").Cells(1 + J, 10 + K).Value = Kn1

If Test > 0 Then
P0min = P0 - pas
P0max = P0 + pas
pas = pas / 10
J = J + 1
Worksheets("feuil3").Cells(1 + J, 1 + K).Value = "P0min"
Worksheets("feuil3").Cells(1 + J, 2 + K).Value = "P0max"
J = J + 1
Worksheets("feuil3").Cells(1 + J, 1 + K).Value = P0min
Worksheets("feuil3").Cells(1 + J, 2 + K).Value = P0max
J = J + 1
If pas < P0 / 100000 Then
GoTo Line2:
End If
'L = L + 1
GoTo Line1:
End If

Next P0
```

```
Line2:
K = 0
J = J + 1
Worksheets("feuil3").Cells(1 + J, 1 + K).Value = "Orif1"
J = J + 1
Worksheets("feuil3").Cells(1 + J, 1 + K).Value = "P0"
Worksheets("feuil3").Cells(1 + J, 2 + K).Value = "P0sant"
Worksheets("feuil3").Cells(1 + J, 3 + K).Value = "P0mol"
Worksheets("feuil3").Cells(1 + J, 4 + K).Value = "Qmol"
Worksheets("feuil3").Cells(1 + J, 5 + K).Value = "Qsant"
Worksheets("feuil3").Cells(1 + J, 6 + K).Value = "Qcraq"
Worksheets("feuil3").Cells(1 + J, 7 + K).Value = "QtranS"
Worksheets("feuil3").Cells(1 + J, 8 + K).Value = "test"
Worksheets("feuil3").Cells(1 + J, 9 + K).Value = "P1"
Worksheets("feuil3").Cells(1 + J, 10 + K).Value = "Kn"

J = J + 1
Worksheets("feuil3").Cells(1 + J, 1 + K).Value = P0
Worksheets("feuil3").Cells(1 + J, 2 + K).Value = P0sant
Worksheets("feuil3").Cells(1 + J, 3 + K).Value = P0mol
Worksheets("feuil3").Cells(1 + J, 4 + K).Value = Qmol
Worksheets("feuil3").Cells(1 + J, 5 + K).Value = Qsant
Worksheets("feuil3").Cells(1 + J, 6 + K).Value = Qcraq
Worksheets("feuil3").Cells(1 + J, 7 + K).Value = QtranS
Worksheets("feuil3").Cells(1 + J, 8 + K).Value = Test
Worksheets("feuil3").Cells(1 + J, 9 + K).Value = P1
Worksheets("feuil3").Cells(1 + J, 10 + K).Value = Kn1

'Sorties des résultats seuls'
L = L + 1
K = 12
Worksheets("feuil3").Cells(1 + L, 1 + K).Value = P2
Worksheets("feuil3").Cells(1 + L, 2 + K).Value = P1
Worksheets("feuil3").Cells(1 + L, 3 + K).Value = P0


Q = K + 9
Worksheets("feuil3").Cells(1 + L, 1 + Q).Value = Log(P2 / Pst) / Log(10)
Worksheets("feuil3").Cells(1 + L, 2 + Q).Value = Log(P1 / Pst) / Log(10)
Worksheets("feuil3").Cells(1 + L, 3 + Q).Value = Log(P0 / Pst) / Log(10)
Q = K + 15
Worksheets("feuil3").Cells(1 + L, 4 + Q).Value = Log(Pcraq / Pst) / Log(10)
Worksheets("feuil3").Cells(1 + L, 5 + Q).Value = Log(Peff / Pst) / Log(10)

K = 0
Porif1s = P1
Ptub1s = P0
J = J + 4
Worksheets("feuil3").Cells(1 + J, 1 + K).Value = "P0"
Worksheets("feuil3").Cells(1 + J, 2 + K).Value = "P0sant"
Worksheets("feuil3").Cells(1 + J, 3 + K).Value = "P0mol"
Worksheets("feuil3").Cells(1 + J, 4 + K).Value = "Qmol"
Worksheets("feuil3").Cells(1 + J, 5 + K).Value = "Qsant"
Worksheets("feuil3").Cells(1 + J, 6 + K).Value = "Qcraq"
Worksheets("feuil3").Cells(1 + J, 7 + K).Value = "QtranS"
Worksheets("feuil3").Cells(1 + J, 8 + K).Value = "test"
Worksheets("feuil3").Cells(1 + J, 9 + K).Value = "P1"
Worksheets("feuil3").Cells(1 + J, 10 + K).Value = "Kn"

'boucle pour calcul de l'écoulement dans le tube 1'
```

```
'les pressions sont calculées en Pa'
P1 = Ptub1s
P2 = P1
P0sant = (Qcraq / Ktub1 + P1 ^ 2) ^ (1 / 2) 'formule d'Hagen-Poiseuille pour le tube de transfert entrée craqueur car pas d'orifice de sortie'
P0mol = (Qcraq / Ctub1) + P1
'Résolution de la transition avec Santeler-Hagen  dans le tube 1'*****************************
J = J + 1
If P0mol > P0sant Then
P0max = P0mol * 1.1
P0min = P0sant * 0.9
Else
P0max = P0sant * 1.1
P0min = P0mol * 0.9
End If
pas = (P0max - P0min) / 10
Line3:
For P0 = P0min To P0max Step pas
Qsant = Ktub1 * (P0 ^ 2 - P1 ^ 2)  ' flux molaire/s tube1 en visqueux-laminaire = Hagen-Poiseuille'
Lmoyen = Lmtub1 / ((P1 + P0) / 2)
Kn1 = Lmoyen / (2 * Rtub1)
Qmol = Ctub1 * (P0 - P1)
'QtranS = Qsant * (1 - Ca ^ -Kn1) + Qmol * (Ca ^ -Kn1)
QtranS = Qsant * (1 - Ca ^ (-1 / Kn1)) + Qmol * (Ca ^ (-1 / Kn1))
Test = QtranS - Qcraq
J = J + 1
Worksheets("feuil3").Cells(1 + J, 1 + K).Value = P0
Worksheets("feuil3").Cells(1 + J, 2 + K).Value = P0sant
Worksheets("feuil3").Cells(1 + J, 3 + K).Value = P0mol
Worksheets("feuil3").Cells(1 + J, 4 + K).Value = Qmol
Worksheets("feuil3").Cells(1 + J, 5 + K).Value = Qsant
Worksheets("feuil3").Cells(1 + J, 6 + K).Value = Qcraq
Worksheets("feuil3").Cells(1 + J, 7 + K).Value = QtranS
Worksheets("feuil3").Cells(1 + J, 8 + K).Value = Test
Worksheets("feuil3").Cells(1 + J, 9 + K).Value = P1
Worksheets("feuil3").Cells(1 + J, 10 + K).Value = Kn1

If Test > 0 Then
P0min = P0 - pas
P0max = P0 + pas
pas = pas / 10
J = J + 1
Worksheets("feuil3").Cells(1 + J, 1 + K).Value = "P0min"
Worksheets("feuil3").Cells(1 + J, 2 + K).Value = "P0max"
J = J + 1
Worksheets("feuil3").Cells(1 + J, 1 + K).Value = P0min
Worksheets("feuil3").Cells(1 + J, 2 + K).Value = P0max
J = J + 1
If pas < P0 / 100000 Then
GoTo Line4:
End If
'L = L + 1
GoTo Line3:
End If

Next P0
Line4:
K = 0
J = J + 1
Worksheets("feuil3").Cells(1 + J, 1 + K).Value = "Tub1"
```

```
J = J + 1
Worksheets("feuil3").Cells(1 + J, 1 + K).Value = "P0"
Worksheets("feuil3").Cells(1 + J, 2 + K).Value = "P0sant"
Worksheets("feuil3").Cells(1 + J, 3 + K).Value = "P0mol"
Worksheets("feuil3").Cells(1 + J, 4 + K).Value = "Qmol"
Worksheets("feuil3").Cells(1 + J, 5 + K).Value = "Qsant"
Worksheets("feuil3").Cells(1 + J, 6 + K).Value = "Qcraq"
Worksheets("feuil3").Cells(1 + J, 7 + K).Value = "QtranS"
Worksheets("feuil3").Cells(1 + J, 8 + K).Value = "test"
Worksheets("feuil3").Cells(1 + J, 9 + K).Value = "P1"
Worksheets("feuil3").Cells(1 + J, 10 + K).Value = "Kn"

J = J + 1
Worksheets("feuil3").Cells(1 + J, 1 + K).Value = P0
Worksheets("feuil3").Cells(1 + J, 2 + K).Value = P0sant
Worksheets("feuil3").Cells(1 + J, 3 + K).Value = P0mol
Worksheets("feuil3").Cells(1 + J, 4 + K).Value = Qmol
Worksheets("feuil3").Cells(1 + J, 5 + K).Value = Qsant
Worksheets("feuil3").Cells(1 + J, 6 + K).Value = Qcraq
Worksheets("feuil3").Cells(1 + J, 7 + K).Value = QtranS
Worksheets("feuil3").Cells(1 + J, 8 + K).Value = Test
Worksheets("feuil3").Cells(1 + J, 9 + K).Value = P1
Worksheets("feuil3").Cells(1 + J, 10 + K).Value = Kn1

K = 15

Worksheets("feuil3").Cells(1 + L, 1 + K).Value = P2
Worksheets("feuil3").Cells(1 + L, 2 + K).Value = P1
Worksheets("feuil3").Cells(1 + L, 3 + K).Value = P0
Q = K + 9
Worksheets("feuil3").Cells(1 + L, 1 + Q).Value = Log(P2 / Pst) / Log(10)
Worksheets("feuil3").Cells(1 + L, 2 + Q).Value = Log(P1 / Pst) / Log(10)
Worksheets("feuil3").Cells(1 + L, 3 + Q).Value = Log(P0 / Pst) / Log(10)


K = 0

'boucle pour calcul de l'écoulement dans la buse GI''''''''''''''''''''''''''''''''''''''''''''''''''''''''''''''''''''''''''''''''''''''''''''''''''''
J = J + 4
Worksheets("feuil3").Cells(1 + J, 1 + K).Value = "P0"
Worksheets("feuil3").Cells(1 + J, 2 + K).Value = "P0sant"
Worksheets("feuil3").Cells(1 + J, 3 + K).Value = "P0mol"
Worksheets("feuil3").Cells(1 + J, 4 + K).Value = "Qmol"
Worksheets("feuil3").Cells(1 + J, 5 + K).Value = "Qsant"
Worksheets("feuil3").Cells(1 + J, 6 + K).Value = "Qcraq"
Worksheets("feuil3").Cells(1 + J, 7 + K).Value = "QtranS"
Worksheets("feuil3").Cells(1 + J, 8 + K).Value = "test"
Worksheets("feuil3").Cells(1 + J, 9 + K).Value = "P1"
Worksheets("feuil3").Cells(1 + J, 10 + K).Value = "Kn"


Ptub1e = P0
P2 = P0
'les pressions sont calculées en Pa'
P1 = Qcraq / Cbchoc1  ' Qchoc en mol./s, P1 pression interne orifice buse seul choqué'
'P0sant = (Qcraq * (1 / Kbvis1 + Qcraq / (Cbchoc1 ^ 2))) ^ (1 / 2) 'élimination de P1'
P0sant = (Cbchoc1 / (2 * Kbvis1)) * ((2 * Kbvis1 * Qcraq / (Cbchoc1 ^ 2) + 1) ^ 2 - 1) ^ 1 / 2
'P0hag = (Qcraq / Kbvis1 + P2 ^ 2) ^ (1 / 2) 'formule d'Hagen-Poiseuille'
P0mol = (Qcraq / Cbmol1) + P2
```

```
'Résolution de la transition avec Santeler dans la buse1'*****************************
If P0mol > P0sant Then
P0max = P0mol * 1.1
P0min = P0sant * 0.9
Else
P0max = P0sant * 1.1
P0min = P0mol * 0.9
End If
pas = (P0max - P0min) / 10
Line5:
For P0 = P0min To P0max Step pas
'Qhag = Kbvis1 * (P0 ^ 2 - P2 ^ 2)  ' flux molaire/s buse entière en visqueux-laminaire = Hagen-Poiseuille'
Qsant = (Cbchoc1 ^ 2 / (2 * Kbvis1)) * ((1 + (2 * Kbvis1 * P0 / Cbchoc1) ^ 2) ^ (1 / 2) - 1) ' débit buse+choc en moles/s'
'QhagS = Kbvis1 * (P0 ^ 2 - P1 ^ 2)  ' flux molaire/s conduit buse en visqueux-laminaire = Hagen-Poiseuille'
Lmoyen = Lmbuse1 / ((P0 + P1) / 2)
Kn1 = Lmoyen / (2 * Rbuse1)
Qmol = Cbmol1 * (P0 - P2)
'QtranS = Qsant * (1 - Ca ^ -Kn1) + Qmol * (Ca ^ -Kn1)
QtranS = Qsant * (1 - Ca ^ (-1 / Kn1)) + Qmol * (Ca ^ (-1 / Kn1))

Test = QtranS - Qcraq
J = J + 1
Worksheets("feuil3").Cells(1 + J, 1 + K).Value = P0
Worksheets("feuil3").Cells(1 + J, 2 + K).Value = P0sant
Worksheets("feuil3").Cells(1 + J, 3 + K).Value = P0mol
Worksheets("feuil3").Cells(1 + J, 4 + K).Value = Qmol
Worksheets("feuil3").Cells(1 + J, 5 + K).Value = Qsant
Worksheets("feuil3").Cells(1 + J, 6 + K).Value = Qcraq
Worksheets("feuil3").Cells(1 + J, 7 + K).Value = QtranS
Worksheets("feuil3").Cells(1 + J, 8 + K).Value = Test
Worksheets("feuil3").Cells(1 + J, 9 + K).Value = P1
Worksheets("feuil3").Cells(1 + J, 10 + K).Value = Kn1


If Test > 0 Then
P0min = P0 - pas
P0max = P0 + pas
pas = pas / 10
J = J + 1
Worksheets("feuil3").Cells(1 + J, 1 + K).Value = "P0min"
Worksheets("feuil3").Cells(1 + J, 2 + K).Value = "P0max"
J = J + 1
Worksheets("feuil3").Cells(1 + J, 1 + K).Value = P0min
Worksheets("feuil3").Cells(1 + J, 2 + K).Value = P0max
J = J + 1
If pas < P0 / 100000 Then
GoTo Line6:
End If
'L = L + 1
GoTo Line5:
End If

Next P0
Line6:
K = 0
J = J + 1
Worksheets("feuil3").Cells(1 + J, 1 + K).Value = "Buse1"
J = J + 1
Worksheets("feuil3").Cells(1 + J, 1 + K).Value = "P0"
```

```
Worksheets("feuil3").Cells(1 + J, 2 + K).Value = "P0sant"
Worksheets("feuil3").Cells(1 + J, 3 + K).Value = "P0mol"
Worksheets("feuil3").Cells(1 + J, 4 + K).Value = "Qmol"
Worksheets("feuil3").Cells(1 + J, 5 + K).Value = "Qsant"
Worksheets("feuil3").Cells(1 + J, 6 + K).Value = "Qcraq"
Worksheets("feuil3").Cells(1 + J, 7 + K).Value = "QtranS"
Worksheets("feuil3").Cells(1 + J, 8 + K).Value = "test"
Worksheets("feuil3").Cells(1 + J, 9 + K).Value = "P1"
Worksheets("feuil3").Cells(1 + J, 10 + K).Value = "Kn"


J = J + 1
Worksheets("feuil3").Cells(1 + J, 1 + K).Value = P0
Worksheets("feuil3").Cells(1 + J, 2 + K).Value = P0sant
Worksheets("feuil3").Cells(1 + J, 3 + K).Value = P0mol
Worksheets("feuil3").Cells(1 + J, 4 + K).Value = Qmol
Worksheets("feuil3").Cells(1 + J, 5 + K).Value = Qsant
Worksheets("feuil3").Cells(1 + J, 6 + K).Value = Qcraq
Worksheets("feuil3").Cells(1 + J, 7 + K).Value = QtranS
Worksheets("feuil3").Cells(1 + J, 8 + K).Value = Test
Worksheets("feuil3").Cells(1 + J, 9 + K).Value = P1
Worksheets("feuil3").Cells(1 + J, 10 + K).Value = Kn1

K = 18

Worksheets("feuil3").Cells(1 + L, 1 + K).Value = P2
Worksheets("feuil3").Cells(1 + L, 2 + K).Value = P1
Worksheets("feuil3").Cells(1 + L, 3 + K).Value = P0
Q = K + 9
Worksheets("feuil3").Cells(1 + L, 1 + Q).Value = Log(P2 / Pst) / Log(10)
Worksheets("feuil3").Cells(1 + L, 2 + Q).Value = Log(P1 / Pst) / Log(10)
Worksheets("feuil3").Cells(1 + L, 3 + Q).Value = Log(P0 / Pst) / Log(10)



K = 0
Next I
End Sub
**************************************************************************
Sub ligneCsOH() ' buse 2 (100 microns) avec un seul tube de liaison pour toute  buse
'= tub1 et pression craqueur imposée '
L = 0
K = 0
J = 0
Tbuse = 1045 'K
Tcraq = 1770
Teff = 1234
Ttub1 = (Tbuse + Tcraq) / 2
Ttub2 = (Tcraq + Teff) / 2

variables
K = 0
Worksheets("feuil6").Cells(1 + J, 1 + K).Value = "P0"
Worksheets("feuil6").Cells(1 + J, 2 + K).Value = "P0sant"
Worksheets("feuil6").Cells(1 + J, 3 + K).Value = "P0mol"
Worksheets("feuil6").Cells(1 + J, 4 + K).Value = "Qmol"
Worksheets("feuil6").Cells(1 + J, 5 + K).Value = "Qsant"
Worksheets("feuil6").Cells(1 + J, 6 + K).Value = "Qcraq"
Worksheets("feuil6").Cells(1 + J, 7 + K).Value = "QtranS"
Worksheets("feuil6").Cells(1 + J, 8 + K).Value = "test"
```

```
Worksheets("feuil6").Cells(1 + J, 9 + K).Value = "P1"
Worksheets("feuil6").Cells(1 + J, 10 + K).Value = "Kn"

K = 12
Worksheets("feuil6").Cells(1 + L, 1 + K).Value = "Orif-1"
Worksheets("feuil6").Cells(1 + L, 4 + K).Value = "Tube-1"
Worksheets("feuil6").Cells(1 + L, 7 + K).Value = "Buse-1"
Q = K + 9
Worksheets("feuil6").Cells(1 + L, 1 + Q).Value = "Orif-1"
Worksheets("feuil6").Cells(1 + L, 4 + Q).Value = "Tube-1"
Worksheets("feuil6").Cells(1 + L, 7 + Q).Value = "Buse-1"
L = L + 1
Worksheets("feuil6").Cells(1 + L, 1 + K).Value = "P2/Pa"
Worksheets("feuil6").Cells(1 + L, 2 + K).Value = "P1/Pa"
Worksheets("feuil6").Cells(1 + L, 3 + K).Value = "P0/Pa"
Q = K + 9
Worksheets("feuil6").Cells(1 + L, 1 + Q).Value = "Log P2/bar"
Worksheets("feuil6").Cells(1 + L, 2 + Q).Value = "Log P1/bar"
Worksheets("feuil6").Cells(1 + L, 3 + Q).Value = "Log P0/bar"
K = K + 3
Worksheets("feuil6").Cells(1 + L, 1 + K).Value = "P2/Pa"
Worksheets("feuil6").Cells(1 + L, 2 + K).Value = "P1/Pa"
Worksheets("feuil6").Cells(1 + L, 3 + K).Value = "P0/Pa"
Q = K + 9
Worksheets("feuil6").Cells(1 + L, 1 + Q).Value = "Log P2/bar"
Worksheets("feuil6").Cells(1 + L, 2 + Q).Value = "Log P1/bar"
Worksheets("feuil6").Cells(1 + L, 3 + Q).Value = "Log P0/bar"
K = K + 3
Worksheets("feuil6").Cells(1 + L, 1 + K).Value = "P2/Pa"
Worksheets("feuil6").Cells(1 + L, 2 + K).Value = "P1/Pa"
Worksheets("feuil6").Cells(1 + L, 3 + K).Value = "P0/Pa"
Q = K + 9
Worksheets("feuil6").Cells(1 + L, 1 + Q).Value = "Log P2/bar"
Worksheets("feuil6").Cells(1 + L, 2 + Q).Value = "Log P1/bar"
Worksheets("feuil6").Cells(1 + L, 3 + Q).Value = "Log P0/bar"
Worksheets("feuil6").Cells(1 + L, 4 + Q).Value = "Log Pcraq/bar"
Worksheets("feuil6").Cells(1 + L, 5 + Q).Value = "Log Peff/bar"

'Calcul de la conductance entre craqueur et condenseur
Ctot = 1 / Centre3 + 1 / Cbaffix3 + 3 / Cbafint3 + 1 / Cbaf13 + 2 / Cbaf33 + 1 / Ccraq
Ctot = Ctot + 1 / Corif2 + 1 / Ctub2 + 1 / Corif3
Ctot = 1 / Ctot + 1 / Centre4 + 1 / Cbaffix4 + 3 / Cbafint4 + 1 / Cbaf14 + 2 / Cbaf34 + 1 / Ccond
Ctot = 1 / Ctot

K = 0
For I = 2 To -3 Step -0.25
'les pressions sont calculées en Pa'
'Pcraq = 10 'Pa'
Pcraq = 10 ^ I 'Pa'
'Peff = 10 ^ (Log(Pcraq) / Log(10) - 0.2359)
'Qcraq = (Pcraq * Corif2) / 3 'même flux dans chacune des 3 lignes'
Peff = Pcraq / (1 + Ceff / Ctot)   'calcule la Peff et le Qeff (flux) correspondant à Pcraq
Qeff = Peff * Ceff
Qcraq = Qeff

Ptub1s = Qcraq / Corif1 + Pcraq
P2 = Pcraq
P1 = Qcraq / Cchocorif1
P0sant = (Cchocorif1 / (2 * Korif1)) * ((2 * Korif1 * Qcraq / (Cchocorif1 ^ 2) + 1) ^ 2 - 1) ^ 1 / 2   'élimination
de P1'
```

```
'P0sant = (Qcraq * (1 / Korif1 + Qcraq / (Cchocorif1 ^ 2))) ^ 1 / 2   ' formule alternative pour elimination de P1
P0mol = (Qcraq / Corif1) + P2
'Résolution de la transition avec Santeler dans l'orifice 1'*******************************
J = J + 1
If P0mol > P0sant Then
P0max = P0mol * 1.2
P0min = P0sant * 0.9
Else
P0max = P0sant * 1.1
P0min = P0mol * 0.9
End If
pas = (P0max - P0min) / 10
Line1:
For P0 = P0min To P0max Step pas
Qsant = (Cchocorif1 ^ 2 / (2 * Korif1)) * ((1 + (2 * Korif1 * P0 / Cchocorif1) ^ 2) ^ (1 / 2) - 1) ' débit buse+choc
en moles/s'
Lmoyen = Lmorif1 / ((P1 + P0) / 2)
Kn1 = Lmoyen / (2 * Rorif1)  'attention DeMuth definit Kn à l'inverse
Qmol = Corif1 * (P0 - P2)
'QtranS = Qsant * (1 - Ca ^ -Kn1) + Qmol * (Ca ^ - Kn1) formule DeMuth
QtranS = Qsant * (1 - Ca ^ (-1 / Kn1)) + Qmol * Ca ^ (-1 / Kn1)  'inversion du Kn
Test = QtranS - Qcraq
J = J + 1
Worksheets("feuil6").Cells(1 + J, 1 + K).Value = P0
Worksheets("feuil6").Cells(1 + J, 2 + K).Value = P0sant
Worksheets("feuil6").Cells(1 + J, 3 + K).Value = P0mol
Worksheets("feuil6").Cells(1 + J, 4 + K).Value = Qmol
Worksheets("feuil6").Cells(1 + J, 5 + K).Value = Qsant
Worksheets("feuil6").Cells(1 + J, 6 + K).Value = Qcraq
Worksheets("feuil6").Cells(1 + J, 7 + K).Value = QtranS
Worksheets("feuil6").Cells(1 + J, 8 + K).Value = Test
Worksheets("feuil6").Cells(1 + J, 9 + K).Value = P1
Worksheets("feuil6").Cells(1 + J, 10 + K).Value = Kn1

If Test > 0 Then
P0min = P0 - pas
P0max = P0 + pas
pas = pas / 10
J = J + 1
Worksheets("feuil6").Cells(1 + J, 1 + K).Value = "P0min"
Worksheets("feuil6").Cells(1 + J, 2 + K).Value = "P0max"
J = J + 1
Worksheets("feuil6").Cells(1 + J, 1 + K).Value = P0min
Worksheets("feuil6").Cells(1 + J, 2 + K).Value = P0max
J = J + 1
If pas < P0 / 100000 Then
GoTo Line2:
End If
'L = L + 1
GoTo Line1:
End If

Next P0
Line2:
K = 0
J = J + 1
Worksheets("feuil6").Cells(1 + J, 1 + K).Value = "Orif1"
J = J + 1
Worksheets("feuil6").Cells(1 + J, 1 + K).Value = "P0"
Worksheets("feuil6").Cells(1 + J, 2 + K).Value = "P0sant"
```

```
Worksheets("feuil6").Cells(1 + J, 3 + K).Value = "P0mol"
Worksheets("feuil6").Cells(1 + J, 4 + K).Value = "Qmol"
Worksheets("feuil6").Cells(1 + J, 5 + K).Value = "Qsant"
Worksheets("feuil6").Cells(1 + J, 6 + K).Value = "Qcraq"
Worksheets("feuil6").Cells(1 + J, 7 + K).Value = "QtranS"
Worksheets("feuil6").Cells(1 + J, 8 + K).Value = "test"
Worksheets("feuil6").Cells(1 + J, 9 + K).Value = "P1"
Worksheets("feuil6").Cells(1 + J, 10 + K).Value = "Kn"

J = J + 1
Worksheets("feuil6").Cells(1 + J, 1 + K).Value = P0
Worksheets("feuil6").Cells(1 + J, 2 + K).Value = P0sant
Worksheets("feuil6").Cells(1 + J, 3 + K).Value = P0mol
Worksheets("feuil6").Cells(1 + J, 4 + K).Value = Qmol
Worksheets("feuil6").Cells(1 + J, 5 + K).Value = Qsant
Worksheets("feuil6").Cells(1 + J, 6 + K).Value = Qcraq
Worksheets("feuil6").Cells(1 + J, 7 + K).Value = QtranS
Worksheets("feuil6").Cells(1 + J, 8 + K).Value = Test
Worksheets("feuil6").Cells(1 + J, 9 + K).Value = P1
Worksheets("feuil6").Cells(1 + J, 10 + K).Value = Kn1

'Sorties des résultats seuls'
L = L + 1
K = 12
Worksheets("feuil6").Cells(1 + L, 1 + K).Value = P2
Worksheets("feuil6").Cells(1 + L, 2 + K).Value = P1
Worksheets("feuil6").Cells(1 + L, 3 + K).Value = P0


Q = K + 9
Worksheets("feuil6").Cells(1 + L, 1 + Q).Value = Log(P2 / Pst) / Log(10)
Worksheets("feuil6").Cells(1 + L, 2 + Q).Value = Log(P1 / Pst) / Log(10)
Worksheets("feuil6").Cells(1 + L, 3 + Q).Value = Log(P0 / Pst) / Log(10)
Q = K + 15
Worksheets("feuil6").Cells(1 + L, 4 + Q).Value = Log(Pcraq / Pst) / Log(10)
Worksheets("feuil6").Cells(1 + L, 5 + Q).Value = Log(Peff / Pst) / Log(10)

K = 0
Porif1s = P1
Ptub1s = P0
J = J + 4
Worksheets("feuil6").Cells(1 + J, 1 + K).Value = "P0"
Worksheets("feuil6").Cells(1 + J, 2 + K).Value = "P0sant"
Worksheets("feuil6").Cells(1 + J, 3 + K).Value = "P0mol"
Worksheets("feuil6").Cells(1 + J, 4 + K).Value = "Qmol"
Worksheets("feuil6").Cells(1 + J, 5 + K).Value = "Qsant"
Worksheets("feuil6").Cells(1 + J, 6 + K).Value = "Qcraq"
Worksheets("feuil6").Cells(1 + J, 7 + K).Value = "QtranS"
Worksheets("feuil6").Cells(1 + J, 8 + K).Value = "test"
Worksheets("feuil6").Cells(1 + J, 9 + K).Value = "P1"
Worksheets("feuil6").Cells(1 + J, 10 + K).Value = "Kn"

'boucle pour calcul de l'écoulement dans le tube 1'
'les pressions sont calculées en Pa'
P1 = Ptub1s
P2 = P1
P0sant = (Qcraq / Ktub1 + P1 ^ 2) ^ (1 / 2) 'formule d'Hagen-Poiseuille pour le tube de transfert entrée craqueur car pas d'orifice de sortie'
P0mol = (Qcraq / Ctub1) + P1
'Résolution de la transition avec Santeler-Hagen  dans le tube 1'*****************************
```

```
J = J + 1
If P0mol > P0sant Then
P0max = P0mol * 1.1
P0min = P0sant * 0.9
Else
P0max = P0sant * 1.1
P0min = P0mol * 0.9
End If
pas = (P0max - P0min) / 10
Line3:
For P0 = P0min To P0max Step pas
Qsant = Ktub1 * (P0 ^ 2 - P1 ^ 2)  ' flux molaire/s tube1 en visqueux-laminaire = Hagen-Poiseuille'
Lmoyen = Lmtub1 / ((P1 + P0) / 2)
Kn1 = Lmoyen / (2 * Rtub1)
Qmol = Ctub1 * (P0 - P1)
'QtranS = Qsant * (1 - Ca ^ -Kn1) + Qmol * (Ca ^ -Kn1)
QtranS = Qsant * (1 - Ca ^ (-1 / Kn1)) + Qmol * (Ca ^ (-1 / Kn1))
Test = QtranS - Qcraq
J = J + 1
Worksheets("feuil6").Cells(1 + J, 1 + K).Value = P0
Worksheets("feuil6").Cells(1 + J, 2 + K).Value = P0sant
Worksheets("feuil6").Cells(1 + J, 3 + K).Value = P0mol
Worksheets("feuil6").Cells(1 + J, 4 + K).Value = Qmol
Worksheets("feuil6").Cells(1 + J, 5 + K).Value = Qsant
Worksheets("feuil6").Cells(1 + J, 6 + K).Value = Qcraq
Worksheets("feuil6").Cells(1 + J, 7 + K).Value = QtranS
Worksheets("feuil6").Cells(1 + J, 8 + K).Value = Test
Worksheets("feuil6").Cells(1 + J, 9 + K).Value = P1
Worksheets("feuil6").Cells(1 + J, 10 + K).Value = Kn1

If Test > 0 Then
P0min = P0 - pas
P0max = P0 + pas
pas = pas / 10
J = J + 1
Worksheets("feuil6").Cells(1 + J, 1 + K).Value = "P0min"
Worksheets("feuil6").Cells(1 + J, 2 + K).Value = "P0max"
J = J + 1
Worksheets("feuil6").Cells(1 + J, 1 + K).Value = P0min
Worksheets("feuil6").Cells(1 + J, 2 + K).Value = P0max
J = J + 1
If pas < P0 / 100000 Then
GoTo Line4:
End If
'L = L + 1
GoTo Line3:
End If

Next P0
Line4:
K = 0
J = J + 1
Worksheets("feuil6").Cells(1 + J, 1 + K).Value = "Tub1"
J = J + 1
Worksheets("feuil6").Cells(1 + J, 1 + K).Value = "P0"
Worksheets("feuil6").Cells(1 + J, 2 + K).Value = "P0sant"
Worksheets("feuil6").Cells(1 + J, 3 + K).Value = "P0mol"
Worksheets("feuil6").Cells(1 + J, 4 + K).Value = "Qmol"
Worksheets("feuil6").Cells(1 + J, 5 + K).Value = "Qsant"
Worksheets("feuil6").Cells(1 + J, 6 + K).Value = "Qcraq"
```

```
Worksheets("feuil6").Cells(1 + J, 7 + K).Value = "QtranS"
Worksheets("feuil6").Cells(1 + J, 8 + K).Value = "test"
Worksheets("feuil6").Cells(1 + J, 9 + K).Value = "P1"
Worksheets("feuil6").Cells(1 + J, 10 + K).Value = "Kn"

J = J + 1
Worksheets("feuil6").Cells(1 + J, 1 + K).Value = P0
Worksheets("feuil6").Cells(1 + J, 2 + K).Value = P0sant
Worksheets("feuil6").Cells(1 + J, 3 + K).Value = P0mol
Worksheets("feuil6").Cells(1 + J, 4 + K).Value = Qmol
Worksheets("feuil6").Cells(1 + J, 5 + K).Value = Qsant
Worksheets("feuil6").Cells(1 + J, 6 + K).Value = Qcraq
Worksheets("feuil6").Cells(1 + J, 7 + K).Value = QtranS
Worksheets("feuil6").Cells(1 + J, 8 + K).Value = Test
Worksheets("feuil6").Cells(1 + J, 9 + K).Value = P1
Worksheets("feuil6").Cells(1 + J, 10 + K).Value = Kn1

K = 15

Worksheets("feuil6").Cells(1 + L, 1 + K).Value = P2
Worksheets("feuil6").Cells(1 + L, 2 + K).Value = P1
Worksheets("feuil6").Cells(1 + L, 3 + K).Value = P0
Q = K + 9
Worksheets("feuil6").Cells(1 + L, 1 + Q).Value = Log(P2 / Pst) / Log(10)
Worksheets("feuil6").Cells(1 + L, 2 + Q).Value = Log(P1 / Pst) / Log(10)
Worksheets("feuil6").Cells(1 + L, 3 + Q).Value = Log(P0 / Pst) / Log(10)


K = 0

'boucle pour calcul de l'écoulement dans la buse 2 du
CsOH"""""""""""""""""""""""""""""""""""""""""""""""""""
J = J + 4
Worksheets("feuil6").Cells(1 + J, 1 + K).Value = "P0"
Worksheets("feuil6").Cells(1 + J, 2 + K).Value = "P0sant"
Worksheets("feuil6").Cells(1 + J, 3 + K).Value = "P0mol"
Worksheets("feuil6").Cells(1 + J, 4 + K).Value = "Qmol"
Worksheets("feuil6").Cells(1 + J, 5 + K).Value = "Qsant"
Worksheets("feuil6").Cells(1 + J, 6 + K).Value = "Qcraq"
Worksheets("feuil6").Cells(1 + J, 7 + K).Value = "QtranS"
Worksheets("feuil6").Cells(1 + J, 8 + K).Value = "test"
Worksheets("feuil6").Cells(1 + J, 9 + K).Value = "P1"
Worksheets("feuil6").Cells(1 + J, 10 + K).Value = "Kn"


Ptub1e = P0
P2 = P0
'les pressions sont calculées en Pa'
P1 = Qcraq / Cbchoc2  ' Qchoc en mol./s, P1 pression interne orifice buse 2 seul choqué'
'P0sant = (Qcraq * (1 / Kbvis2 + Qcraq / (Cbchoc2 ^ 2))) ^ (1 / 2) 'élimination de P1'
P0sant = (Cbchoc2 / (2 * Kbvis2)) * ((2 * Kbvis2 * Qcraq / (Cbchoc2 ^ 2) + 1) ^ 2 - 1) ^ 1 / 2
'P0hag = (Qcraq / Kbvis2 + P2 ^ 2) ^ (1 / 2) 'formule d'Hagen-Poiseuille'
P0mol = (Qcraq / Cbmol2) + P2

'Résolution de la transition avec Santeler dans la buse2'******************************
If P0mol > P0sant Then
P0max = P0mol * 1.1
P0min = P0sant * 0.9
Else
P0max = P0sant * 1.1
```

```
P0min = P0mol * 0.9
End If
pas = (P0max - P0min) / 10
Line5:
For P0 = P0min To P0max Step pas
'Qhag = Kbvis2 * (P0 ^ 2 - P2 ^ 2)  ' flux molaire/s buse entière en visqueux-laminaire = Hagen-Poiseuille'
Qsant = (Cbchoc2 ^ 2 / (2 * Kbvis2)) * ((1 + (2 * Kbvis2 * P0 / Cbchoc2) ^ 2) ^ (1 / 2) - 1) ' débit buse+choc en moles/s'
'QhagS = Kbvis2 * (P0 ^ 2 - P1 ^ 2)  ' flux molaire/s conduit buse en visqueux-laminaire = Hagen-Poiseuille'
Lmoyen = Lmbuse2 / ((P0 + P1) / 2)
Kn1 = Lmoyen / (2 * Rbuse2)
Qmol = Cbmol2 * (P0 - P2)
'QtranS = Qsant * (1 - Ca ^ -Kn1) + Qmol * (Ca ^ -Kn1)
QtranS = Qsant * (1 - Ca ^ (-1 / Kn1)) + Qmol * (Ca ^ (-1 / Kn1))

Test = QtranS - Qcraq
J = J + 1
Worksheets("feuil6").Cells(1 + J, 1 + K).Value = P0
Worksheets("feuil6").Cells(1 + J, 2 + K).Value = P0sant
Worksheets("feuil6").Cells(1 + J, 3 + K).Value = P0mol
Worksheets("feuil6").Cells(1 + J, 4 + K).Value = Qmol
Worksheets("feuil6").Cells(1 + J, 5 + K).Value = Qsant
Worksheets("feuil6").Cells(1 + J, 6 + K).Value = Qcraq
Worksheets("feuil6").Cells(1 + J, 7 + K).Value = QtranS
Worksheets("feuil6").Cells(1 + J, 8 + K).Value = Test
Worksheets("feuil6").Cells(1 + J, 9 + K).Value = P1
Worksheets("feuil6").Cells(1 + J, 10 + K).Value = Kn1


If Test > 0 Then
P0min = P0 - pas
P0max = P0 + pas
pas = pas / 10
J = J + 1
Worksheets("feuil6").Cells(1 + J, 1 + K).Value = "P0min"
Worksheets("feuil6").Cells(1 + J, 2 + K).Value = "P0max"
J = J + 1
Worksheets("feuil6").Cells(1 + J, 1 + K).Value = P0min
Worksheets("feuil6").Cells(1 + J, 2 + K).Value = P0max
J = J + 1
If pas < P0 / 100000 Then
GoTo Line6:
End If
'L = L + 1
GoTo Line5:
End If

Next P0
Line6:
K = 0
J = J + 1
Worksheets("feuil6").Cells(1 + J, 1 + K).Value = "Buse2"
J = J + 1
Worksheets("feuil6").Cells(1 + J, 1 + K).Value = "P0"
Worksheets("feuil6").Cells(1 + J, 2 + K).Value = "P0sant"
Worksheets("feuil6").Cells(1 + J, 3 + K).Value = "P0mol"
Worksheets("feuil6").Cells(1 + J, 4 + K).Value = "Qmol"
Worksheets("feuil6").Cells(1 + J, 5 + K).Value = "Qsant"
Worksheets("feuil6").Cells(1 + J, 6 + K).Value = "Qcraq"
Worksheets("feuil6").Cells(1 + J, 7 + K).Value = "QtranS"
```

```
Worksheets("feuil6").Cells(1 + J, 8 + K).Value = "test"
Worksheets("feuil6").Cells(1 + J, 9 + K).Value = "P1"
Worksheets("feuil6").Cells(1 + J, 10 + K).Value = "Kn"


J = J + 1
Worksheets("feuil6").Cells(1 + J, 1 + K).Value = P0
Worksheets("feuil6").Cells(1 + J, 2 + K).Value = P0sant
Worksheets("feuil6").Cells(1 + J, 3 + K).Value = P0mol
Worksheets("feuil6").Cells(1 + J, 4 + K).Value = Qmol
Worksheets("feuil6").Cells(1 + J, 5 + K).Value = Qsant
Worksheets("feuil6").Cells(1 + J, 6 + K).Value = Qcraq
Worksheets("feuil6").Cells(1 + J, 7 + K).Value = QtranS
Worksheets("feuil6").Cells(1 + J, 8 + K).Value = Test
Worksheets("feuil6").Cells(1 + J, 9 + K).Value = P1
Worksheets("feuil6").Cells(1 + J, 10 + K).Value = Kn1

K = 18

Worksheets("feuil6").Cells(1 + L, 1 + K).Value = P2
Worksheets("feuil6").Cells(1 + L, 2 + K).Value = P1
Worksheets("feuil6").Cells(1 + L, 3 + K).Value = P0
Q = K + 9
Worksheets("feuil6").Cells(1 + L, 1 + Q).Value = Log(P2 / Pst) / Log(10)
Worksheets("feuil6").Cells(1 + L, 2 + Q).Value = Log(P1 / Pst) / Log(10)
Worksheets("feuil6").Cells(1 + L, 3 + Q).Value = Log(P0 / Pst) / Log(10)



K = 0
Next I
End Sub
*************************************************************************
Sub ligneGVH() ' buse 1 (50 microns) avec un seul tube de liaison pour toute  buse
'= tub1 vers craqueur'
L = 0
K = 0
J = 0
Tbuse = 1045 'K
Tcraq = 1770
Teff = 1234
Ttub1 = (Tbuse + Tcraq) / 2
variables
K = 0
Worksheets("feuil7").Cells(1 + J, 1 + K).Value = "P0"
Worksheets("feuil7").Cells(1 + J, 2 + K).Value = "P0sant"
Worksheets("feuil7").Cells(1 + J, 3 + K).Value = "P0mol"
Worksheets("feuil7").Cells(1 + J, 4 + K).Value = "Qmol"
Worksheets("feuil7").Cells(1 + J, 5 + K).Value = "Qsant"
Worksheets("feuil7").Cells(1 + J, 6 + K).Value = "Qcraq"
Worksheets("feuil7").Cells(1 + J, 7 + K).Value = "QtranS"
Worksheets("feuil7").Cells(1 + J, 8 + K).Value = "test"
Worksheets("feuil7").Cells(1 + J, 9 + K).Value = "P1"
Worksheets("feuil7").Cells(1 + J, 10 + K).Value = "Kn"

K = 12
Worksheets("feuil7").Cells(1 + L, 1 + K).Value = "Orif-1"
Worksheets("feuil7").Cells(1 + L, 4 + K).Value = "Tube-1"
Worksheets("feuil7").Cells(1 + L, 7 + K).Value = "Buse-1"
Q = K + 9
```

```
Worksheets("feuil7").Cells(1 + L, 1 + Q).Value = "Orif-1"
Worksheets("feuil7").Cells(1 + L, 4 + Q).Value = "Tube-1"
Worksheets("feuil7").Cells(1 + L, 7 + Q).Value = "Buse-1"
L = L + 1
Worksheets("feuil7").Cells(1 + L, 1 + K).Value = "P2/Pa"
Worksheets("feuil7").Cells(1 + L, 2 + K).Value = "P1/Pa"
Worksheets("feuil7").Cells(1 + L, 3 + K).Value = "P0/Pa"
Q = K + 9
Worksheets("feuil7").Cells(1 + L, 1 + Q).Value = "Log P2/bar"
Worksheets("feuil7").Cells(1 + L, 2 + Q).Value = "Log P1/bar"
Worksheets("feuil7").Cells(1 + L, 3 + Q).Value = "Log P0/bar"
K = K + 3
Worksheets("feuil7").Cells(1 + L, 1 + K).Value = "P2/Pa"
Worksheets("feuil7").Cells(1 + L, 2 + K).Value = "P1/Pa"
Worksheets("feuil7").Cells(1 + L, 3 + K).Value = "P0/Pa"
Q = K + 9
Worksheets("feuil7").Cells(1 + L, 1 + Q).Value = "Log P2/bar"
Worksheets("feuil7").Cells(1 + L, 2 + Q).Value = "Log P1/bar"
Worksheets("feuil7").Cells(1 + L, 3 + Q).Value = "Log P0/bar"
K = K + 3
Worksheets("feuil7").Cells(1 + L, 1 + K).Value = "P2/Pa"
Worksheets("feuil7").Cells(1 + L, 2 + K).Value = "P1/Pa"
Worksheets("feuil7").Cells(1 + L, 3 + K).Value = "P0/Pa"
Q = K + 9
Worksheets("feuil7").Cells(1 + L, 1 + Q).Value = "Log P2/bar"
Worksheets("feuil7").Cells(1 + L, 2 + Q).Value = "Log P1/bar"
Worksheets("feuil7").Cells(1 + L, 3 + Q).Value = "Log P0/bar"
Worksheets("feuil7").Cells(1 + L, 4 + Q).Value = "Log Pcraq/bar"
Worksheets("feuil7").Cells(1 + L, 5 + Q).Value = "Log Peff/bar"

'Calcul de la conductance entre craqueur et condenseur
Ctot = 1 / Centre3 + 1 / Cbaffix3 + 3 / Cbafint3 + 1 / Cbaf13 + 2 / Cbaf33 + 1 / Ccraq
Ctot = Ctot + 1 / Corif2 + 1 / Ctub2 + 1 / Corif3
Ctot = 1 / Ctot + 1 / Centre4 + 1 / Cbaffix4 + 3 / Cbafint4 + 1 / Cbaf14 + 2 / Cbaf34 + 1 / Ccond
Ctot = 1 / Ctot

K = 0
For I = 2 To -3 Step -0.25
'les pressions sont calculées en Pa'
'Pcraq = 10 'Pa'
Pcraq = 10 ^ I 'Pa'
'Peff = 10 ^ (Log(Pcraq) / Log(10) - 0.2359)   'pour argon mais aussi valable pour les autres car compensation des racines des masses
'Qcraq = (Pcraq * Corif2) / 3     'même flux dans chacune des 3 lignes'
'Qcraq = (Pcraq * Ceff) / 3 / 5
Peff = Pcraq / (1 + Ceff / Ctot)   'calcule la Peff et le Qeff (flux) correspondant à Pcraq
Qeff = Peff * Ceff
Qcraq = Qeff
Ptub1s = Qcraq / Corif1 + Pcraq
P2 = Pcraq
P1 = Qcraq / Cchocorif1
'P0sant = (Qcraq * (1 / Korif1 + Qcraq / (Cchocorif1 ^ 2))) ^ (1 / 2) 'élimination de P1'
P0sant = (Cchocorif1 / (2 * Korif1)) * ((2 * Korif1 * Qcraq / (Cchocorif1 ^ 2) + 1) ^ 2 - 1) ^ 1 / 2
P0mol = (Qcraq / Corif1) + P2
'Résolution de la transition avec Santeler dans l'orifice 1'*****************************
J = J + 1
If P0mol > P0sant Then
P0max = P0mol * 1.2
P0min = P0sant * 0.9
Else
```

```
P0max = P0sant * 1.1
P0min = P0mol * 0.9
End If
pas = (P0max - P0min) / 10
Line1:
For P0 = P0min To P0max Step pas
Qsant = (Cchocorif1 ^ 2 / (2 * Korif1)) * ((1 + (2 * Korif1 * P0 / Cchocorif1) ^ 2) ^ (1 / 2) - 1) ' débit buse+choc en moles/s'
Lmoyen = Lmorif1 / ((P1 + P0) / 2)
Kn1 = Lmoyen / (2 * Rorif1)  'attention DeMuth definit Kn à l'inverse
Qmol = Corif1 * (P0 - P2)
'QtranS = Qsant * (1 - Ca ^ -Kn1) + Qmol * (Ca ^ - Kn1) formule DeMuth
QtranS = Qsant * (1 - Ca ^ (-1 / Kn1)) + Qmol * Ca ^ (-1 / Kn1)  'inversion du Kn
Test = QtranS - Qcraq
J = J + 1
Worksheets("feuil7").Cells(1 + J, 1 + K).Value = P0
Worksheets("feuil7").Cells(1 + J, 2 + K).Value = P0sant
Worksheets("feuil7").Cells(1 + J, 3 + K).Value = P0mol
Worksheets("feuil7").Cells(1 + J, 4 + K).Value = Qmol
Worksheets("feuil7").Cells(1 + J, 5 + K).Value = Qsant
Worksheets("feuil7").Cells(1 + J, 6 + K).Value = Qcraq
Worksheets("feuil7").Cells(1 + J, 7 + K).Value = QtranS
Worksheets("feuil7").Cells(1 + J, 8 + K).Value = Test
Worksheets("feuil7").Cells(1 + J, 9 + K).Value = P1
Worksheets("feuil7").Cells(1 + J, 10 + K).Value = Kn1

If Test > 0 Then
P0min = P0 - pas
P0max = P0 + pas
pas = pas / 10
J = J + 1
Worksheets("feuil7").Cells(1 + J, 1 + K).Value = "P0min"
Worksheets("feuil7").Cells(1 + J, 2 + K).Value = "P0max"
J = J + 1
Worksheets("feuil7").Cells(1 + J, 1 + K).Value = P0min
Worksheets("feuil7").Cells(1 + J, 2 + K).Value = P0max
J = J + 1
If pas < P0 / 100000 Then
GoTo Line2:
End If
'L = L + 1
GoTo Line1:
End If

Next P0
Line2:
K = 0
J = J + 1
Worksheets("feuil7").Cells(1 + J, 1 + K).Value = "Orif1"
J = J + 1
Worksheets("feuil7").Cells(1 + J, 1 + K).Value = "P0"
Worksheets("feuil7").Cells(1 + J, 2 + K).Value = "P0sant"
Worksheets("feuil7").Cells(1 + J, 3 + K).Value = "P0mol"
Worksheets("feuil7").Cells(1 + J, 4 + K).Value = "Qmol"
Worksheets("feuil7").Cells(1 + J, 5 + K).Value = "Qsant"
Worksheets("feuil7").Cells(1 + J, 6 + K).Value = "Qcraq"
Worksheets("feuil7").Cells(1 + J, 7 + K).Value = "QtranS"
Worksheets("feuil7").Cells(1 + J, 8 + K).Value = "test"
Worksheets("feuil7").Cells(1 + J, 9 + K).Value = "P1"
Worksheets("feuil7").Cells(1 + J, 10 + K).Value = "Kn"
```

```
J = J + 1
Worksheets("feuil7").Cells(1 + J, 1 + K).Value = P0
Worksheets("feuil7").Cells(1 + J, 2 + K).Value = P0sant
Worksheets("feuil7").Cells(1 + J, 3 + K).Value = P0mol
Worksheets("feuil7").Cells(1 + J, 4 + K).Value = Qmol
Worksheets("feuil7").Cells(1 + J, 5 + K).Value = Qsant
Worksheets("feuil7").Cells(1 + J, 6 + K).Value = Qcraq
Worksheets("feuil7").Cells(1 + J, 7 + K).Value = QtranS
Worksheets("feuil7").Cells(1 + J, 8 + K).Value = Test
Worksheets("feuil7").Cells(1 + J, 9 + K).Value = P1
Worksheets("feuil7").Cells(1 + J, 10 + K).Value = Kn1

'Sorties des résultats seuls'
L = L + 1
K = 12
Worksheets("feuil7").Cells(1 + L, 1 + K).Value = P2
Worksheets("feuil7").Cells(1 + L, 2 + K).Value = P1
Worksheets("feuil7").Cells(1 + L, 3 + K).Value = P0

Q = K + 9
Worksheets("feuil7").Cells(1 + L, 1 + Q).Value = Log(P2 / Pst) / Log(10)
Worksheets("feuil7").Cells(1 + L, 2 + Q).Value = Log(P1 / Pst) / Log(10)
Worksheets("feuil7").Cells(1 + L, 3 + Q).Value = Log(P0 / Pst) / Log(10)
Q = K + 15
Worksheets("feuil7").Cells(1 + L, 4 + Q).Value = Log(Pcraq / Pst) / Log(10)
Worksheets("feuil7").Cells(1 + L, 5 + Q).Value = Log(Peff / Pst) / Log(10)

K = 0
Porif1s = P1
Ptub1s = P0
J = J + 4
Worksheets("feuil7").Cells(1 + J, 1 + K).Value = "P0"
Worksheets("feuil7").Cells(1 + J, 2 + K).Value = "P0sant"
Worksheets("feuil7").Cells(1 + J, 3 + K).Value = "P0mol"
Worksheets("feuil7").Cells(1 + J, 4 + K).Value = "Qmol"
Worksheets("feuil7").Cells(1 + J, 5 + K).Value = "Qsant"
Worksheets("feuil7").Cells(1 + J, 6 + K).Value = "Qcraq"
Worksheets("feuil7").Cells(1 + J, 7 + K).Value = "QtranS"
Worksheets("feuil7").Cells(1 + J, 8 + K).Value = "test"
Worksheets("feuil7").Cells(1 + J, 9 + K).Value = "P1"
Worksheets("feuil7").Cells(1 + J, 10 + K).Value = "Kn"

'boucle pour calcul de l'écoulement dans le tube 1'
'les pressions sont calculées en Pa'
P1 = Ptub1s
P2 = P1
P0sant = (Qcraq / Ktub1 + P1 ^ 2) ^ (1 / 2) 'formule d'Hagen-Poiseuille pour le tube de transfert entrée craqueur car pas d'orifice de sortie'
P0mol = (Qcraq / Ctub1) + P1
'Résolution de la transition avec Santeler-Hagen  dans le tube 1'******************************
J = J + 1
If P0mol > P0sant Then
P0max = P0mol * 1.1
P0min = P0sant * 0.9
Else
P0max = P0sant * 1.1
P0min = P0mol * 0.9
End If
pas = (P0max - P0min) / 10
```

```
Line3:
For P0 = P0min To P0max Step pas
Qsant = Ktub1 * (P0 ^ 2 - P1 ^ 2)  ' flux molaire/s tube1 en visqueux-laminaire = Hagen-Poiseuille'
Lmoyen = Lmtub1 / ((P1 + P0) / 2)
Kn1 = Lmoyen / (2 * Rtub1)
Qmol = Ctub1 * (P0 - P1)
'QtranS = Qsant * (1 - Ca ^ -Kn1) + Qmol * (Ca ^ -Kn1)
QtranS = Qsant * (1 - Ca ^ (-1 / Kn1)) + Qmol * (Ca ^ (-1 / Kn1))
Test = QtranS - Qcraq
J = J + 1
Worksheets("feuil7").Cells(1 + J, 1 + K).Value = P0
Worksheets("feuil7").Cells(1 + J, 2 + K).Value = P0sant
Worksheets("feuil7").Cells(1 + J, 3 + K).Value = P0mol
Worksheets("feuil7").Cells(1 + J, 4 + K).Value = Qmol
Worksheets("feuil7").Cells(1 + J, 5 + K).Value = Qsant
Worksheets("feuil7").Cells(1 + J, 6 + K).Value = Qcraq
Worksheets("feuil7").Cells(1 + J, 7 + K).Value = QtranS
Worksheets("feuil7").Cells(1 + J, 8 + K).Value = Test
Worksheets("feuil7").Cells(1 + J, 9 + K).Value = P1
Worksheets("feuil7").Cells(1 + J, 10 + K).Value = Kn1

If Test > 0 Then
P0min = P0 - pas
P0max = P0 + pas
pas = pas / 10
J = J + 1
Worksheets("feuil7").Cells(1 + J, 1 + K).Value = "P0min"
Worksheets("feuil7").Cells(1 + J, 2 + K).Value = "P0max"
J = J + 1
Worksheets("feuil7").Cells(1 + J, 1 + K).Value = P0min
Worksheets("feuil7").Cells(1 + J, 2 + K).Value = P0max
J = J + 1
If pas < P0 / 100000 Then
GoTo Line4:
End If
'L = L + 1
GoTo Line3:
End If

Next P0
Line4:
K = 0
J = J + 1
Worksheets("feuil7").Cells(1 + J, 1 + K).Value = "Tub1"
J = J + 1
Worksheets("feuil7").Cells(1 + J, 1 + K).Value = "P0"
Worksheets("feuil7").Cells(1 + J, 2 + K).Value = "P0sant"
Worksheets("feuil7").Cells(1 + J, 3 + K).Value = "P0mol"
Worksheets("feuil7").Cells(1 + J, 4 + K).Value = "Qmol"
Worksheets("feuil7").Cells(1 + J, 5 + K).Value = "Qsant"
Worksheets("feuil7").Cells(1 + J, 6 + K).Value = "Qcraq"
Worksheets("feuil7").Cells(1 + J, 7 + K).Value = "QtranS"
Worksheets("feuil7").Cells(1 + J, 8 + K).Value = "test"
Worksheets("feuil7").Cells(1 + J, 9 + K).Value = "P1"
Worksheets("feuil7").Cells(1 + J, 10 + K).Value = "Kn"
J = J + 1
Worksheets("feuil7").Cells(1 + J, 1 + K).Value = P0
Worksheets("feuil7").Cells(1 + J, 2 + K).Value = P0sant
Worksheets("feuil7").Cells(1 + J, 3 + K).Value = P0mol
Worksheets("feuil7").Cells(1 + J, 4 + K).Value = Qmol
```

```
Worksheets("feuil7").Cells(1 + J, 5 + K).Value = Qsant
Worksheets("feuil7").Cells(1 + J, 6 + K).Value = Qcraq
Worksheets("feuil7").Cells(1 + J, 7 + K).Value = QtranS
Worksheets("feuil7").Cells(1 + J, 8 + K).Value = Test
Worksheets("feuil7").Cells(1 + J, 9 + K).Value = P1
Worksheets("feuil7").Cells(1 + J, 10 + K).Value = Kn1

K = 15

Worksheets("feuil7").Cells(1 + L, 1 + K).Value = P2
Worksheets("feuil7").Cells(1 + L, 2 + K).Value = P1
Worksheets("feuil7").Cells(1 + L, 3 + K).Value = P0
Q = K + 9
Worksheets("feuil7").Cells(1 + L, 1 + Q).Value = Log(P2 / Pst) / Log(10)
Worksheets("feuil7").Cells(1 + L, 2 + Q).Value = Log(P1 / Pst) / Log(10)
Worksheets("feuil7").Cells(1 + L, 3 + Q).Value = Log(P0 / Pst) / Log(10)


K = 0

'boucle pour calcul de l'écoulement dans la buse GVH'""""""""""""""""""""""""""""""""""""""""""""""""""""""""""""""""""""
J = J + 4
Worksheets("feuil7").Cells(1 + J, 1 + K).Value = "P0"
Worksheets("feuil7").Cells(1 + J, 2 + K).Value = "P0sant"
Worksheets("feuil7").Cells(1 + J, 3 + K).Value = "P0mol"
Worksheets("feuil7").Cells(1 + J, 4 + K).Value = "Qmol"
Worksheets("feuil7").Cells(1 + J, 5 + K).Value = "Qsant"
Worksheets("feuil7").Cells(1 + J, 6 + K).Value = "Qcraq"
Worksheets("feuil7").Cells(1 + J, 7 + K).Value = "QtranS"
Worksheets("feuil7").Cells(1 + J, 8 + K).Value = "test"
Worksheets("feuil7").Cells(1 + J, 9 + K).Value = "P1"
Worksheets("feuil7").Cells(1 + J, 10 + K).Value = "Kn"

Ptub1e = P0
P2 = P0
'les pressions sont calculées en Pa'
P1 = Qcraq / Cbchoc1  ' Qchoc en mol./s, P1 pression interne orifice buse seul choqué'
'P0sant = (Qcraq * (1 / Kbvis1 + Qcraq / (Cbchoc1 ^ 2))) ^ (1 / 2) 'élimination de P1'
P0sant = (Cbchoc1 / (2 * Kbvis1)) * ((2 * Kbvis1 * Qcraq / (Cbchoc1 ^ 2) + 1) ^ 2 - 1) ^ 1 / 2
'P0hag = (Qcraq / Kbvis1 + P2 ^ 2) ^ (1 / 2) 'formule d'Hagen-Poiseuille'
P0mol = (Qcraq / Cbmol1) + P2

'Résolution de la transition avec Santeler dans la buse1'******************************
If P0mol > P0sant Then
P0max = P0mol * 1.1
P0min = P0sant * 0.9
Else
P0max = P0sant * 1.1
P0min = P0mol * 0.9
End If
pas = (P0max - P0min) / 10
Line5:
For P0 = P0min To P0max Step pas
'Qhag = Kbvis1 * (P0 ^ 2 - P2 ^ 2)  ' flux molaire/s buse entière en visqueux-laminaire = Hagen-Poiseuille'
Qsant = (Cbchoc1 ^ 2 / (2 * Kbvis1)) * ((1 + (2 * Kbvis1 * P0 / Cbchoc1) ^ 2) ^ (1 / 2) - 1) ' débit buse+choc en
moles/s'
'QhagS = Kbvis1 * (P0 ^ 2 - P1 ^ 2)  ' flux molaire/s conduit buse en visqueux-laminaire = Hagen-Poiseuille'
Lmoyen = Lmbuse1 / ((P0 + P1) / 2)
Kn1 = Lmoyen / (2 * Rbuse1)
Qmol = Cbmol1 * (P0 - P2)
```

```
'QtranS = Qsant * (1 - Ca ^ -Kn1) + Qmol * (Ca ^ -Kn1)
QtranS = Qsant * (1 - Ca ^ (-1 / Kn1)) + Qmol * (Ca ^ (-1 / Kn1))

Test = QtranS - Qcraq
J = J + 1
Worksheets("feuil7").Cells(1 + J, 1 + K).Value = P0
Worksheets("feuil7").Cells(1 + J, 2 + K).Value = P0sant
Worksheets("feuil7").Cells(1 + J, 3 + K).Value = P0mol
Worksheets("feuil7").Cells(1 + J, 4 + K).Value = Qmol
Worksheets("feuil7").Cells(1 + J, 5 + K).Value = Qsant
Worksheets("feuil7").Cells(1 + J, 6 + K).Value = Qcraq
Worksheets("feuil7").Cells(1 + J, 7 + K).Value = QtranS
Worksheets("feuil7").Cells(1 + J, 8 + K).Value = Test
Worksheets("feuil7").Cells(1 + J, 9 + K).Value = P1
Worksheets("feuil7").Cells(1 + J, 10 + K).Value = Kn1


If Test > 0 Then
P0min = P0 - pas
P0max = P0 + pas
pas = pas / 10
J = J + 1
Worksheets("feuil7").Cells(1 + J, 1 + K).Value = "P0min"
Worksheets("feuil7").Cells(1 + J, 2 + K).Value = "P0max"
J = J + 1
Worksheets("feuil7").Cells(1 + J, 1 + K).Value = P0min
Worksheets("feuil7").Cells(1 + J, 2 + K).Value = P0max
J = J + 1
If pas < P0 / 100000 Then
GoTo Line6:
End If
'L = L + 1
GoTo Line5:
End If

Next P0
Line6:
K = 0
J = J + 1
Worksheets("feuil7").Cells(1 + J, 1 + K).Value = "Buse3"
J = J + 1
Worksheets("feuil7").Cells(1 + J, 1 + K).Value = "P0"
Worksheets("feuil7").Cells(1 + J, 2 + K).Value = "P0sant"
Worksheets("feuil7").Cells(1 + J, 3 + K).Value = "P0mol"
Worksheets("feuil7").Cells(1 + J, 4 + K).Value = "Qmol"
Worksheets("feuil7").Cells(1 + J, 5 + K).Value = "Qsant"
Worksheets("feuil7").Cells(1 + J, 6 + K).Value = "Qcraq"
Worksheets("feuil7").Cells(1 + J, 7 + K).Value = "QtranS"
Worksheets("feuil7").Cells(1 + J, 8 + K).Value = "test"
Worksheets("feuil7").Cells(1 + J, 9 + K).Value = "P1"
Worksheets("feuil7").Cells(1 + J, 10 + K).Value = "Kn"
J = J + 1
Worksheets("feuil7").Cells(1 + J, 1 + K).Value = P0
Worksheets("feuil7").Cells(1 + J, 2 + K).Value = P0sant
Worksheets("feuil7").Cells(1 + J, 3 + K).Value = P0mol
Worksheets("feuil7").Cells(1 + J, 4 + K).Value = Qmol
Worksheets("feuil7").Cells(1 + J, 5 + K).Value = Qsant
Worksheets("feuil7").Cells(1 + J, 6 + K).Value = Qcraq
Worksheets("feuil7").Cells(1 + J, 7 + K).Value = QtranS
Worksheets("feuil7").Cells(1 + J, 8 + K).Value = Test
```

```
Worksheets("feuil7").Cells(1 + J, 9 + K).Value = P1
Worksheets("feuil7").Cells(1 + J, 10 + K).Value = Kn1

K = 18

Worksheets("feuil7").Cells(1 + L, 1 + K).Value = P2
Worksheets("feuil7").Cells(1 + L, 2 + K).Value = P1
Worksheets("feuil7").Cells(1 + L, 3 + K).Value = P0
Q = K + 9
Worksheets("feuil7").Cells(1 + L, 1 + Q).Value = Log(P2 / Pst) / Log(10)
Worksheets("feuil7").Cells(1 + L, 2 + Q).Value = Log(P1 / Pst) / Log(10)
Worksheets("feuil7").Cells(1 + L, 3 + Q).Value = Log(P0 / Pst) / Log(10)

K = 0
Next I
End Sub
*************************************************************************
Sub Viscosité()

Etabusear = (18.497 * Tbuse / 300 + 3.22) * 10 ^ -6        'viscosité Ar '
Etaorif1ar = (18.497 * Tcraq / 300 + 3.22) * 10 ^ -6
Etatub1ar = (18.497 * Ttub1 / 300 + 3.22) * 10 ^ -6
MAr = 0.04                                  'kg pour Ar(g)'
Deltaar = 2.9 * 10 ^ -10                    'diamètre de la molécule
Gammaar = 5 / 3                             'rapport Cp/Cv monoatomique

EtabuseH2 = (6.0514 * Tbuse / 300 + 2.6067) * 10 ^ -6      'viscosité H2 selon lissage'
Etaorif1H2 = (6.0514 * Tcraq / 300 + 2.6067) * 10 ^ -6
Etatub1H2 = (6.0514 * Ttub1 / 300 + 2.6067) * 10 ^ -6
MH2 = 0.002                                 'kg pour H2(g)'
DeltaH2 = 1 * 10 ^ -10                      'diamètre de la molécule
GammaH2 = 7 / 5                             'rapport Cp/Cv diatomique = air

EtabuseW = (11.46 * Tbuse / 300 - 1.69) * 10 ^ -6          'viscosité H2O'
Etaorif1W = (11.46 * Tcraq / 300 - 1.69) * 10 ^ -6
Etatub1W = (11.46 * Ttub1 / 300 - 1.69) * 10 ^ -6
MW = 0.018                                  'kg pour H2O(g)'
DeltaW = 1.6 * 10 ^ -10                     'diamètre de la molécule
GammaW = 7 / 5                              'rapport Cp/Cv diatomique = air

'Etabuse = EtabuseAr
'Etaorif1 = Etaorif1Ar
'Etatub1 = Etatub1Ar
'M = MAr
'Delta = DeltaAr
'Gamma = GammaAr

'Etabuse = EtabuseH2
'Etaorif1 = Etaorif1H2
'Etatub1 = Etatub1H2
'M = MH2
'Delta = DeltaH2
'Gamma = GammaH2

Etabuse = Etabusear
Etaorif1 = Etaorif1ar
Etatub1 = Etatub1ar
M = MAr
Delta = Deltaar
Gamma = Gammaar
```

```
'Etabuse = EtabuseAr / 2 + EtabuseH2 / 2      'cas 50% H2 dans 50% Ar'
'Etaorif1 = Etaorif1Ar / 2 + Etaorif1H2 / 2
'Etatub1 = Etatub1Ar / 2 + Etatub1H2 / 2
'Delta = DeltaAr / 2 + DeltaH2 / 2
'Gamma = GammaAr / 2 + GammaH2 / 2

End Sub
*****************************************************
```

APPENDIX V-B

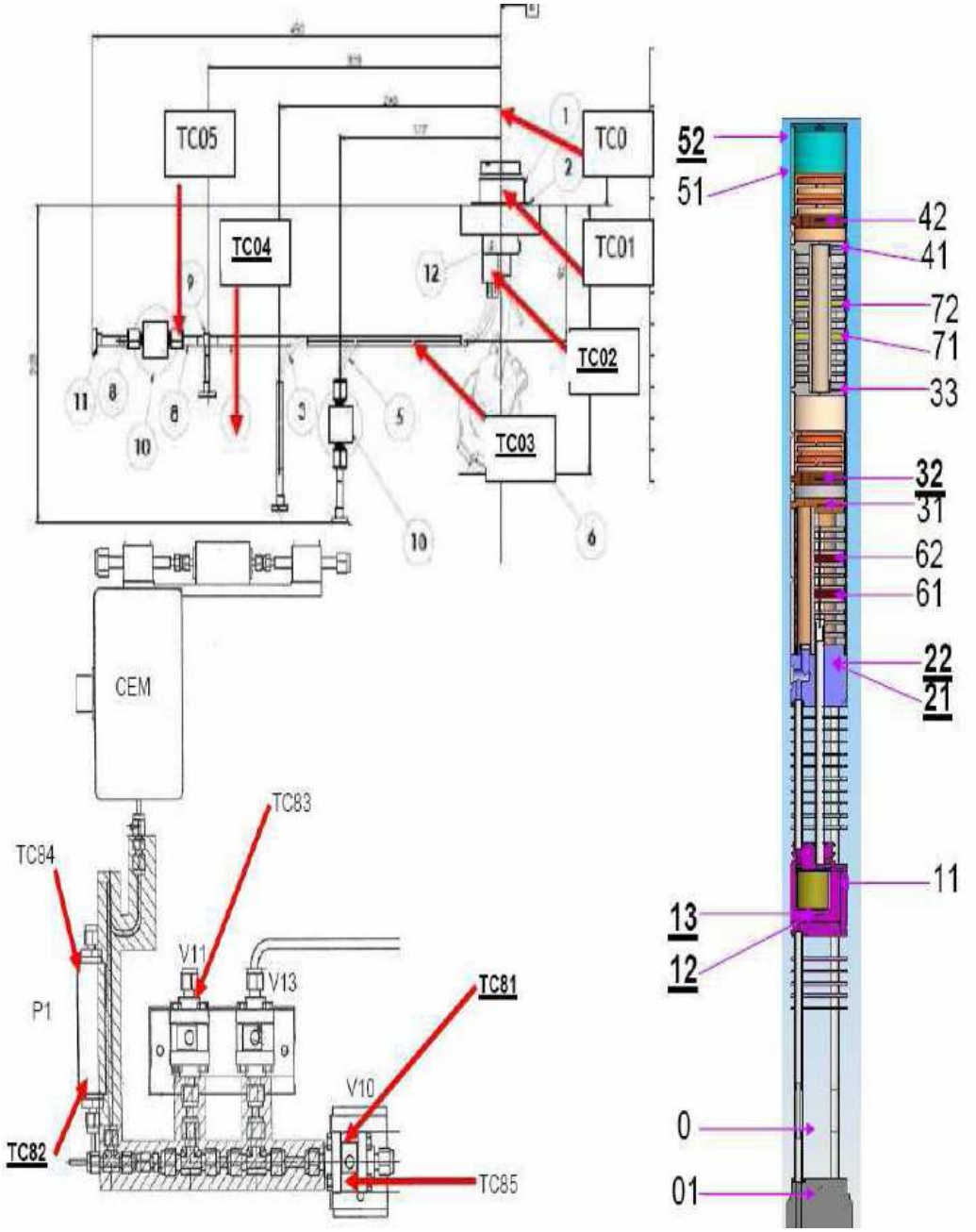

Figure V-A1: Thermocouples location in CHIP reactor

repère thermocouple S2IE	repère thermocouple SIMAP	Proposition	Zone	Position	Type	Regulation	T nominale en °C
52	B215		Condenseur	Trou droit enveloppe Molybdène haut	B	Regulation etage 4	1600
51	B213 @214		Condenseur	Trou gauche enveloppe Molybdène bas	B		
42	B213		Condenseur	Baffle fixe condenseur	B		
41	B211 @212		Condenseur	Partie basse condenseur	B		
72	B219		entre craqueur et condenseur	Tube de transfert (position haute à travers sole haute four étage 4	B		
71	B217 @218		entre craqueur et condenseur	Tube de transfert (position basse) à travers disque céramique four étage 4	B		
33	B211		Craqueur	Partie haute craqueur	B		
32	B209 @210		Craqueur	Baffle fixe craqueur	B	Regulation etage 3	1600
31	B209		Craqueur	Partie basse craqueur	B		
62	B217		entre buse et craqueur	Tube amont craqueur (position haute) à travers sole haute four étage 3	B		
22	K45 & K206		Buses	Trou latéral droit	K	Regulation etage 2	900
21	K205		Buses	Trou latéral gauche	K		
13	K35 & K204		Évaporateur	Trou latéral droit	K	Regulation etage 1	700
12	K203		Évaporateur	Trou latéral gauche	K		
11	K202		Évaporateur	Trou inférieur	K		
0	K201		Ambiance four	Lové entre les arrivées gaz	K		
01		K201	Embase réacteur	à cœur de l'embase	J		
02	J26		Embase réacteur	proche crayon chauffant	J	Regulation crayon Réacteur	150
03	J27		Lignes injecteurs	entre les 3 lignes gaz horizontales	J	Regulation injecteurs	150
04	J28		Lignes injecteurs	dans l'air entre BOA iode et BOA vapeur : coques chauffantes	J	Regulation coques	150
05			Lignes injecteurs	Aval vanne V15 (vanne vide ligne iode)	J		
81	J17		caisson GVH zone externe	Vanne V10 amont BOA vapeur	J	Regulation caisson externe	150
85			caisson GVH zone externe	Vanne V10 amont BOA vapeur	K		
83			caisson GVH zone externe	Vanne V11 purge sortie CEM	J		
82	J18		caisson GVH zone interne	P1 - regulateur de pression CEM	J	Regulation caisson interne	70
84			caisson GVH zone interne	P1 - regulateur de pression CEM	K		

Table V-A: Thermocouples description

APPENDIX V-C

Ionisation cross section (10^{-10} m^2) and isotopic abundance of the measured isotope

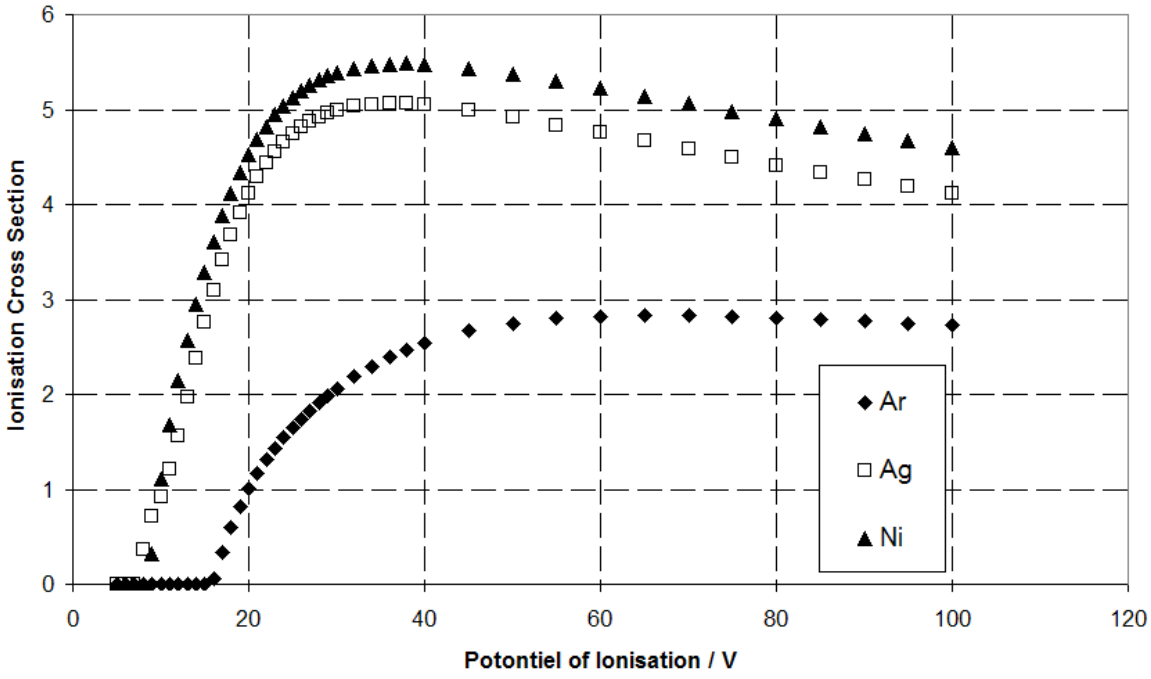

Figure V-B1: Ionisation cross section of Ar, Ag and Ni as function of the ionisation potential

Component	Isotopic abundance for the measured isotope
Ar	0.996
Ag	0.518
Ni	0.680769

Table V-B1: Isotopic abundance for Ar, Ag and Ni

APPENDIX V-D

Calculated Ar pressures at the cracker entrance as well as in the condenser are presented for the two experiments retained at the melting temperature of Ag and Ni in the two following figures. Temperatures of the different stages are those of the experiments. The geometry is the same for the two experiments.

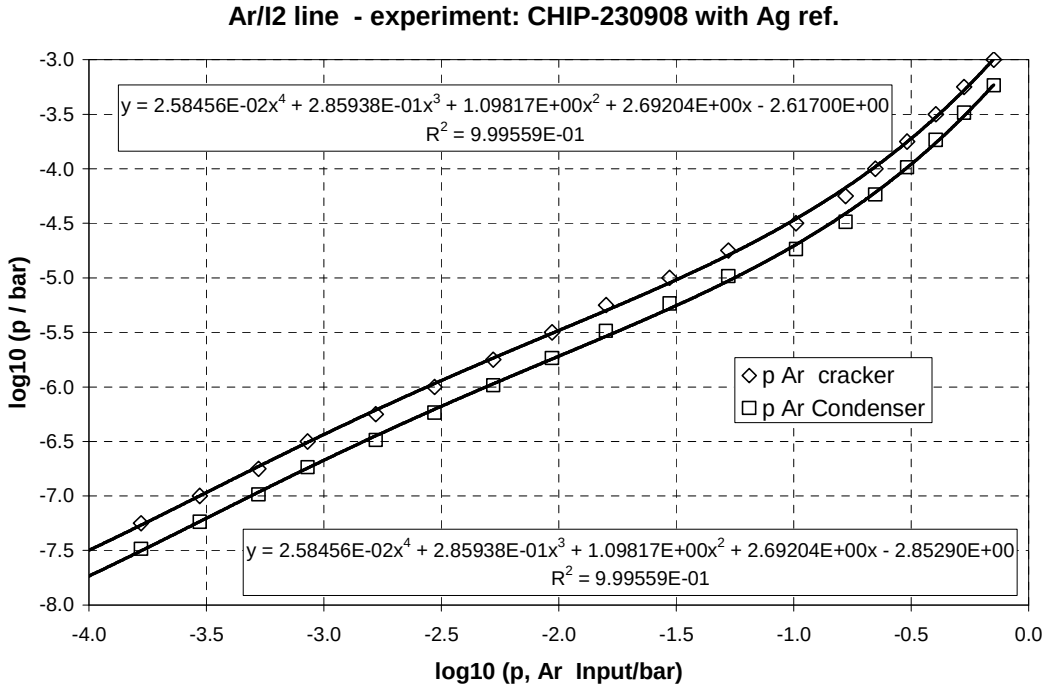

Figure V-C1: Calculated pressures of Ar at the cracker entrance and at the condenser (effusion orifice) as a function of the input pressure in the Ar/iodine line (nozzle 50 microns diameter. T condenser = 1234 K, T nozzles = 1045 K, T cracker = 1770 K, p(Ar/CsOH) = 50 mbar, p(Ar/I_2) = 632 mbar, p(Ar/H_2/H_2O) = 0 (clogged)

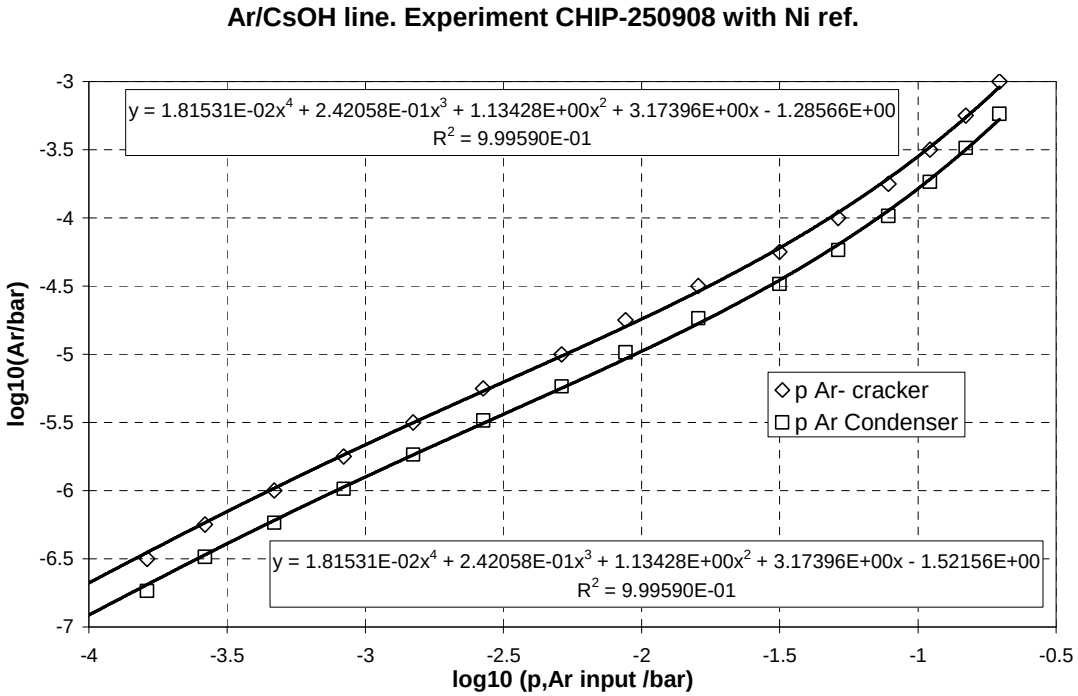

Figure V-C2: Calculated pressures of Ar at the cracker entrance and at the condenser (effusion orifice) as a function of the input pressure in the Ar/CsOH line (nozzle 100 microns diameter). T condenser = 1726 K, T nozzles = 1012 K, T cracker = 1853 K, p(Ar/CsOH) = 51 mbar, p(Ar/I_2) = 99.3 mbar, p(Ar/H_2/H_2O) = 0 (clogged)

CONCLUSIONS GENERALES ET PERSPECTIVES

Le présent travail a porté sur l'étude thermodynamique et cinétique de l'iode dans un environnement chimique représentatif de celui existant dans le cas d'un accident nucléaire grave sur un réacteur à eau pressurisée. Le système chimique de base choisi était le système quaternaire {Cs-I-O-H}, système dans lequel des composés stables à base d'iode existent comme CsI sous forme solide, liquide ou gazeuse avec la présence de polymères. Les composés hydroxydes comme CsOH sont aussi très stables et existent sous forme liquide et de vapeurs complexes. La compétition entre la formation des composés iodés condensés et gazeux va se produire et sera fonction, entre autre, des rapports H_2 / H_2O qui caractérisent le milieu accidentel. Tout l'enjeu du programme CHIP lancé par l'IRSN est d'expliquer comment cette compétition se règle dans les circuits de refroidissement, et notamment pour ce qui concerne cette étude analytique, dans la zone dite de «brèche en branche chaude». Les essais intégraux Phébus, menés à l'échelle 1/5000 par rapport aux réacteurs à eau pressurisée de type 900MWe, ont montré que de l'iode sous forme très volatile se propageait dans ce circuit jusqu'à l'enceinte de confinement, contrairement à ce que les calculs thermodynamiques laissaient prévoir à partir des données existantes dans les bases thermodynamiques. Le transfert de matière dans cette zone se produisant dans un temps relativement court, une des hypothèses envisagées était alors que la recombinaison des espèces atomiques issues du cœur du réacteur ne se faisait que lentement en ce qui concerne l'iode.

Sur le plan des données thermodynamiques, le présent travail a porté sur trois aspects relatifs au problème de la fiabilité des données utilisées dans les calculs:

- compiler et critiquer les données existantes afin de proposer des valeurs plus fiables pour les fonctions thermodynamiques comme cela a été fait pour le composé CsI: description plus fine du liquide (fusion et capacité calorifique), et nouvelles enthalpies de formation pour le monomère et le dimère gazeux. Ces nouvelles données correspondent à une augmentation relative des pressions de l'ordre de 30% par rapport aux données actuellement retenues (compilation de Glushko et al. 1982).
- Déterminer des grandeurs thermodynamiques en supplément pour des composés dont la compilation critique montrait des incertitudes importantes: ce fût le cas pour la vaporisation de CsOH, composé important dans le milieu accidentel en présence d'un excès de vapeur d'eau. Ces déterminations ont permis de modifier très sensiblement la température de fusion du composé, et ont fourni – après analyse critique de la littérature sur la base de ces déterminations – de nouvelles enthalpies de formation

pour le monomère et le dimère gazeux de l'hydroxyde. Les pressions proposées sont inférieures de 36% à celles compilées récemment par Gurvich et al. (1997). Il faut noter que le présent travail satisfait exactement aux recommandations proposées par les auteurs de cette compilation.

- Rechercher des espèces nouvelles à base d'iode qui pourrait expliquer le transport, c'est-à-dire des espèces plus stables que les composés CsI et CsOH. Un travail expérimental par spectrométrie de masse haute température a donc été entrepris pour confirmer et/ou infirmer la présence de la molécule complexe $Cs_2IOH(g)$ proposée par Blackburn et Johnson en 1986. Ce type de complexe dans la chimie gazeuse des molécules ioniques avait déjà été observé sur des molécules à base de Bore, puis soupçonné pour des mélanges de type NaCl-NaOH. La molécule $Cs_2IOH(g)$ a bien été observée mais avec des difficultés supplémentaires dues aux modes d'ionisation propres à ce type de molécule ionique. Les fonctions thermodynamiques proposées dans ce travail correspondent à une molécule plus stable que proposé par Blackburn et Johnson avec une pression supérieure d'un facteur 13. Des fonctions thermodynamiques complètes sont proposées pour être intégrées dans les banques de données.

En terme de bilan thermodynamique, le présent travail permettra une évaluation plus précise des quantités d'iode transportées d'une part parce que les propriétés thermodynamiques sont plus fiables, mais aussi parce que la présence d'une molécule nouvelle change la distribution de l'iode dans le système accidentel considéré. Le transport de l'iode va augmenter non seulement parce qu'avec ces nouvelles données, CsI(g) et $Cs_2I_2(g)$ sont plus volatiles de 30%, mais aussi parce que $Cs_2IOH(g)$ est 13 fois plus volatile que les composés de base CsI(g) et CsOH(g). Un effet de levier dans la compétition entre CsI et CsOH va aussi se produire car CsOH est pour sa part moins volatile de 36%.

En ce qui concerne l'obtention de données cinétiques, le présent travail a consisté à entreprendre la construction et la mise au point d'un réacteur expérimental associé à un spectromètre de masse pouvant à la fois analyser le milieu réactionnel - tout au moins en le simplifiant du point de vue chimique – et fournir des constantes cinétiques. Les différentes phases de la mise au point de ce réacteur au cours de ce travail ont été:

- Le calcul des régimes de flux qui permettent de satisfaire au transit de flux très faibles, compatibles avec les flux d'effusion mesurés par spectrométrie de masse, le réacteur ne devant pas perdre de matière.
- La conception d'une architecture permettant d'introduire plusieurs réactifs simultanément afin de satisfaire à l'observation – même simplifiée – de réactions dans des systèmes quaternaires du type {Cs-I-O-H}. L'introduction indépendante des réactifs, - CsOH, H_2O/H_2 et I_2 – doit permettre de porter un diagnostic sur les réactions ou espèces limitantes lors de la recombinaison se produisant dans la branche chaude du circuit primaire. Le réacteur est donc muni de trois lignes d'introduction de gaz débouchant dans un craqueur à haute température (1900 K) suivi d'un condenseur dont la température peut varier et qui satisfait aux caractéristiques d'une cellule d'effusion, ce qui est une première en spectrométrie de masse.
- Les tests assurant des conditions de fonctionnement satisfaisantes qui permettent d'envisager au moins une fonction diagnostique, et au mieux, à la suite de modifications en cours ou proposées, des études cinétiques.

Ce réacteur complexe a nécessité beaucoup de travail et a fait l'objet d'une collaboration étroite avec le service d'ingénierie de la DPAM à l'IRSN qui en a assuré la conception technique et une bonne part du suivi méthodologique. Si la mise au point du réacteur a pris un certain temps du notamment à sa complexité technologique et aux contraintes de son intégration dans le spectromètre de masse, sans compter les armoires pilotes de régulation (gaz et électricité), des évènements imprévus sont apparus ayant pour cause principale la méconnaissance scientifique des réactions de l'iode. En effet, la chimie haute température de l'iode est bien moins connue que celle des conditions standards, et est peu quantifiée. Ainsi, l'absence de données thermodynamiques pertinentes ne permet pas de choisir avec assurance les matériaux les mieux adaptés. Un effort de connaissance thermodynamique générale des réactions de l'iode avec l'ensemble des matériaux du nucléaire serait utile et va sans doute devenir nécessaire.

Les perspectives qui peuvent être dégagées du présent travail sont:

- Conserver un axe de recherche sur la thermodynamique des systèmes à base d'iode: deux aspects doivent être développés en parallèle, (i) conserver un œil critique sur les

données publiées, ce qui demande un travail minutieux et du temps, (ii) établir de nouvelles données en recherchant des espèces nouvelles stables.

- Faire précéder toute étude cinétique d'un effort thermodynamique comme cela a été fait ici pour le système {Cs-I-O-H} car la spectrométrie de masse aura besoin de références fiables pour déterminer si une réaction observée est en régime thermodynamique ou présente une limitation cinétique: c'est l'enjeu de la phase de diagnostique du réacteur CHIP.
- Améliorer sensiblement les qualités du réacteur CHIP pour aborder de façon certaine et fiable l'ajustement des modèles cinétiques de réactions en phase gazeuse. Cette amélioration porte sur trois points importants que sont – (i) le choix du matériau ne présentant pas d'interaction avec l'iode aux températures d'intérêt, (ii) le gradient thermique entre craqueur et condenseur, - (iii) les conditions de l'écoulement moléculaire dans l'étage haute température de l'Ar qui servira de référence de pression à l'ensemble des espèces analysées. .

Le réacteur CHIP associé au spectromètre de masse reste un outil de compréhension indispensable, et peut devenir une méthode de validation des modèles cinétiques de réactions en phase gazeuse. Cette méthode a la possibilité d'application large apte à aborder la complexité des problèmes posés par le comportement des matériaux du nucléaire.

TITLE / *TITRE*

KINETIC AND THERMODYNAMIC STUDIES OF REACTIONEL SYSTEM (X-I-O-H) BY HIGH TEMPERATURE MASS SPECTROMETRY

ETUDE DE LA CINETIQUE ET DE LA THERMODYNAMIQUE DES SYSTEMES REACTIONNELS (X-I-O-H) PAR SPECTROMETRIE DE MASSE HAUTE TEMPERATURE

ABSTRACT

High temperature mass spectrometry is used for analysis of vapors coming from iodine reaction with fission products in case of a severe nuclear accident in a pressurized water reactor. Two main ways are used, - (i) thermodynamic analysis of vaporization processes of CsOH, CsI and mixtures CsI-CsOH. - (ii) building a dedicated reactor for kinetic analysis of the recombination of atoms into these stables molecular species. The present study confirms the existence of $Cs_2IOH(g)$ molecule. Vapor pressures of gaseous molecules CsOH(g), $Cs_2O_2H_2(g)$ and $Cs_2IOH(g)$ have been determined. Molecular parameters of the mixed molecule have been estimated on the basis of the pure dimmers $Cs_2O_2H_2(g)$ and $Cs_2I_2(g)$ and its enthalpy of formation are established. The acquisition of kinetic data needs a new reactor, the conception of which is presented in this work as well as qualification tests: thermal, flow regimes and pressure calibration tests.

RESUME

La spectrométrie de masse haute température a été utilisée pour analyser les vapeurs simulant la réaction entre l'iode et les produits de fissions issus d'un accident grave de réacteur nucléaire à eau pressurisée. Deux voies principales ont été explorées, -(i) l'analyse thermodynamique des processus de vaporisation de CsOH, CsI et des mélanges CsI-CsOH. – (ii) la conception d'un réacteur spécifique pour l'analyse de la cinétique de recombinaison d'atomes pour former des molécules stables. La présente étude a confirmé l'existence de la molécule mixte $Cs_2IOH(g)$. Les pressions de vapeurs CsOH(g), $Cs_2O_2H_2(g)$ et $Cs_2IOH(g)$ ont été déterminées. Les paramètres moléculaires de la molécule mixte ont été estimés sur la base des dimères purs $Cs_2O_2H_2(g)$ and $Cs_2I_2(g)$ et l'enthalpie de formation proposée. L'acquisition de données cinétiques nécessite un réacteur dédié dont la conception est présentée dans ce travail ainsi que les tests de qualifications associés.

KEYWORDS / *MOT-CLES*

High temperature mass spectrometry, severe nuclear accident, iodine compounds vaporisation thermodynamic, kinetic reactor.

Spectrométrie de masse haute température, accident nucléaire grave, vaporisation des composés iodés, thermodynamique, réacteur cinétique.

Laboratoire: Science et Ingénierie des Matériaux et Procédés, 1130 rue de la piscine, BP 75, 38402 St Martin d'Hères.